UNIVERSITAS INDONESIA

**PERILAKU GESER PADA KOLOM
DENGAN SENGKANG MULTI SPIRAL DAN PERSEGI
MENGGUNAKAN MATERIAL BETON DAN BAJA MUTU
TINGGI DAN BEBAN TEKAN AKSIAL RENDAH**

TESIS

NURAZIZ HANDIKA
1006788214
**(Peserta Dual Degree Universitas Indonesia –
National Taiwan University of Science and Technology)**

FAKULTAS TEKNIK
PROGRAM STUDI TEKNIK SIPIL
DEPOK
JUNI 2012

UNIVERSITAS INDONESIA

PERILAKU GESER PADA KOLOM
DENGAN SENGKANG MULTI SPIRAL DAN PERSEGI
MENGGUNAKAN MATERIAL BETON DAN BAJA MUTU
TINGGI DAN BEBAN TEKAN AKSIAL RENDAH

TESIS

Diajukan sebagai salah satu syarat untuk memperoleh gelar Magister Teknik

NURAZIZ HANDIKA
1006788214
(Peserta Dual Degree Universitas Indonesia –
National Taiwan University of Science and Technology)

FAKULTAS TEKNIK
PROGRAM STUDI TEKNIK SIPIL
KEKHUSUSAN STRUKTUR
DEPOK
JUNI 2012

HALAMAN PERNYATAAN ORISINALITAS

Tesis ini adalah hasil karya saya sendiri,

dan semua sumber baik yang dikutip maupun dirujuk

telah saya nyatakan dengan benar

Nama : Nuraziz Handika

NPM : 1006788214

Tanda Tangan :

Tanggal : Juni 2012

HALAMAN PENGESAHAN

Tesis ini diajukan oleh   :
Nama   :   Nuraziz Handika
NPM   :   1006788214
Program Studi   :   Teknik Sipil
Judul Tesis   :   Perilaku Geser Pada Kolom dengan Sengkang
                                           Persegi dan Multi Spiral Menggunakan Material
                                           Beton dan Baja Mutu Tinggi dan Beban Tekan
                                           Aksial Rendah

Telah berhasil dipertahankan di hadapan De wan Penguji dan diterima sebagai bagian persyaratan yang di perlukan untuk memper oleh gelar Magister Teknik pada Pr ogram Studi Teknik Sipil Kekhususan Struktur , Fakultas Teknik, Universitas Indonesia

DEWAN PENGUJI
1. Cheng-Cheng CHEN
2. Shyh-Jiann HWANG

PEMBIMBING
Yu-Chen OU

Ditetapkan di : Taipei, Taiwan
Tanggal   : 19 Juni 2012

碩士學位考試委員會審定書

Qualification Form by Master's Degree Examination Committee

Department:Department of Construction Engineering

Student's Name:NURAZIZ HANDIKA

Thesis Title:

Shear Behavior of Tied and Multi-Spiral Columns with High-Strength Steel and Concrete under Low Axial Load

This is to certify that the dissertation submitted by the student named above, is qualified and approved by the Examination Committee.

Degree Examination Committee

Members' Signatures:

Advisor:

Program Director's Signature:

Department/Institute Chairman's Signature:

Date: _____2012____ / __6__ / __19__ (yyyy/mm/dd)

iv

碩士學位論文指導教授推薦書
Master's Thesis Recommendation Form

Department :　Department of Construction Engineering

Student's Name:　NURAZIZ HANDIKA

Thesis title:　Shear Behavior of Tied and Multi-Spiral Columns with High-Strength Steel and Concrete under Low Axial Load

This is to certify that the thesis submitted by the student named above, has been written under my supervision. I hereby approve this thesis to be applied for examination.

Advisor:YU-CHEN OU

Co-advisor:

Advisor's Signature: _____

Date: 2012 / 6 / 19 (yyyy/mm/dd)

v

ACKNOWLEDGEMENT

HALAMAN PERNYATAAN PERSETUJUAN PUBLIKASI
TUGAS AKHIR UNTUK KEPENTINGAN AKADEMIS

Sebagai sivitas akademik Universitas Indonesia, saya yang bertanda tangan di bawah ini:

Nama : Nuraziz Handika
NPM : 1006788214
Program Studi : Teknik Sipil
Departemen : Teknik Sipil
Fakultas : Teknik
Jenis karya : Tesis

demi pengembangan ilmu pengetahuan, menyetujui untuk memberikan kepada Universitas Indonesia **Hak Bebas Royalti Nonekslusif (** *Non-exclusive Royalty-Free Right*) atas karya ilmiah saya yang berjudul:

PERILAKU GESER PADA KOLOM DENGAN SENGKANG MULTI SPIRAL DAN PERSEGI MENGGUNAKAN MATERIAL BETON DAN BAJA MUTU TINGGI DAN BEBAN TEKAN AKSIAL RENDAH

beserta perangkat yang ada (jika diperlukan). Dengan Hak Bebas Royalti Nonekslusif ini Universitas Indonesia berhak menyimpan, mengalihmedia/formatkan, mengelola dalam bentuk pangkalan data (*database*), merawat, dan mempublikasikan tugas akhir saya tanpa meminta izin dari saya selama tetap mencantumkan nama saya sebagai penulis/pencipta dan sebagai pemilik Hak Cipta.

Demikian pernyataan ini saya buat dengan sebenarnya.

Dibuat di : Taipei
Pada tanggal : Juni 2012
Yang menyatakan,

(Nuraziz Handika)

ABSTRAK

Nama   : Nuraziz Handika

Program Studi : Teknik Sipil

Judul   : Perilaku Geser Pada Kolom dengan Sengkang Persegi dan Multi Spiral Menggunakan Material Beton dan Baja Mutu Tinggi dan Beban Tekan Aksial Rendah
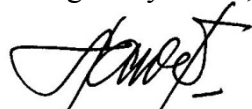
Penelitian ini bertujuan mengenali perilaku geser dua jenis sengkang dengan material baja dan beton mutu tinggi. Kolom dengan sengkang persegi dan multi-spiral diuji dengan rasio beban tekan aksial sebesar 20% dan 10%. Kuat tekan beton (70 MPa dan 100 MPa) dan spasi tulangan transversal menjadi dua parameter, dengan baja longitudinal dan transversal berkekuatan 685 MPa dan 785 MPa. Sudut retak kritis; regangan geser; kurvatur; tegangan tulangan transversal; efek dari beban tekan aksial akan dijelaskan. Hasil pengujian menunjukkan kekuatan geser maksimum kolom terjadi sebelum tulangan transversal mencapai titik lelehnya. Selain itu, sudut retak kritis yang lebih kecil, kekakuan kolom dan kekuatan lateral yang lebih tinggi terjadi pada beban aksial yang lebih besar. Peraturan desain kekuatan geser memberikan estimasi konservatif, 45 derajat sebagai sudut retak.

Kata kunci : *kolom, multi-spiral, baja mutu tinggi, beton mutu tinggi, beban siklis, beban tekan aksial rendah, kuat geser.*

Universitas Indonesia

ABSTRACT

Name   : Nuraziz Handika

Study Program   : Structure, Civil Engineering

Title   : Shear Behavior of Tied and Multi-Spiral Columns with High Strength Steel and Concrete under Low Axial Load

This research has objective to recognize the shear behavior of two types of stirrups with high strength steel and concrete under low axial load. The square hoops columns and multi-spiral columns are tested under 20% and 10% axial load ratio. Concrete compressive strength (70 MPa and 100 MPa) and spacing of the transverse reinforcement are two parameters that will be examined. Longitudinal and transversal reinforcements with specified yield strengths of 685 MPa and 785 MPa, respectively, are considered. Critical crack angle; shear strain and curvature; stress of transverse reinforcement; effect of axial compression load of six large-scale columns will be explained. Test results show that the maximum strength of columns appears before the yielding of stirrups. Moreover, smaller critical crack angle, stiffer column and higher lateral strength will be occurred from higher axial load application. Current codes provisions in shear strength provide the conservative estimation as 45 degrees of crack angle applied.

Keywords: *column, multi-spiral, high strength steel, high strength concrete, cyclic loading, low axial load, shear strength.*

TABLE OF CONTENTS

LIST OF TABLES

TABLE OF FIGURES

Universitas Indonesia

xxii

Universitas Indonesia

CHAPTER I
INTRODUCTION

1.1. INTRODUCTION

Nowadays, reinforced concrete is the most widely used construction material for buildings in the world, especially in the Asian region. Tony C Liu and Jenn-Chuan Chern[1] mentioned that in the year of 2007, Taiwan produced 150 million tons of concrete, which was the one percent of total world concrete production. Also, about 84% of the buildings in Taiwan are reinforced concrete structures (Samuel Yin[2]).

As the population will continue to increase, the infrastructure needs will grow. Consequently, construction, repair, rehabilitation needs, and demand of material sources for reinforced concrete are increasing. On the other hand, natural resources and renewal energy are becoming scarce. High-Strength Steel (HSS) and High-Strength Concrete (HSC) technology are two important innovations in order to face this condition. Research in combination of these two types of materials has been developed in past decades. The development of their definition and characteristics changes slightly as the continuation improvement of the new methods, innovation in materials and technology.

Caldarone[3] stated that high-strength concrete technology has been continually evolving for decades, and it has extensive records of accomplishment with respect to both its mechanical and its durability-enhancing properties. Definition and term of high strength concrete could depend on region and needs for the development. The definition of high-strength concrete is by no means static. Where high-strength concrete has been defined in terms of a precise numerical value, its

1

definition has changed over the years.

In the last sixty years, compressive strength of commercially produced concrete has increased approximately quadruple as the advancements in chemical admixtures technology, the increased availability of mineral admixtures and the increased knowledge of the principles governing higher-strength concretes.

High-strength concrete has high load carrying capacity per unit weight, which permits construction of very tall building. Smaller size of structural components may be used, resulting in reduced consumption of material. Furthermore, high-strength concrete allows for uniform column section along the height, with higher strength concrete used in lower stories.

Furthermore, HSC permits early form removal, resulting from sufficiently high early age strength, increasing construction speed. Lower deflections due to increased elastic modulus, lower creep, and greater resistance to physical and chemical deterioration form additional advantages associated with improved performance.

Although high-strength concrete has many advantages, it has a major drawback for seismic applications. As the physical strength of the material increases, the characteristic of concrete becomes increasingly brittle, and as a result, failure takes on more of an explosive nature (Caldarone[3]). Stated differently, since strength and ductility of concrete are inversely proportional, higher strength concretes are significantly more brittle than concretes within the normal-strength range.

As the demand of reinforced concrete is getting higher, the production of the concrete is needed to be considered more efficiently. Consequently, recent research creates innovations on the design and construction technology of

reinforced concrete, for example multi-spiral shear reinforcement. Building with construction automation technologies and precast components is one of the solutions in order to answer the economical and high quality construction problem these days. This innovative reinforcement provides both technical and cost advantages (Samuel Yin[2]).

1.2. PROBLEM DEFINITION

As mentioned before, the increasing needs of the material appear as the high demand of high rise buildings these days. An important benefit of using High-Strength Concrete (HSC) in high rise building is reducing the dimension of structural members. The reducing dimension of structural member, such as columns, means reducing the material consumption. In seismic region, when the column is subjected to earthquake lateral loading, shear force has a very significant influence on this structural member.

Effect of shear force on High-Strength Concrete in terms of strength at failure, has been an interesting subject of research. Also, as the definition of HSC is continually developing, the range of the concrete compressive strength is also changing. High rise building's columns are subjected to high axial load from the upper stories. Varying axial load ratio in the column has been an interesting research related the seismic behavior of the column during earthquake. Research using large scale specimens is rarely done since there are some merits of using high-strength re-bars.

Shear strength behavior under lateral loading for HSC is the main focus on this research. The elastic shear becomes interesting part of this research regarding

prediction of the shear demand of the HSC column.

Current codes have limitation for maximum strength of concrete and steel. Therefore, it is not clear whether or not the shear design models from these current codes can be implemented in design of columns with high strength steel and concrete. For example, the current shear design models in ACI 318R-08 may not be applicable for columns that have strength of steel and concrete larger 70 MPa.

Some researchers proposed equations for shear strength of concrete considering inelastic shear. Therefore, it is reasonable to examine the implementation of proposed equations in elastic shear condition.

Moreover, most of these current codes do not provide the formulation for multi-spiral columns with square cross-section. The idea of shear strength prediction of spiral shear reinforcement with circle cross-section will be applied.

1.3. OBJECTIVE AND SCOPE

The main objective of this research is to investigate the shear behavior of columns with High-Strength Steel (HSS) and High-Strength Concrete (HSC) under low axial load. Another objective is to compare the existing shear models with the test results and end up with design recommendation.

Some past researches on shear mentioned in the next chapter, has more focus on estimating shear strength in normal-strength concrete and quite a few shear strength estimations are available today. Hence, it was decided to put more effort towards predicting the shear strength of HSC columns.

The accuracy of existing proposed models was checked first. Some of the existing

proposed model used the normal-strength concrete and normal-strength steel but since the HSS and HSC are continually developing, the design suggestions and recommendations are needed for HSS and HSC columns. The details are provided in subsequent chapters.

As a sequence of previous study (Dimas Pramudya Kurniawan[28]), this research will compare test result especially in term of axial compression load effect to shear strength and lateral stiffness of the columns. Moreover, critical cracking angle; shear strain and curvature of columns; stress of transverse reinforcement, its limitation according to codes and a statistical study will be discussed.

In the final, it is expected that a design equation for shear design of reinforced concrete columns with high strength steel and concrete under low axial load could be proposed.

1.4. ORGANIZATION

First chapter contains a brief description of the report including background, objective and scope of this research.

Chapter 2 consists of previous research and literature review including the preceding research in HSC columns with square and spiral hoops and also some proposed shear strength models.

Specimen design of the columns and also properties of the materials for each specimen are provided in Chapter 3. The comparison of shear strength prediction of columns with low axial load is also reported here.

Detail of the test program as construction of specimens, test setup, applied loading and the instrumentations that were used during the experiment are provided in

Chapter 4.

Test result including material strength, applied axial load and test of specimens are provided in Chapter 5. The critical crack angle and its comparison to prediction value, strain reading, shear strain, curvature and displacement obtained from experimental data are also provided in this chapter. Statistical study of strain gauges reading is also given. The effect of axial compression load to shear strength and lateral stiffness will be explained in this part.

The evaluation of test results and analytical studies are provided in Chapter 6. This chapter will discuss about the comparison of test result and analytical studies.

Chapter 7 provides conclusion of this study and also future work that needed to be performed.
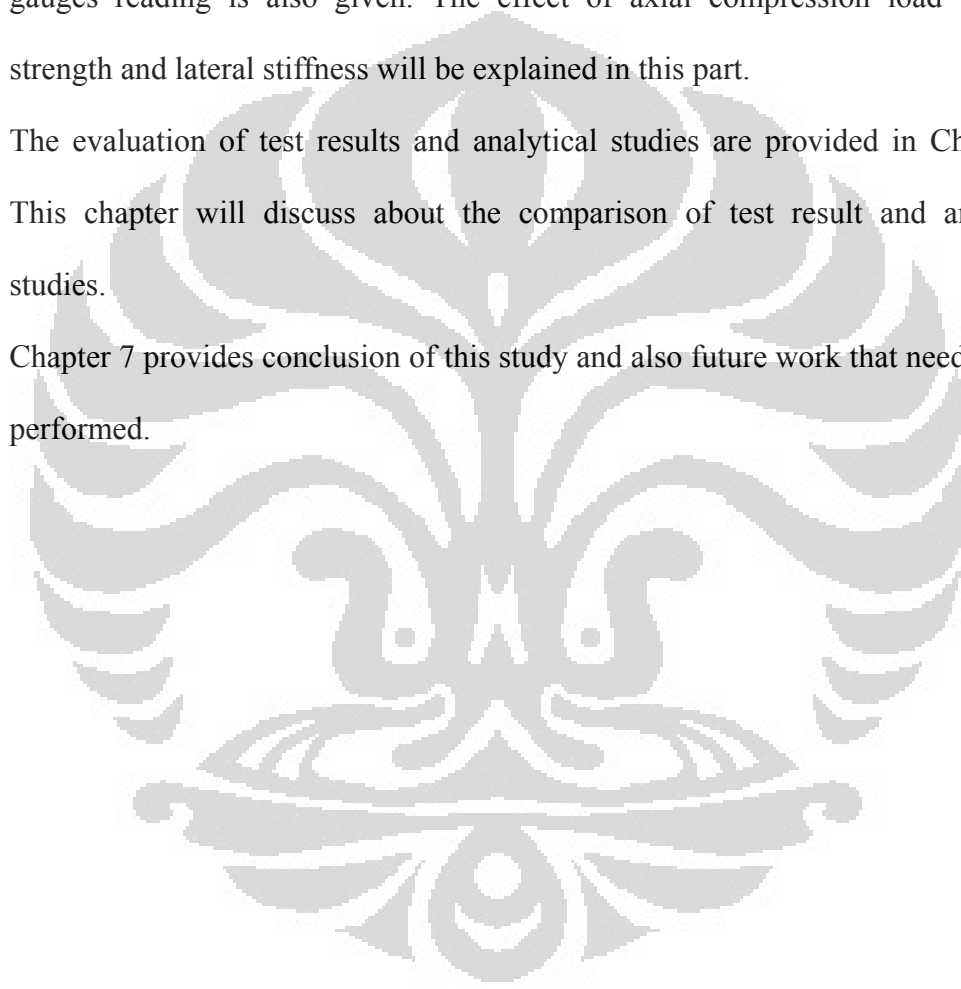
CHAPTER II
PREVIOUS RESEARCH & LITERATURE REVIEW

This chapter provides an overview of existing experimental and analytical research on the shear behavior of the High-Strength Concrete (HSC) columns. The definition of high-strength concrete and steel will be discussed in the beginning followed by the used of some parameters as axial load ratio, diameter of transverse reinforcement and yield strength of transverse reinforcement bar. Shear strength models proposed by some researchers are also discussed in this chapter. In the end of this chapter, the innovation of the multi-spiral reinforcement research will be explained.

2.1. HIGH STRENGTH CONCRETE MATERIAL

Before discussing about the model, the definition of the high-strength concrete will be explained first. Then, this section will continue to describe the confinement model for HSC.

2.1.1. Definition of High-Strength Concrete

Concrete Basics[4] stated that The American Concrete Institute (ACI) defines a High-strength Concrete as concrete that has a specified compressive strength for design of 41 MPa or greater but as mentioned before that the definition of HSC is continually developing. The primary difference between high-strength concrete and normal-strength concrete relates to the compressive strength that refers to the maximum resistance of the concrete sample to the applied pressure.

Besides HSC, another term which is also very important in the innovations of concrete is High-Performance Concrete (HPC). In the same source, it is stated that

the ACI defines high-performance concrete as concrete meeting special combinations of performance and uniformity requirements that cannot always be achieved routinely when using conventional constituents and normal mixing, placing and curing practices. A high performance concrete is mouthing which demands much higher performance from concrete as compared to performance expected from routine concrete. The HPC is normally designed for parameters (one or more) falling under the strength criterion or/and under the durability criterion. It could be concluded that a High-strength Concrete (HSC) is always a High-performance Concrete (HPC) but a HPC is not always HSC.

2.1.2. Confinement Model for High-Strength Concrete

In spite of many advantages to offer, high-strength concrete has a major drawback for seismic applications (Razvi[5]). Higher strength concretes are significantly more brittle than concretes within the normal-strength range. Therefore, concrete confinement becomes even more critical for high-strength concrete columns.

Confinement models developed for normal-strength concrete may not be applicable to high-strength concrete. In fact, these models were shown to overestimate ductility when applied to high-strength concrete (Razvi[5]). Presently, most of the models proposed for high-strength concrete are modified versions of models developed for normal-strength concrete. The modifications were usually introduced on the basis of limited test data, often restricting them to data used for the modifications. Hence, these models were often modified more than once as additional test data became available. The review of existing confinement models conducted by Razvi[5] indicates that there is a need for an analytical model that is relatively simple to use and general enough to cover normal-strength and

high-strength materials, as well as the cross-sectional shapes and reinforcement arrangements used in practice.

Confined models developed for normal-strength concrete may not be applicable to high-strength concrete (Razvi[5], Razvi Saatcioglu[6]). Presently most of the models proposed for high-strength concrete are modified versions of models developed for normal-strength concrete. The modifications were usually introduced on the basis of limited data, often restricting them to data used for the modifications. Hence, these models were often modified more than once as additional test data became available. The review of existing confinement model conducted by Razvi[5] indicates that there is a need for an analytical model that is relatively simple to used and general enough to cover normal-strength and high-strength materials, as well as the cross-sectional shapes and reinforcement arrangements used in practice.

2.1.1.1. Confined Concrete Strength

Confinement model proposed by Razvi Saatcioglu[6] is based on the computation of equivalent uniform pressure that gives the same effect as the non-uniform confinement pressures as shown in Figure 2.1. Accordingly, the strength of confined concrete can be written as shown below, where f_{le} is the equivalent uniform lateral pressure.

Universitas Indonesia
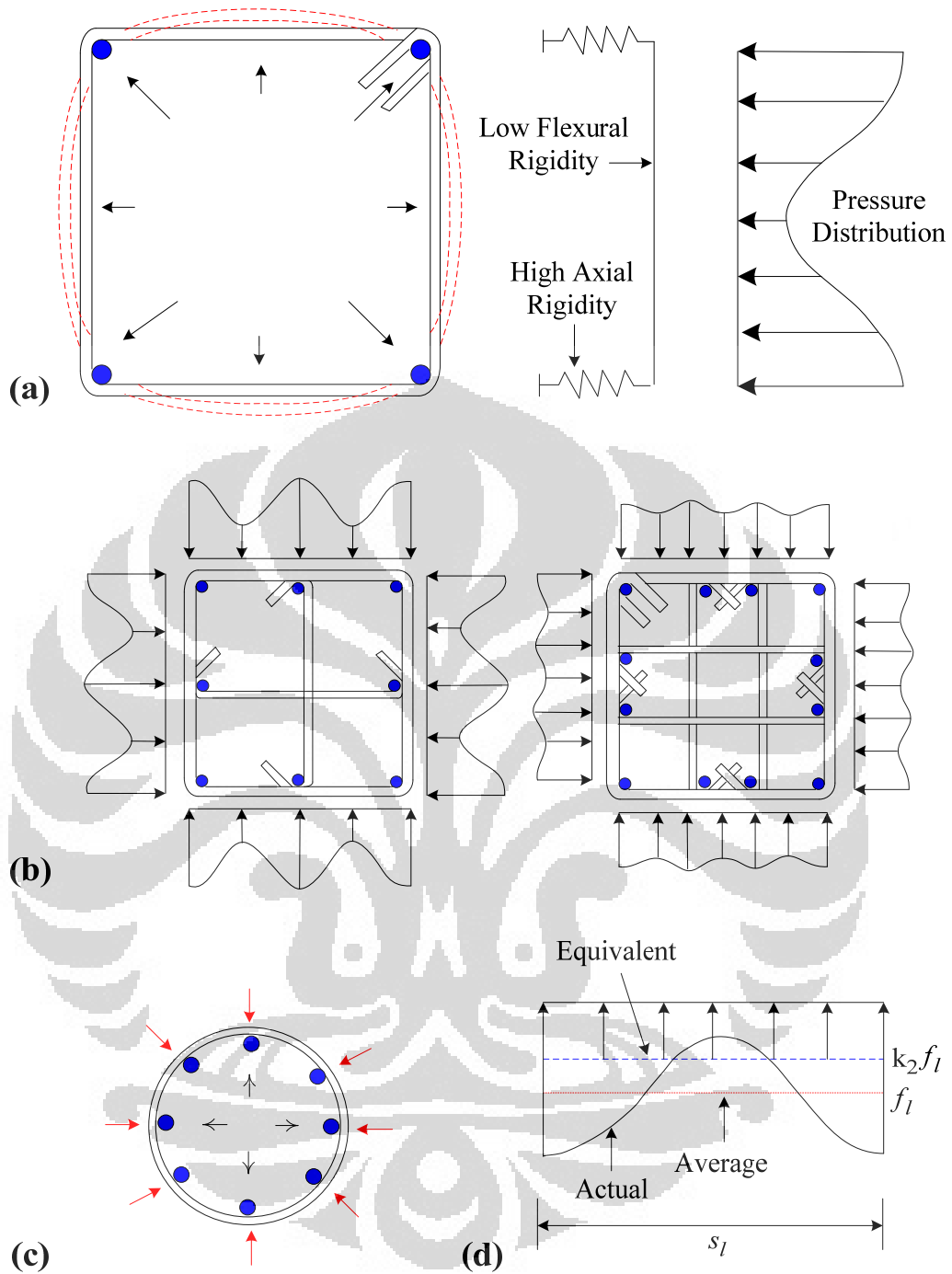
Figure 2.1 Passive Confinement Pressure

(a) Development of Passive Confinement Pressure in Square Column; (b) Variation of

Confinement Pressure with Reinforcement Arrangement; (c) Uniform Lateral Pressure in Circular

Columns; (d) Equivalent Uniform Pressure in Square Column (Razvi Saatcioglu[6])

$$f'_{cc} = f'_{co} + k_1 f_{le} \qquad (2.1)$$

$$k_1 = 6.7(f_{le})^{-0.17} \tag{2.2}$$

$$f_{le} = k_2 f_1 \tag{2.3}$$

$$f_1 = \frac{\sum_{i=1}^{q}(A_s f_s \sin\alpha)_i}{s b_c} \tag{2.4}$$

Where:

q = number of ties legs that cross the side of core concrete;

f_1 = average lateral pressure (Where f_1 is in megapascals);

f_{le} = equivalent uniform pressure (in MPa), it is computed by dividing the perpendicular components of tensile forces in transverse reinforcement acting on each side of concrete core by the core surface area, defined as $s b_c$ and reducing it by k_2;

f_s = tensile stress in transverse reinforcement at peak concrete stress

$$f_s = E_s \left(0.0025 + 0.04 \sqrt[3]{\frac{k_2 \rho_c}{f'_{co}}} \right) \le f_{yt} \tag{2.5}$$

Where f'_{co} is in megapascals. The upper limit for yield strength f_{yt} may be taken as 1,400 MPa, as this was maximum yield strength considered in the experimental data evaluated.

The equivalent uniform lateral pressure f_{le} used in Equation (2.2) is often smaller than the average uniform pressure f_1, because of non-uniformity of lateral pressure. The reduction in pressure is reflected through coefficient k_2, which is a function of tie spacing s and the spacing of laterally supported longitudinal reinforcement s_l. This coefficient reflects the efficiency of reinforcement arrangement and is equal to unity when the confinement pressure is near-uniform as in the case of closely spaced circular spirals, indicating highest efficiency. The

formulation (2.4) is applicable to circular and square sections having the same confinement pressure in two orthogonal directions.

$$k_2 = 0.15 \sqrt{\left(\frac{b_c}{s}\right)\left(\frac{b_c}{s_l}\right)} \leq 1.0 \qquad (2.6)$$

A proposed model by Razvi and Saatcioglu is shown in Figure 2.2. This model were used to compute the strength of 40 confined high-strength concrete columns, as well as 124 additional high-strength concrete columns tested by six other group researchers. The columns were either circular or square in section. The concrete strength ranged approximately between 50 and 130 MPa, and the steel yield strength ranged from 400 to 1,400 MPa.
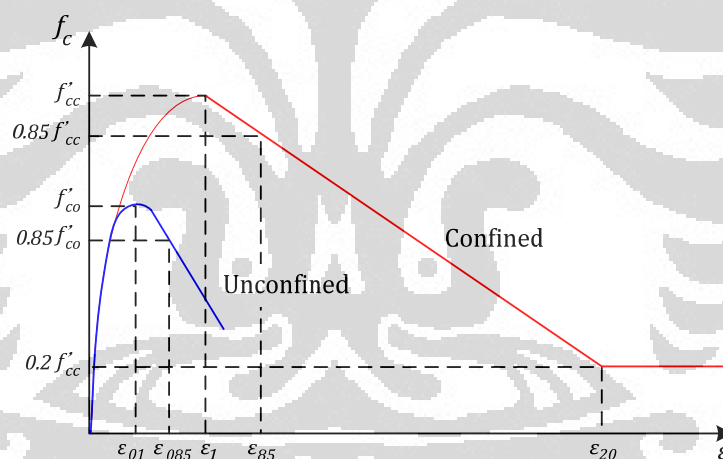
Figure 2.2 Proposed Confinement Model (Razvi Saatcioglu[6])

2.1.1.2. Ductility of Confined Concrete and Descending Branch

Defining the strain at peak concrete stress ε_1 and the descending branch of the stress-strain relationship could be the model of confined concrete ductility. The descending branch adopted in the model is the same as that proposed by Saatcioglu and Razvi[7]. In their original model developed for normal-strength concrete and consists of a linear segment originating from the peak. The slope of

this segment is defined by the strain corresponding to 85% of the peak stress ε_{85}. The expression proposed earlier for normal-strength concrete were modified to introduce the effects of increased concrete and steel strength through coefficient k_3 and k_4, respectively. The new expressions, which are applicable to both normal-strength and high strength concretes, are given below.

$$\varepsilon_1 = \varepsilon_{01}(1 + 5k_3K) \qquad (2.7)$$

$$\varepsilon_{85} = 260k_3\rho_c\varepsilon_1[1 + 0.5k_2(k_4 - 1) + \varepsilon_{085}] \qquad (2.8)$$

Where:

$$k_3 = \frac{40}{f'_{co}} \leq 1.0 \qquad (2.9)$$

$$k_4 = \frac{f_{yt}}{500} \geq 1.0 \qquad (2.10)$$

$$K = \frac{k_1 f_{le}}{f'_{co}} \qquad (2.11)$$

$$\rho_c = \frac{\sum_{i=1}^{n}(A_{sx})_i + \sum_{i=1}^{m}(A_{sy})_i}{[s(b_{cx} + b_{cy})]} \qquad (2.12)$$

Numbers of tie legs in x- and y-directions are n and m, respectively. It should be noted that the stress in transverse steel is assumed to reach the yield strength in defining ε_{85} on the descending branch. Unconfined, in-place concrete properties (ε_{01} and ε_{085}) are often determined through tests. If experimental value is available, they should not exceed the value specified in Equation (2.13) and (2.14) for modeling purposes. In the absence of experimental data, however, the values obtained by the same two equations, given below, may be used

$$\varepsilon_{01} = 0.0028 - 0.0008k_3 \qquad (2.13)$$

$$\varepsilon_{085} = \varepsilon_{01} + 0.0018k_3{}^2 \qquad (2.14)$$

Equation (2.12) was obtained from test data that included columns with lateral reinforcement ratio, ρ_c, less than $0.03 - 0.01k_3$. Therefore, this may be used as an upper limit for the applicability of Equation (2.12).

2.1.1.3. Ascending Branch

Modified version of Hognestad's curve was used as the ascending branch of the stress-strain relationship, proposed by Saatcioglu and Razvi[7] for normal-strength concrete. It was confirmed experimentally that the applicability of this curve was limited to normal-strength concrete. The relationship overestimated the initial modulus of elasticity when applied to high-strength concrete. For high-strength concrete, was adopted for the ascending branch of the proposed model. The mathematical expression for the curve is given below

$$f_c = \frac{f'_{cc}\left(\frac{\varepsilon_c}{\varepsilon_1}\right)r}{r - 1 + \left(\frac{\varepsilon_c}{\varepsilon_1}\right)^r} \qquad (2.15)$$

$$r = \frac{E_c}{E_c - E_{sec}} \qquad (2.16)$$

Where E_{sec} = secant modulus of elasticity of confined concrete and can be calculated from:

$$E_{sec} = \frac{f'_{cc}}{\varepsilon_1} \qquad (2.17)$$

Where E_c = modulus of elasticity of unconfined concrete.

Saatcioglu and Razvi used proposed equation by Carrasquillo et.al[8] as shown in Equation (2.18) below.

$$E_c = 3,320\sqrt{f'_c} + 6,900 \qquad (2.18)$$

Where f'_c is in megapascals. However E_c should be greater than E_{sec}.

Bechtoula et. al.[9] found that the equation (2.18) gives good estimation of the Modulus of elasticity for a concrete having a compressive strength of 80 MPa, however beyond the results are overestimated. The equation proposed by Nemati et. al.[10] will be used in this research.

2.1.1.4. Modulus of Elasticity of High-Strength Concrete

Nemati et. al.[10] stated that modulus of elasticity of concrete is a key factor for estimating the deformation of structural elements. New equation of Modulus of Elasticity which can be applied for concrete with compressive strength more than 36 MPa given as below:

$$E = k \cdot 1486\sigma_B{}^{1/3}\gamma^{1/2} = k_1 k_2 \cdot 1486\sigma_B{}^{1/3}\gamma^{1/2} \qquad (2.19)$$

The value of k_1 and k_2 are the correction factor corresponding to coarse aggregates and mineral admixtures respectively. Table 2.1 and Table 2.2 show Practical Correction Factor for each.

Table 2.1 Practical Correction Factor k_1 (Nemati et. al.[10])

k_1	Lithological Type of Coarse Aggregate
1.20	Crushed Limestone, Calcined Bauxite
0.95	Crushed Quartzitic Aggregate, Crushed Andesite, Crushed Basalt, Crushed Clayslate, Crushed Cobble Stone
1.00	Coarse Aggregate, other than the above

Table 2.2 Practical Correction Factor k_2 (Nemati et. al.[10])

k_2	Type of Addition
0.95	Silica Fume, Ground Granulated-furnace Slag, Fly Ash Fume
1.10	Fly Ash
1.00	Addition other than the above

Equation (2.19) was derived as an equation for modulus of elasticity. Conventional equations that can be obtained simply by substituting standard values of compressive strength and unit weight in equation, have been convenient in such a way in order to obtain the modulus of elasticity. Nemati et. al.[10] proposed Equation (2.20) as the equation to be used for modulus of elasticity calculations. This equation is based on 60 MPa, a typical compressive strength of high-strength concrete, and uses a unit weight of $2.4\,\text{t/m}^3$, which leads to the compressive strength of 60 MPa. σ_B is concrete compressive strength in MPa.

$$E = k_1 k_2 \cdot 3.35 \times 10^4 (\gamma/2.4)^2 (\sigma_B/60)^{1/3} \qquad (2.20)$$

2.2. PREVIOUS RESEARCH

2.2.1. Makoto Maruta

Maruta[12] tested 14 specimens with 1/4.5 of scale. Table 2.3 shows the list of specimens. All specimens were designed for shear failure prior to flexural failure. The shear span ratio (M/QD hereafter) was fixed at 1.0. The main longitudinal reinforcement comprised 13 mm deformed bar with a high yield strength of 785 MPa. Figure 2.3 and Figure 2.4 show the shape, size and section of the columns.

The parameters of this test were hoop configuration (square or rectangular (sub-tie) combination, square hoop-circular spiral hoop combination), hoop ratio $P_w\,(0.3, 0.6, 1.2, 1.8\,\%)$, axial force ratio (0.15, 0.3, 0.6), and the combination of strength and hoop diameter. In order to determine a column's shear capacities under high axial load, 8 specimens subjected to a high axial load ratio of 0.6. The target concrete strength was 130 MPa.

Table 2.3 List of Specimens (Maruta[12])

Specimen	Hoop Configuration	Axial Force Ratio	Hoop			σ_B (MPa)
			P_w (%)	σ_{xv} (MPa)	$P_w.\sigma_{xv}$ (MPa)	
H-0.6-0.15	S+N (HN)	0.15	0.6	D6 785	4.7	128
H-0.6-0.3		0.3				125
H-0.6-0.6		0.6				120
HS-0.6-0.3	S+C (HS)	0.3				128
HS-0.6-0.6						128
HS-1.2-0.6			1.2	D6 785	9.4	129
H-0.3-0.6	S+N (HN)	0.6	0.3		2.4	128
H-1.2-0.6			1.2		9.4	121
H-1.8-0.6			1.8		14.1	130
H-0.3-0.3		0.3	0.3		2.4	130
H-1.2-0.3			1.2		9.4	121
H-1.8-0.3			1.8		14.1	121
U-0.4-0.6	S+C (U)	0.6	0.37	φ 5.1 1275	4.7	130
U-0.7-0.6			0.74		9.4	129

Figure 2.3 Shape and size of Makoto Maruta column specimen (Maruta[12])
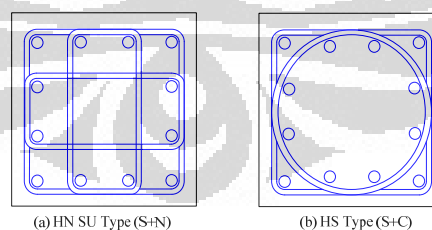
Figure 2.4 Section of Makoto Maruta column specimen (Maruta[12])

All of the specimens were ensured that no yielding of longitudinal bar before maximum strength, except for specimen H-1.8-0.6. Hence, the maximum strength is shear strength. Shear cracking strength of a column $_cQ_{sc}$ was calculated by Equation (2.21). These calculations are based on the principle stress method.

$$_cQ_{SC} = bD\sqrt{\sigma_T^2 + \sigma_T\sigma_0}/\kappa \ (kN) \qquad (2.21)$$

b = Width of section ;

D = Depth of section ;

σ_T = Tensile strength of concrete = $0.313\sqrt{\sigma_B}$ (MPa);

σ_0 = Axial compressive stress ;

κ = Shape factor of section

From the results shown in Table 2.3 and 2.4, the restoring responses of the specimens differ depending on hoop ratio and axial load. The maximum rotation angle increases as hoop ratio increases and axial load ratio decreases.

Table 2.4 List of Makoto Maruta test results (Maruta[12])

Specimen	Test Result (kN)		Calculated Value (kN)		
	$_RQ_{SCR}$[1]	Q_{SMAX}[2]	$_cQ_{SC}$[3]	$Q_{S\text{-}AIJ}$[4] $R_p = 0$	$_cQ_{SC}$[3]
H-0.6-0.15	270	522	244 (1.08)	439 (1.19)	455 (1.15)
H-0.6-0.3	367	516	330 (1.07)	439 (1.18)	475 (1.09)
H-0.6-0.6	466	523	452 (0.98)	439 (1.19)	641 (0.82)
HS-0.6-0.3	400	494	332 (1.17)	439 (1.13)	475 (1.04)
HS-0.6-0.6	445	508	460(0.91)	4.39 (1.16)	641 (0.79)
HS-1.2-0.6	533	588	461 (1.13)	604 (0.97)	802 (0.73)
H-0.3-0.6	431	485	460 (0.91)	312 (1.51)	561 (0.86)
H-1.2-0.6	555	681	453 (1.17)	604 (1.13)	802 (0.85)
H-1.8-0.6	588	778	4.62 (1.24)	664 (1.17)	962 (0.81)
H-0.3-0.3	394	524	334 (1.16)	321 (1.63)	409 (1.28)
H-1.2-0.3	354	689	327 (1.29)	604 (1.14)	607 (1.13)
H-1.8-0.3	439	798	327 (1.29)	664 (1.20)	739 (1.08)
U-0.4-0.6	478	508	462 (1.01)	408 (1.25)	605 (0.84)
U-0.7-0.6	506	561	461 (1.07)	578 (0.97)	728 (0.77)

1) Shear Cracking Strength 2) Maximum Strength 3) Shear Cracking Strength by Eq 2.1
4) Shear Strength by AIJ 5) Shear Strength by New RC ( ): Test Result/Calculated Value

The tests showed that higher hoop reinforcement ensures high maximum strength.

Axial force does not influence the maximum shear strength but the ductility does.

Comparison among the 30% axial force ratio specimen shows that the strain of the

$P_w = 0.6$ specimen at the same rotation angle is the largest. Many specimens did

not reach their hoop yield strength, therefore concrete crushing occurred prior to hoop yield. The maximum strengths of the same P_w specimens are nearly the same even for different axial force ratios.

From this study, could be concluded that the experimental shear strength is influenced mainly by P_w, not axial load ratio. In the next part, AIJ and New RC calculation methods will be discussed which show rough agreement with this test results. However the New RC shows underestimation for some specimens. The AIJ calculation method has a higher safety margin than the New RC calculation method.

2.3. MULTI-SPIRAL CONFINEMENT IN RECTANGULAR COLUMNS

As mentioned before, building with construction automation technologies and precast components is one of the solutions to answer the economical and high quality construction problem nowadays. Instead of conventional stirrups, the continuous spirals that are formed mechanically can reduce the labor demand, enhanced the quality and efficiency of stirrups is a widely used alternative for column with circular cross-section (Yin et.al[13]).

Current codes specify the requirements for rectangular RC columns which typically have rectangular perimeter hoops and cross ties configuration. The detail requirements that was designed to ensure the structural member to provide sufficient ductility brings the assembly of re-bars cages into a complicated, time-consuming, and expensive operation.

On the other hand, the effectiveness of circular spiral confinement steel are able to present better ductility capacity because they tend to transfer the dilatation

deformation of concrete into axial elongation of spiral (Yin et.al[13]). In general, demand of confinement steel for spiral reinforcement columns could be 30% less than the tie reinforcement.

Because of superfluous unconfined area at the four corners of the rectangular cross section, application of spiral cages in rectangular columns is not normal. Yin et.al[13] designed the combination of central spiral and four corner spirals to extend the area of confined concrete core to solve this problem.

Yin et.al performed two phases of test to evaluate a large number of concrete columns of large number of concrete columns specimens in axial compression and lateral cyclic loading. Axial compression tests for columns with various confinement details were evaluated in Phase I. Detailed axial compression test and lateral cyclic loading tests were carried out in the Phase II study.

2.3.1. Phase I Study

Ten confinement designs, including four rectilinear configurations and six different multi-spiral configurations were evaluated in a series of axial compression tests in the first phase of test. All specimens are 600 mm square and 1200 mm in height. The compressive strength concrete in 28 days is 35 MPa. The tensile strength of both transverse and longitudinal re-bars is 280 MPa. Volumetric ratio of the transverse steel for all specimens is set close to 2.0%, as mentioned in ACI-318[14] building codes. The detail layouts of ten specimens could be seen in Figure 2.5 below.

(a)	(b)	(c)	(d)	(e)
Conventional	One-bar	Wire-mesh	3 Welded Hoops	Twin-Hexagon Confinement

(f)	(g)	(h)	(i)	(j)
Twin-ellipse	4 Spirals	5 Spirals	Spiral + Cross Ties	Spiral + 4 tie ears
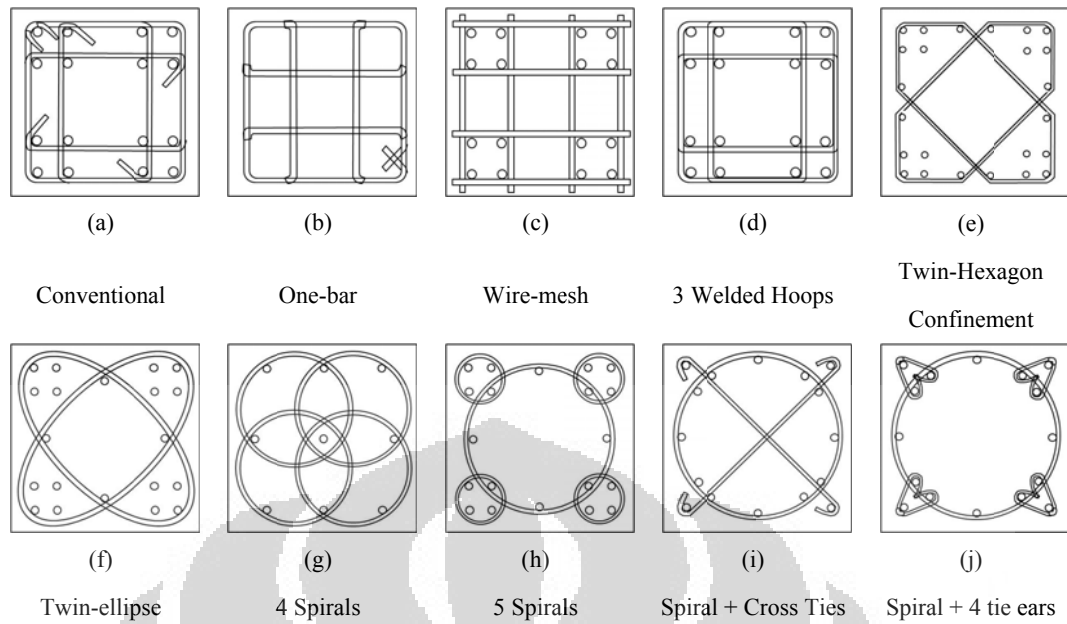
Figure 2.5 Confinement detail of the Phase I test (Yin et.al[13])

The experimental results of Phase I tests are listed below.

Table 2.5 Result of Phase I Tests (Yin et.al[13])
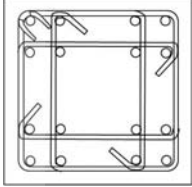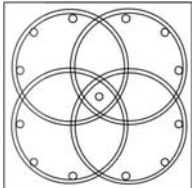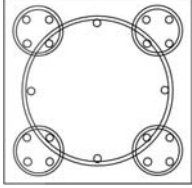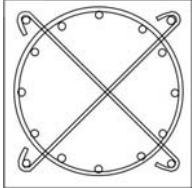
No.	Confinement	Strength (MPa)			Strain Energy (MPa)	
		f'_c	f'_{cc}	f'_{cc}/f'_c	E_{80}	$E_{80}/E_{80(a)}$
1	35.6	54.2	1.52	0.19	1.00	35.6
2	35.6	42.1	1.18	0.14	0.74	35.6
3	35.6	37.0	1.04	0.05	0.28	35.6
4	35.6	41.4	1.17	0.11	0.57	35.6
5	43.0	64.9	1.51	0.66	3.44	43.0
6	43.0	53.5	1.25	0.40	2.07	43.0
7	43.0	59.2	1.38	1.04	5.44	43.0
8	37.6	57.7	1.53	1.21	6.34	37.6
9	37.6	63.2	1.68	0.80	4.15	37.6
10	37.6	50.6	1.34	0.55	2.86	37.6

As shown in Table 2.5 above, the most of the test specimens with spiral

confinements exhibit higher compressive strength and energy capacity (see specimen (g), (h) and (i)). In the next phase of study, three configurations will be selected.

2.3.2. Phase II Study

Table 2.6 Design Detailst of Phase II Axial Compression Tests (Yin et.al[13])

Specimen	Concrete f'_c (MPa)	Confinement Reinforcement Spacing (mm)		Size (mm)	f_{yt} (MPa)	ρ_d (%)	ρ_{req} (%)	Shape
T1	34.4	85		13	274.7(SD280)	2.20	2.26	
T2	68.7	65		12	412.0(SD420)	2.55	3.01	
4S1	34.4	75		13	274.7(SD280)	2.0	1.63	
4S2	68.7	50		12	412.0(SD420)	2.6	2.17	
4S3	34.4	50		16	274.7(SD280)	4.5	1.63	
4S4	34.4	65		16	274.7(SD280)	3.5	1.63	
4S5	34.4	100		13	274.7(SD280)	1.47	1.63	
5S1	34.4	50		13	274.7(SD280)	2.56	1.64	
5S2	68.7	75		12	274.7(SD280)	1.56	2.19	
5S3	34.4	70		16	274.7(SD280)	2.2	1.64	
		70		13	274.7(SD280)		1.64	
5S4	34.4	60		13	274.7(SD280)	2.2	1.64	
5S5	34.4	50		10	274.7(SD280)	1.44	/	
ST1	34.4	spiral	60	13	274.7(SD280)	1.58	/	
		ties	60	10	274.7(SD280)			
ST2	68.7	spiral	95	16	412.0(SD420)	2.06	/	
		ties	95	16	412.0(SD420)			
ST3	34.4	spiral	75	16	274.7(SD280)	2.06	/	
		ties	75	13	274.7(SD280)			
ST4	34.4	spiral	45	16	274.7(SD280)	2.75	/	
		ties	45	10	274.7(SD280)			
ST5	34.4	spiral	55	16	274.7(SD280)	2.2	/	
		ties	55	10	274.7(SD280)			
ST6	34.4	spiral	80	16	274.7(SD280)	1.54	/	
		ties	80	10	274.7(SD280)			

Detailed axial compression test and lateral cyclic loading tests were carried out for four confinement designs that include one conventional stirrup design, combination of four spirals and five spirals designs, and a spiral with cross ties. Detail of the design could be seen in Table 2.6 in the previous page. The volumetric ratio of the confinement reinforcement to the gross area of concrete section (ρ_d) is related to the required volumetric ratio (ρ_{req}). For f'_c equals to 34.4 MPa and 68.7 MPa, the required volumetric ratios respectively are 2.26% and 3.01%.

Test results of the axial compression tests show that the behavior of confined concrete can be improved with closer spiral spacing and higher volumetric ratios of confinement steel. Also, it shows that the multi-spiral confinement design behave much better than the traditional stirrups for rectangular columns.

Cyclic loading test was done for three column specimens, such as: a traditional stirrup design as benchmark (T), two multi-spiral designs (4S and 5S) with 3000 mm height and square 600 mm × 600 mm cross section. Constant axial force of 126 tons is applied at the top of the specimens by a 200 ton jack. Detail of the design could be seen below.

Table 2.7 Design Detailst of Phase II Cyclic Loading Tests (Yin et.al[13])

Specimens	f'_c (MPa)	Longitudinal Bars	Confinement Reinforcement		
			Size (mm)	Grade	Spacing
T	34.4		13	SD280	85
S4	34.4	SD42 16-#8	13	SD280	75
S5	34.4		13	SD280	60

Specimen S5 exhibits the best strength and ductility capacity among the three columns (as shown in Figure 2.6). Response of S4 column is close to S5, and the T specimen displayed the lowest strength and ductility capacity as is expected

(Yin et.al[13]).
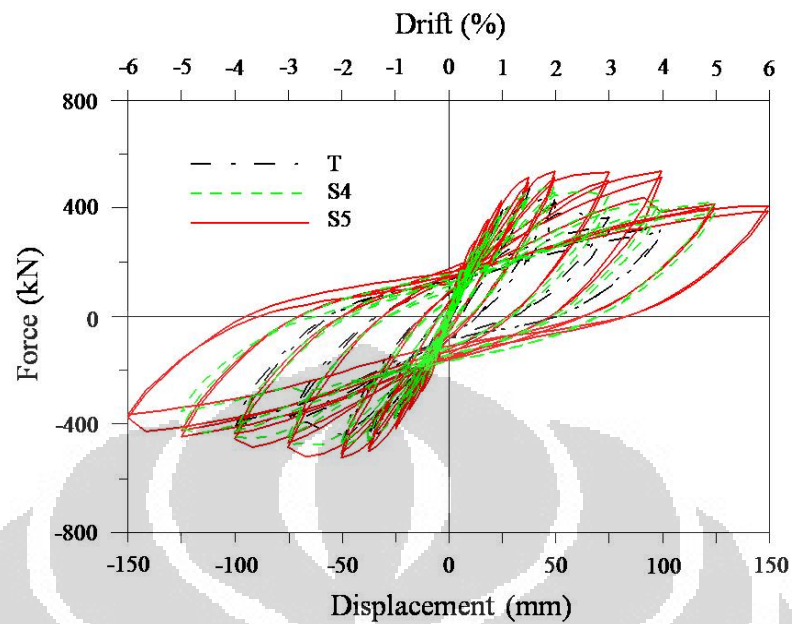
Figure 2.6 Force-Displacement Relations Phase II Cyclic Loading Test Result (Yin et.al[13])

2.3.3. Multi-Spiral Confinement

As mentioned before, S5 designs have the best confinement effectiveness among others given the same amount of confinement reinforcement and also the most effective layout in terms of automatic assembly.
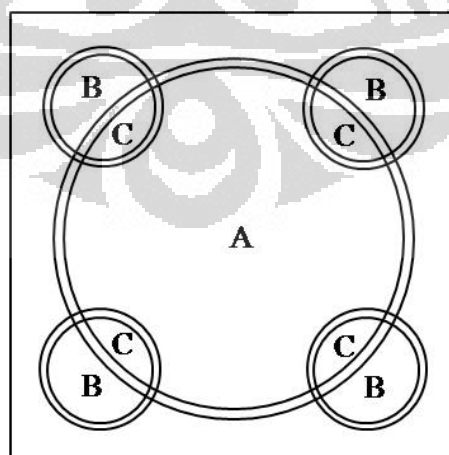
Figure 2.7 Confinement detail of the Phase I test (Yin et.al[13])

Multi-spiral confinement type S5 cold be divided into three regions A, B and C as

shown in Figure 2.6 above, where Region A and B are the large central circle and the small corner circle, respectively, and Region C is their overlapped area. The respective volumetric ratio is defined as follow.

$$\rho_{sA} = \frac{V_{sA}}{S_A \times A_A}, \qquad \rho_{sB} = \frac{V_{sB}}{S_B \times A_B}, \qquad \rho_{sA} = \frac{V_{sC}}{S_C \times A_C}, \quad (2.22)$$

Where:

ρ_{si} =   Volumetric ratios of confinement steel in region i;

V_{si} =   Volume of confinement steel in region i;

S_i =   Spacing of spirals in region i;

A_i =   Confined area in region i

The experimental stress-strain response can be estimated accurately through rational separations of the concrete core. The influence of the large circle on the core area is more significant than that of the small circles.

2.4. EQUIVALENT RECTANGULAR STRESS-BLOCK (ACI ITG-4.3R-07)

ACI ITG-4.3R-07[31] (Report on Structural Design and Detailing for High-Strength Concrete in Moderate to High Seismic Applications) presents a literature review on seismic design using high-strength concrete. As mentioned in the report that ACI 318, "Building Code Requirement for Structural Concrete," governs for the design and construction of buildings and is applicable for designs using high-strength concrete in moderate to high seismic applications. ITG 4.3R-07 does not supersede ACI 318. User of ITG 4.3R-07 should not infer that the recommendations it contains are future ACI 318 Code requirements. There are a

series of recommended modifications to ACI 318-05. The recommendations for the modification of the equivalent rectangular stress block will be discussed in this part.

$\frac{1}{2}\beta_1 = k_2$

$\alpha_1\beta_1 = k_1k_3$

a) Strain Distribution b) 2nd order Parabolic Stress Distribution and Equivalent Force c) ACI Rectangular Stress Block and Equivalent Force
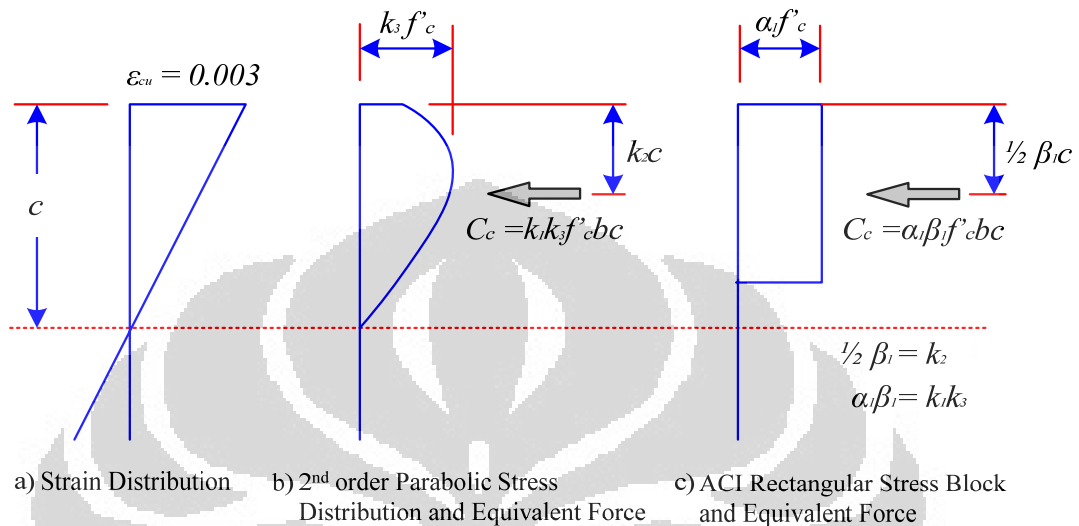
Figure 2.8 Parameters equivalent rectangular stress block (ACI ITG-4.3R-07[31])

For some elements with high axial load demands, such as lower-story columns in tall buildings, lower story columns in narrow moment-resisting frame, and columns supporting the ends of discontinuous walls, the shape of the stress block may have a significant effect on the estimated strength.

The accuracy of the stress block is of concern in earthquake-resistant design because overestimating the flexural strength of column leads to overestimating the ratio of column-to-beam moment strength, which increases the probability of hinging in the columns due to the development of a strong beam-weak column mechanism.

Even though the stress-strain characteristics of high-strength concrete are different from those of normal-strength concrete, there is no well-defined compressive strength boundary between two; there is instead a gradual change with the

increasing concrete strength. The ascending branch of the stress-strain relationship is steeper of HSC, indicating higher elastic modulus. Failure becomes more sudden and brittle as the concrete strength increases.
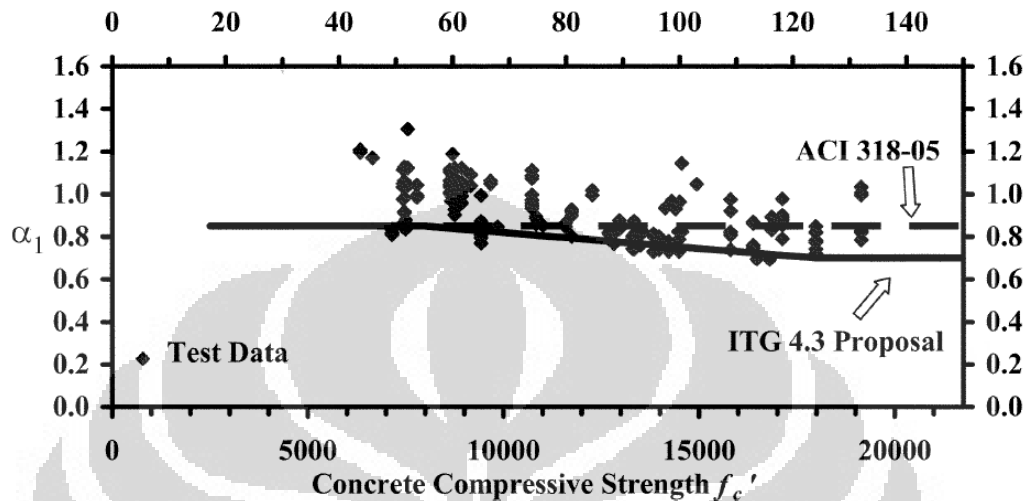
Figure 2.9 Observed Stress intensity factor for concentrically loaded columns
(ACI ITG-4.3R-07[31])

Figure 2.9 provides a comparison of the aforementioned recommendations with experimental data and the nominal strength calculated using the provisions in ACI 318-05. The proposed parameters α_1, β_1, and χ_1 were selected based on what was deemed an acceptable level of conservatism in the judgment of the committee. Another factor considered by the committee in selecting the aforementioned parameters was that there is no experimental evidence to suggest that the parameters in ACI 318-05 result in non conservative estimates of strength for columns with normal-strength concrete. For this reason, the stress block parameters proposed by the committee were selected so that there would be no change in the stress block parameters of ACI 318-05 for columns with normal-strength concrete.

The following changes are proposed to the rectangular stress in ACI 318-05.

α_1 $\equiv$ Factor relating magnitude of uniform stress in the equivalent

rectangular compressive stress block to specified compressive strength of concrete.

For $17 \leq f'_c \leq 55$ MPa, α_1 shall be taken as 0.85. For $f'_c \geq 55$ MPa, α_1 shall be reduced linearly at a rate of 0.015 for each 7 MPa of strength in excess of 55 MPa, but α_1 shall not be taken less than 0.70.

β_1 =   Factor relating depth of equivalent rectangular compressive stress block to neutral axis depth.

For $17 \leq f'_c \leq 28$ MPa, β_1 shall be taken as 0.85. For 28 MPa $\leq f'_c$, β_1 shall be reduced linearly at a rate of 0.05 for each 7 MPa of strength in excess of 28 MPa, but β_1 shall not be taken less than 0.65.

χ_1 $\equiv$ Factor relating mean concrete compressive stress at axial load failure of concentrically loaded columns to specified compressive strength of concrete.

For $17 \leq f'_c \leq 55$ MPa, χ_1 shall be taken as 0.85. For 55 MPa $\leq f'_c$, χ_1 shall be reduced linearly at a rate of 0.015 for each 7 MPa of strength in excess of 55 MPa, but χ_1 shall not be taken less than 0.70.

2.5. LITERATURE REVIEW

Several shear strength models will be applied to predict the shear strength of all specimens. Although each model has its own parameter and approximation, generally, shear strength of column could be computed as the summation of strength contribution from concrete and transverse reinforcement.

Several shear models that would be examined were proposed by several researcher such as Priestley et.al., Aschheim & Moehle, Sezen, Kowalsky, Xiao &

Martirossyan and also shear models from codes, provision and also Guidelines (ACI 318, ASCE-ACI 426, AIJ 1990, AIJ 1999, New RC equation, AASHTO LRFD, Caltrans). Each of them has their own database, consideration and engineering judgment related to the equation.

2.3.1. ACI 318-08

The ACI 318-08[14] adopts the 45° truss model with an additional term for concrete contribution.

$$V_n = V_c + V_s \qquad (2.23)$$

Where:

V_n = Nominal shear strength ;

V_c = Nominal shear strength provided by concrete ;

V_s = Nominal shear strength provided by shear reinforcement

$$V_c = 0.166 \left(1 + \frac{N_u}{13.8 A_g} \right) \sqrt{f'_c}\, b_w d \qquad (2.24)$$

V_c can be calculated using the more detailed calculation as follow:

$$V_c = \left(0.16 \sqrt{f'_c} + 17 \rho_w \frac{V_u d}{M_m} \right) b_w d \qquad (2.25)$$

Where:

$$M_m = M_u - N_u \frac{(4h - d)}{8} \qquad (2.26)$$

V_c should not be taken greater than following equation

$$V_c = 0.29 \sqrt{f'_c}\, b_w d \sqrt{1 + \frac{0.29 N_u}{A_g}} \qquad (2.27)$$

f'_c = Concrete compressive strength ;

b_w = Effective web width ;

d = Effective depth ;

h = Height of the section area ;

N_u = The factored axial compression load (positive in compression) ;

A_g = The gross area of the concrete cross-section ;

ρ_w = Longitudinal reinforcement ratio ;

V_u = Factored shear due to the total factored loads ;

M_u = Factored moment due to the total factored loads

For the stirrup contribution to shear, the conservative 45° truss solution is used:

$$V_s = \frac{A_v f_y d}{s} \qquad (2.28)$$

Where

A_v = Cross-sectional area of shear reinforcement ;

f_y = Yield stress of shear reinforcement ;

d = Effective depth ;

s = Spacing of shear reinforcement

2.3.2. American Code ASCE-ACI 426 Shear Strength Approach (1973)

The ASCE-ACI Joint Committee 426 published a report on the shear strength of reinforced concrete members in 1973. For the calculation of shear strength, the ACI 426R-74[15] proposed an approach that similar to the one provided in the ACI 318-08[14]. The shear strength is provided by both concrete and the shear reinforcement.

$$V_n = V_c + V_s \qquad (2.29)$$

Where:

V_n = Nominal shear strength ;

V_c = Nominal shear strength provided by concrete ;

V_s = Nominal shear strength provided by shear reinforcement

$$V_c = (0.066 + 10\rho_t)\left(1 + \frac{3N_u}{f'_c A_g}\right)\sqrt{f'_c}\, b_w d \qquad (2.30)$$

V_c should not be taken greater than following equation.

$$V_c = 0.2\left(1 + \frac{3N_u}{f'_c A_g}\right)\sqrt{f'_c}\, b_w d \qquad (2.31)$$

And

f'_c = Concrete compressive strength ;

ρ_t = Tension steel reinforcement ratio ;

b_w = Effective web width ;

d = Effective depth ;

N_u = The factored axial compression load (positive in compression) ;

A_g = The gross area of the concrete cross-section

The transverse reinforcement contribution is the same as given in ACI 318-08. For the stirrup contribution to shear, the conservative 45° truss solution is used:

$$V_s = \frac{A_v f_y d}{s} \qquad (2.32)$$

Where:

A_v = Cross-sectional area of shear reinforcement ;

f_y = Yield stress of shear reinforcement ;

d = Effective depth ;

s = Spacing of shear reinforcement

2.3.3. Japanese Equation

2.3.3.1. Architectural Institute of Japan (AIJ) 1990

AIJ 1990[16] Design Guidelines for Earthquake Resistant Reinforced Concrete Building Based on Ultimate Strength Concept stated that the equation to predict shear strength V_u of reinforced concrete members with rectangular cross section is given by

$$V_{u-AIJ\ 1990} = \rho_w f_{yt} b j_t \cot\phi + \tan\theta(1-\beta)\frac{bDvf'_c}{2} \qquad (2.33)$$

Where:

$$\rho_w = \frac{\pi N_w d_{bw}^2}{4b_e s} \qquad (2.34)$$

$$\cot\phi = \min\left(2 - 50R_p, \frac{j_t}{D\tan\theta}, \sqrt{\frac{vf'_c}{\rho_w f_{yt}} - 1}\right) \qquad (2.35)$$

$$v = (1.0 - 15R_p)v_0 \qquad (2.36)$$

$$\beta = \frac{(1 + \cot^2\phi)\rho_w f_{yt}}{vf'_c} \qquad (2.37)$$

v = effective concrete strength factor. Before yielding, it is a constant equal to the basic value v_0

$$v = v_0 = 0.7 - \frac{f'_c}{200} \qquad (2.38)$$

Effective concrete strength vf'_c from Equation (2.33) may not be applicable to high strength concrete, and the following equation by CEB was found to be applicable to high strength concrete up to 120 MPa in the various existing studies

$$v_0 = 1.7f'_c{}^{\left(-\frac{1}{3}\right)} \qquad (2.39)$$

$$tan\ \theta\ \ = \sqrt{\left(\frac{L}{D}\right)^2 + 1} - \frac{L}{D} \qquad (2.40)$$

Where:

b = Width of member ;

b_e = Effective width of member ;

d_{bw} = Diameter of shear reinforcement ;

D = Depth of member ;

j_t = Distance between top and bottom longitudinal bars ;

L = Clean span length ;

s = Spacing of shear reinforcement ;

N_w = Number of flexural bars ;

R_p = Hinge rotation angle ;

ϕ = Angle of concrete truss strut ;

θ = Angle of concrete arch strut ;

f'_c = Concrete compressive strength (MPa)

f_{yt} = Yield strength of transverse reinforcement (MPa)

Effect of axial load on the shear strength is not considered in the AIJ Guidelines. Shear strength degradation is related to the plastic hinge rotation through a reduction in the concrete contribution (AIJ 1990[16]). The concrete contribution is reduced as much as seventy-five percent at large displacement (through v in Figure 2.10). Similarly, the steel contribution is reduced as much as fifty percent at large displacements (through cot ϕ in Figure 2.10).
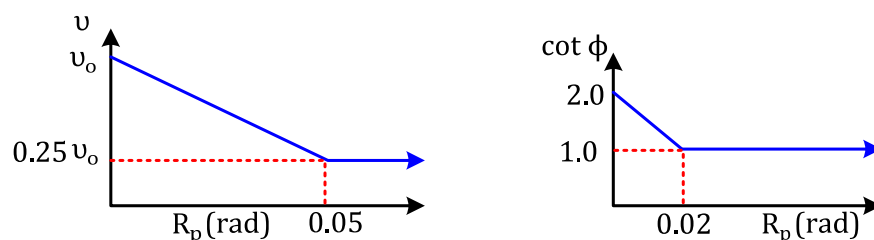
Figure 2.10 Relation between observed angles of the critical cracks and axial load

2.3.3.2. Architectural Institute of Japan (AIJ) 1999

Different with AIJ 1999[17] Design Guidelines, Design Guidelines for Earthquake Resistant Reinforced Concrete Buildings Based on Inelastic Displacement Concept published by the Architectural Institute of Japan (AIJ) in 1999 proposed shear strength prediction by using the minimum value of the following equations. The shear strength V_u is given by

$$V_u = min(V_{u1}, V_{u2}, V_{u3}) \tag{2.41}$$

$$V_{u1} = \rho_w f_{yt} b_e j_e cot\phi + \left(vf'_c - \frac{5\rho_w f_{yt}}{\lambda} \right) \frac{bD}{2} tan\,\theta \tag{2.42}$$

$$V_{u2} = \frac{\lambda v f'_c + \rho_w f_{yt}}{3} b_e j_e \tag{2.43}$$

$$V_{u3} = \frac{\lambda v f'_c}{2} b_e j_e \tag{2.44}$$

Where

$$\rho_w = \frac{\pi N_w d_{bw}^{\,2}}{4 b_e s} \tag{2.45}$$

$$cot\,\phi = 2 - 20 R_p \tag{2.46}$$

$$\lambda = 1 - \frac{s}{2 j_e} - \frac{b_s}{4 j_e} \tag{2.47}$$

$$v = \left(1.0 - 20 R_p \right) v_0 \tag{2.48}$$

Before yielding, it is a constant equal to the basic value v_0

$$v = v_0 = 0.7 - \frac{f'_c}{200} \tag{2.49}$$

Effective concrete strength vf'_c from Equation (2.42), (2.43) and (2.44) may not be applicable to high strength concrete, and the following equation by CEB was found to be applicable to high strength concrete up to 120 MPa in the various

existing studies

$$v_0 = 1.7f'_c{}^{\left(-\frac{1}{3}\right)} \tag{2.50}$$

$$\tan\theta = \sqrt{\left(\frac{L}{D}\right)^2 + 1} - \frac{L}{D} \tag{2.51}$$

Where:

b = Width of member ;

b_e = Effective width of member ;

d_{bw} = Diameter of shear reinforcement ;

D = Depth of member ;

j_t = Distance between top and bottom longitudinal bars ;

L = Clean span length ;

s = Spacing of shear reinforcement ;

N_w = Number of flexural bars ;

R_p = Hinge rotation angle ;

ϕ = Angle of concrete truss strut ;

θ = Angle of concrete arch strut ;

f'_c = Concrete compressive strength (MPa)

f_{yt} = Yield strength of transverse reinforcement (MPa)

v = Effective concrete strength factor ;

λ = Effective area factor for truss action ;

b_s = Largest distance between ties ;

j_e = Effective depth of member ;

Note that the effect of axial load on the shear strength is not considered in the AIJ Guidelines. Shear strength degradation is related to the plastic hinge rotation through a reduction in the concrete contribution (AIJ 1999[17]). The concrete contribution is reduced as much as seventy-five percent at large displacement (through v in Figure 2.11). Similarly, the steel contribution is reduced as much as fifty percent at large displacements (through $\cot\phi$ in Figure 2.9).

Universitas Indonesia
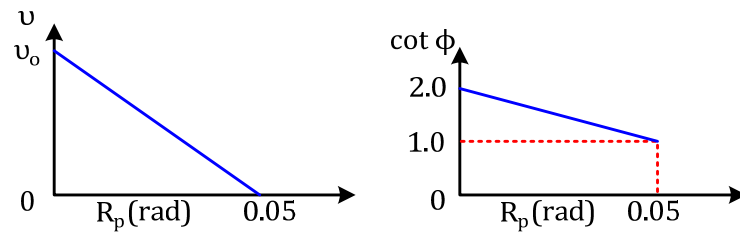
Figure 2.11 Relation between observed angles of the critical cracks and axial load

2.3.3.3. New RC (1993)

Maruta[12] mentioned that New RC report published by Japan Institute of Construction Engineering in 1993 proposed new shear strength equation that modified from AIJ 1990 Design Guidelines. The axial load ratio as parameter that affects the shear strength is mentioned in this equation. Also, limit of transverse reinforcement yield strength is mentioned since the stress of re-bar that has yield strength more than certain value cannot reach the yield stress.

The shear strength V_u is given by

$$V_{u-New\,RC} = \rho_w f_{yt} b j_t cot\phi + \alpha(1-\beta)bDvf'_c \qquad (2.52)$$

Where

$$\rho_w = \frac{\pi N_w d_{bw}^2}{4 b_e s} \qquad (2.53)$$

$$cot\,\phi = min\left(2.0 - 3n - 50R_p, \frac{j_t}{2\alpha D}, \sqrt{\frac{vf'_c}{\rho_w f_{yt}} - 1} \right) \qquad (2.54)$$

$$f_{yt} \leq 125\sqrt{v_0 f'_c} \qquad (2.55)$$

$$\alpha = \frac{\sqrt{\left(\frac{L}{D}\right)^2 + 1} - \frac{L}{D}}{2} \qquad (2.56)$$

$$\beta = \frac{(1 + cot^2\phi)\rho_w f_{yt}}{vf'_c} \qquad (2.57)$$

Universitas Indonesia

$$v = (1.0 - 15R_p)v_0 \qquad\qquad (2.58)$$

$$v_0 = 1.7(1 + 2n)f'_c{}^{\left(-\frac{1}{3}\right)} \qquad\qquad (2.59)$$

Where:

b = Width of member ;

b_e = Effective width of member ;

d_{bw} = Diameter of shear reinforcement ;

D = Depth of member ;

j_t = Distance between top and bottom longitudinal bars ;

L = Clean span length ;

s = Spacing of shear reinforcement ;

N_w = Number of flexural bars ;

R_p = Hinge rotation angle ;

ϕ = Angle of concrete truss strut ;

f'_c = Concrete compressive strength (MPa)

f_{yt} = Yield strength of transverse reinforcement (MPa)

v = Effective concrete strength factor ;

n = Axial load ratio

2.3.4. Caltrans

Sezen[18] mentioned that California Department of Transportation (Caltrans) proposed equation to evaluate the shear strength of the existing reinforced concrete columns. The equation proposed by Caltrans was developed for the evaluation of prismatic reinforced concrete members.

$$V_n = V_c + V_s \qquad\qquad (2.60)$$

Where:

V_n =   Nominal shear strength ;

V_c =   Nominal shear strength provided by concrete ;

V_s =   Nominal shear strength provided by shear reinforcement

$$V_c = (F_1)(F_2)\sqrt{f'_c}\left(0.8\,A_g\right) \text{ (psi)} \qquad (2.61)$$

V_c should not be taken greater than following equation.

$$V_c = 4\sqrt{f'_c}\left(0.8\,A_g\right) \text{ (psi)} \qquad (2.62)$$

And

$$0.3 \leq F_1 = \frac{\rho''\,f_{yh}}{150} + 3.67 - \mu \leq 3.0 \text{ (psi)} \qquad (2.63)$$

$$1.0 \leq F_2 = 0.0005\left(\frac{P}{A_g}\right) + 1 \leq 1.5 \text{ (psi)} \qquad (2.64)$$

Where

f'_c =   Concrete compressive strength ;

A_g =   The gross area of the concrete cross-section ;

P =   The factored axial compression load (positive in compression) ;

ρ'' =   Ratio of the transverse reinforcement volume to column core volume ;

f_{yh} =   Yield strength of transverse steel

For the stirrup contribution to shear, the conservative $45°$ truss solution is used:

$$V_s = \frac{A_v f_y d}{s} \qquad (2.65)$$

Where

A_v =   Cross-sectional area of shear reinforcement ;

f_y =   Yield stress of shear reinforcement ;

d =   Effective depth ;

s =   Spacing of shear reinforcement

2.3.5. AASHTO LRFD (2007)

The AASHTO LRFD 2007[19] proposed equation to calculate the nominal shear resistance. The nominal shear resistance, V_n, shall be determined as:

$$V_n = V_c + V_s + V_p \qquad (2.66)$$

Where

V_n = Nominal shear strength ;
V_c = Nominal shear strength provided by concrete ;
V_s = Nominal shear strength provided by shear reinforcement ;
V_p = Nominal shear strength provided by pre-stressing force

$$V_c = 0.083\beta\sqrt{f'_c}\, b_V\, d_V \qquad (2.67)$$

Where:

f'_c = Concrete compressive strength ;
b_v = Effective web width ;
d_v = Effective shear depth ;
β = Factor indicating ability of diagonally cracked concrete to transmit tension

For the stirrup contribution to shear, truss mechanism is used:

$$V_s = \frac{A_v f_y d_v (cot\,\theta + cot\,\alpha) sin\alpha}{s} \qquad (2.68)$$

Where

A_v = Cross-sectional area of shear reinforcement ;
f_y = Yield stress of shear reinforcement ;
d_v = Effective shear depth ;
s = Spacing of shear reinforcement ;
θ = Angle of inclination of diagonal compressive stresses ;
α = Angle of inclination of transverse reinforcement to longitudinal axis

As component in the direction of the applied shear of the effective pre-stressing force, V_p is taken as zero if the columns are non pre-stressed. β and θ values are the contribution value of axial compression. These two values are listed in Table 2.8 obtained from calculating the stresses that can be transmitted across diagonally cracked concrete that contains at least the minimum amount of transverse reinforcement required for crack control. This minimum amount is specified by AASHTO as

$$A_{v,min} = 0.083\sqrt{f'_c}\frac{b_v s}{f_y}$$
(2.69)

Where:

$A_{v,min}$ = Cross-sectional area of shear reinforcement ;

f'_c = Concrete compressive strength ;

b_v = Effective web width ;

s = Spacing of shear reinforcement ;

f_y = Yield stress of shear reinforcement

Table 2.8 Value of β and θ for sections with transverse reinforcement

v/f'_c		ε_x x 1000								
		$\leq$ -0.20	$\leq$ -0.10	$\leq$ -0.05	$\leq$ 0.00	$\leq$ 0.125	$\leq$ 0.25	$\leq$ 0.50	$\leq$ 0.75	$\leq$ 1.00
$\leq$ 0.075	θ	22.3	20.4	21.0	21.8	24.3	26.6	30.5	33.7	36.4
	β	6.32	4.75	4.10	3.75	3.24	2.94	2.59	2.38	2.23
$\leq$ 0.100	θ	18.1	20.4	21.4	22.5	24.9	27.1	30.8	34.0	36.7
	β	3.79	3.38	3.24	3.14	2.91	2.75	2.50	2.32	2.18
$\leq$ 0.125	θ	19.9	21.9	22.8	23.7	25.9	27.9	31.4	34.4	37.0
	β	3.18	2.99	2.94	2.87	2.74	2.62	2.42	2.26	2.13
$\leq$ 0.150	θ	21.6	23.3	24.2	25.0	26.9	28.8	32.1	34.9	37.3
	β	2.88	2.79	2.78	2.72	2.60	2.52	2.36	2.21	2.08
$\leq$ 0.175	θ	23.2	24.7	25.5	26.2	28.0	29.7	32.7	35.2	36.8
	β	2.73	2.66	2.65	2.60	2.52	2.44	2.28	2.14	1.96
$\leq$ 0.200	θ	24.7	26.1	26.7	27.4	29.0	30.6	32.8	34.5	36.1
	β	2.63	2.59	2.52	2.51	2.43	2.37	2.14	1.94	1.79
$\leq$ 0.225	θ	26.1	27.3	27.9	28.5	30.0	30.8	32.3	34.0	35.7
	β	2.53	2.45	2.42	2.40	2.34	2.14	1.86	1.73	1.64
$\leq$ 0.250	θ	27.5	28.6	29.1	29.7	30.6	31.3	32.8	34.3	35.8
	β	2.39	2.39	2.33	2.33	2.12	1.93	1.70	1.58	1.50

It can be seen from Table 2.8 that β and θ depend on the shear stress on the concrete v_u and the longitudinal strain at mid-depth of the section ε_x, where

$$v_u = \frac{|V_u - \phi V_p|}{\phi b_v d_v}$$ (2.70)

Where:

V_u = Factored shear force at section;

b_v = Effective web width ;

d_v = Effective shear depth ;

ϕ = Resistance factor for shear

In using Table 2.8, ε_x shall be taken as the calculated longitudinal strain at the mid-depth of the members when the section subjected to N_u, M_u and V_u.

For non pre-stressed columns subjected to axial compression and the section contains at least the minimum transverse reinforcement, the longitudinal tensile strain in the flexural tension can be calculated as

$$\varepsilon_x = \frac{\left(\frac{|M_u|}{d_v} + 0.5 N_u + 0.5 |V_u - V_p| \cot\theta - A_{ps} f_{po} \right)}{2(E_s A_s + E_p A_{ps})}$$ (2.71)

If the value from Equation (2.71) is negative, the strain shall be taken as:

$$\varepsilon_x = \frac{\left(\frac{|M_u|}{d_v} + 0.5 N_u + 0.5 |V_u - V_p| \cot\theta - A_{ps} f_{po} \right)}{2(E_c A_c + E_s A_s + E_p A_{ps})}$$ (2.72)

The initial value of ε_x should not be taken greater than 0.001 and it is convenient to take the value of $0.5 \cot\theta = 1$.

Where:

ε_x = Longitudinal strain at mid-depth of section ;

d_v = Effective shear depth ;

M_u = Factored moment applied to section ;

N_u = Factored axial compression applied to section ;

V_u = Factored shear applied to section ;

A_c = Area of concrete on flexural compression side ;

A_s = Area of longitudinal reinforcement on flexural tension side;

A_{ps} = Area of pre-stressing steel on the flexural tension side of the member;

E_c = Elastic modulus of concrete ;

E_s = Elastic modulus of steel

E_p = Elastic modulus of pre-stressing tendon ;

f_{po} = Elastic modulus of pre-stressing tendon multiplied by the locked-in difference in strain between the pre-stressing tendon and the surrounding concrete;

2.3.6. Priestley et al. (1994)

Priestley et.al.[20] proposed an additive shear equation as shown below.

$$V_n = V_c + V_s + V_a \qquad (2.73)$$

Where:

V_n = Nominal shear strength ;

V_c = Nominal shear strength provided by concrete ;

V_s = Nominal shear strength provided by shear reinforcement ;

V_a = Nominal shear strength provided by axial load

$$V_c = k\sqrt{f'_c}\, A_e \qquad (2.74)$$

f'_c is concrete compression strength (MPa). k depends on the displacement ductility factor μ_Δ that can be shown in Figure 2.12, which reduces from 0.29 in MPa units for $\mu_\Delta \leq 2.0$ to 0.1 in MPa unit for $\mu_\Delta \leq 4.0$ and A_e is taken as

$0.8A_g$.
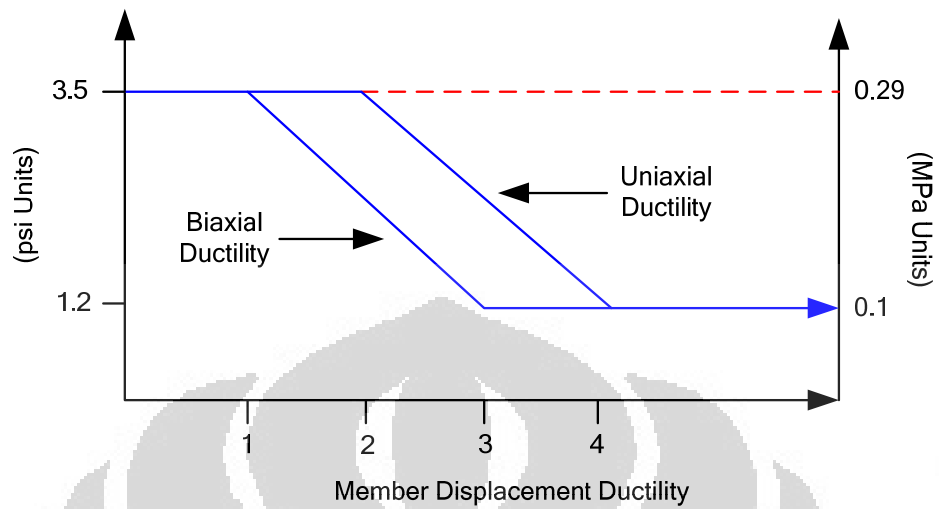
Figure 2.12 Concrete Shear Strength Degradation with Displacement Ductility (Priestley et.al.[20])
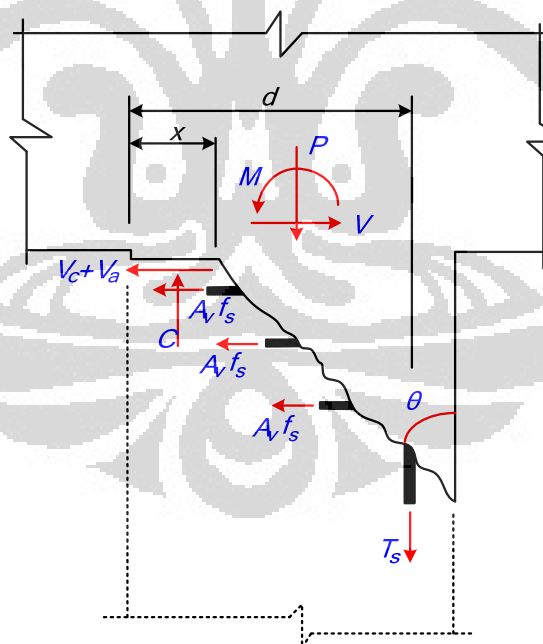
Figure 2.13 Schematic Critical Section for Flexural and Shear (Priestley et.al.[20])

Obtained from equilibrium truss model, the shear strength contribution by truss mechanism for rectangular columns is given by

Universitas Indonesia

$$V_s = \frac{A_v f_y h_c}{s} \cot \theta \qquad (2.75)$$

Where:

A_v = Cross-sectional area of shear reinforcement ;

f_y = Yield stress of shear reinforcement ;

h_c = The core dimension measured center-to-center of the peripheral transverse reinforcement ;

θ = The angle of truss mechanism, taken as 30º. In general, the truss mechanism angle θ should be considered as variable for different columns conditions

For circular sections reinforced with spirals or circular hoops, Ang et.el.[21] proposed the following equation as shear strength contribution obtained by truss mechanisms:

$$V_s = \frac{\pi}{2} \frac{A_{sh} f_{yh} D'}{s} \cot \theta \qquad (2.76)$$

Where:

A_{sh} = The area of the steel transverse reinforcement;

f_{yh} = The strength of the steel transverse reinforcement;

D' = Diameter of the spiral or hoop;

s = Spacing between two transverse reinforcement;

θ = The angle of truss mechanism, taken as 30º. In general, the truss mechanism angle θ should be considered as variable for different columns conditions

The derivation of Equation (2.76) is illustrated in Figure 2.14 by considering circular column section reinforced by circular hoops.

Universitas Indonesia
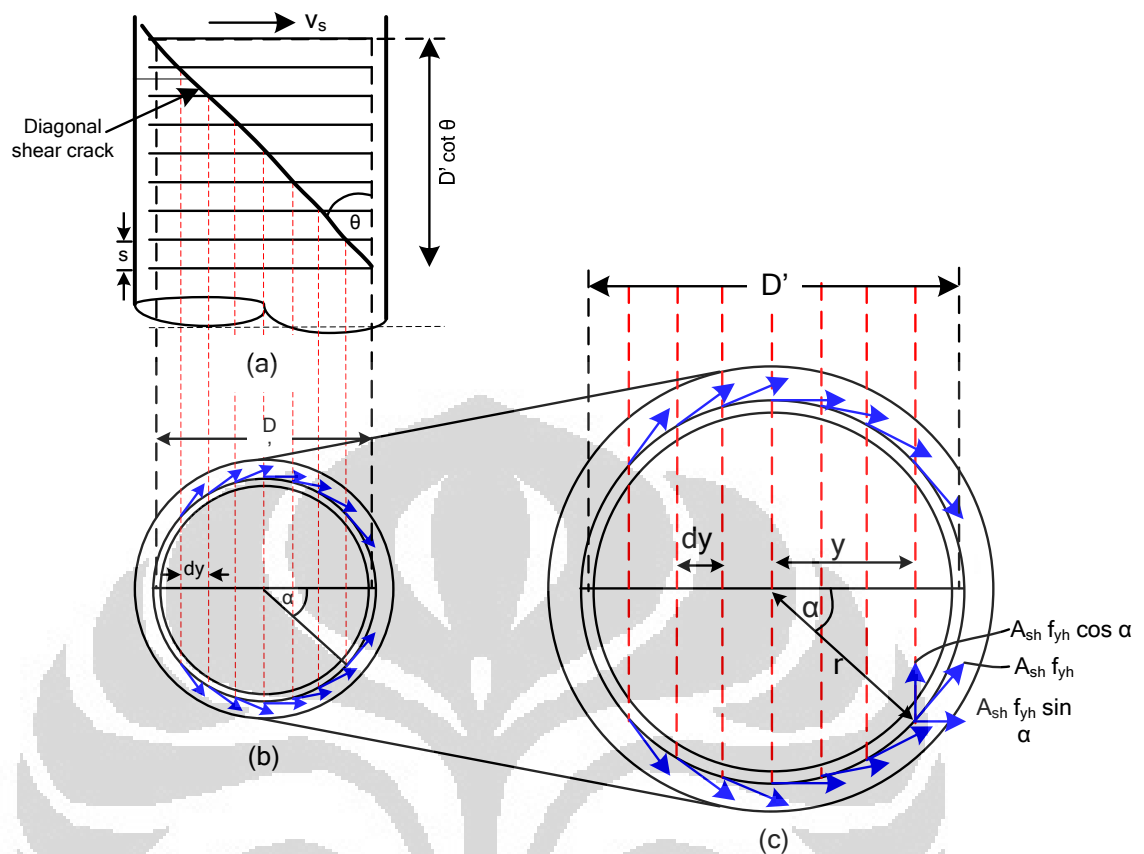
Figure 2.14 Shear carried by transverse reinforcement for circular column (Ang et.al.[21])
(a). Elevation. (b). Plan. (c). Plan zoomed view

Due to diagonal shear crack, the circular hoops are crossed by crack at two points as shown in Figure 2.14. Horizontal distance between two adjacent transverse reinforcement that crossed by diagonal shear crack is defined as dy. Figure 2.14 depicts the tension forces on the transverse reinforcement in which each of them has horizontal and vertical components. The vertical components of the lower and upper part eliminate each other. That means only the horizontal component remains.

$$V_s = \int_{y_1}^{y_2} \frac{2\, A_{sh} f_{yh} \sin\alpha\, dy}{D'} \frac{D' \cot\theta}{s} \tag{2.77}$$

Since that

$$\cos\alpha = \frac{y}{r} \; ; \; \sin\alpha = \frac{\sqrt{r^2 - y^2}}{r} \tag{2.78}$$

$$\sin\alpha = \sqrt{\sin^2\alpha} = \sqrt{1 - \cos^2\alpha} \tag{2.79}$$

Equation (2.77) can be considered as

$$V_s = \int_{y_1}^{y_2} 2\, A_{sh} f_{yh} \sqrt{1 - \left(\frac{y}{r}\right)^2} \frac{dy}{D'} \frac{D' \cot\alpha}{s}$$

or

$$V_s = 2\, A_{sh} f_{yh} \frac{D' \cot\alpha}{s} \int_{y_1}^{y_2} \sqrt{1 - \left(\frac{y}{r}\right)^2} \frac{dy}{D'} \tag{2.80}$$

If $y_1 = -r$ and $y_2 = r$ are considered as upper and lower boundary where r is equal to half of the hoops diameter.

$$\int_{-r}^{r} \sqrt{1 - \left(\frac{y}{r}\right)^2} \frac{dy}{D'} \tag{2.81}$$

Equation (2.81) is developed to represent the total tension force of the entire level of transverse reinforcement. The integration result of Equation (2.81) will be equal to $\pi/4$. Equation (2.80) is approximation value by assuming tension force occurs at continuous point along the transverse reinforcement. Whereas tension force actually occurs in certain points that crossed by the diagonal shear crack only. The following figure shows calculated shear strength provided by transverse reinforcement in certain points. Based on the result, it can clearly be seen that the

Equation (2.80) is approximation value.
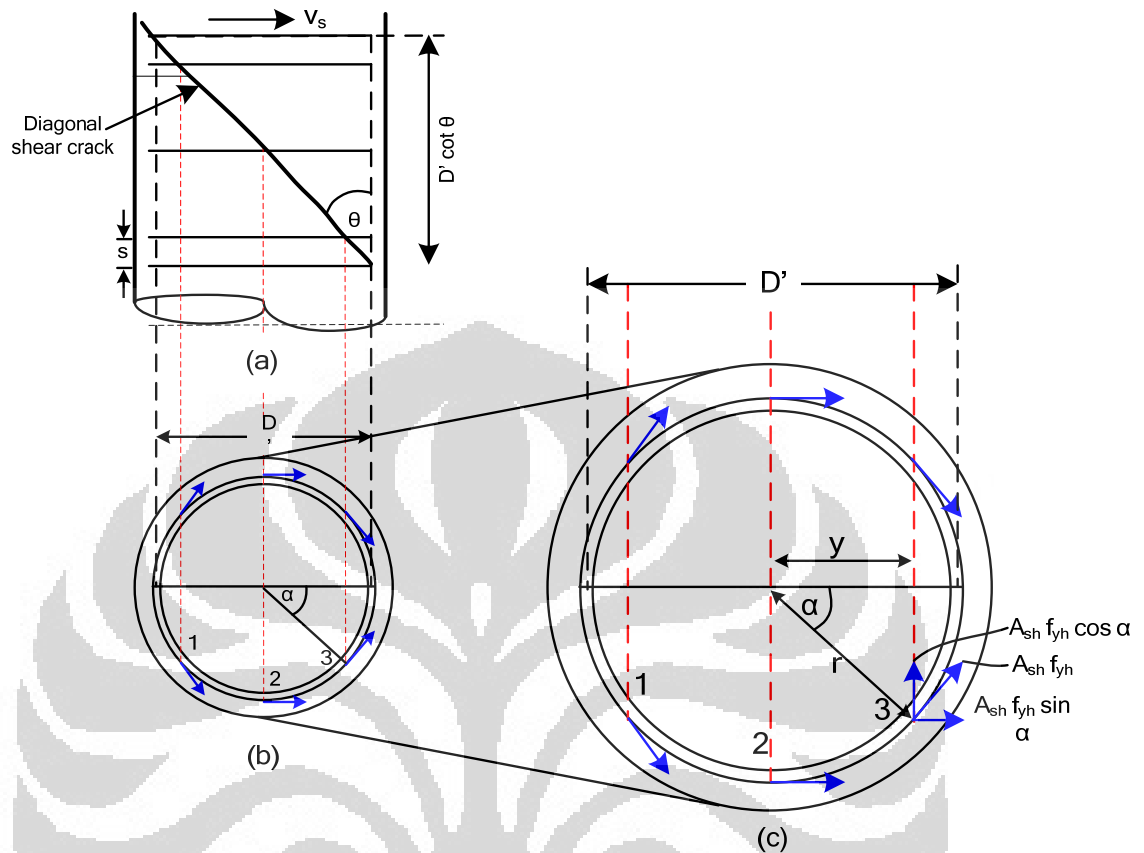
Figure 2.15 Shear carried by transverse reinforcement considering three intersection points of diagonal shear crack and transverse reinforcement.
(a). Elevation. (b). Plan. (c). Plan zoomed view.

Three layers of the transverse reinforcement are crossed by diagonal shear crack (assume $\theta = 45^o$) at three different points. Each point has its own value of α. Since the vertical components eliminate each other, only the horizontal component of $A_{sh}f_{yh}\sin\alpha$ that is considered.

Table 2.9 Three different considered points

Point	θ (°)	$2\,A_{sh}f_{yh}\sin\theta$
1	45	$\sqrt{2}\,A_{sh}f_{yh}$
2	90	$2\,A_{sh}f_{yh}$
3	135	$\sqrt{2}\,A_{sh}f_{yh}$
V_s		$(2 + 2\sqrt{2})\,A_{sh}f_{yh}$

From Table 2.9, the value of shear strength provided by transverse reinforcement that calculated in three different points is $V_s = 4.83\ A_{sh}f_{yh}$.

The result mentioned above can be compared by the result from Equation (2.76)

$$V_s = \frac{\pi}{2}\frac{A_{sh}f_{yh}\ D'}{s}\cot\theta$$

$$V_s = \frac{\pi}{2}A_{sh}f_{yh}\frac{D'\cot\theta}{s}$$

$$V_s = \frac{\pi}{2}A_{sh}f_{yh}(3)$$

$$V_s = 4.71\ A_{sh}f_{yh}$$

The value of shear strength provided by transverse reinforcement that calculated in continuous points is $V_s = 4.71\ A_{sh}f_{yh}$. Exact value and approximation value are almost the same. If there are more transverse reinforcement crossed by diagonal shear crack, that means there are more points that will be considered. If more points are consider the approximation value will be closer to the exact value.

Crack angle

Elwood and Moehle[23] stated that there are few reliable models exist for estimating the inclination θ of the shear failure plane. A basic principles approach is to define θ as the angle of the nominal principal tension stress at instant when it reaches the tensile capacity of the concrete under combined shear and axial load, using a Mohr's circle representation of the state of stress.

An Experiment for columns tested by Lynn and Sezen, the critical angle estimated by the model range from 65 to 71 degrees, with an average 68 degrees. Lynn and Sezen (in Elwood and Moehle[23]) has different definition related the crack angle with the Priestley et.al[20] as shown in Figure 2.16 and 2.18. In order to have a same

perception, the critical crack angle defined by Lynn and Sezen is noted as α_r and critical angle by Priestley as θ.
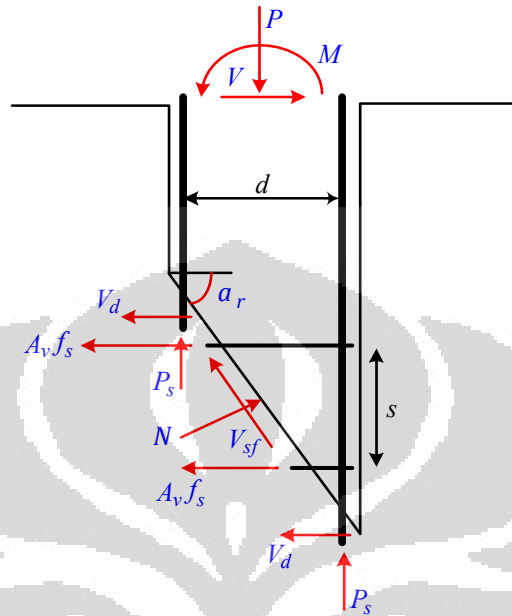
Figure 2.16 Free body Diagram of Column after shear failure (Elwood and Moehle[23])

The observed average angle of critical shear crack from the tests is plotted in Figure 2.17 (The angles were subjectively estimated from photographs).
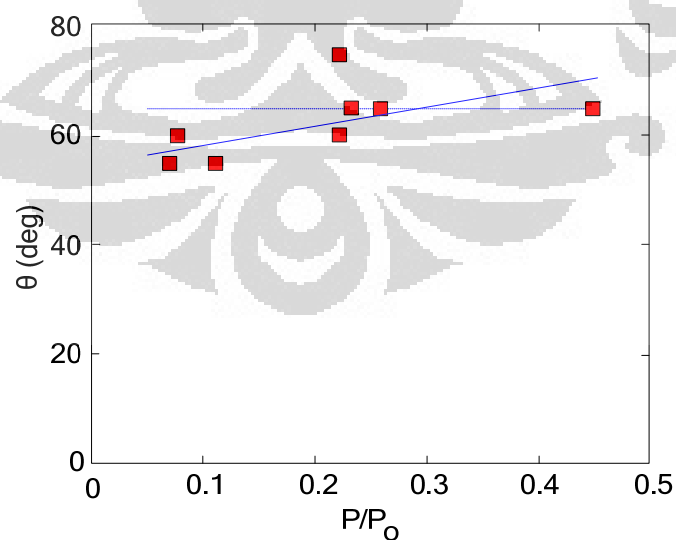
Figure 2.17 Relation between observed angles of the critical cracks and axial load

(Elwood and Moehle[23])

The angle could have the linear variation suggested by the solid line as:

Universitas Indonesia

$$\alpha_r = 55 + 35\frac{P}{P_0} \qquad (2.82)$$

Where:

P = Axial load ;

P_0 = The axial capacity of the undamaged column ;

    = $0.85f'_c(A_g - A_{sl}) + f_{yl}A_{sl}$;

f'_c = The concrete compressive strength ;

A_g = The gross concrete area ;

A_{sl} = The area of longitudinal steel ;

f_{yl} = The yield strength of the longitudinal reinforcement
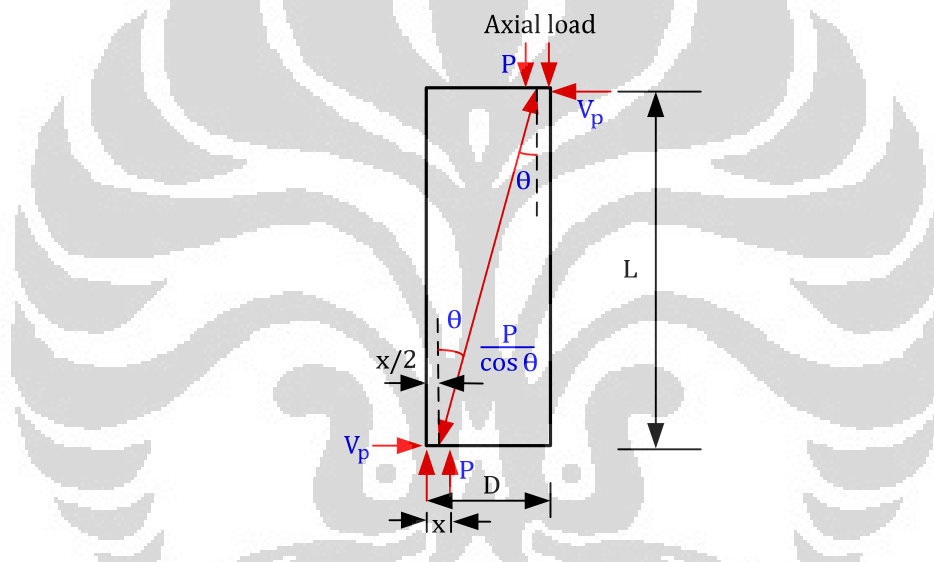
Figure 2.18 Axial Load Contribution for Shear Strength (Priestley et. al.[20])

The shear strength enhancement by axial load is considered to result from an inclined compression strut (Figure 2.18), given by

$$V_a = P \tan\theta = \frac{D - x}{L}P \qquad (2.83)$$

Where:

D = Section depth or diameter ;

x = The compression zone depth ;

a = Shear span ;

P = Axial load

2.3.7. Sezen

Sezen[18] proposed a shear strength model for lightly reinforced columns, which also considers a concrete component and a transverse reinforcement component. The model considers the effect of aspect ratio a/d in addition to the other parameters considered by previous researchers.

$$V_n = V_c + V_s \qquad (2.84)$$

Where:

V_n = Nominal shear strength ;

V_c = Nominal shear strength provided by concrete ;

V_s = Nominal shear strength provided by shear reinforcement ;

$$V_c = k \left(\frac{0.5\sqrt{f'_c}}{a/d} \sqrt{1 + \frac{P}{0.5\sqrt{f'_c}A_g}} \right) 0.8A_g \qquad (2.85)$$

Where:

f'_c = Concrete compressive strength ;

b_w = Effective web width ;

a/d = Aspect ratio ;

P = The factored axial compression load (positive in compression) ;

A_g = The gross area of the concrete cross-section

k = Factor based of displacement ductility

For the stirrup contribution to shear, the conservative 45° truss solution is used:

$$V_s = k \frac{A_v f_{yt} d}{s} \qquad (2.86)$$

Where:

A_v = Cross-sectional area of shear reinforcement ;

f_{yt} = Yield stress of shear reinforcement ;

d = Effective depth ;

s = Spacing of shear reinforcement

k =   Factor based of displacement ductility

Figure 2.19 shows the effect of displacement ductility on shear strength. Note that this equation is defined for the shear-flexure failure range, i.e., $2 \leq a/d \leq 4$.
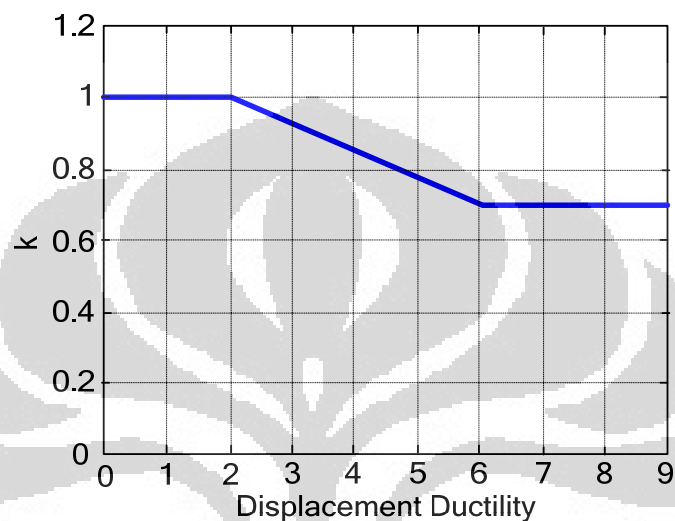
Figure 2.19 Effect of Displacement Ductility on Shear Strength (Sezen[18])

2.3.8. Kowalsky and Priestley (2000)

Kowalsky and Priestley[25] improved the shear design equation in both truss and concrete mechanism as proposed below:

$$V_n = V_c + V_s + V_p \tag{2.87}$$

Where:

V_n =   Nominal shear strength ;

V_c =   Nominal shear strength provided by concrete ;

V_s =   Nominal shear strength provided by shear reinforcement ;

V_p =   Nominal shear strength provided by axial load

The concrete contribution is given by

$$V_c = \alpha \, \beta \, \gamma \sqrt{f'_c} \, 0.8 A_g \tag{2.88}$$

Universitas Indonesia

Where

α = $1 \leq (3 - a/h) \leq 1.5$;

β = $(0.5 + 20\rho_i) \leq 1$;

a/h = Aspect ratio ;

ρ_i = Longitudinal reinforcement ratio ;

γ = factor based on displacement ductility ;

As shown in Figure 2.20, the strength degradation factor γ, is reduced at larger displacement ductility. Figure 2.20 indicates that the reduction in the concrete contribution could be as much as 83 percent at large displacement ductility.

Truss mechanism component, V_s is given by

$$V_s = \frac{A_{sw}f_{yw}(D - c - cover)}{s} \cot 30^o \qquad (2.89)$$

Where:

A_{sw} = Cross-sectional area of shear reinforcement ;

f_{yw} = Yield stress of shear reinforcement ;

D = Effective depth ;

c = Compression depth ;

30° = The angle of truss mechanism ;

s = Spacing of shear reinforcement

The axial load component, V_p is given by

$$V_p = P \tan \alpha = \frac{D - x}{2a} P \qquad (2.90)$$

Where:

D = Section depth or diameter ;

x = The compression zone depth ;

a = Shear span ;

P = Axial load
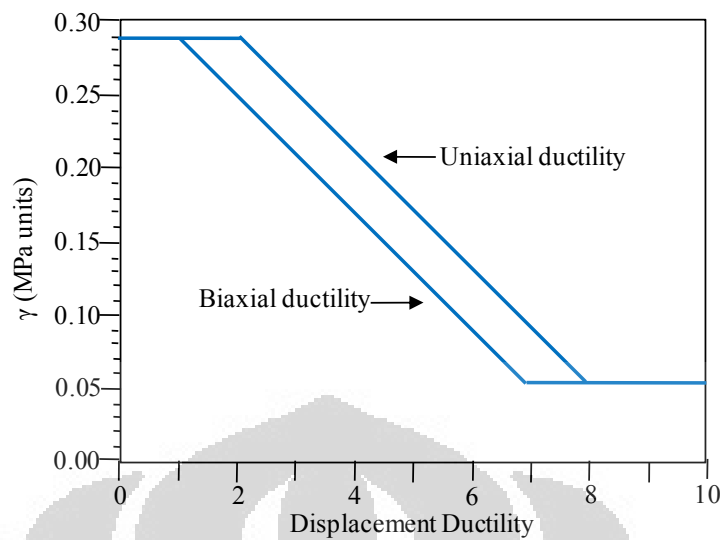
Figure 2.20 γfactor (Kowalsky and Priestley[25])

2.3.9. Aschheim and Moehle

The study by Aschheim and Moehle[26] used laboratory data from cantilever bridge column tests. The shear strength is calculated as the summation of strength contributions from transverse reinforcement and concrete.

$$V_n = V_c + V_s \qquad (2.91)$$

Where:

V_n = Nominal shear strength ;

V_c = Nominal shear strength provided by concrete ;

V_s = Nominal shear strength provided by shear reinforcement ;

The concrete contribution, V_c, is defined as

$$V_c = 0.29 \left(k + \frac{N_u}{13.8 A_g} \right) \sqrt{f'_c} \left(0.8 A_g \right) \qquad (2.92)$$

$$1 \geq k = \frac{4 - \mu_\Delta}{3} \geq 0 \qquad (2.93)$$

Where

f'_c = Concrete compressive strength ;

N_u = The factored axial compression load (positive in compression) ;

A_g = The gross area of the concrete cross-section

μ_Δ = Displacement ductility ;

For the stirrup contribution to shear, the 30° truss solution is used:

$$V_s = \frac{A_v f_y d}{s} \cot 30^\circ \qquad (2.94)$$

Where

A_v = Cross-sectional area of shear reinforcement ;

f_y = Yield stress of shear reinforcement ;

d = Effective depth ;

s = Spacing of shear reinforcement

2.3.10. Xiao and Martirossyan

Xiao and Martirossyan[27] have modified the shear strength equation proposed by Priestley et.al[20] as given below

$$V_n = V_c + V_s + V_a \qquad (2.95)$$

Where:

V_n = Nominal shear strength ;

V_c = Nominal shear strength provided by concrete ;

V_s = Nominal shear strength provided by shear reinforcement ;

V_a = Nominal shear strength provided by axial load ;

$$V_c = k\sqrt{f'_c}\, A_e \qquad (2.96)$$

Where:

f'_c = Concrete compression strength (MPa);

k = Coefficient depends on displacement ductility factor μ_Δ

Xiao and Martirossyan[27] stated that the concrete shear contributions in HSC columns degrade more dramatically than that described by Priestley et.al[20]'s

relationship. At a displacement ductility factor of $\mu_\Delta = 6.0$, the contribution from almost disappears. The modification of the coefficient k (Xiao and Martirossyan[27]) for high-strength concrete defined as follow:

$$k = 0.29 \qquad\qquad\qquad \text{for } \mu_\Delta < 2.0$$
$$k = 0.29 - 0.12(\mu_\Delta - 2) \qquad \text{for } 2.0 \leq \mu_\Delta \leq 4.0$$
$$k = 0.05 - 0.025(\mu_\Delta - 4) \quad \text{for } 4.0 \leq \mu_\Delta \leq 6.0 \tag{2.97}$$
$$k = 0 \qquad\qquad\qquad\qquad \text{for } \mu_\Delta > 6.0$$

Eq. 2.97 is also shown in Figure 2.21. It should be point out that Equation (2.97) has not been calibrated for HSC columns that suffered shear failure with $\mu_\Delta < 4.0$.
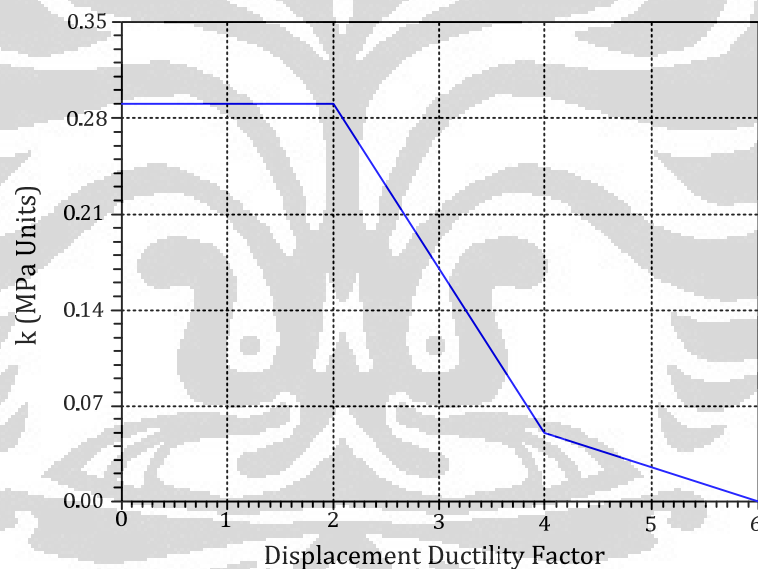
Figure 2.21 Concrete Shear Strength Degradation with Displacement Ductility
(Xiao and Martirossyan[27])

Figure 2.22 illustrates the three components of shear strength in Equation (2.95). It is assumed that at large displacements, the major shear crack sufficiently opens and the shear transfer mechanism of concrete can be lump-summed into the shear resistance of the compression zone, along which the strut mechanism V_a, is also applied.

Universitas Indonesia
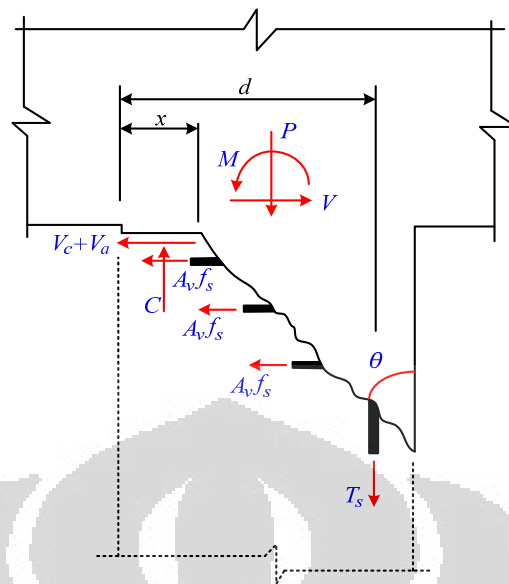
Figure 2.22 Schematic Critical Section for Flexural and Shear (Xiao and Martirossyan[27])

Thus, the shear contribution of the truss mechanism can be estimated as

$$V_s = \frac{A_v f_y (d - x)}{s} \cot\theta \qquad (2.98)$$

Where

A_v = Cross-sectional area of shear reinforcement ;

f_y = Yield stress of shear reinforcement ;

d = The effective depth of the column section ;

x = The depth of the compression zone at the critical section ;

θ = The inclination angle of the major shear crack to the column axis.

Equation (2.99) shown the estimated critical crack angle proposed by Lynn and Sezen. The shear strength enhancement by axial load is considered to result from an inclined compression strut (Figure 2.22), given by

$$V_a = P \tan \alpha = \frac{D - x}{2a} P \qquad (2.99)$$

D = Section depth or diameter ;

x = The compression zone depth ;

a = Shear span

CHAPTER III
SPECIMENS DESIGN & SHEAR STRENGTH PREDICTION

Two types of specimens were designated and varied in several parameters. The first type of specimen consists of eight columns with square transverse reinforcement varied in concrete compressive strength and vertical spacing of hoops. Four of eight columns, named type A columns, were already tested before (Dimas Pramudya Kurniawan[28]); the four rest specimens, named type B columns will be tested. The second type of specimen, named type S columns, consists of two columns with multi-spiral transverse reinforcement varied in vertical spacing of large spiral transverse reinforcement.

3.1. SPECIMEN DESIGN

Four type B columns and two type S columns were designed in different parameter. Both types of columns had a clear height of 1,800 mm with a square cross section of 600×600 mm. The columns reinforced laterally with D13 (no. #4) re-bars with designed yield strength of 785 MPa. Axial re-bars are D32 (No. #10), have designed yield strength of 685 MPa.

As mentioned before, there are three parameters that were used for type A and B columns: axial load ratio, concrete compressive strength and spacing of transverse reinforcement. Ten and twenty percent axial load ratio is classified to low axial load. The columns were made of 70 and 100 MPa concrete. The vertical spacing used in the columns are 450 and 260 mm. On the other hand, only one parameter used for type S columns, which is spacing of transverse reinforcement. These two columns were made of 100 MPa concrete and will be subjected to ten percent axial load ratio.

58

Table 3.1 High Strength Concrete Columns Test Parameters shows the experimental parameters, including the parameters used for type A columns.

Table 3.1 High Strength Concrete Columns Test Parameters

Specimen	Axial Load Ratio	Transverse Bar		Longitudinal Bar		Concrete compressive f'_c (MPa)	Spacing s (mm)
		Size	f_{yt} (MPa)	Size	f_y (MPa)		
A1	10%	D13	785	D32	685	70	450
A2						100	
A3						70	260
A4						100	
B1	20%	D13	785	D32	685	70	450
B2						100	
B3						70	260
B4						100	
S1	10%	D13	785	D32	685	100	125
S2						100	180

Eight first columns were designed based on the analytical study that was done before (Dimas Pramudya Kurniawan[28]). The flexural capacity of the section could be expected by conducting a sectional analysis using Xtract software. Moreover, the shear strength corresponding to the flexural failure from this analysis could be known.

In order to ensure whether or not the shear failure will occur in all columns, the shear strength predictions should be smaller than the shear strength corresponding to the flexural failure of each column (this comparison would be shown in section 3.3 about shear strength prediction of specimens).

There are two possibilities in order to obtain high probability of shear failure during the analytical study: by increasing the flexural capacity that means will also increase the shear strength corresponding to the flexural failure and by reducing shear strength predictions. Larger spacing of the transverse

reinforcement would reduce the shear strength predictions (Dimas Pramudya Kurniawan[28]).

The ratio of longitudinal reinforcement (ρ) of 3.63% is not typically used. That ratio was used in order to increase the flexural capacity that was obtained from sectional analysis. The spacing of transverse reinforcement of 450 mm does not meet code requirement. However, the spacing of transverse reinforcement of 450 mm is still used but preceded by ensuring that at least one hoop will be crossed by diagonal crack during the test. The cracking angle predicted by Elwood and Moehle[23] was used to predict the diagonal crack. So, the high probability of occurrence of the shear failure can be reached by increasing the flexural capacity that means will also increase the shear strength corresponding to the flexural failure and by reducing shear strength capacity (shear strength predicted by codes and researchers).

3.2. MATERIALS

3.2.1. Longitudinal Reinforcement
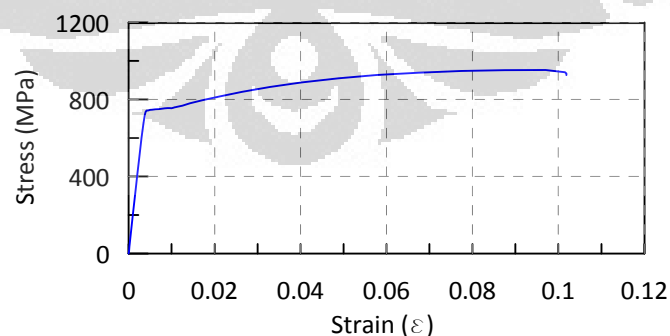
Figure 3.1 Stress-strain Relationship of D32 Longitudinal Reinforcement

All longitudinal reinforcement used in the columns is D32 (No. #10). The longitudinal re-bars had yield strength of 685 MPa and actual yield strength of

735.06 MPa (from the test result). Figure 3.1 shows the stress-strain relationship of the D32 longitudinal reinforcement.

3.2.2. Transverse Reinforcement
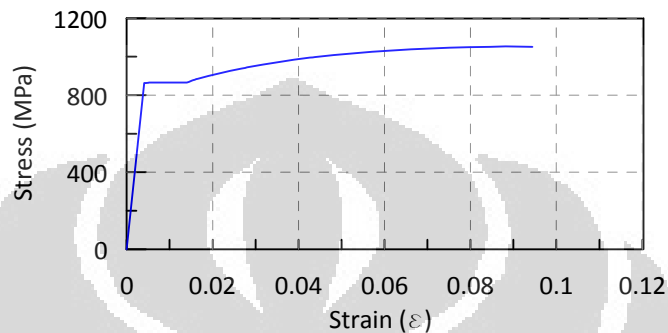
Figure 3.2 Stress-strain Relationship of D13 Transverse Reinforcement

All transversal reinforcement used in the columns is D13 (No. #4). The transverse re-bars had yield strength of 785 MPa and actual yield strength of 862 MPa (from the test result). Figure 3.2 shows the stress-strain relationship of the D13 transverse reinforcement.

3.2.1. Concrete

Concrete compressive strength was one of the parameters in this research. Two value of compressive strength of concrete used in the columns during the design, 70 MPa and 100 MPa. In order to predict the shear strength nominal value, it is better to use the actual value.

Table 5.1 shows the actual and design of concrete compressive strength for each specimen.

(a) Column A1   (b) Column A2

(c) Column A3   (d) Column A4
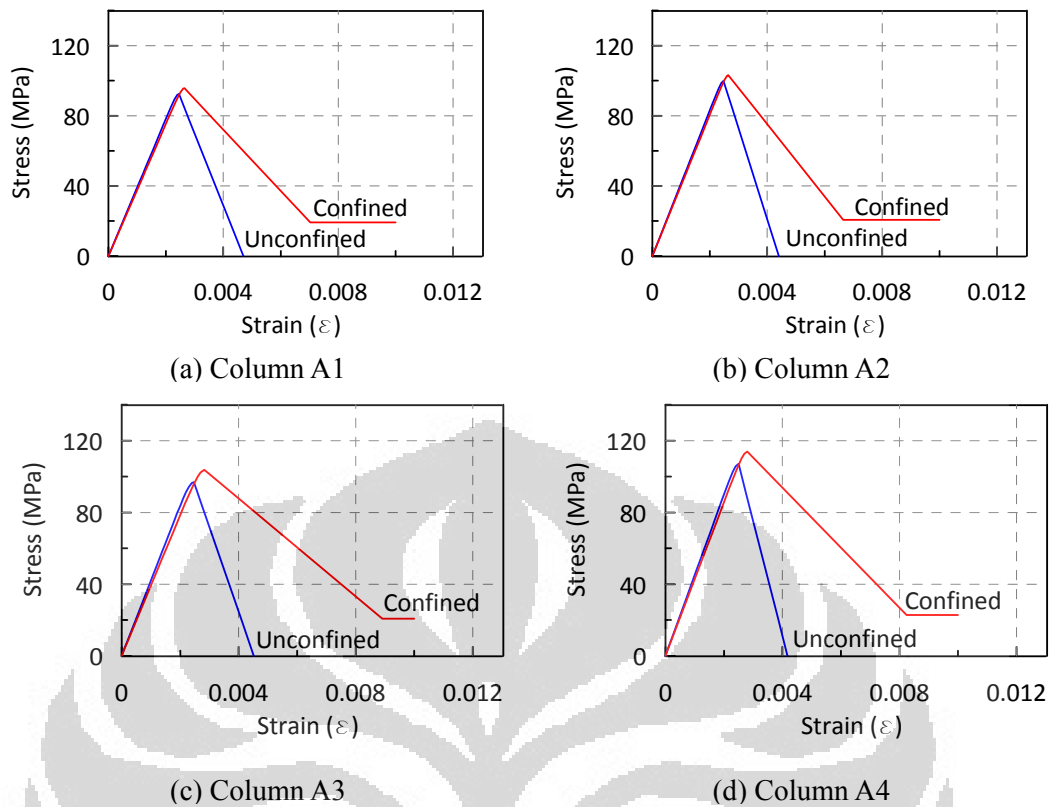
Figure 3.3 Stress-strain relationship of Type A Columns

(a) Column B1   (b) Column B2

(c) Column B3   (d) Column B4
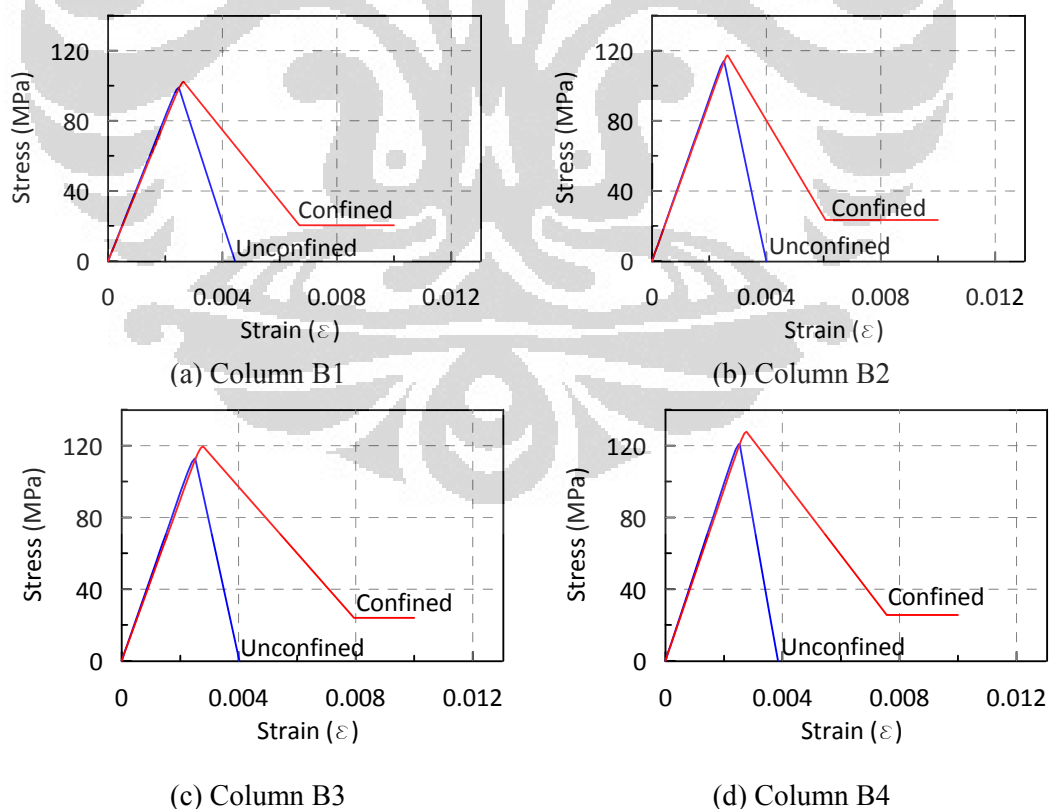
Figure 3.4 Stress-strain relationship of Type B Columns

Universitas Indonesia

Figure 3.4 and Figure 3.4 show the confined concrete models in different concrete compressive strength and transverse reinforcement spacing for each specimen. It could be seen from Figure 3.4 (b) and (d), apart from the different value of actual concrete compressive strength, specimen with smaller vertical spacing of transverse reinforcement has steeper confined concrete model.

Multi-spiral specimens (type S) have three different parts of reinforced concrete. The entire confined concrete strength and stress-strain model depicted in these ten relationship graph used Saatcioglu and Razvi (1992) equations. Further explanation about multi-spiral confined concrete model would be described in the next part 3.3.
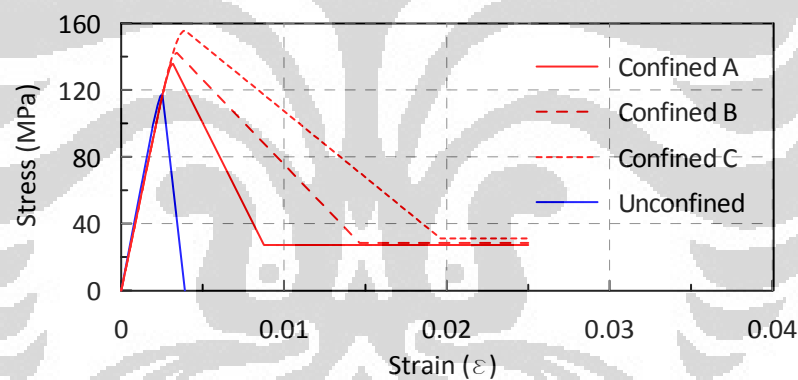
(a) Column S1
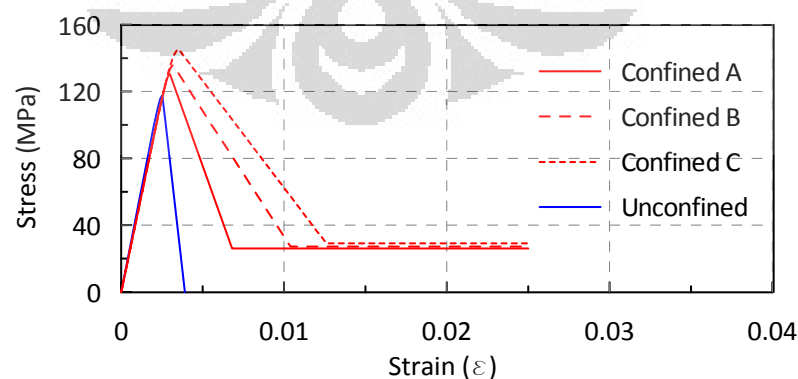
(b) Column S2

Figure 3.5 Stress-strain relationship of Type S Columns

Universitas Indonesia

3.3. SHEAR STRENGTH PREDICTION OF SPECIMENS

Figure 3.6 and Figure 3.7 show the specimen design of type B specimens with 450 mm 260 mm spacing. Figure 3.8 and Figure 3.9 show the design of type S specimen.

Multi-spiral specimens consist of one large and four small spirals transverse reinforcement. As shown in Figure 3.5 in part 3.2.1., in order to facilitate the analysis, the area inside the reinforcement was divided into three different parts, such as: Confined A, B and C. Confined A is the area which is only surrounded by the large spiral, Confined B is only surrounded by the small spiral, and the Confined C is the intersection area of large and small spiral. Previous figure shows that Confined C has the higher concrete compressive stress since it is confined by large and small spiral.

The comparison between shear strength corresponding to flexural failure and shear strength equations mentioned in Chapter 0 and the ratio between shear strength corresponding to flexural failure and shear strength predictions are shown in Table 3.2 and Table 3.3 respectively. For this calculation, the actual value for each specimen and 862 MPa of transverse reinforcement yield stress are used. Calculation for multi-spiral specimens are performed twice: consider and do not consider small spiral reinforcement. From these two tables, it could be seen that, in general, the ratios of shear strength corresponding to flexural failure and shear strength predictions (V_n/V_f) are smaller than 1.00 which means based on the shear models that will be used as comparison, the probability of shear failure occurring in those columns is high enough. Almost all the shear strength prediction for type S specimens that considers the small spiral, is larger than 1.00.
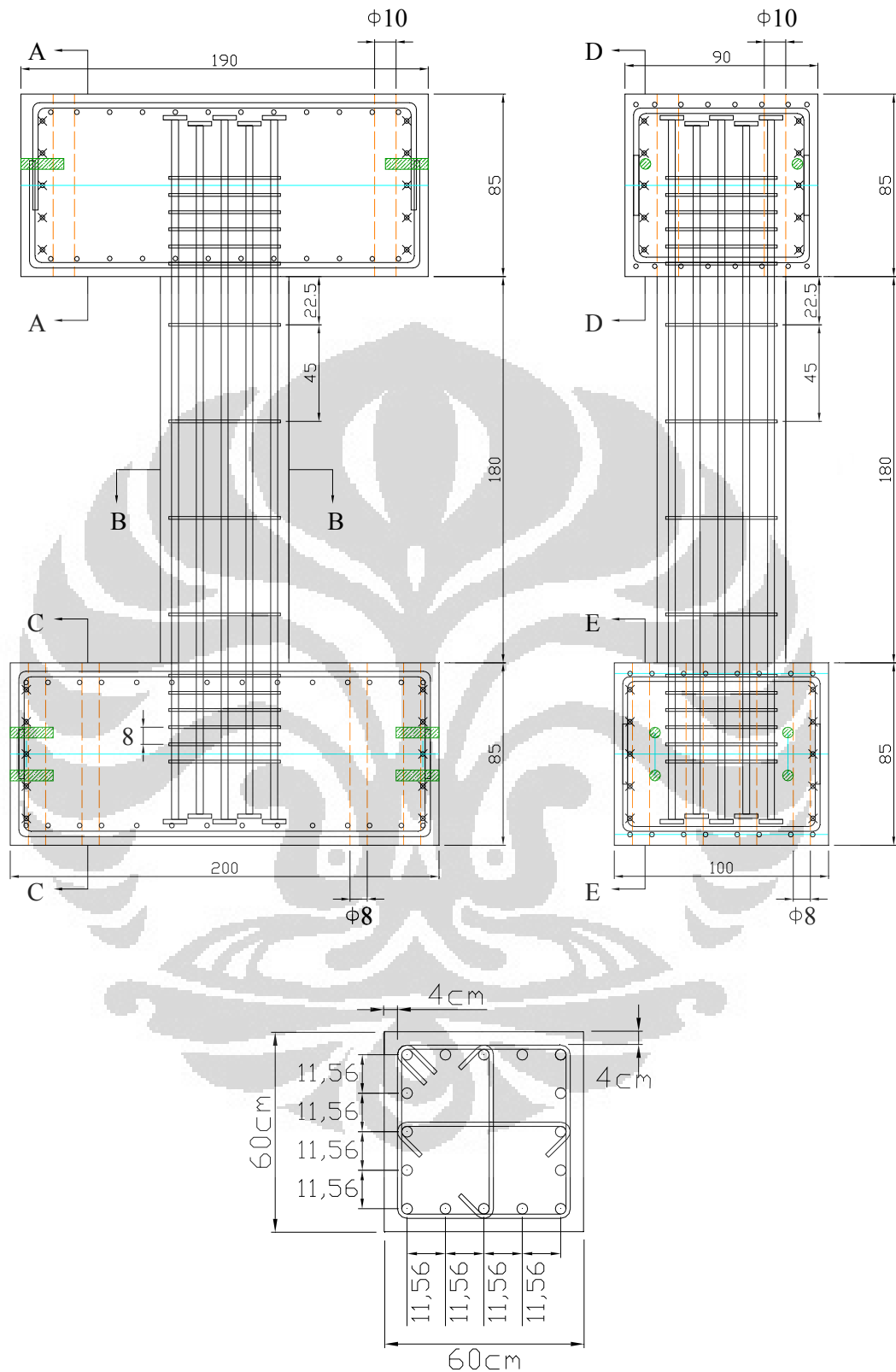
Figure 3.6 HSC Columns Design in cm with 450 mm transverse reinforcement spacing
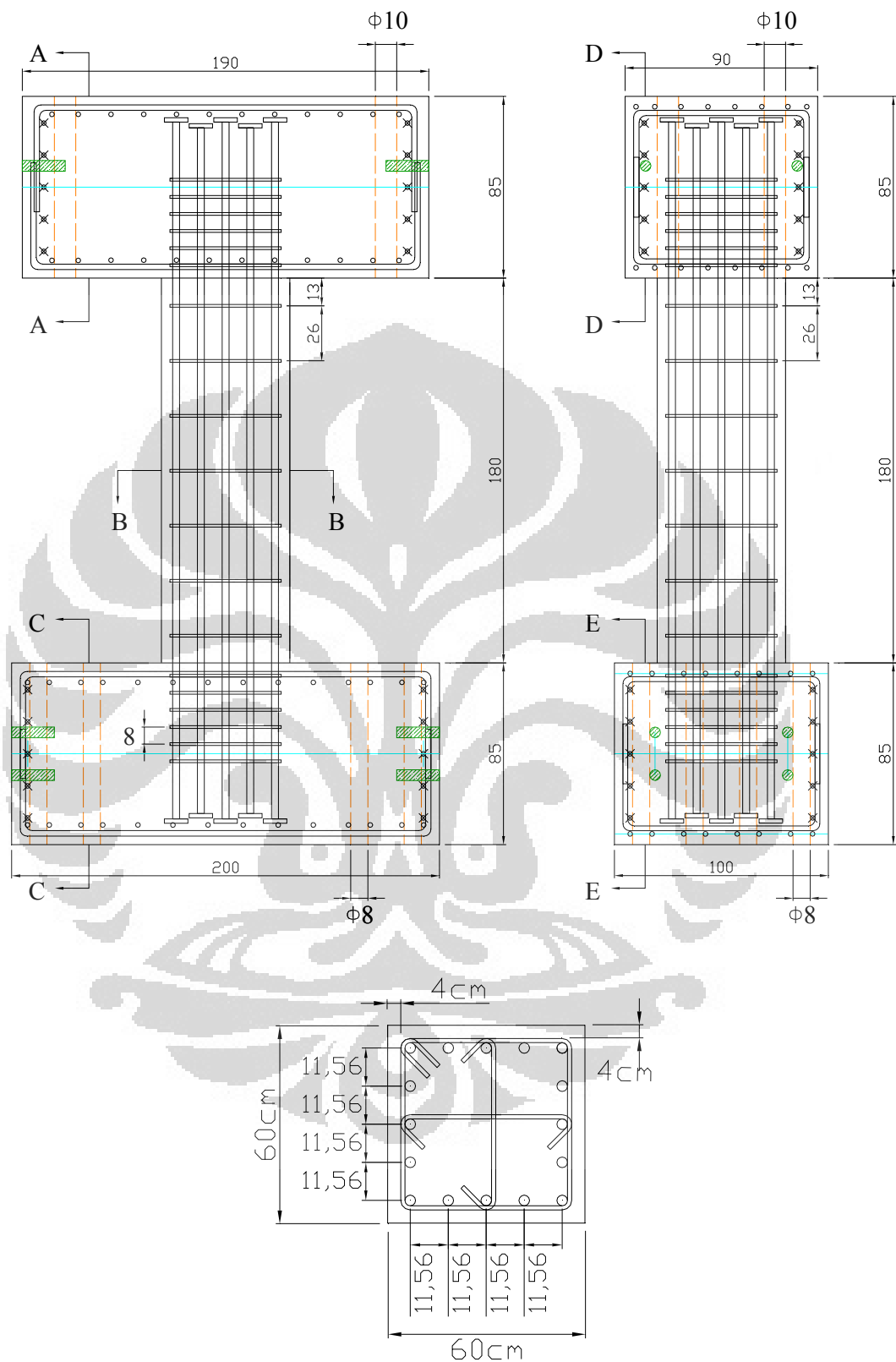
Figure 3.7 HSC Columns Design in cm with 260 mm transverse reinforcement spacing
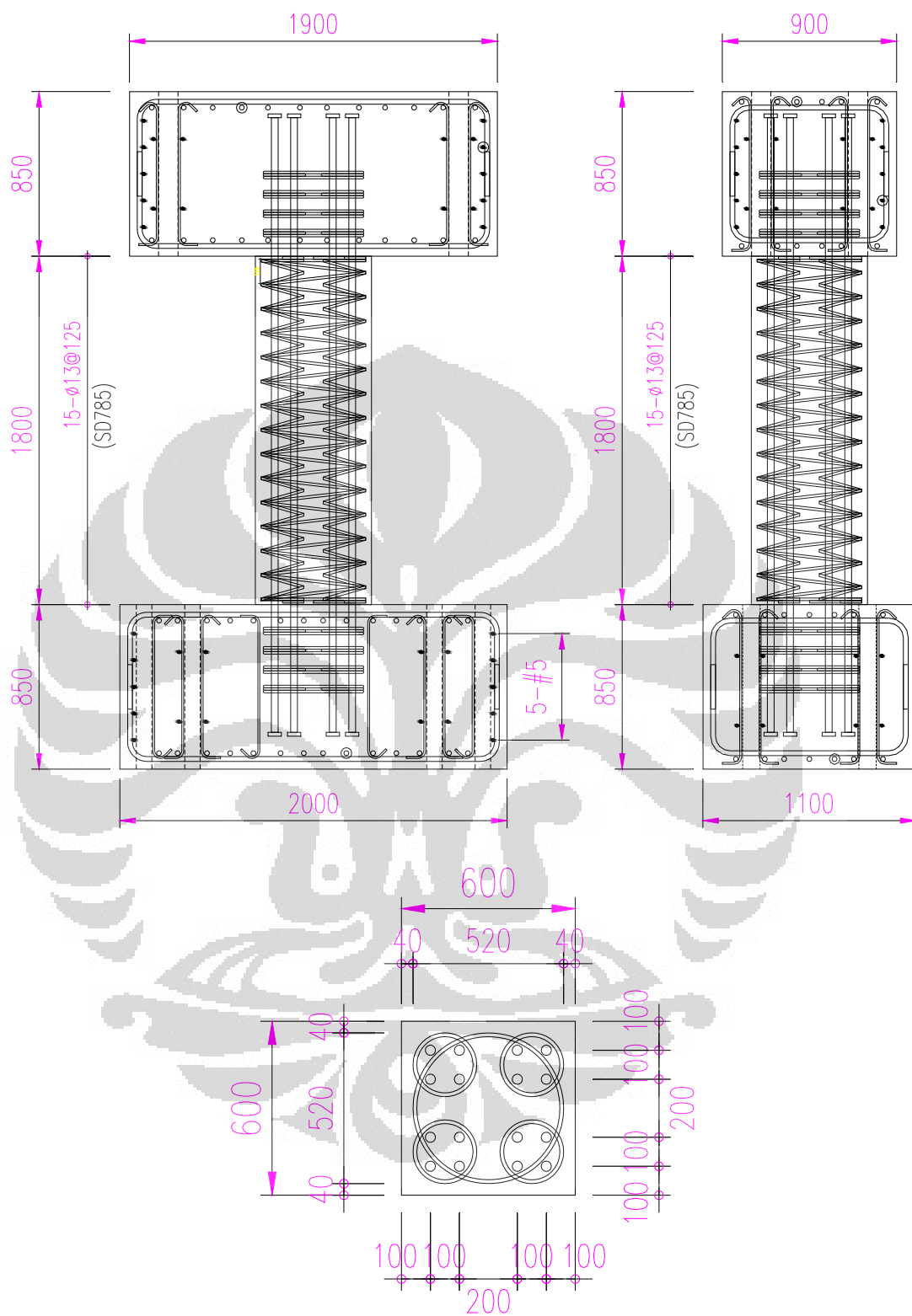
Figure 3.8 HSC Columns Design in mm with 125 mm spiral transverse reinforcement spacing

(S1)
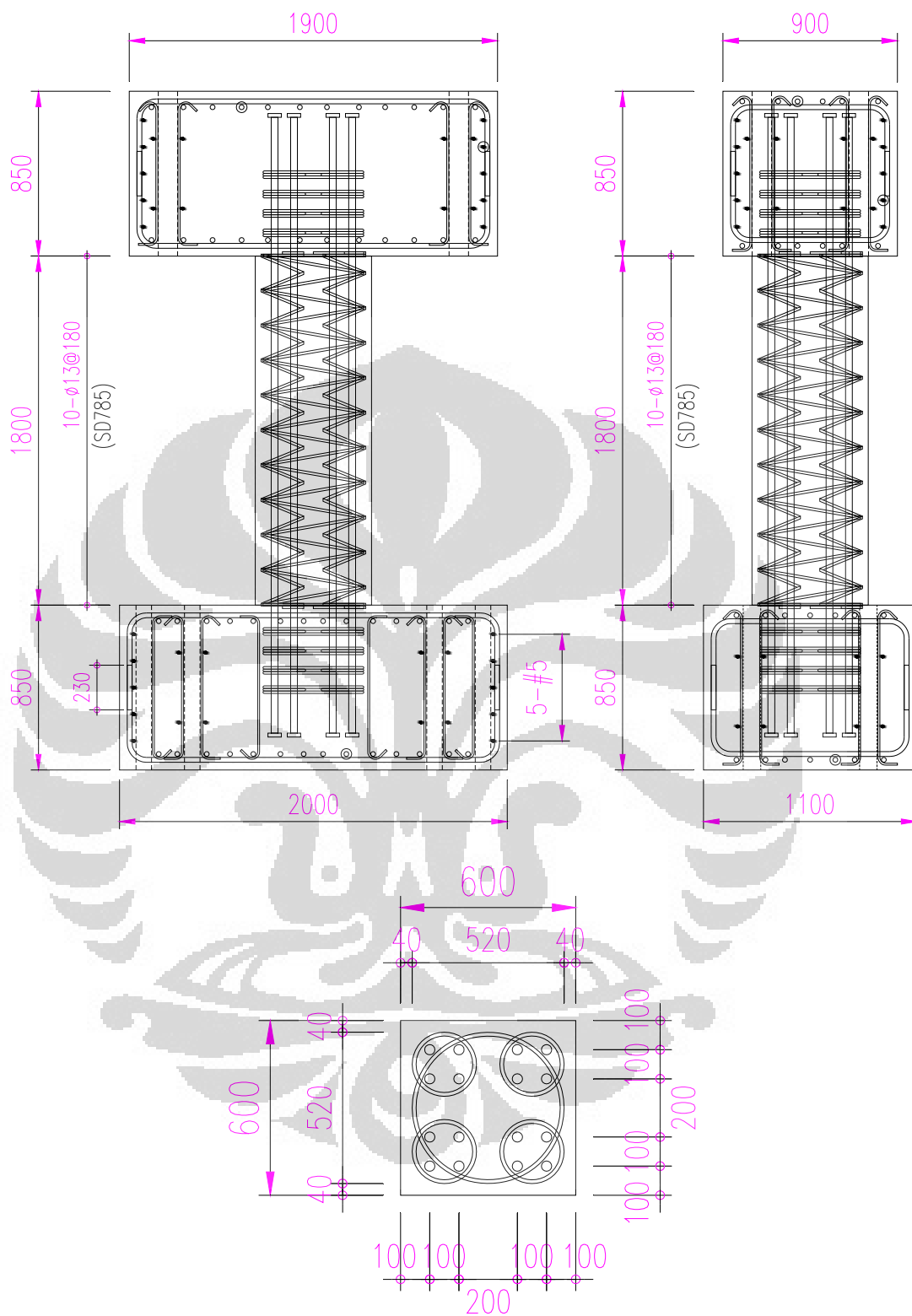
Figure 3.9 HSC Columns Design in mm with 180 mm spiral transverse reinforcement spacing

(S2)

Ratios of V_n/V_f smaller than 1.00 means very important since all of the shear

models give different shear strength prediction. Table 3.3 shows that the ratios of V_n/V_f from shear strength predicted by researchers are generally lower than from codes, provisions and guidelines. The shear strength equations provided by codes, provisions and guidelines have different consideration compared to the shear strength prediction by researchers. The current codes usually use a lower boundary from the database they have for safety reason while shear strength models proposed by researchers try to predict shear strength as accurate as possible. Comparing the value obtained from both sides will be important to observe how accurate the prediction and also how good the current codes can perform.

Some formulations from researchers, codes, provisions and guidelines do not provide the exact formulation for spiral transverse reinforcement. Therefore, in order to calculate the shear strength prediction, some formulations were adapted.

Figure 3.10 to Figure 3.21 show the displacement ductility vs. shear strength predictions for each column compared to the shear strength corresponding to the flexural failure. As mentioned before that all of the shear models proposed by researchers consider shear degradation corresponding to displacement ductility. For shear models from codes, only AIJ 1990, AIJ 1999 and New RC Equation that consider shear degradation. Moreover, from AIJ 1999, the formulation gives the possibility that the shear strength could reach zero value. From these figures, generally prediction from Kowalsky gives the higher value and shear predictions from the codes, provision and guidelines are lower than shear prediction from equation proposed by researchers.

Table 3.2 Comparison of Shear Strength Corresponding to Flexural Failure vs. Several Shear Strength Predictions

Specimen	Shear at flexural failure V_f (kN)	Shear Strength V_n (kN)												
		ACI 318 simplified	ACI 318 detailed	ACI - 426	AIJ 1990	AIJ 1999	New RC	AASHTO	CALTRANS	Aschheim & Moehle	Priestley	Kowalsky	Sezen	Xiao Martirossyan
A1	2943.33	1112.56	958.00	968.30	1602.07	1262.80	1699.65	1032.23	1267.74	1486.96	2157.24	2355.85	1922.39	1827.51
A2	3012.22	1190.35	986.62	1000.96	1678.84	1339.58	1809.65	1100.20	1318.66	1654.12	2289.63	2513.68	2040.60	1962.41
A3	2987.78	1399.00	1226.02	1335.46	2062.75	1734.87	2102.64	1474.82	1543.33	1641.85	2592.53	2685.27	2172.38	2000.60
A4	3078.89	1471.79	1252.33	1368.80	2135.27	1807.39	2218.46	1562.30	1589.86	1817.56	2775.50	2876.79	2316.66	2203.23
B1	3317.78	1571.75	1150.41	1191.58	1649.00	1309.74	1920.57	1092.44	1315.91	2162.71	2736.18	2864.71	2490.59	2391.23
B2	3478.89	1776.81	1231.60	1251.97	1754.80	1415.53	2068.69	1172.77	1385.93	2559.49	2994.73	3154.89	2713.71	2653.16
B3	3480.00	2025.82	1480.19	1651.09	2175.00	1847.12	2373.40	1642.20	1646.56	2637.43	3400.76	3364.13	2931.19	2798.53
B4	3578.89	2139.84	1524.87	1686.81	2230.47	1902.59	2451.06	1660.21	1682.55	2856.98	3576.97	3543.99	3076.70	2987.52
S1	2927.78	1445.10	1127.11	1297.01	1826.25	1797.34	1924.24	1598.97	1522.21	1821.95	2995.60	3098.00	2309.34	2301.17
S2	2923.33	1296.88	978.80	1148.79	1472.67	1566.37	1581.61	1293.56	1373.99	1828.41	2668.20	2867.18	2185.31	2193.45
Considering Small Spiral														
S1	2927.78	2225.12	1907.13	2077.02	2289.99	2012.94	2387.98	1822.64	2302.23	2601.97	3775.62	3878.02	2699.35	2892.23
S2	2923.33	1881.89	1563.81	1733.80	1794.72	1716.09	1903.66	1529.92	1959.00	2413.43	3253.21	3452.19	2477.82	2647.24

Universitas Indonesia

Table 3.3 Ratio of Shear Strength Corresponding to Flexural Failure vs. Several Shear Strength Predictions

Specimen	Shear at flexural failure V_f (kN)	Ratio of Shear Strength Prediction &Shear at flexural failure (V_n/V_f)												
		ACI 318 simplified	ACI 318 detailed	ACI - 426	AIJ 1990	AIJ 1999	New RC	AASHTO	CALTRANS	Aschheim & Moehle	Priestley	Kowalsky	Sezen	Xiao Martirossyan
A1	2943.33	0.38	0.33	0.33	0.54	0.43	0.58	0.35	0.43	0.51	0.73	0.80	0.65	0.62
A2	3012.22	0.39	0.32	0.33	0.55	0.44	0.60	0.36	0.43	0.54	0.75	0.83	0.67	0.65
A3	2987.78	0.47	0.41	0.45	0.69	0.58	0.70	0.49	0.52	0.55	0.87	0.90	0.73	0.67
A4	3078.89	0.48	0.41	0.44	0.69	0.59	0.72	0.51	0.52	0.59	0.90	0.93	0.75	0.72
B1	3317.78	0.47	0.35	0.36	0.50	0.39	0.58	0.33	0.40	0.65	0.82	0.86	0.75	0.72
B2	3478.89	0.51	0.35	0.36	0.50	0.41	0.59	0.34	0.40	0.74	0.86	0.91	0.78	0.76
B3	3480.00	0.58	0.43	0.47	0.62	0.53	0.68	0.47	0.47	0.76	0.98	0.97	0.84	0.80
B4	3578.89	0.60	0.43	0.47	0.62	0.53	0.68	0.46	0.47	0.80	1.00	0.99	0.86	0.83
S1	2927.78	0.49	0.38	0.44	0.62	0.61	0.66	0.55	0.52	0.62	1.02	1.06	0.79	0.79
S2	2923.33	0.44	0.33	0.39	0.50	0.54	0.54	0.44	0.47	0.63	0.91	0.98	0.75	0.75
Considering Small Spiral														
S1	2927.78	0.76	0.65	0.71	0.78	0.69	0.82	0.62	0.79	0.89	1.29	1.32	0.92	1.05
S2	2923.33	0.64	0.53	0.59	0.61	0.59	0.65	0.52	0.67	0.83	1.11	1.18	0.85	0.95

Universitas Indonesia
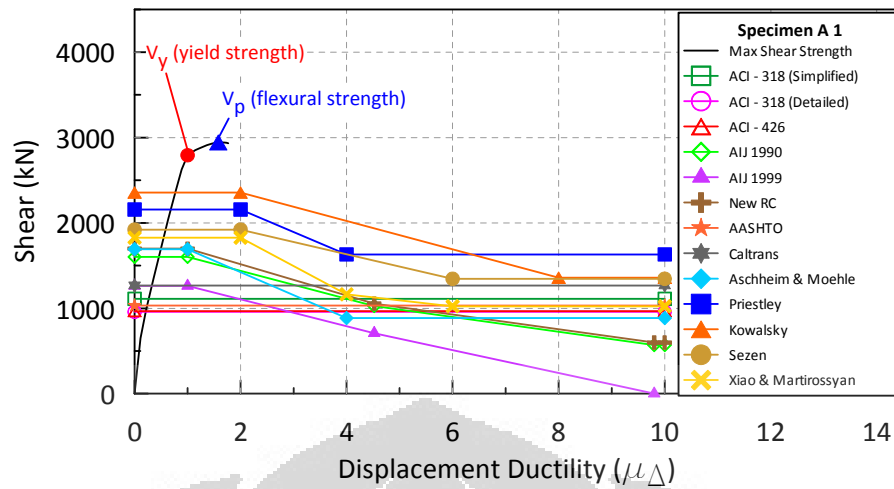
Figure 3.10 Displacement Ductility vs. Shear Strength Prediction of Specimen A1
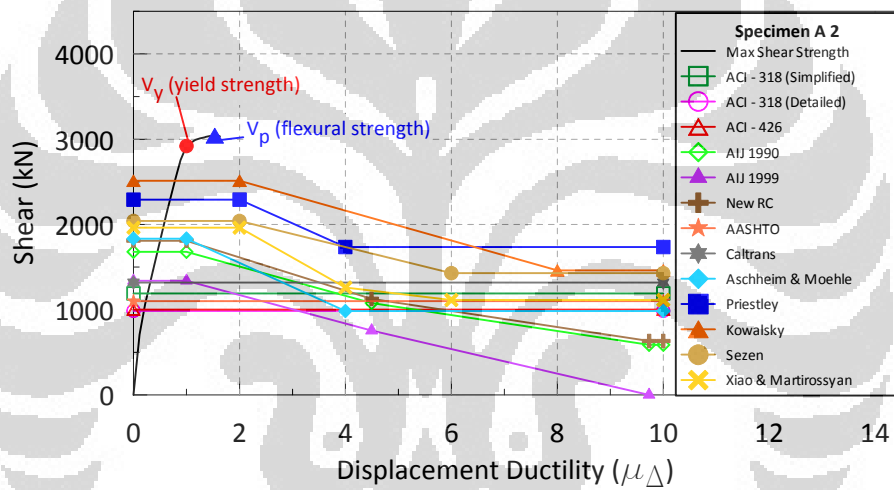
Figure 3.11 Displacement Ductility vs. Shear Strength Prediction of Specimen A2
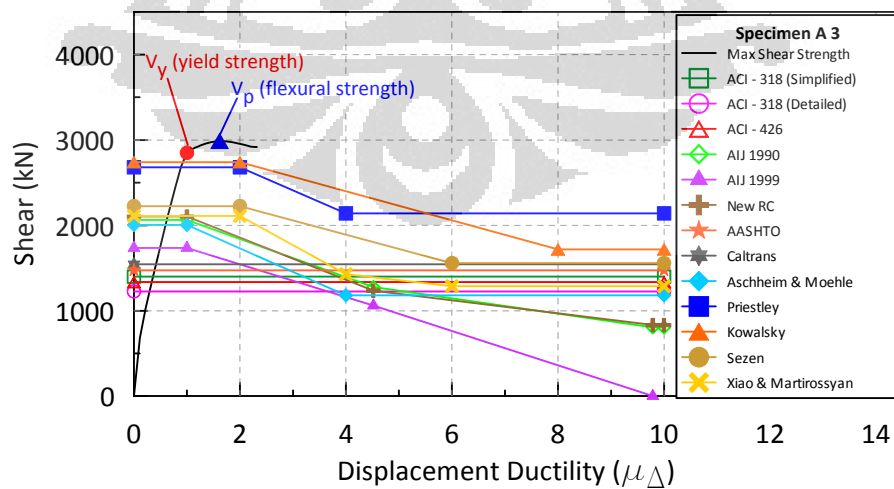
Figure 3.12 Displacement Ductility vs. Shear Strength Prediction of Specimen A3
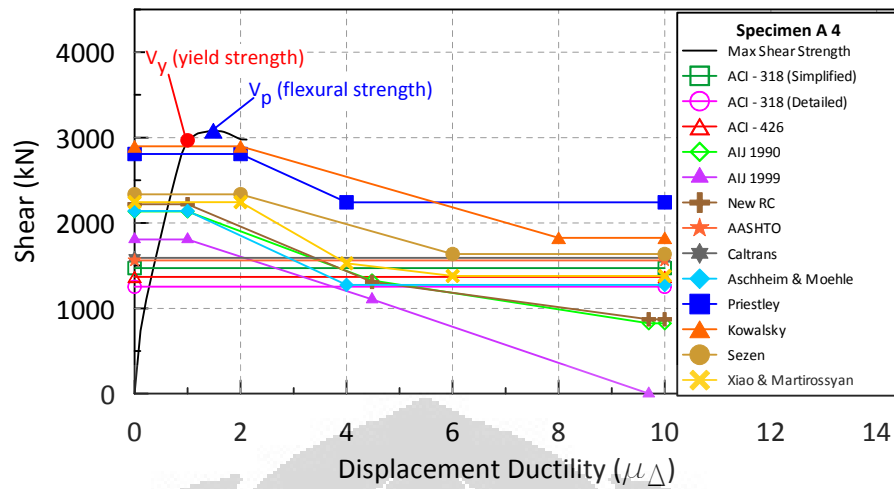
Figure 3.13 Displacement Ductility vs. Shear Strength Prediction of Specimen A4
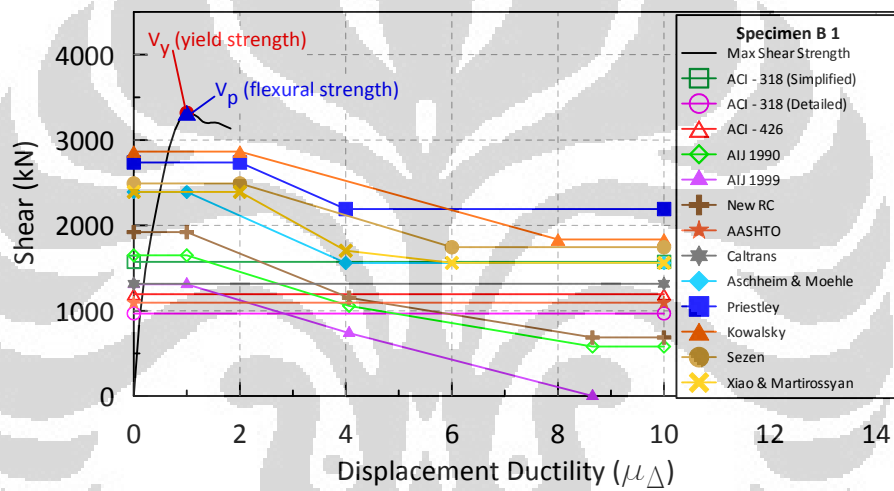
Figure 3.14 Displacement Ductility vs. Shear Strength Prediction of Specimen B1
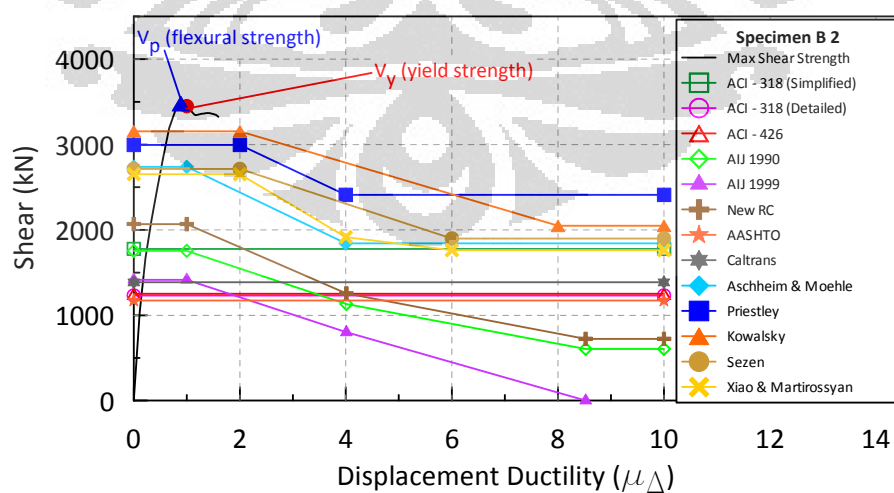
Figure 3.15 Displacement Ductility vs. Shear Strength Prediction of Specimen B2
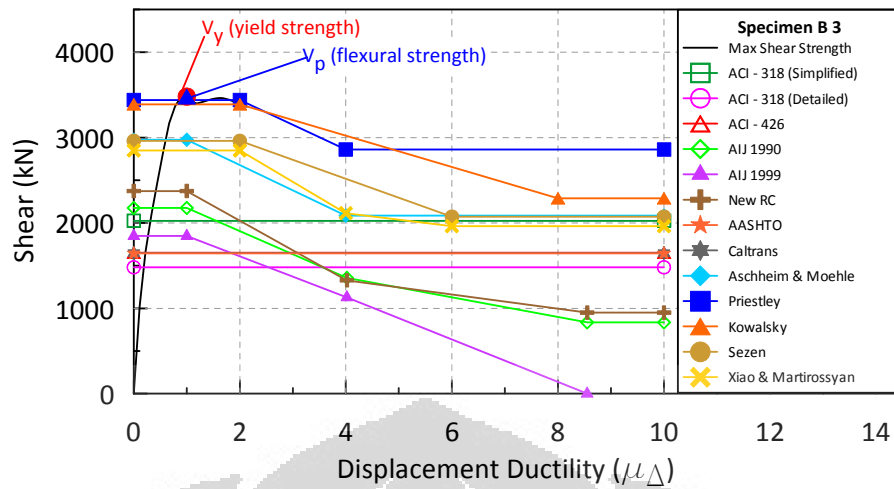
Figure 3.16 Displacement Ductility vs. Shear Strength Prediction of Specimen B3
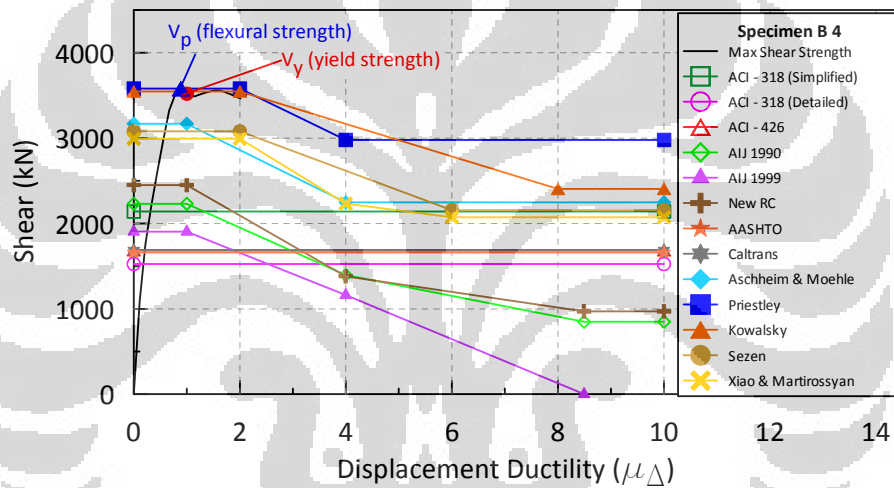
Figure 3.17 Displacement Ductility vs. Shear Strength Prediction of Specimen B4
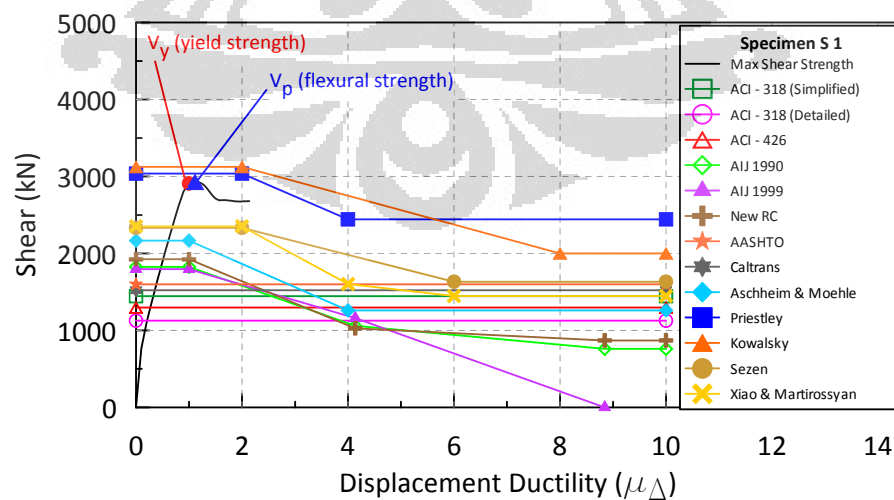
Figure 3.18 Displacement Ductility vs. Shear Strength Prediction of Specimen S1
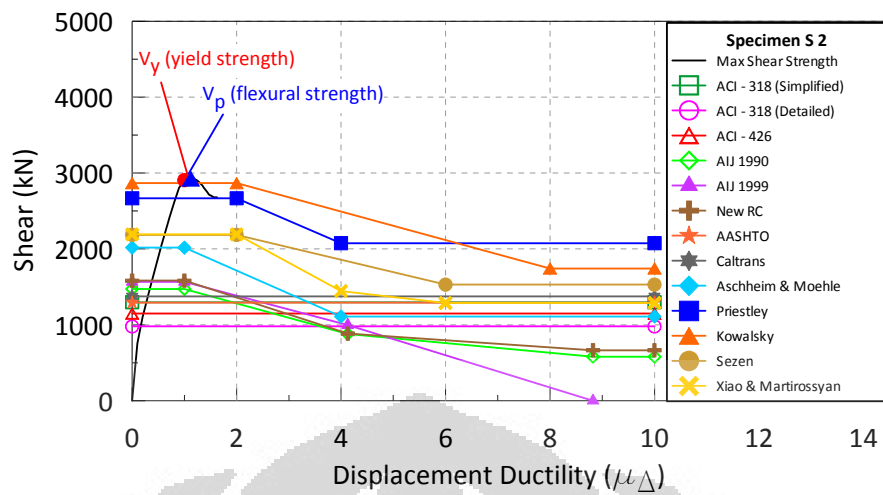
Figure 3.19 Displacement Ductility vs. Shear Strength Prediction of Specimen S2
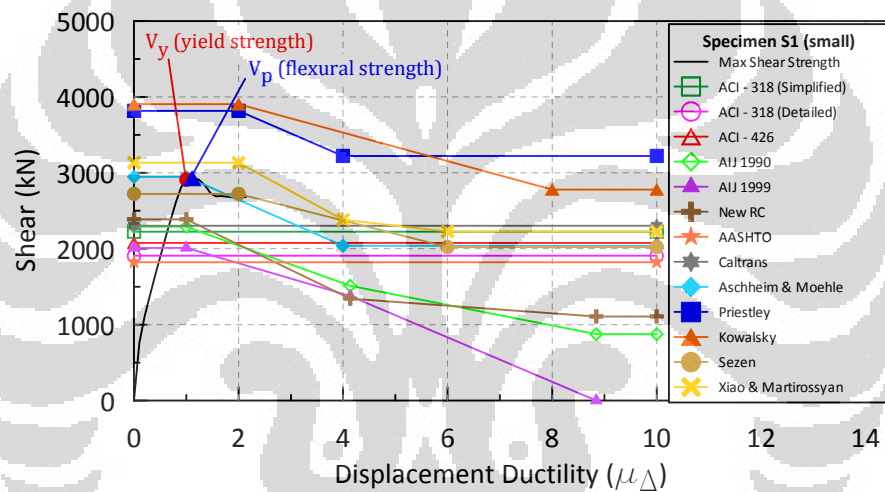
Figure 3.20 Displacement Ductility vs. Shear Strength Prediction of Specimen S1
(Considering small spiral)
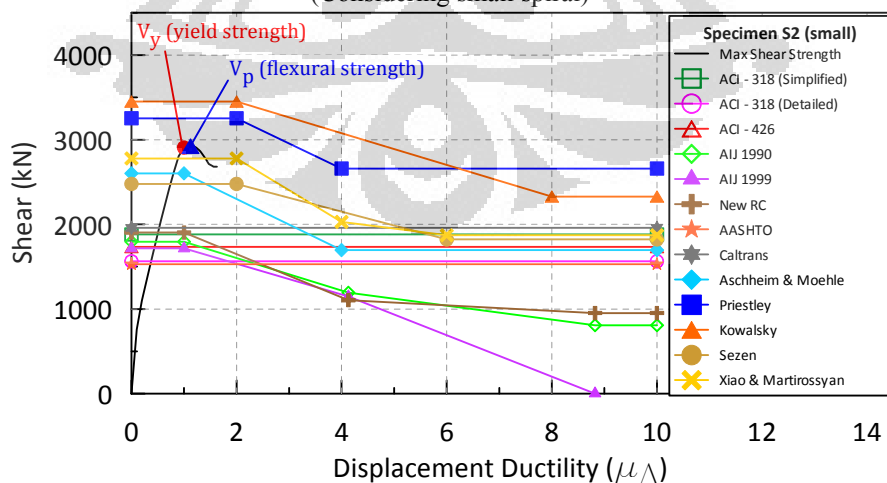
Figure 3.21 Displacement Ductility vs. Shear Strength Prediction of Specimen S2
(Considering small spiral)
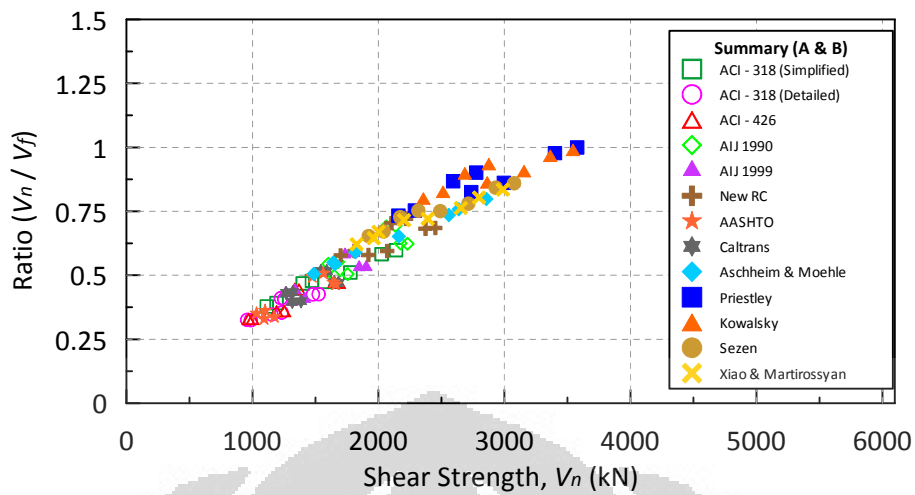
Figure 3.22 Shear Strength vs. Ratio (V_n/V_f) of type A and B specimens.

(a) Not considering small spiral

(b) Considering small spiral
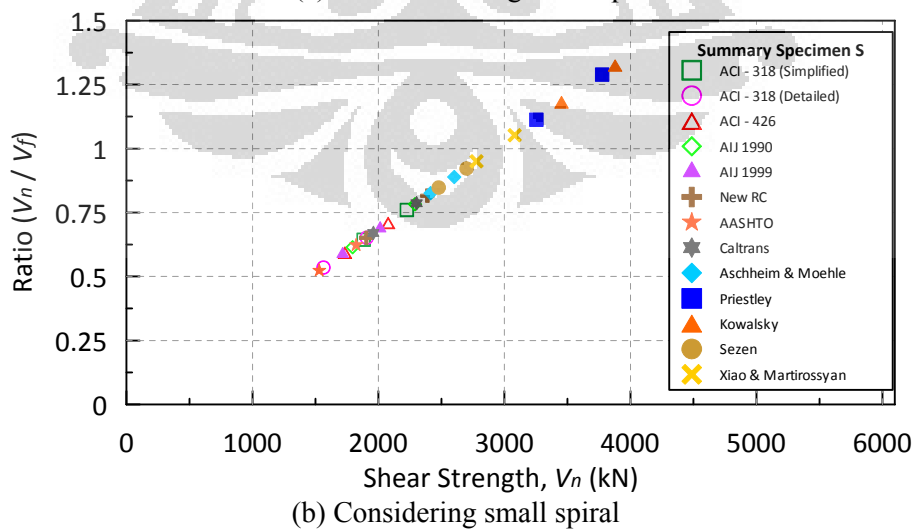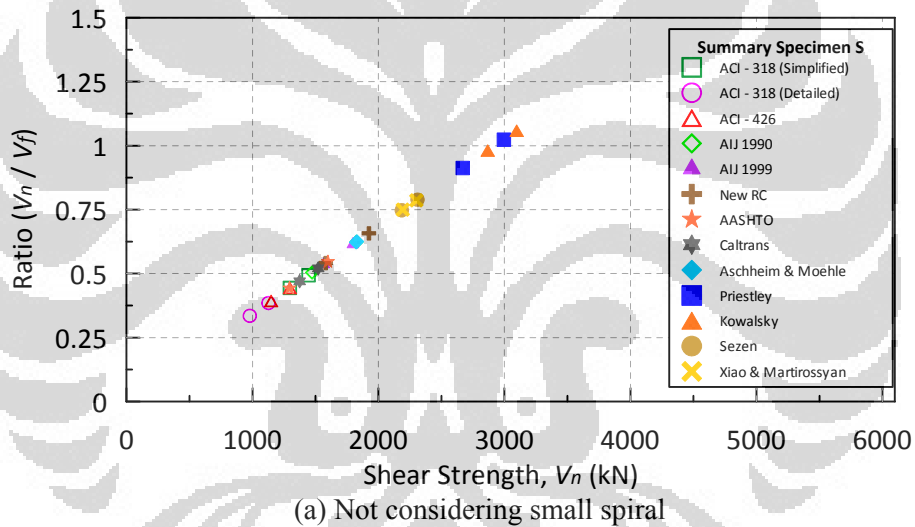
Figure 3.23 Shear Strength vs. Ratio (V_n/V_f) of type S specimens.

As shown in previous figures and Table 3.3 most of the ratios of nominal shear strength to shear at flexural failure are less than one. Certain shear models by researcher have the ratio larger than 1.00, such as: model of Priestley et.al.[20], Kowalsky and Priestley[25]. Figure 3.22 in the previous page shows the summary of specimen A and B. Type S specimen, as shown in Figure 3.23, the ratio reached 1.40, which means the prediction value of nominal shear strength is higher than the cross section analysis.

3.3.1. Effect of Axial Load Ratio
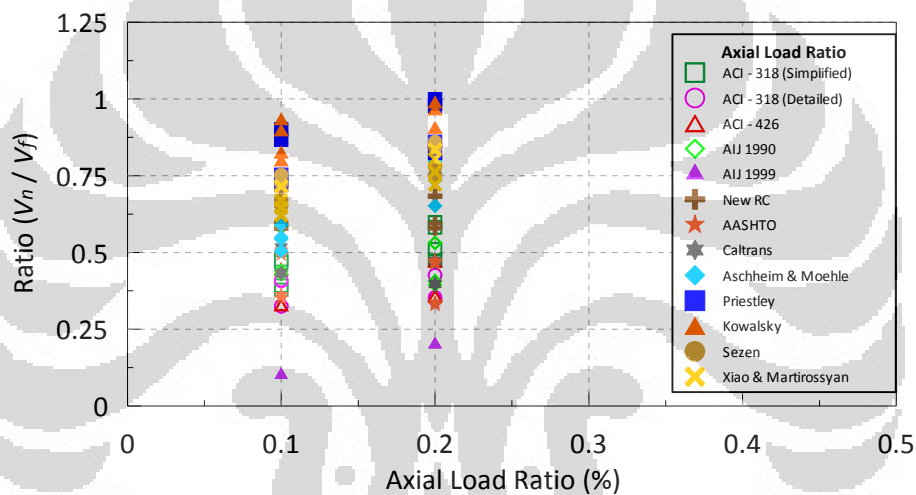
Figure 3.24 Axial load ratio's vs. Ratio (V_n/V_f) of type A and B specimens.

As the applied axial load ratio become larger, the ratio of V_n/V_f diverge too. Three methods proposed by Priestley et.al.[20]; Kowalsky and Priestley[25] and Xiao; and Martirossyan[27] use the new term V_a in shear strength calculation as shear strength provided by axial load. Figure 3.24 shows that the ratio values from these three methods are the higher.

3.3.2. Effect of Concrete Compressive Strength

Figure 3.25 shows the actual value of concrete compressive strength vs. ratio V_n/V_f. When concrete compressive strength becomes higher the ratio V_n/V_f will become higher either.
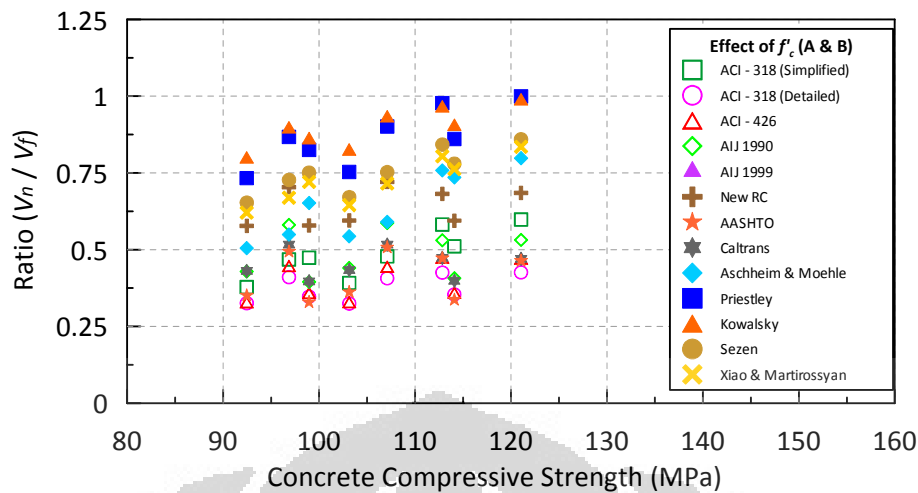
Figure 3.25 Concrete Compressive Strength vs. Ratio (V_n/V_f) of type A and B specimens.

3.3.3. Effect of Transverse Reinforcement Spacing

Larger of the spacing means the volumetric ratio of the transverse reinforcement to the concrete (ρ_s) is getting lower. Figure 3.26 and Figure 3.27 show specimens with lower of vertical spacing s have the higher ratio V_n/V_f than specimens with higher s. Since the spacing of transverse reinforcement (s) is one of the parameters of shear strength provided by transverse reinforcement (V_s) and most of the shear strength models use the similar formulation of V_s so it will be interesting to know whether the existing shear models (especially V_s component) are sufficient and quite accurate or the new developed shear models is needed.
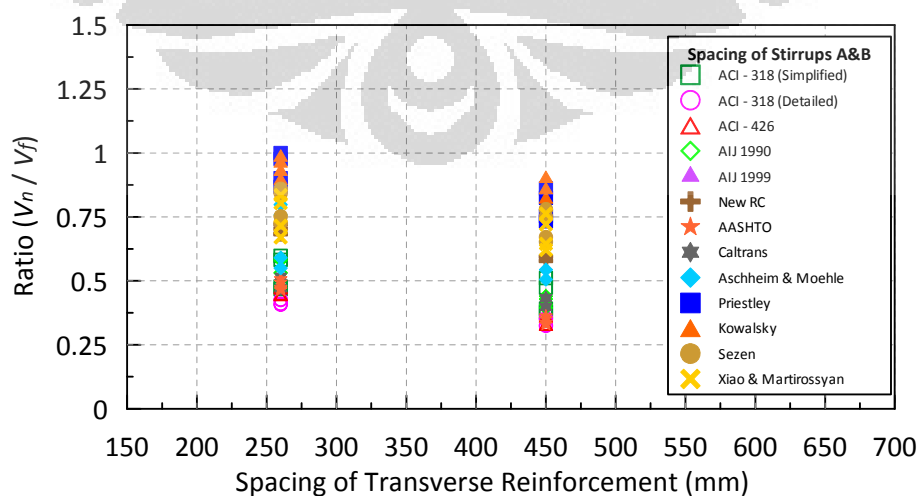
Figure 3.26 Spacing of Transverse Reinforcement vs. Ratio (V_n/V_f) of type A & B specimens.

(a) Not considering small spiral

(b) Considering small spiral
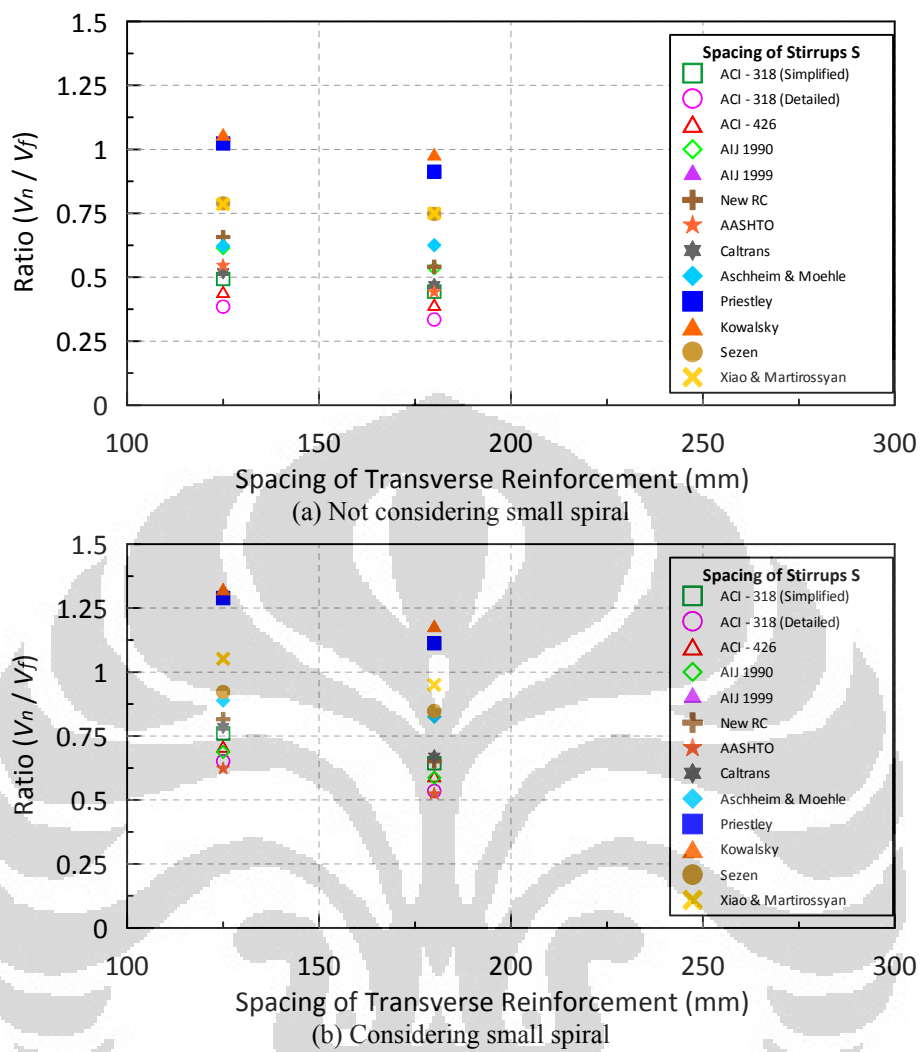
Figure 3.27 Spacing of Transverse Reinforcement vs. Ratio (V_n/V_f) of type S specimens.

CHAPTER IV
TEST PROGRAM

4.1. CONSTRUCTION OF SPECIMENS

Ten specimens were fabricated by Ruentex in Yangmei (杨梅), Taoyuan County, Taiwan. Eight specimens are designated with square hoops; the two rests are with spiral hoops.
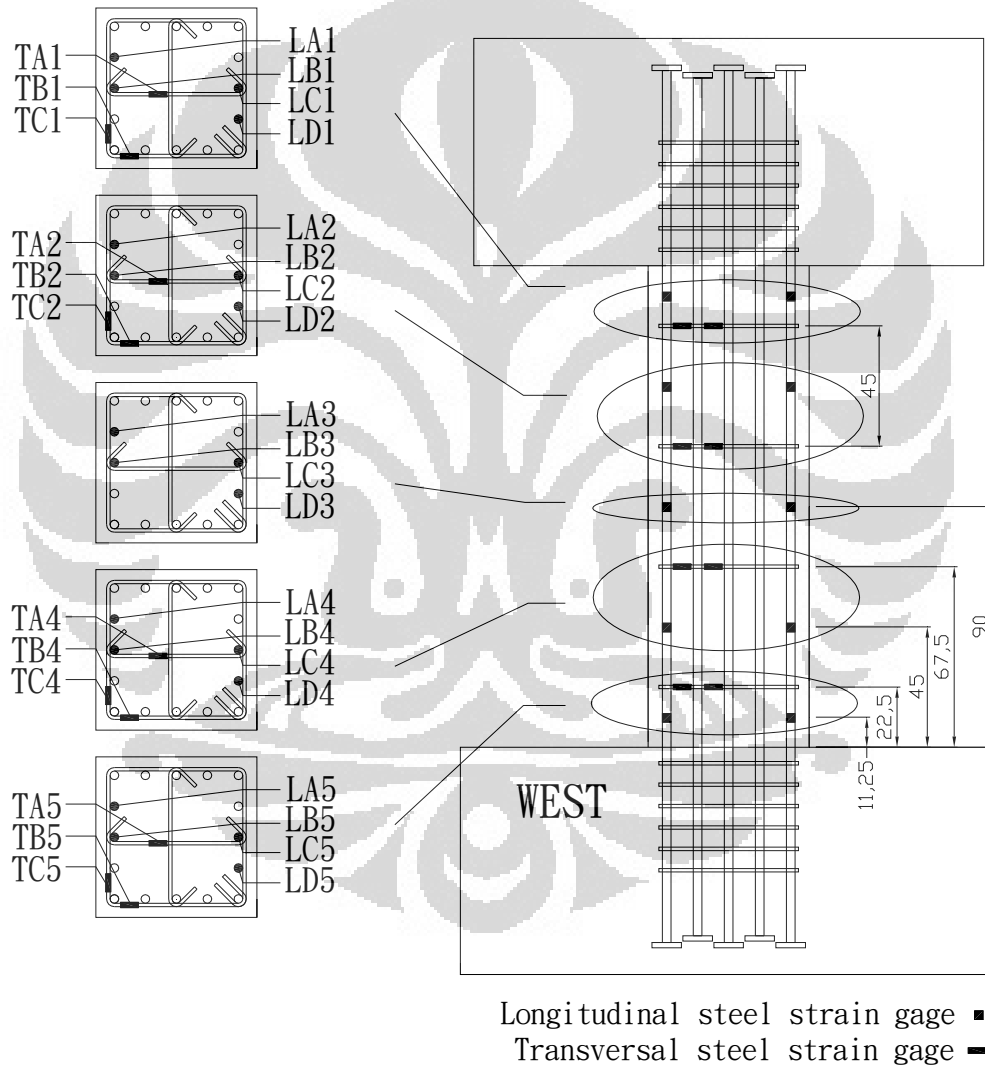
Figure 4.1 Arrangement and numbering of strain gauges on the transverse and longitudinal bars for specimens with 450 mm of transverse reinforcement spacing

A total of 252 strain gauges were attached on both longitudinal (124 strain gauges) and transversal (128 strain gauges) reinforcement in the factory. Figure 4.1

80

Arrangement and numbering of strain gauges on the transverse and longitudinal bars for specimens with 450 mm of transverse reinforcement spacing and Figure 4.2 Arrangement and numbering of strain gauges on the transverse and longitudinal bars for specimens with 260 mm of transverse reinforcement spacing show the arrangement and numbering of strain gauges for type A and B specimens. Strain gauges were attached from bottom to upper part of column.
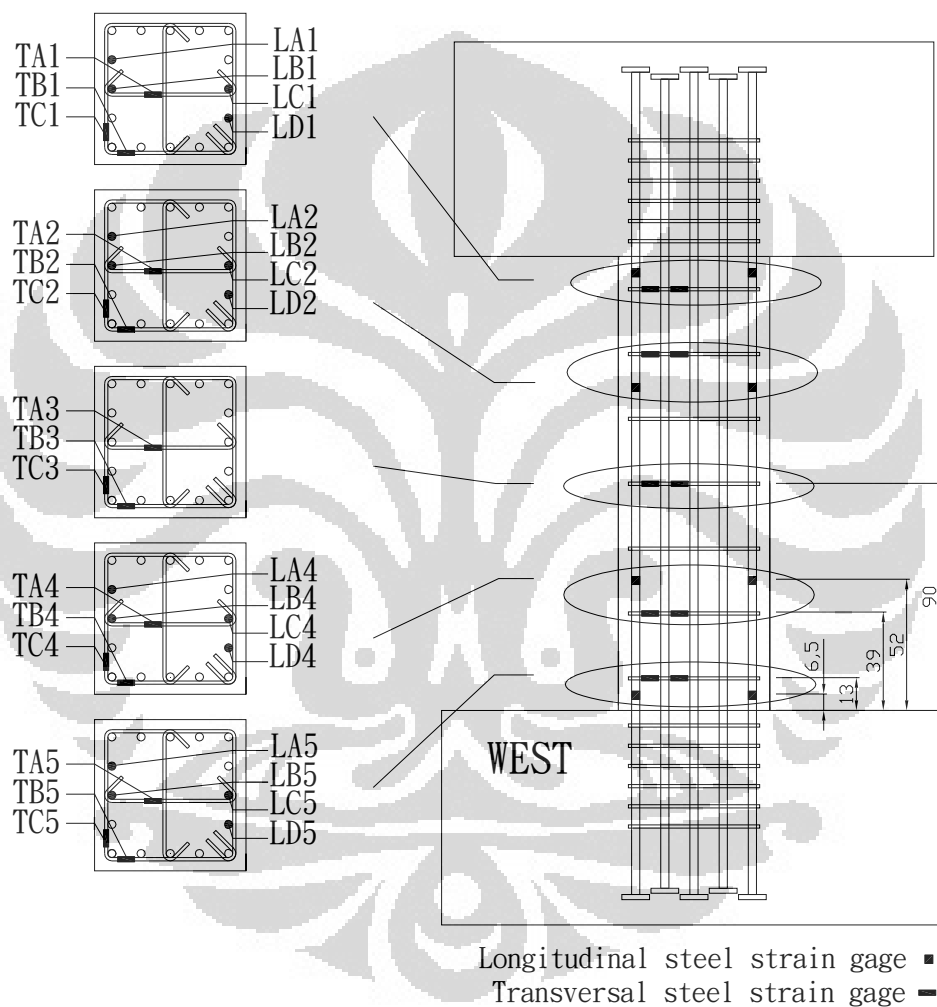
Figure 4.2 Arrangement and numbering of strain gauges on the transverse and longitudinal bars for specimens with 260 mm of transverse reinforcement spacing

A total of 24 strain gauges were attached on both longitudinal (4 strain gauges) and transversal (20 strain gauges) reinforcement in the factory for type S specimens. Strain gauges were attached only on the bottom to mid-height part of column. Figure 4.3 Arrangement and numbering of strain gauges on the transverse and longitudinal bars for

type S1 specimen with 125 mm of transverse reinforcement spacing and Figure 4.4 Arrangement and numbering of strain gauges on the transverse and longitudinal bars for type S2 specimen with 180 mm, of transverse reinforcement spacing show the arrangement and numbering of strain gauges for this type of specimen.
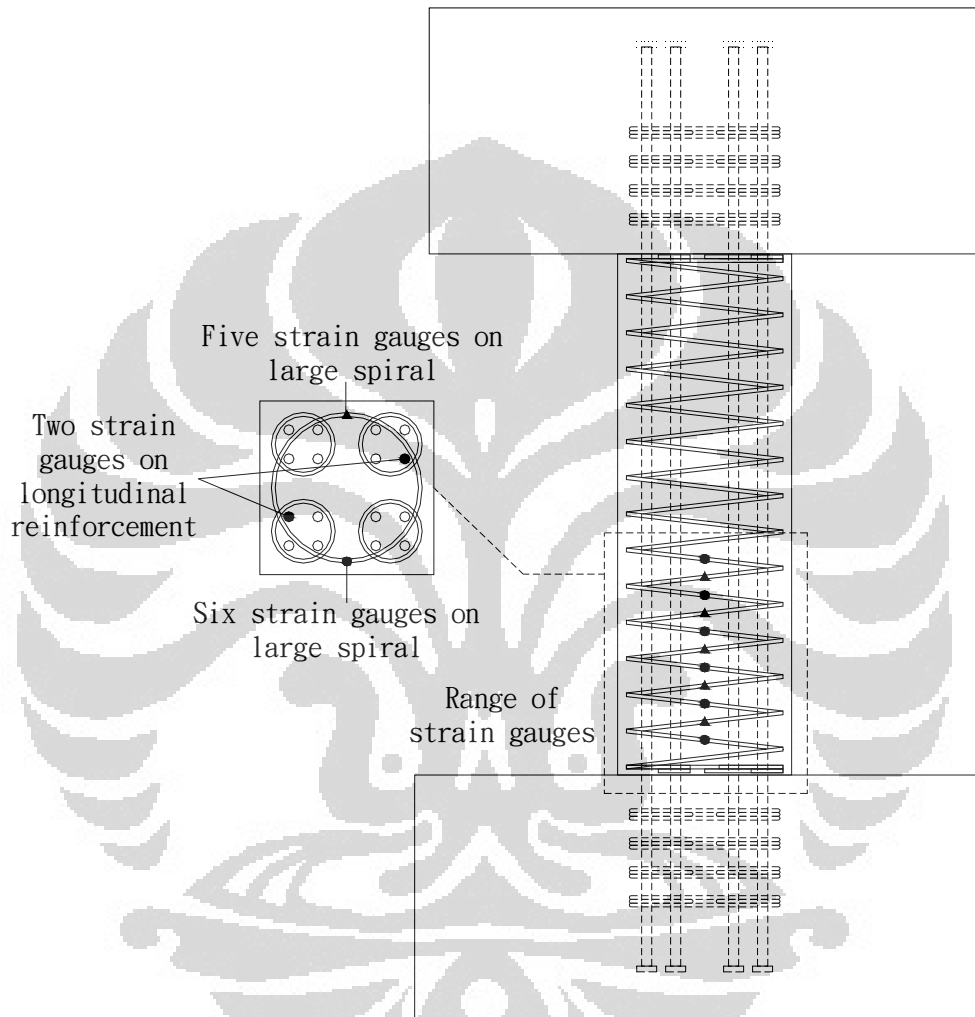
Figure 4.3 Arrangement and numbering of strain gauges on the transverse and longitudinal bars for type S1 specimen with 125 mm of transverse reinforcement spacing

A section of the bar approximately 2-3 centimeter long was filed and cleaned before attaching a strain gauge. After the strain gauges were attached and wired, they were sealed by coating agent. Then, the strain gauges were wrapped by vinylmastic to protect them from damage during concrete casting as shown in Figure 4.6 Step of attaching strain gauge to the bar. Electrical resistance strain gauges were produced by Tokyo Sokki Kenkyujo Co. Type TFLA-5 and YFLA-3 strain gauge with 5 mm and 3 mm gauge length were attached on the longitudinal and transverse reinforcement,

Universitas Indonesia

respectively.

The strain gauges were installed after rebar cage fabrication. The reinforcement cages were tied and the test specimens were constructed inside at the Ruentex manufactory. The specimens were cast in the horizontal position. First, the steel formwork was constructed. Then, the reinforcement cages were tied inside the formwork. The typical reinforcement cage is shown in Figure 4.5 Typical reinforcement cage.
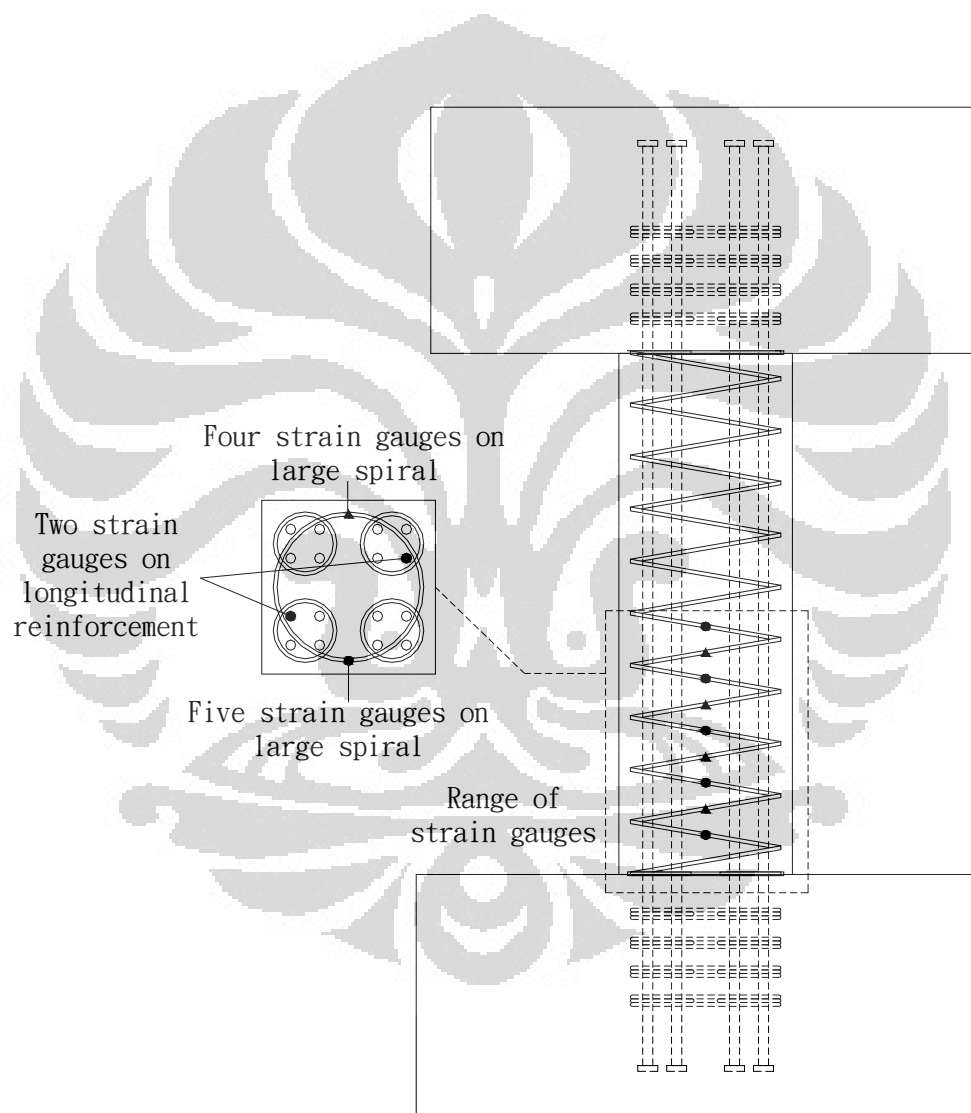
Figure 4.4 Arrangement and numbering of strain gauges on the transverse and longitudinal bars for type S2 specimen with 180 mm of transverse reinforcement spacing

<div align="center">(a)　　　　　　　　　　　　　　　　(b)</div>

Figure 4.5 Typical reinforcement cage
(a) Square hoops column; (b) Multi-spiral hoop column
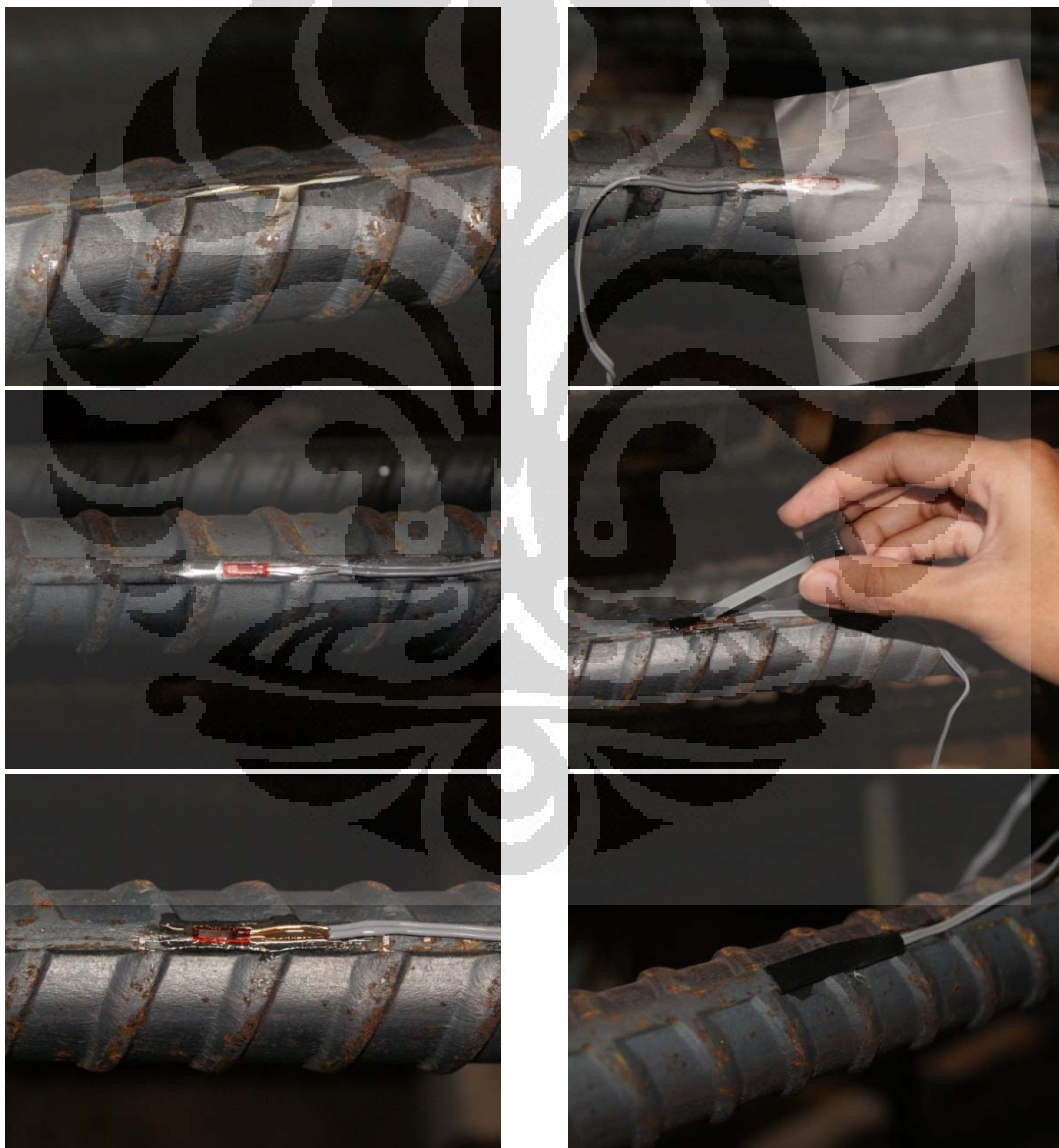
Figure 4.6 Step of attaching strain gauge to the bar

The casting of the specimens could not be done in the same time because only one steel formwork that be used. Figure 4.7 Process of casting, vibrating and curing of the specimen shows the process of casting, vibrating and curing of the specimen and Figure 4.8 Specimen ready for testing shows the specimens that ready for testing.

Figure 4.7 Process of casting, vibrating and curing of the specimen

Figure 4.8 Specimen ready for testing

4.2. TEST SET UP

The test of the specimens was performed in National Center for Research on Earthquake Engineering (NCREE) using Multi-Axial Resting System (MATS) that was built in 2007. The test setup which is shown in Figure 4.9 was used to simulate the axial and lateral loads. The MATS conducted double-curvature deformation pushover.
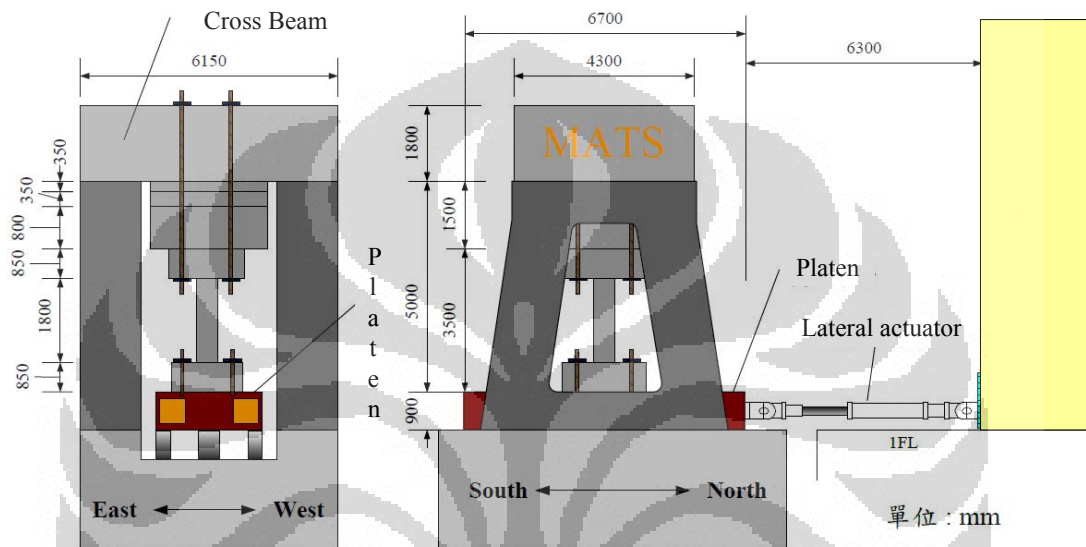
Figure 4.9 Layout of Multi-Axial Resisting System (MATS) (Kurniawan[28])
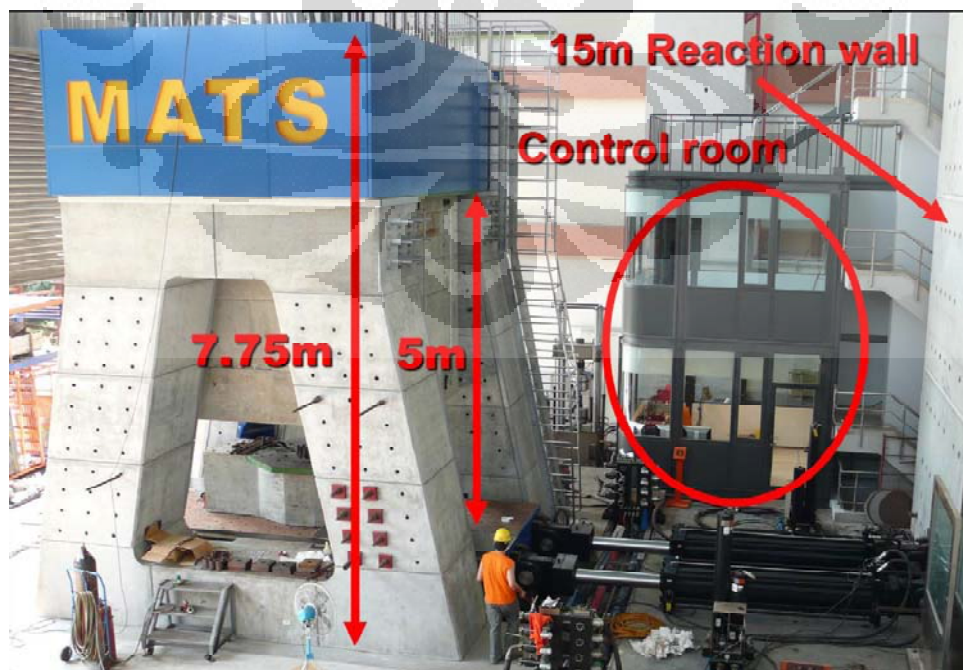
Figure 4.10 Appearance of actual MATS system (Kurniawan[28])

The maximum axial load that can be applied by MATS is 60 MN. The lateral force was set from the hydraulic actuator that placed in the bottom as shown in Figure 4.9. Some block of concrete pads can be hanged in the reaction beam (Cross beam) that placed in the top of the MATS. The total height of the MATS is 7.75 m and effective measured height is 5 mm.

The actuators could be used under either load control or displacement control depending on the input command. The horizontal actuator was controlled by a prescribed horizontal displacement history. For all of the specimens, the axial load was maintained constant.

4.3. APPLIED LOADING

Type B columns were tested under low axial load ratio (20 %) and type S columns were tested under 10 % load ratio. All of these six specimens were tested under the same applied lateral loading; Figure 4.11 below shows the lateral loading protocol. Each level of drift ratio was applied in three cycles. During the test, the displacement controlled was applied to the load platform; therefore, the value measured from the column tested could be different.
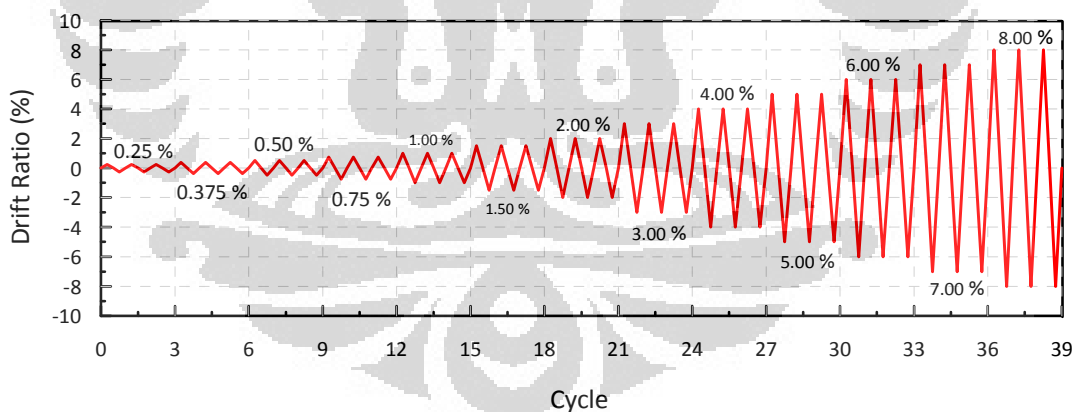
Figure 4.11. Applied lateral loading.

4.4. INSTRUMENTATIONS AND MEASUREMENTS OF LOAD, STRAIN AND DISPLACEMENTS

Two kinds of measurements system such as mechanical measurement and image measurement were attached on the columns to measure the lateral displacement. Those instrumentations can support one to another and also can be a backup data if some problems happen during the test.

Figure 4.12 shows the configuration detail of instrumentation and measurement of displacement. The position of strain measurement has been described in Figure 4.1 to 4.4. During each test, fifty eight channels of data were recorded. Two load cells, two MTS, thirty five strain gauges, twelve LVDT (linear Voltage Displacement Transducer) and seven rotation gauges were used for the load strain and displacement measurement.
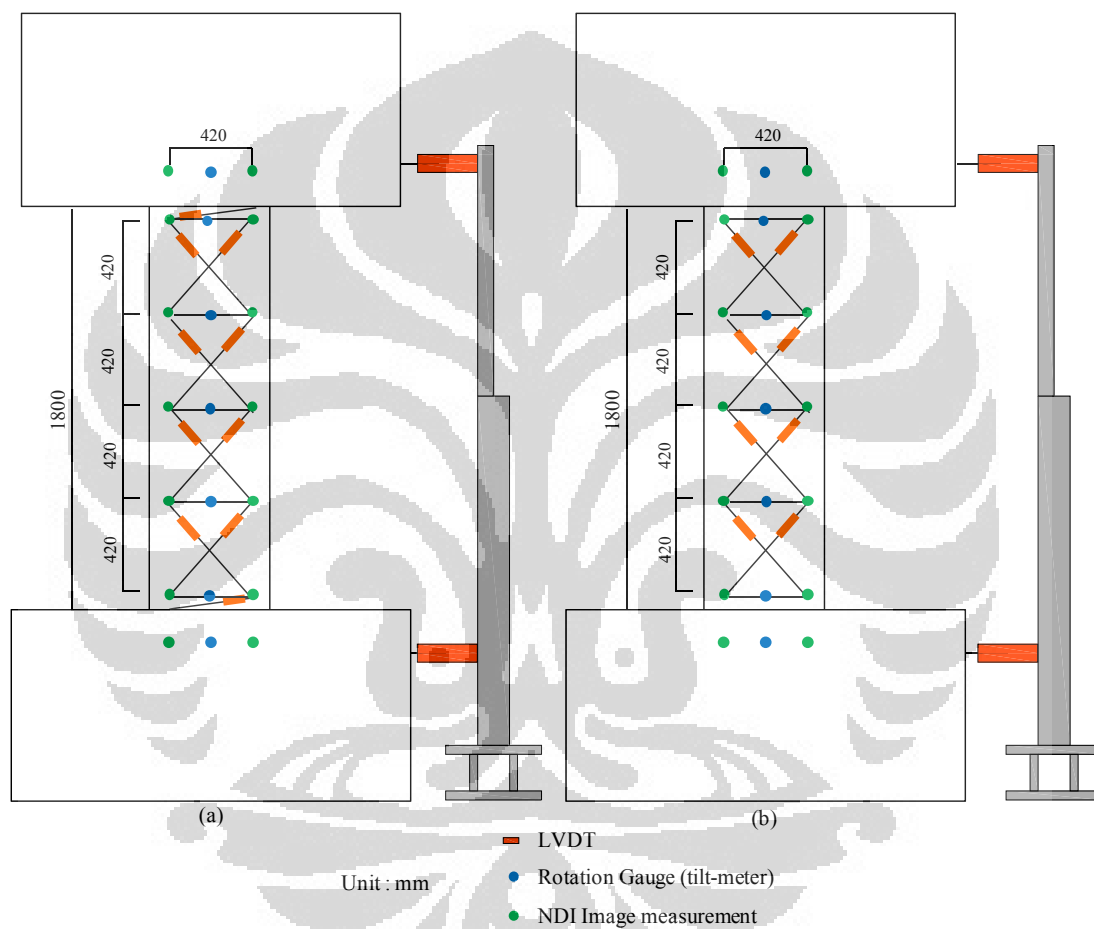
Figure 4.12 Instrumentation and measurement of displacement (a) Configuration for Type B specimens; (b) Configuration for Type S specimens

At the both top and bottom blocks in the north side two LVDT and rotation gauges were installed and have 5 cm toward the end of the column. Ten LVDT and five rotation gauges were install along the column with 42 cm in distance except the two LVDT in the top and bottom of the column which have 6 cm toward the end of the column as shown in Figure 4.12. The LVDT along the column were used to measure the shear displacement. The rotation gauges were used to measure the curvature along the column due to flexure and can be used to calculate the flexural

displacement. The instrumentation setup of the specimen is shown in Figure 4.13.

(a)   Rotation gauge in bottom block

(b)   LVDT in bottom block

(c)   LVDT and rotation gauge in column

(d)   LVDT in top and bottom block
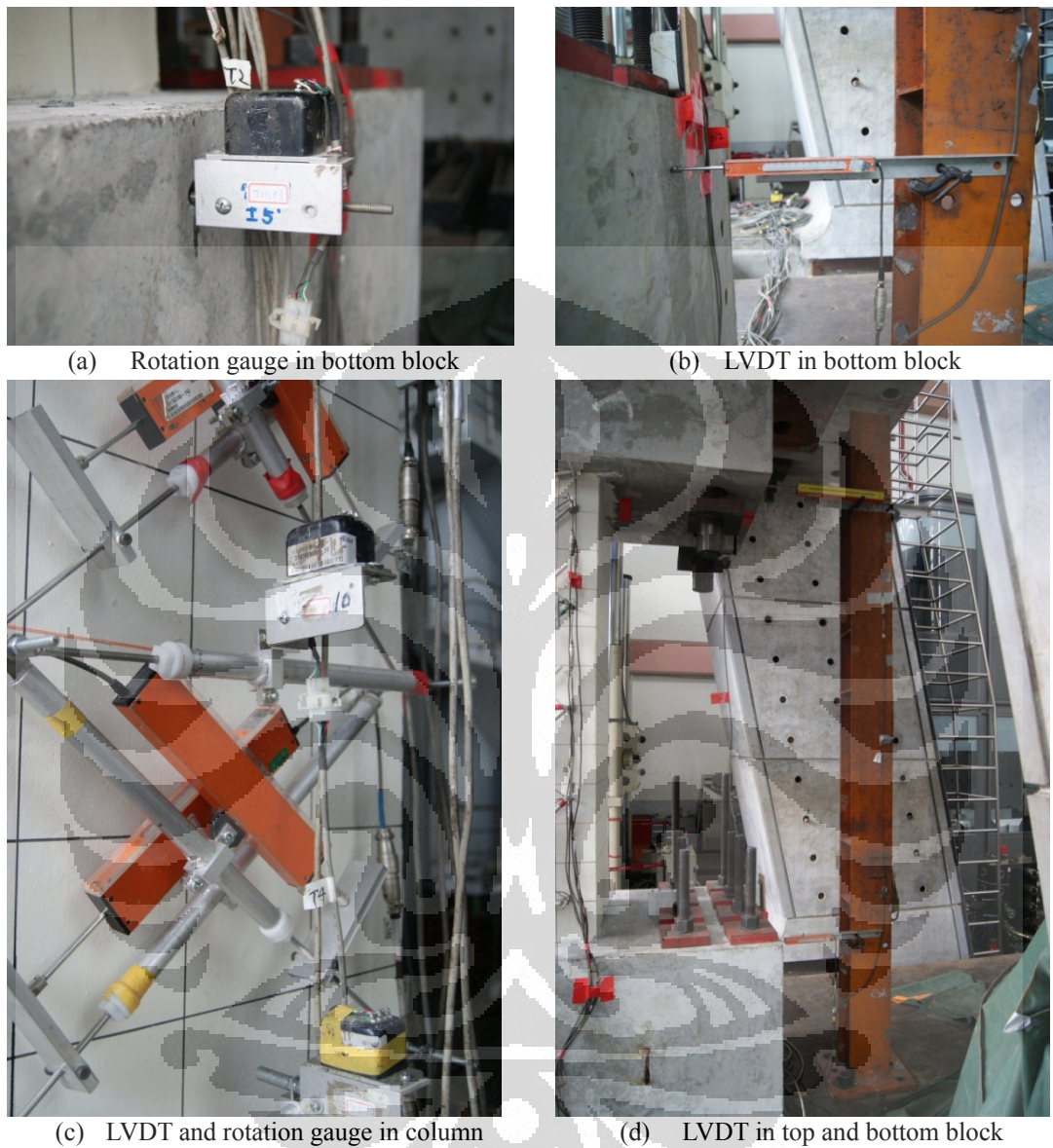
Figure 4.13 The instrumentation of LVDT and rotation gauges in Column and Top-bottom block

The NDI image system was used to measure displacement during the test. The NDI can record three dimensional movement of the marker that attached to the column. The 3D image measurement consists of NDI Optical Measurement System, Base Stand, Marker Stober and Small Diameter Marker as shown in Figure 4.14. Fourteen markers were used and attached on the column as depicted in Figure 4.15.

Universitas Indonesia

(a) NDI Optical Measurement System   (b) Base Stand

(c) Marker Strober   (d) Small Diameter Marker

Figure 4.14 NDI Optical Measurement System (courtesy of www.ndigital.com)

As mentioned before, the set up of the measurement and instrumentation were slightly different for two types of columns as shown in Figure 4.15. Type B specimen have 10 LVDT attached on the column while only 8 LVDT attached for type S specimen. The instrumentations include LVDT, rotation gauge and NDI markers in the column and top-bottom block.

(a)   (b)

Figure 4.15 The instrumentation setup
(a) Type B specimen; (b) Type S specimen

CHAPTER V
TEST RESULTS AND DISCUSSIONS

Test result of six specimens will be discussed in this chapter. As mentioned before, there are two types of specimens: four specimens of type B (columns with square hoops) and two specimens of type S (columns with multi-spiral hoops). The following sections will discuss about the material strength, the applied axial load, response and observation of each specimen. The damage behavior of the specimens will be discussed based on visual observations and recorded test data from instrumentation.

5.1. MATERIAL STRENGTH

Material samples were tested before the test. Table 5.1 below shows the concrete compressive strength (f'_c) for six specimens.

Table 5.1 Concrete compressive strength of six specimens.

Specimen	Spacing s (mm)	Sample	Design Strength f'_c (MPa)	Test Strength f'_c (MPa)	Average f'_c (MPa)
B1	450	No. 1	70	97.40	98.95
		No. 2		103.10	
		No. 3		96.35	
B2	450	No. 1	100	115.58	114.10
		No. 2		92.23	
		No. 3		134.48	
B3	260	No. 1	70	111.14	112.85
		No. 2		117.58	
		No. 3		109.83	
B4	260	No. 1	100	131.23	121.04
		No. 2		111.43	
		No. 3		120.47	
S1	125	No. 1	100	123.40	117.57
		No. 2		101.83	
		No. 3		127.48	
S2	180	No. 1	100	123.40	117.57
		No. 2		101.83	
		No. 3		127.48	

As indicated in the Table 5.1 above, the actual strength is significantly larger than the design. In the preliminary design, the (f'_c) of specimen B1 and B3 are 70 MPa, and

the (f'_c) of specimen B2 and B4 are 100 MPa. Moreover, the difference of the actual concrete compressive strength (f'_c) from specimen B1 and B3 is very significant. The actual value of B3 is 42.85 MPa larger than its design value. On the other hand, the actual value of specimen B4 only 10.55 MPa larger than its design value.

Table 5.2 below shows the yield and ultimate strength of both transverse and longitudinal reinforcement. D13 (#4) of transverse reinforcement type SD 785 has yield strength (f_y) of 862 MPa and ultimate strength of 1052 MPa. D32 (#10) of transverse reinforcement type SD 685 has yield strength (f_y) of 735 MPa and ultimate strength of 951 MPa. Multi-spiral specimens have two types of transverse reinforcement: large and small spiral. The properties of large spiral reinforcement are indicated in Table 5.2 named transverse rebar.

Table 5.2 Strength of SD 785 and SD 685 high strength rebars.

Rebar	Type	Size	f_y (MPa)	f_u (MPa)
Transverse	SD 785	D13 (#4)	862	1052
Longitudinal	SD 685	D32 (#10)	735	951

5.2. APPLIED AXIAL LOAD

Four columns B1, B2, B3 and B4 were tested using 20 % of axial load ratios. On the other hand, two spiral column specimens, S1 and S2, were tested using 10% of axial load ratios. Table 5.3 below shows the exact axial load that was applied to all six columns.

Table 5.3 Concrete compressive strength and axial load of columns.

Specimen	B1	B2	B3	B4	S1	S2
f'_c (MPa)	98.95	114.10	112.85	121.04	117.57	117.57
Axial Load (kN)	7124.530	8214.87	8125.14	8715.11	4232.49	4232.49

5.3. TEST OF THE SPECIMENS

Six specimens were tested by applying the same cyclic increments of lateral displacements as described in previous chapter. There are several objectives of testing the specimens. Identifying the contribution of the transverse reinforcement and the high strength material to the strength of column will be the first objective since the parameter varied in the distance of vertical spacing of transverse

reinforcement and also the concrete compressive strength. Another objective is recognizing the damage level of the column due to elastic shear strength based on observation and the data obtained from the test. The effect of P-Δ will be taken out from the result.

5.4.1. Column B

There are four columns type B, column B1 and B2 which have 450 mm vertical spacing of hoop; column B3 and B4 with 260 mm vertical spacing.

5.3.2.1. Column B1

Specimen B1 was subjected to constant compressive axial load of 7124.53 kN ($0.2\,f'_c\,A_g$ where f'_c = the concrete compressive strength and A_g is the gross cross-sectional area) and cyclic increments of lateral displacements as described in chapter 4.

During the initial displacement cycles of 0.25 % drift ratio, the flexural cracks (width of less than 0.05 mm) developed near the top and bottom of the column (around 15 cm length). At this displacement level, no cracks were observed around the mid-height region of the column (see Figure 5.1). The width of the cracks became larger as 0.10 mm for 0.375 % and 0.50 % drift ratio. The number of the cracks increased as the number and magnitude of the displacement cycle increased.

The shear cracks started to develop at 0.75 % drift ratio (width crack of 0.15 mm) and soft cracking sound was heard. The initial shear cracks developed in the bottom of the column continued from the flexural crack with crack angle approximately 45°. Until the end of the third cycle of 0.75 % drift ratio, the shear crack was not found on the mid-height of column (see Figure 5.3).

In the first cycle of 1.00 % drift ratio (positive direction), a hard cracking sound was heard simultaneously with the developing of a large diagonal shear crack from the right hand of upper part to the left hand of bottom part from west face (width crack of 0.40 mm). Moreover, another two shear crack was developed parallel to the large one with width crack of 0.15 mm, and the rest of the flexural crack is reaching to 0.25 mm of width.
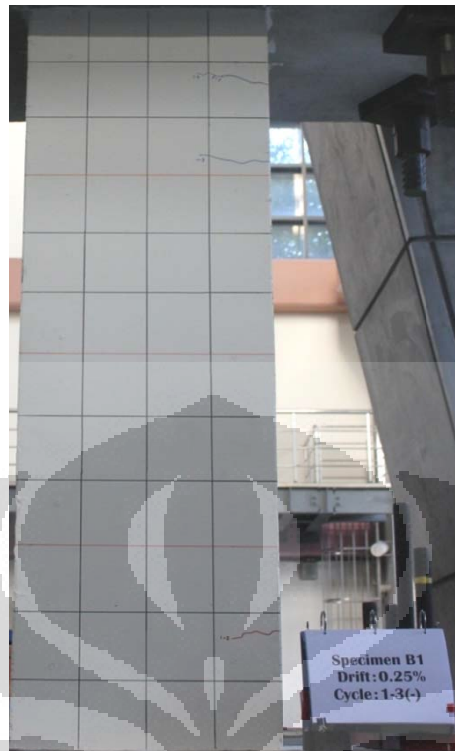
Figure 5.1 Flexural cracks during the initial displacements of column B1 (west side).
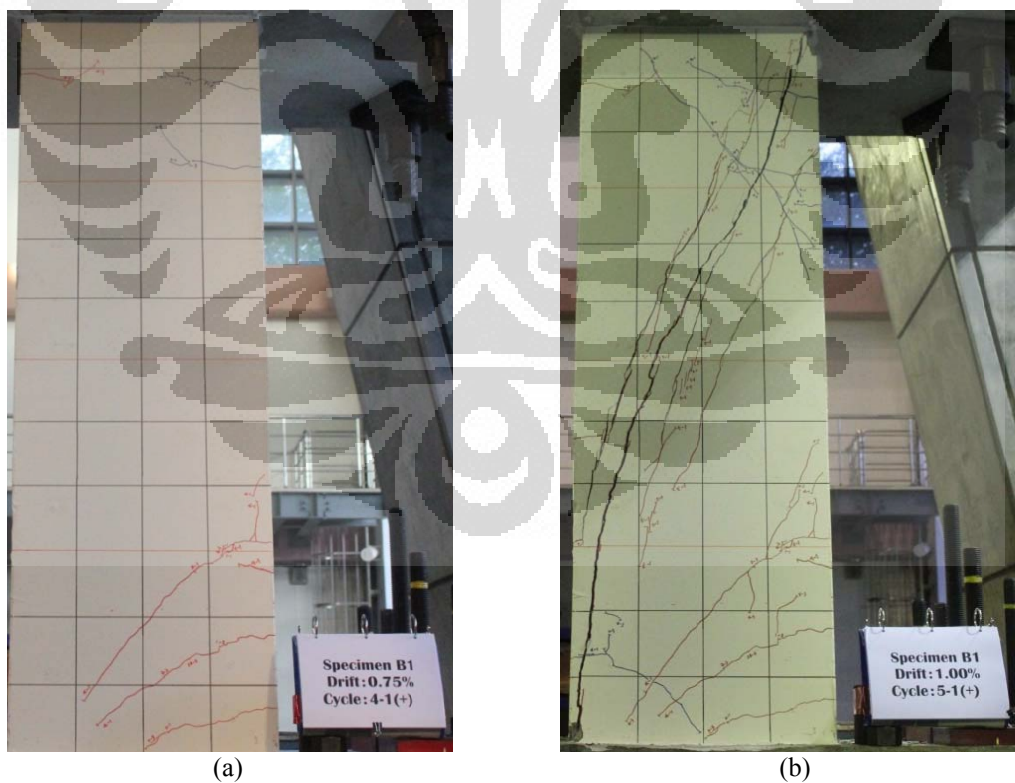
| (a) | (b) |

Figure 5.2 Shear crack column B1
(a) First shear crack at 0.75 % drift ratio (west side); (b). Large diagonal shear crack at the first cycle
of 1.00 % drift.

Universitas Indonesia

During the second cycle of 1.00 % drift ratio, as the specimen was laterally forced for the second time, at around the diagonal shear crack, the cover concrete started to spall. The number of shear cracks increased as the number and magnitude of the displacement cycle increased. The test was stopped at 1.5 % drift ratio with the condition noticed almost all the cover concrete spalled, particularly in the mid-height part of west and east face after an explosive sound was heard. Bending of the longitudinal reinforcement appeared as the failure of transverse reinforcement. Furthermore, some part of concrete inside the reinforcement was broken to pieces.

Figure 5.4 shows the hysteretic loop of Column B1. This figure also noted several important points that indicate starting point of flexural and shear crack, maximum strength, loss of lateral strength, first yield of the transverse reinforcement, big explosive sound and also 20% drop of ultimate strength. Table 5.4 below mentions the exact value of these seven points and their drift level. After reaching the maximum strength which firstly happened at the second cycle of 0.75 % drift ratio (1815.70 kN, negative direction) and secondly at the first cycle of 1.00 % drift ratio (2184.94 kN, positive direction), these values declined to 1932.61 kN and 1011.24 kN in the next cycle. Strain gauges data recorded that the maximum point of transverse reinforcement occurred at the same cycle of the maximum strength point (cycle 4-2).

Table 5.4. Important points of column B1

Points	Displacement (mm)	Lateral load (kN)	Cycle / drift ratio
First flexural crack	2.55	728.73	Cycle 1-3 (0.25 %)
	-1.65	-790.10	Cycle 1-3 (0.25 %)
First shear crack	8.88	1980.10	Cycle 4-1 (0.75 %)
	-7.41	-1797.47	Cycle 4-1 (0.75 %)
Maximum strength	11.16	2184.94	Cycle 5-1 (1.00 %)
	-7.47	-1815.70	Cycle 4-2 (0.75 %)
Loss lateral strength	25.08	611.41	Cycle 6-1 (1.50 %)
	-15.36	-739.99	Cycle 5-1 (1.00 %)
Explosive sound	14.67	1228.63	Cycle 5-1 (1.00 %)
Maximum strain	8.94	1952.34	Cycle 4-2 (0.75 %)
20% drop of lateral strength	12.76	1747.96	After Cycle 5-1 (1.00 %)
	-9.80	-1452.56	After Cycle 4-2 (0.75 %)

Figure 5.5 depicts the envelopes for each cycle. The first two cycles have passed up

to 1.50 % drift ratio while another one has passed up to 1.00 % drift ratio only.
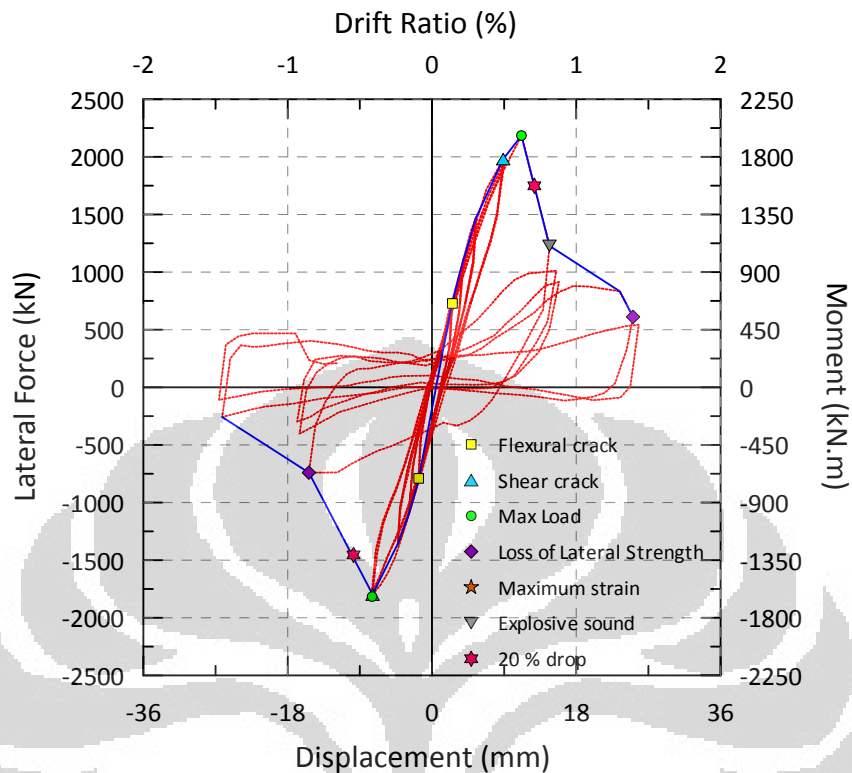
Figure 5.3 Lateral load-Displacement relationship of column B1
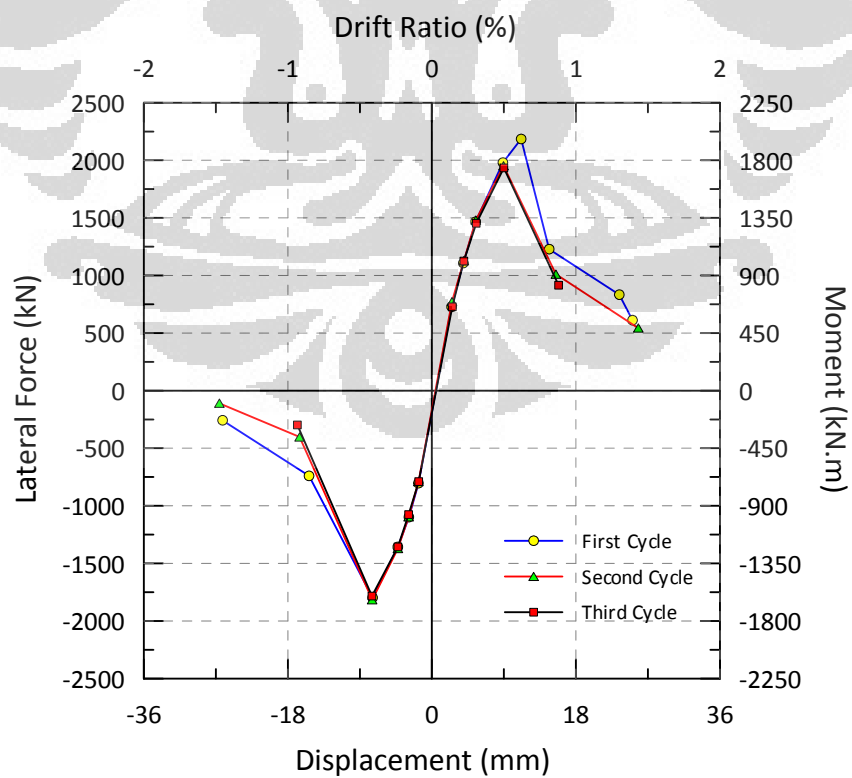
Figure 5.4 Envelope of column B1.

The location of the strain gauge and the strain reading of the reliable strain gauge (red color) during the minimum strength cycle 4-2 could be seen in the figure 5.5 below. The black color means unreliable strain reading or malfunction of the strain gauge. This figure can be clearly seen that small cracks on the top and the bottom of the column did not pass through strain gauges. Strain reading in TA4 and TC 5 are mostly very small, around 0.0006 for both locations. On the other hand, strain reading in TA1 indicates big enough value of strain reading 0.00110 that could be happened due to small crack on the top of the column. No reliable strain reading installed in transverse reinforcement indicated a yielding of the hoops.
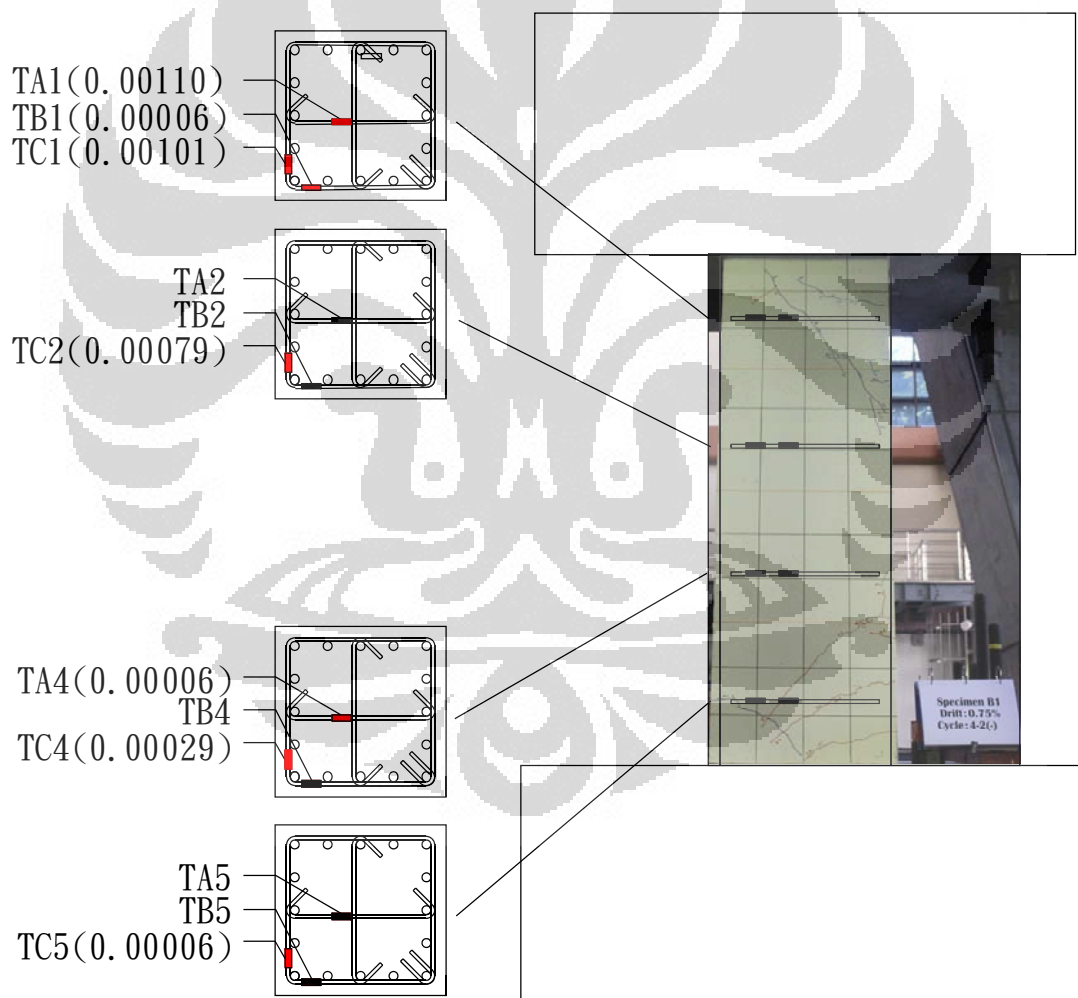
Figure 5.5 Strain reading and crack pattern of column B1 at the peak/maximum strength (negative directions).

The location of the strain gauge and the strain reading of the reliable strain gauge during the maximum strength cycle 5-1 could be seen in the Figure 5.6 below. As we

could see in this figure, diagonal shear crack passed through some strain gauges, such as TB2, TC2, TB4, TC4 and TC5. Strain reading in TC2 and TC5 recorded the high enough value of maximum strain reading, consecutively, 0.00236 and 0.00257 that could be happened due to large diagonal shear crack. The crack leads the cover concrete to spall and the movement of this cracked concrete deformed the hoop. Strain gauges in TA1 and TC1 recorded some small cracks occurred on the top of the column but not as significant as the large diagonal shear crack. No reliable strain reading installed in transverse reinforcement indicated any yielding of the hoops.
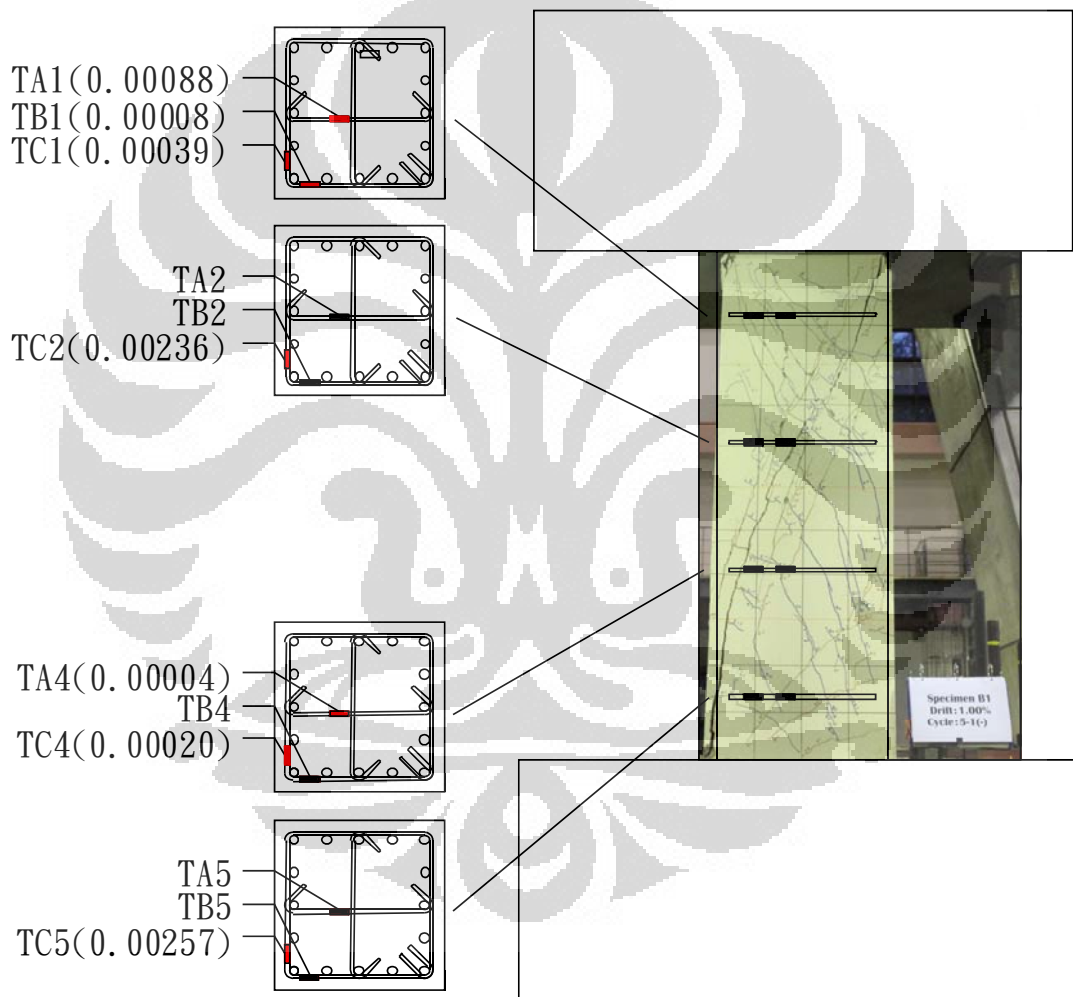
Figure 5.6 Strain reading and crack pattern of column B1 at the peak/maximum strength (positive directions).

Figure 5.7 below shows the final stage of column B1. As shown in this figure, most of the cover concrete in the mid-height of column spalled. Transverse reinforcement in two different levels fractured. As mention before, a hard cracking sound was heard at 1.00 % drift ratio, which was expected as a result of the fracture hoop.

Universitas Indonesia
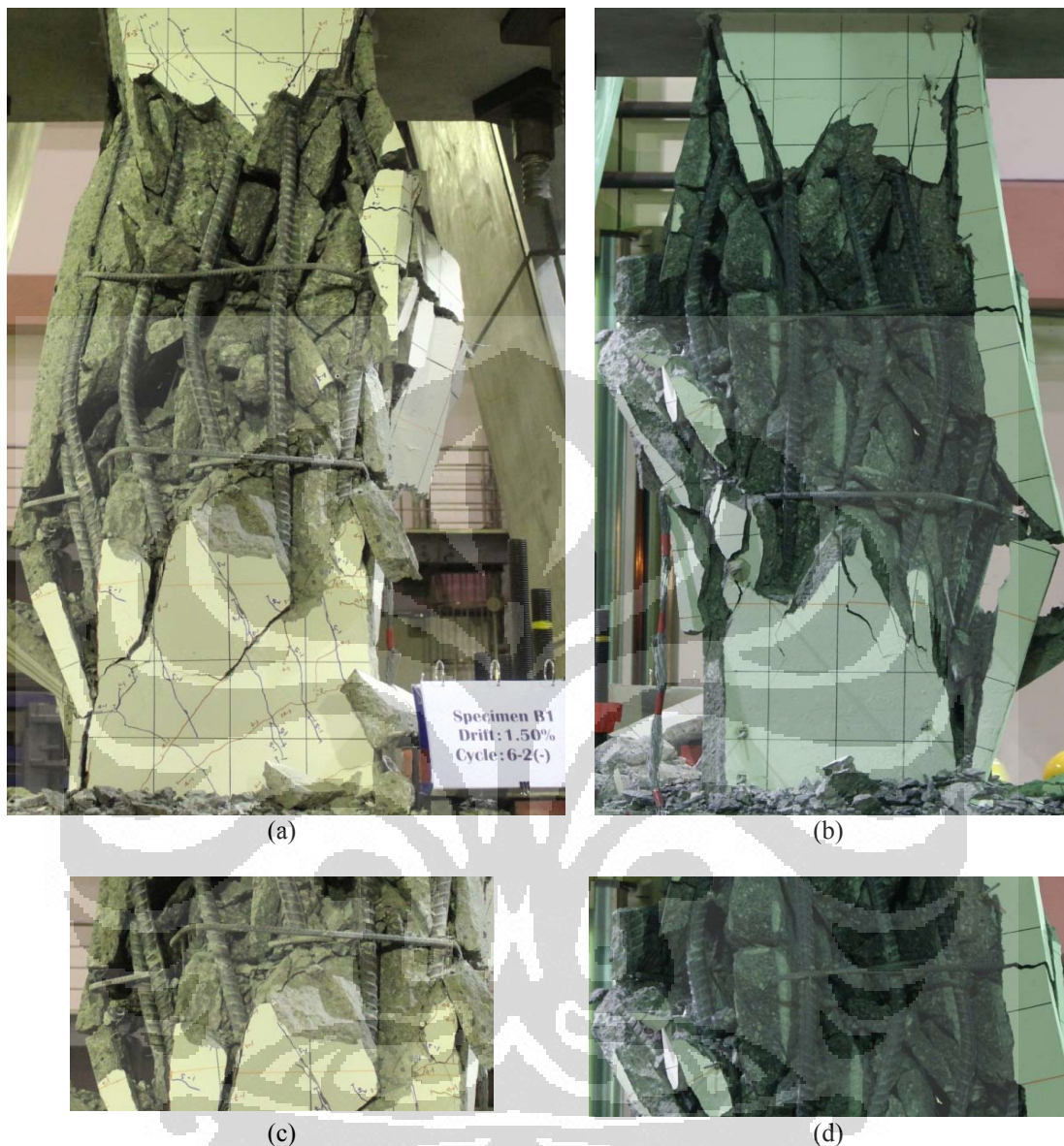
Figure 5.7 Final stage of column B1 (1.5% drift ratio).
(a) At 1.5 % drift ratio (west side); (b) At 1.5 % drift ratio (east side); (c) Failure of transverse reinforcement at height of 67.5 cm from the bottom of the column (west side); (d) Failure of transverse reinforcement at height of 112.5 cm from the bottom of the column (east side).

5.3.2.2. Column B2

Specimen B2 was subjected to constant compressive axial load of 8214.87 kN ($0.2\, f'_c\, A_g$ where f'_c = the concrete compressive strength and A_g is the gross cross-sectional area) and cyclic increments of lateral displacements as described in chapter 4.

During the initial displacement cycles of 0.25 % drift ratio, the flexural cracks (width of less than 0.05 mm) developed near the top of the column in south side (around 60

cm length). At this displacement level, no cracks were observed around the mid-height region of the column. The width of the cracks remained the same for 0.375 % drift ratio. Moreover, it became larger as 0.05 mm for 0.5 % drift ratio. The number of the cracks increased as the number and magnitude of the displacement cycle increased.

(a)   (b)

Figure 5.8 Flexural cracks during the initial displacements of column B2.
(a) First flexural crack in west side; (b) First flexural crack in south side.

The shear cracks started to develop at 0.75 % drift ratio (width crack of 0.15 mm) and the cracking sound was heard. The initial shear cracks developed in the bottom and right hand side of the column continued from the flexural crack with crack angle approximately 45°. In the second cycle the crack appeared in the top of the column. In the end of the third cycle of 0.75 % drift ratio, the shear crack was not found in the mid-height.
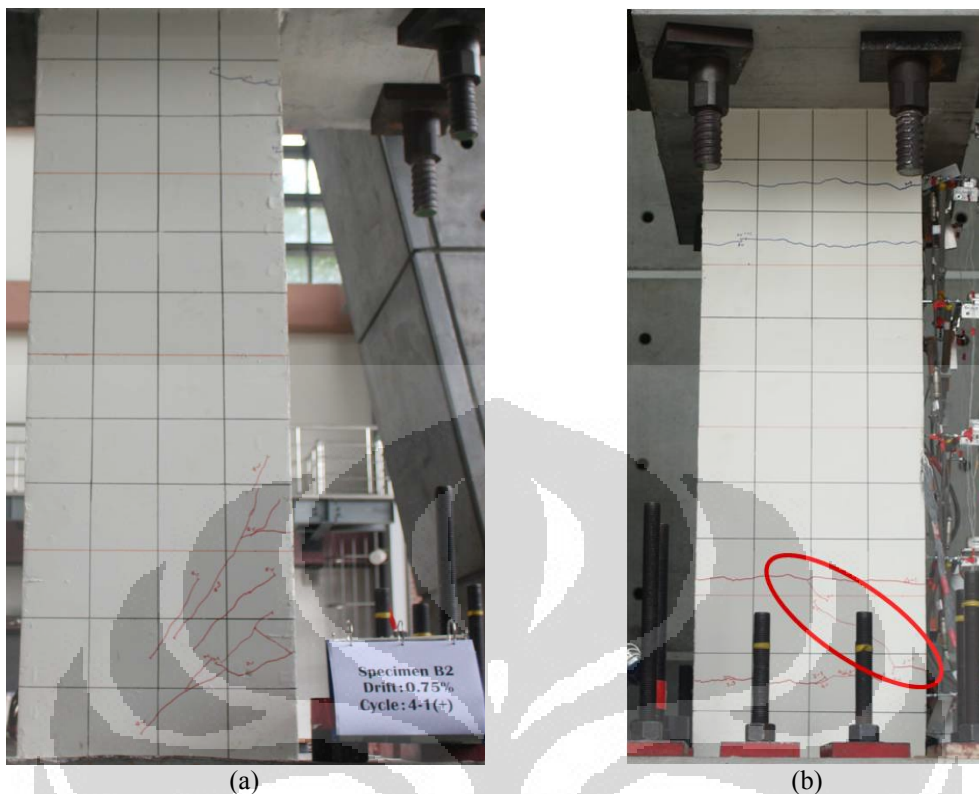
Figure 5.9 First shear crack at drift 0.75 % width crack of 0.15 mm column B2.
(a) West side; (b) South side.

In the first cycle of 1.00 % drift ratio (positive direction), a hard cracking sound was heard simultaneously with the developing of a large diagonal shear crack from the right hand of upper part to the left hand of bottom part from west face (width of shear crack maximum 5.0 mm). Moreover, another two shear crack developed parallel to the large one with width crack of 2.0 mm, and the rest of the flexural crack is reaching to 0.15 mm of width. After this first cycle of testing, all the measurement tools attached to the column were uninstalled.

At the negative direction stage of the first cycle, as the specimen was laterally forced on the opposite direction, the cover concrete started to spall especially in south side. The number of shear cracks increased as the number and magnitude of the displacement cycle increased.

The test was stopped at the end of the second cycle of 1.00 % drift ratio with the condition noticed almost all the cover concrete spalled, particularly in the mid-height part of west and east face after an explosive sound was heard. Bending of the longitudinal reinforcement appeared and the failure of transverse reinforcement did not occur. Furthermore, some part of concrete inside the reinforcement was broken to

pieces.

(a)   (b)
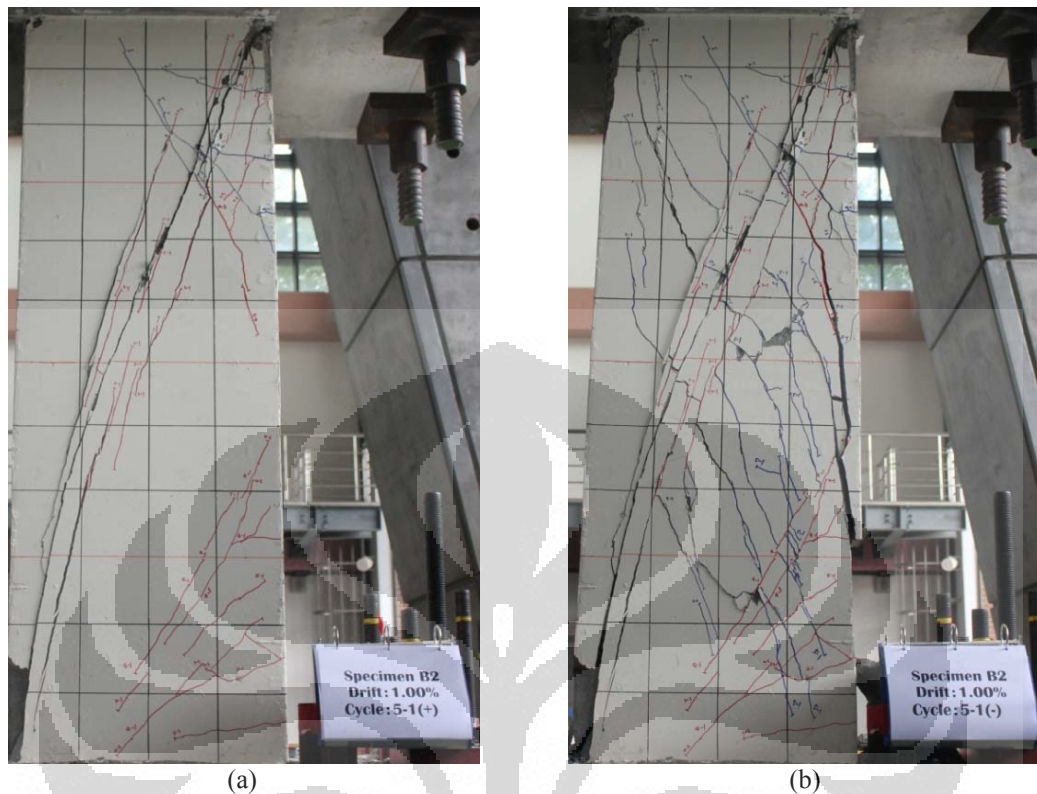
Figure 5.10 Large diagonal shear crack of column B2 (1.0% drift ratio) in west side.
(a) Positive direction in first cycle; (b) Negative direction in first cycle.

Figure 5.11 shows the hysteretic loop of Column B2. This figure noted several important points that indicate when the flexural and shear crack started to develop, maximum strength loss of lateral strength, big explosive sound and also 20% drop of ultimate strength. Table 5.5 below shows the summary of these seven important points. After reaching the maximum strength which firstly happened at the first cycle of 0.75 % drift ratio (2139.68 kN, negative direction) and secondly at the first cycle of 1.00 % drift ratio (2202.54 kN, positive direction), these values declined significantly to 653.01 kN and 1146.68 kN in the next cycle. The first yield of the transverse reinforcement occurred at the same time with the loss lateral strength and the point which explosive sound was heard. Figure 5.12 depicts the envelopes for each cycle where the first cycle reached up to 1.00 % drift ratio while two others are up to 075 % drift ratio only.
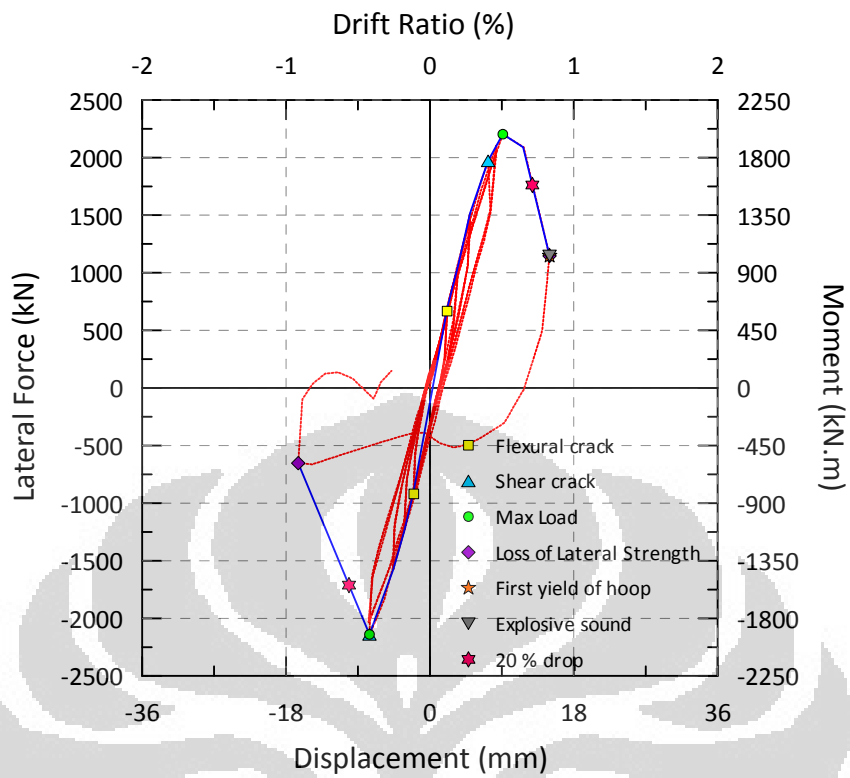
Figure 5.11 Lateral load-Displacement relationship for column B2
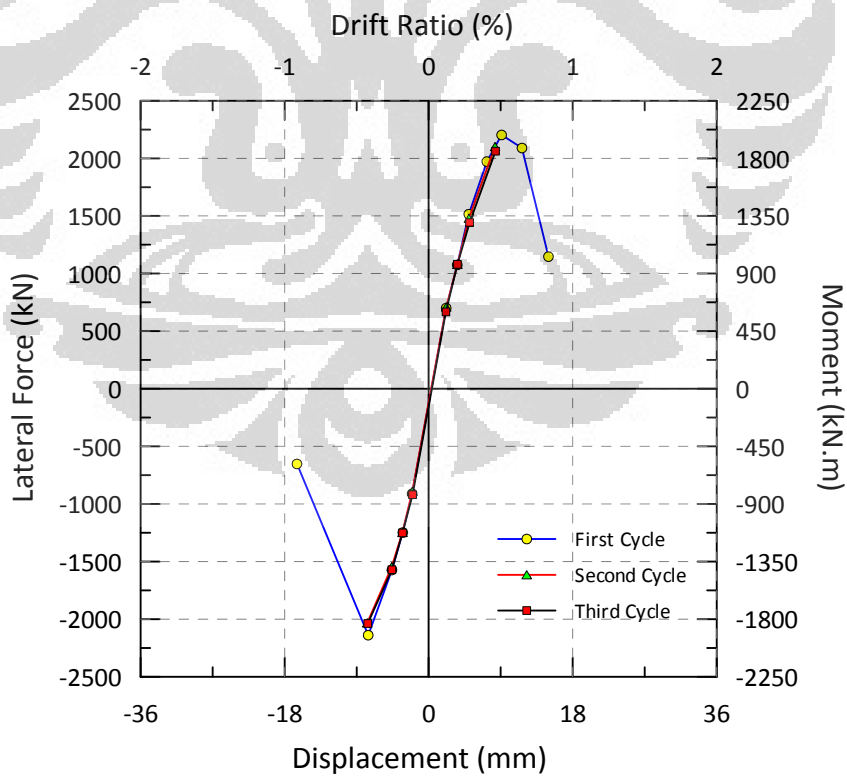
Figure 5.12 Envelope of column B2.

Table 5.5. Important points of column B2

Points	Displacement (mm)	Lateral load (kN)	Level of drift ratio
First flexural crack	2.16	666.34	Cycle 1-3 (0.25 %)
	-2.01	-919.54	Cycle 1-3 (0.25 %)
First shear crack	7.59	1530.50	Cycle 4-1 (0.75 %)
	-7.56	-2139.68	Cycle 4-1 (0.75 %)
Maximum strength	9.12	2202.54	Cycle 5-1 (1.00 %)
	-7.56	-2139.68	Cycle 4-1 (0.75 %)
Loss lateral strength	14.97	1146.68	Cycle 6-1 (1.50 %)
	-16.47	-653.01	Cycle 5-1 (1.00 %)
Explosive sound	14.97	1146.68	Cycle 5-1 (1.00 %)
1st Yield of hoop	14.97	1146.68	Cycle 5-1 (1.00 %)
20% drop of lateral strength	12.81	1762.03	After Cycle 5-1 (1.00 %)
	-10.12	-1711.75	After Cycle 4-1 (0.75 %)

TA1(0.00028)
TB1(0.00210)
TC1(0.00067)

TA2(0.00089)
TB2(0.00032)
TC2(0.00025)

TA4
TB4(0.00011)
TC4(0.00014)

TA5(0.00007)
TB5(0.00032)
TC5(0.00016)
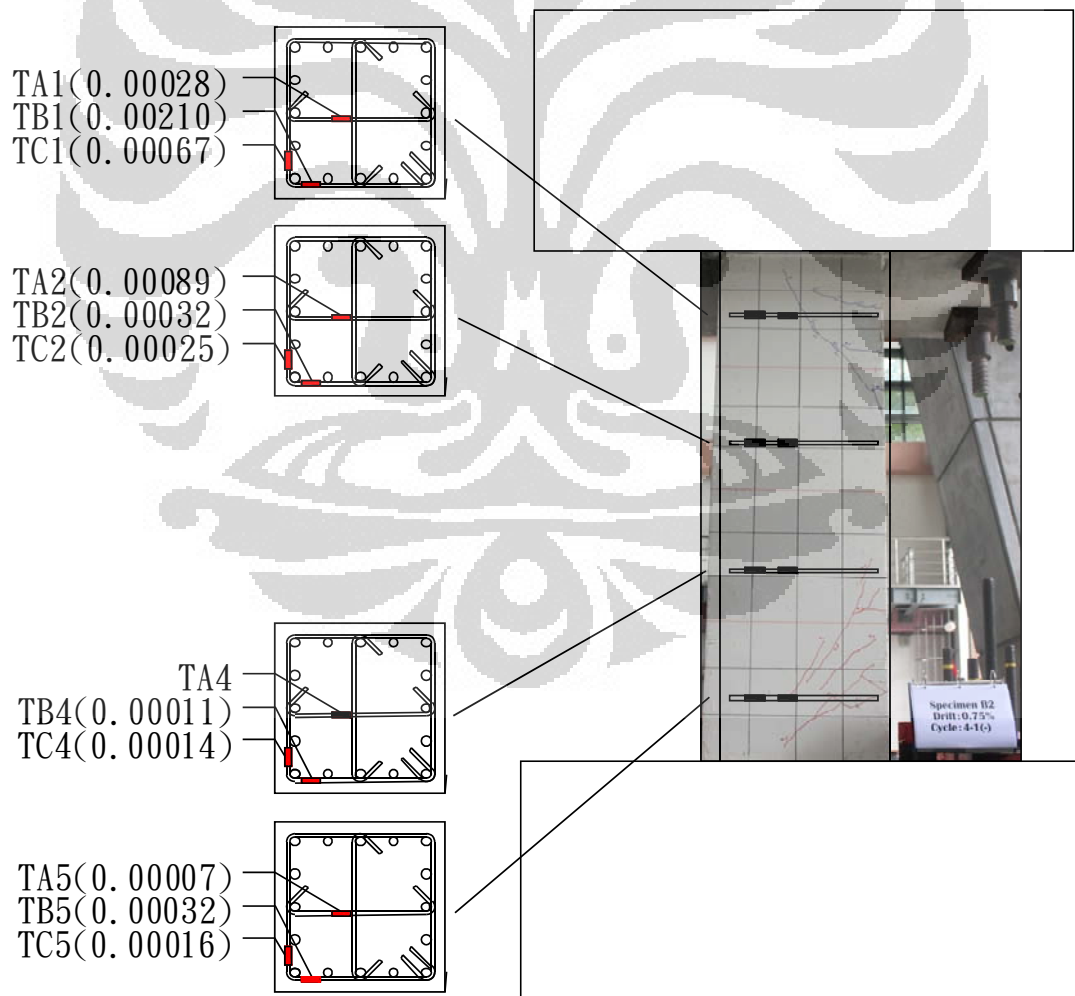
Figure 5.13 Strain reading and crack pattern of column B2 at the peak/maximum strength (negative directions).

Figure 5.13 below depicts the location of the strain gauge and the strain reading of the reliable strain gauge (red color) during the minimum strength cycle 4-1. The black color means unreliable strain reading or malfunction of the strain gauge. This figure can be clearly seen that small cracks on the top and the bottom of the column did not pass through strain gauges. This condition gives the reason why the strain reading is mostly very small. On the other hand, strain reading in TA2 indicates big enough value of strain reading 0.00089 that could be happened due to small crack inside the top of the column (prediction). No reliable strain reading installed in transverse reinforcement indicated a yielding of the hoops at this condition.

TA1(0.00023)
TB1(0.00026)
TC1(0.00051)

TA2(0.00115)
TB2(0.00038)
TC2(0.00019)

TA4
TB4(0.00004)
TC4(0.00010)

TA5(0.00020)
TB5(0.00110)
TC5(0.00053)

Specimen B2
Drift:1.00%
Cycle:5-1(-)
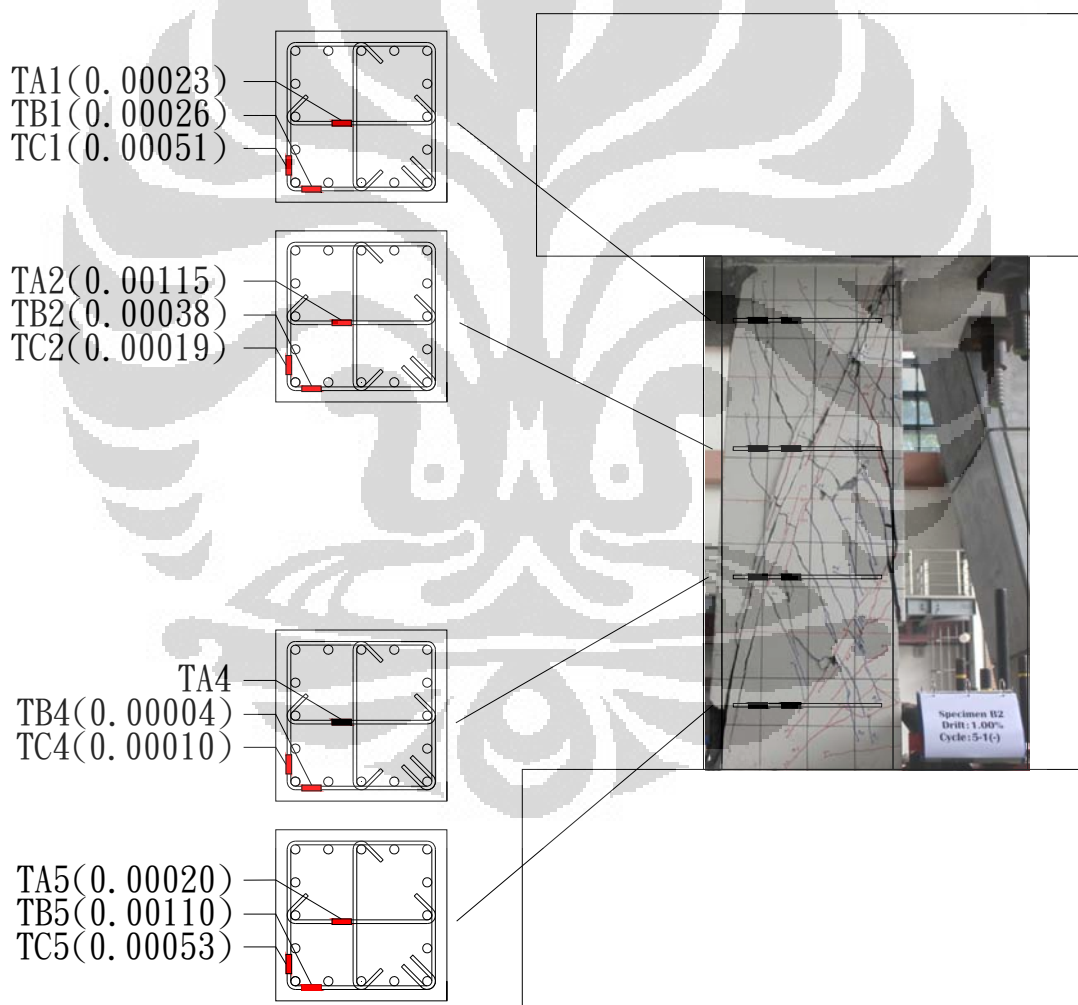
Figure 5.14 Strain reading and crack pattern of column B2 at the peak/maximum strength (positive directions).

The location of the strain gauge and the strain reading of the reliable strain gauge when the transverse reinforcement reached the first yield at the maximum strength

cycle 5-1 could be seen in the figure 5.14 above. As we could see in this figure, diagonal shear crack passed through some strain gauges, such as TB2, TC2, TB4, TC4 and TC5. Strain reading in TA2 and TB5 recorded the high enough value of maximum strain reading, consecutively, 0.00115 and 0.00110 that could be happened due to large diagonal shear crack. No reliable strain reading installed in transverse reinforcement indicated a yielding of the hoops.

(a)   (b)

(c)   (d)

Figure 5.15 Final stage of column B2 (1.00 % drift ratio).
(a) West side; (b) East side; (c) Buckling of longitudinal reinforcement (north-west side); (d) Buckling of longitudinal reinforcement (south-east side).

Figure 5.15 shows the final stage of column B2. Most of the cover concrete in the

Universitas Indonesia

mid-height of column spalled in diagonal pattern following the shear crack location. Transverse reinforcement in two different levels fractured. As mention before, a hard cracking sound was heard at 1.00 % drift ratio, which was expected as a result of the fracture hoop.

5.3.2.3. Column B3

Specimen B3 was subjected to constant compressive axial load of 8125.14 kN ($0.2\, f'_c\, A_g$ where f'_c = the concrete compressive strength and A_g is the gross cross-sectional area) and cyclic increments of lateral displacements as described in chapter 4.
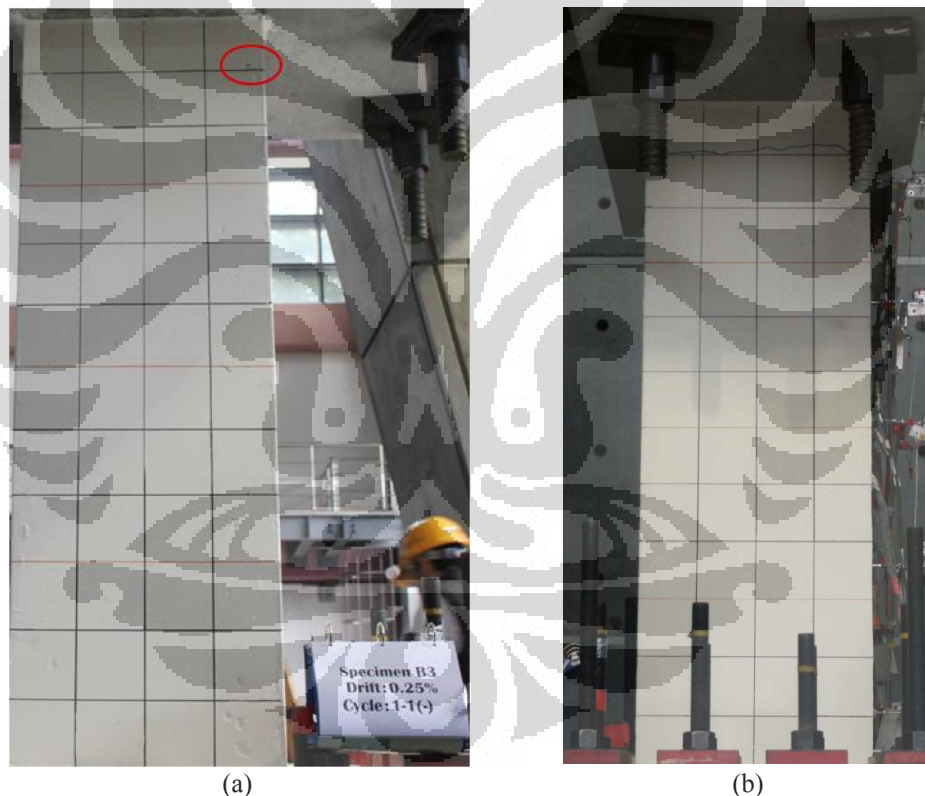
Figure 5.16 Flexural cracks during the initial displacements column B3.
(a) First flexural crack in west side; (b) First flexural crack in south side.

During the initial displacement cycles of 0.25 % drift ratio, the flexural cracks (width of less than 0.05 mm) developed near the top of the column in south side (60 cm length) and continued to west side. At this displacement level, no cracks were observed around the mid-height region of the column. The width of the cracks

remained the same for 0.375 % drift ratio. Moreover, it remained the same for 0.5 % drift ratio. The number of the cracks increased as the number and magnitude of the displacement cycle increased.

The shear cracks started to develop at 0.75 % drift ratio (width crack of 0.10 mm) and the cracking sound was heard. The initial shear cracks developed in the bottom and right hand side of the column continued from the flexural crack with crack angle approximately 45° formed flexural-shear crack pattern. In the end of the third cycle of 0.75 % drift ratio, the shear crack was not found in the mid-height (the maximum width of flexural crack was 0.3 mm) and all the measurement tools attached to the column were uninstalled.

Figure 5.17 First shear crack at drift 0.75 % width crack of 0.15 mm (west side).

In the first cycle of 1.00 % drift ratio, a hard cracking sound was heard simultaneously with the developing of a large diagonal shear crack from the right hand of upper part to the left hand of bottom part from west face (width shear crack maximum 2.75 mm). Moreover, a lot of shear minor crack was developed parallel to the large one with width crack of 0.05 mm, and the rest of the flexural crack is reaching to 0.25 mm of width. Moreover, some vertical minor cracks occurred in south and north side.

(a)   (b)

(c)   (d)
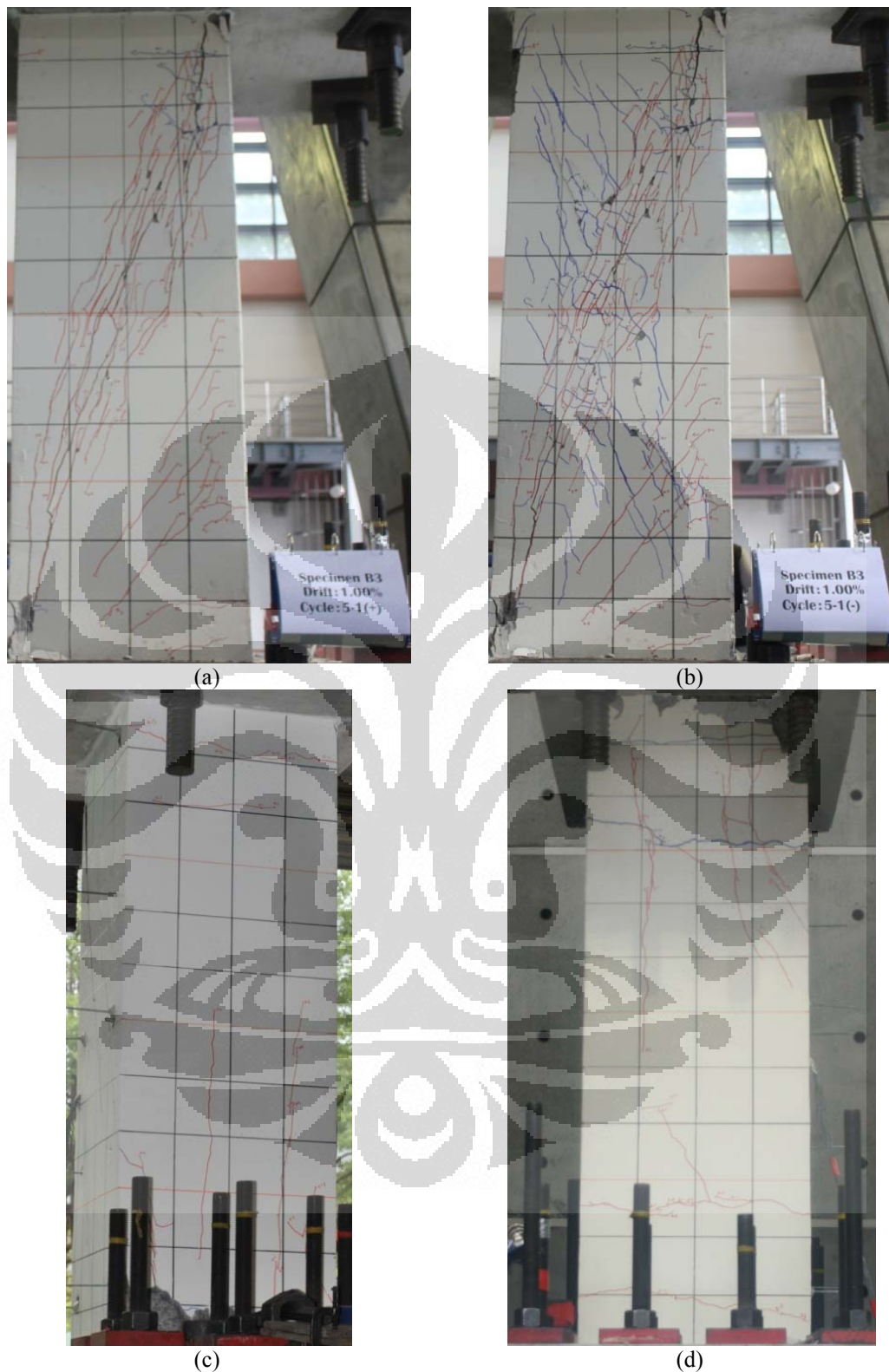
Figure 5.18 Shear crack of column B3 (1.0% drift ratio).
(a) Positive direction in first cycle (west side); (b) Negative direction in first cycle (west side); (c) vertical crack (north side); (d) vertical crack (south side).

At the negative direction stage of the first cycle, as the specimen was laterally forced

on the opposite direction, minor shear crack (width crack of 0.75 mm) developed

perpendicularly to the large one. The number of shear cracks increased as the number and magnitude of the displacement cycle increased. The test was stopped at the third cycle of 1.00 % drift ratio with the condition noticed almost all the cover concrete spalled, particularly in the mid-height part of west and north face after an explosive sound was heard.

Figure 5.19 shows the hysteretic loop of Column B3. This figure noted several important points that indicate when the flexural and shear crack started to develop, maximum strength, loss of lateral strength, first yield of the transverse reinforcement, big explosive sound and also 20% drop of ultimate strength. Table 6 below shows the summary of these seven points. The first shear crack appeared coincidentally to the maximum lateral strength in negative direction. The maximum strength occurred at cycle 4-1 for negative direction and at cycle 5-1 for positive direction.

Table 5.6. Important points of column B3

Points	Displacement (mm)	Lateral load (kN)	Level of drift ratio
First flexural crack	2.12	655.22	Cycle 1-1 (0.25 %)
	-1.33	-912.09	Cycle 1-1 (0.25 %)
First shear crack	8.17	2117.35	Cycle 4-1 (0.75 %)
	-6.37	-2144.78	Cycle 4-1 (0.75 %)
Maximum strength	10.36	2374.04	Cycle 5-1 (1.00 %)
	-6.37	-2144.78	Cycle 4-1 (0.75 %)
Loss lateral strength	13.58	900.59	Cycle 6-1 (1.50 %)
	-14.63	-1045.48	Cycle 5-1 (1.00 %)
Explosive sound	15.28	1081.55	Cycle 5-2 (1.00 %)
Max strain of hoop	-14.63	-1045.48	Cycle 5-1 (1.00 %)
20% drop of lateral strength	12.58	1899.24	After Cycle 5-1 (1.00 %)
	-9.59	-1715.82	After Cycle 4-1 (0.75 %)

Figure 5.20 depicts the envelopes for each cycle. The first two cycles were up to 1.00 % of drift ratio and the other one was up to 0.75 % of drift ratio.

Drift Ratio (%)
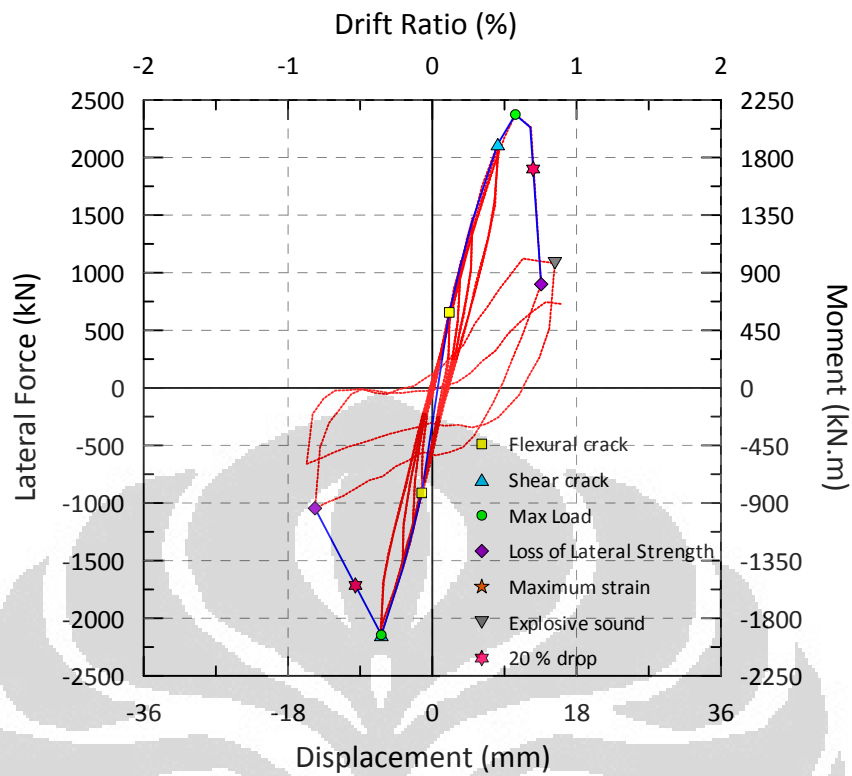
Figure 5.19 Lateral load – Displacement relationship for column B3

Drift Ratio (%)
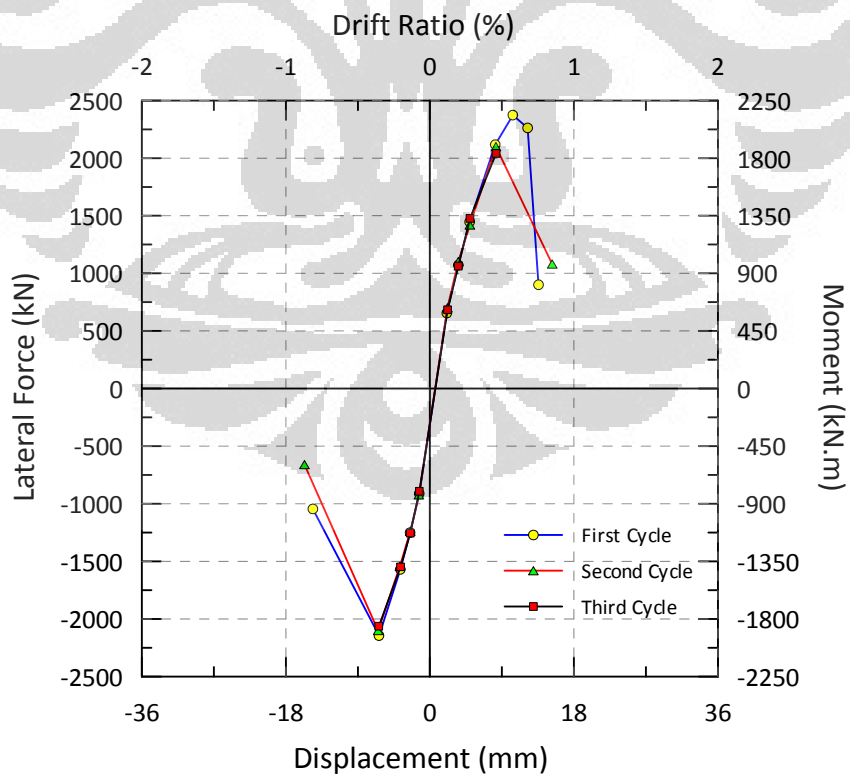
Figure 5.20 Envelope of column B3.

Universitas Indonesia

Figure 5.21 below depicts the location of the strain gauge during the peak (maximum) strength cycle 5-1. This figure can be clearly seen that some small cracks on the top and the bottom of the column passed through strain gauges. Due to problems during the test, the exact location of strain gauges of this column could not be recognized. Nevertheless, among the reliable strain gauges, no strain reading that placed in transverse reinforcement indicated a yielding of the hoops.
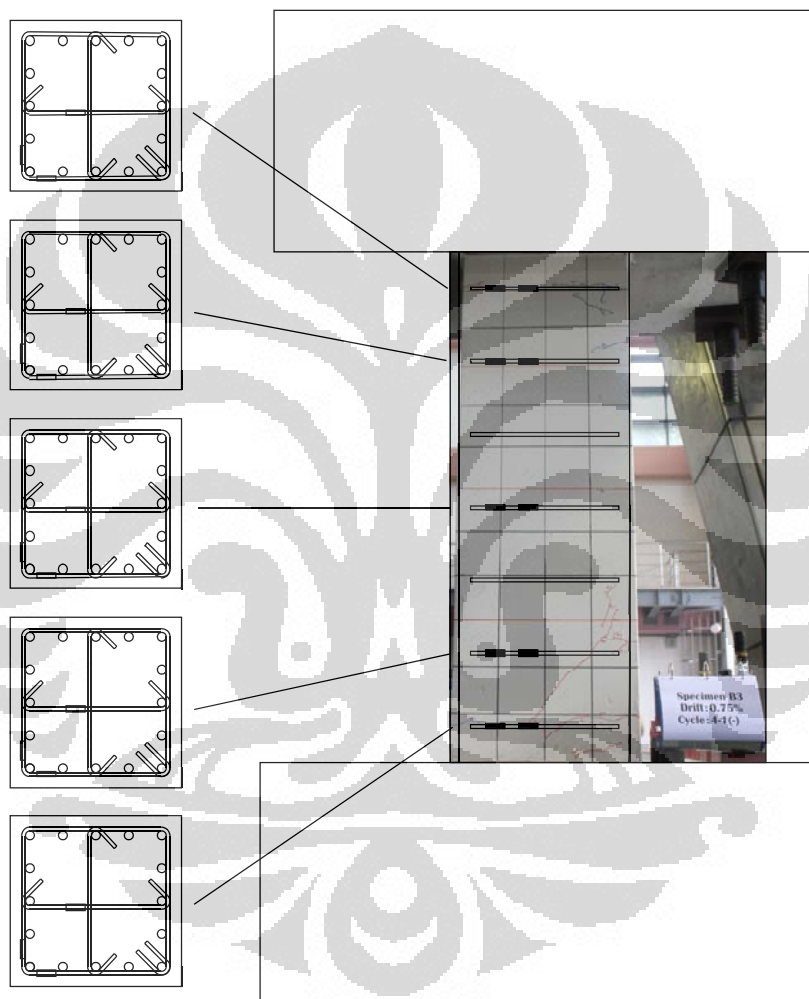
Figure 5.21 The strain gauge and crack pattern of column B3 at the peak (maximum) strength

Figure 5.22 above shows the final stage of column B3. Most of the cover concrete in the mid-height of column spalled. Bending of the longitudinal reinforcement appeared as the failure of transverse reinforcement occurred. Furthermore, some part of concrete inside the reinforcement was broken to pieces.

Figure 5.22 Final stage of column B3 (1.00 % drift ratio).
(a) West side; (b) East side; (c) Failure of transverse reinforcement at the bottom of the column north-west side; (d) Buckling of lateral reinforcement at the upper of the column south-east side.

5.3.2.4. Column B4

Specimen B4 was subjected to constant compressive axial load of 8715.11 kN ($0.2\,f'_c\,A_g$ where f'_c = the concrete compressive strength and A_g is the gross

cross-sectional area) and cyclic increments of lateral displacements.

During the initial displacement cycles of 0.25 % drift ratio, the flexural cracks (width of less than 0.05 mm) developed near the top of the column in south side (40 cm length) and continued to west side. At this displacement level, no cracks were observed around the mid-height region and bottom of the column.
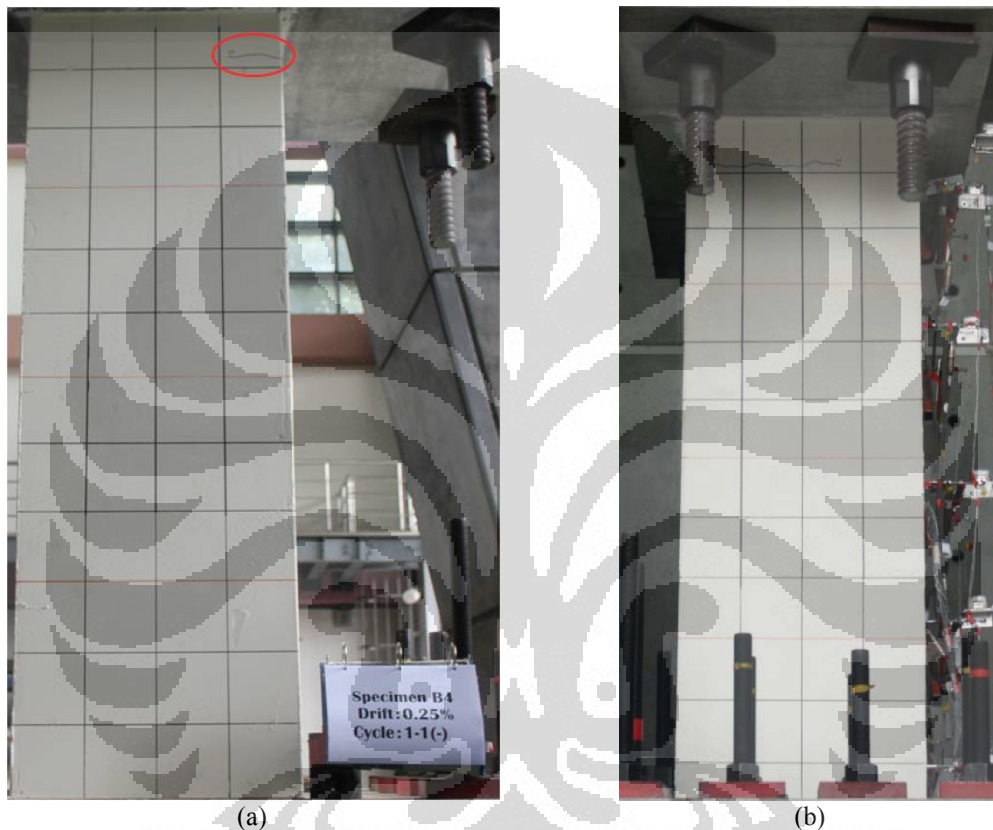
Figure 5.23 Flexural cracks during the initial displacements of column B4.
(a) First flexural crack in west side; (b) First flexural crack in south side.

The width of the cracks remained the same for 0.375 % drift ratio. It widened for 0.5 % drift ratio (width crack of 0.1 mm) and the first flexure crack near the bottom of the column appeared. The number of the cracks increased as the number and magnitude of the displacement cycle increased.

The shear cracks started to develop at 0.75 % drift ratio (width crack of 0.10 mm) and soft cracking sound was heard. The initial shear cracks developed in the bottom and right hand side of the column continued from the flexural crack with crack angle approximately 45° formed flexural-shear crack pattern. In the end of the third cycle of 0.75 % drift ratio, the shear crack was not found in the mid-height (the maximum

width of flexural crack was 0.4 mm).

Figure 5.24. First shear crack at drift ratio 0.75 % width crack of 0.10 mm (west side).

At the first cycle of 1.00 % drift ratio, the first hard cracking sound was heard simultaneously with the developing of a large diagonal shear crack from the right hand of upper part to the left hand of bottom part from west face (width shear crack maximum 1.00 mm). Moreover, two shear minor cracks developed parallel to the large one with width crack of 0.10 mm, and the rest of the flexural crack is reaching to 1.2 mm of width. Moreover, a vertical minor crack occurred in south side at the mid-height of column.
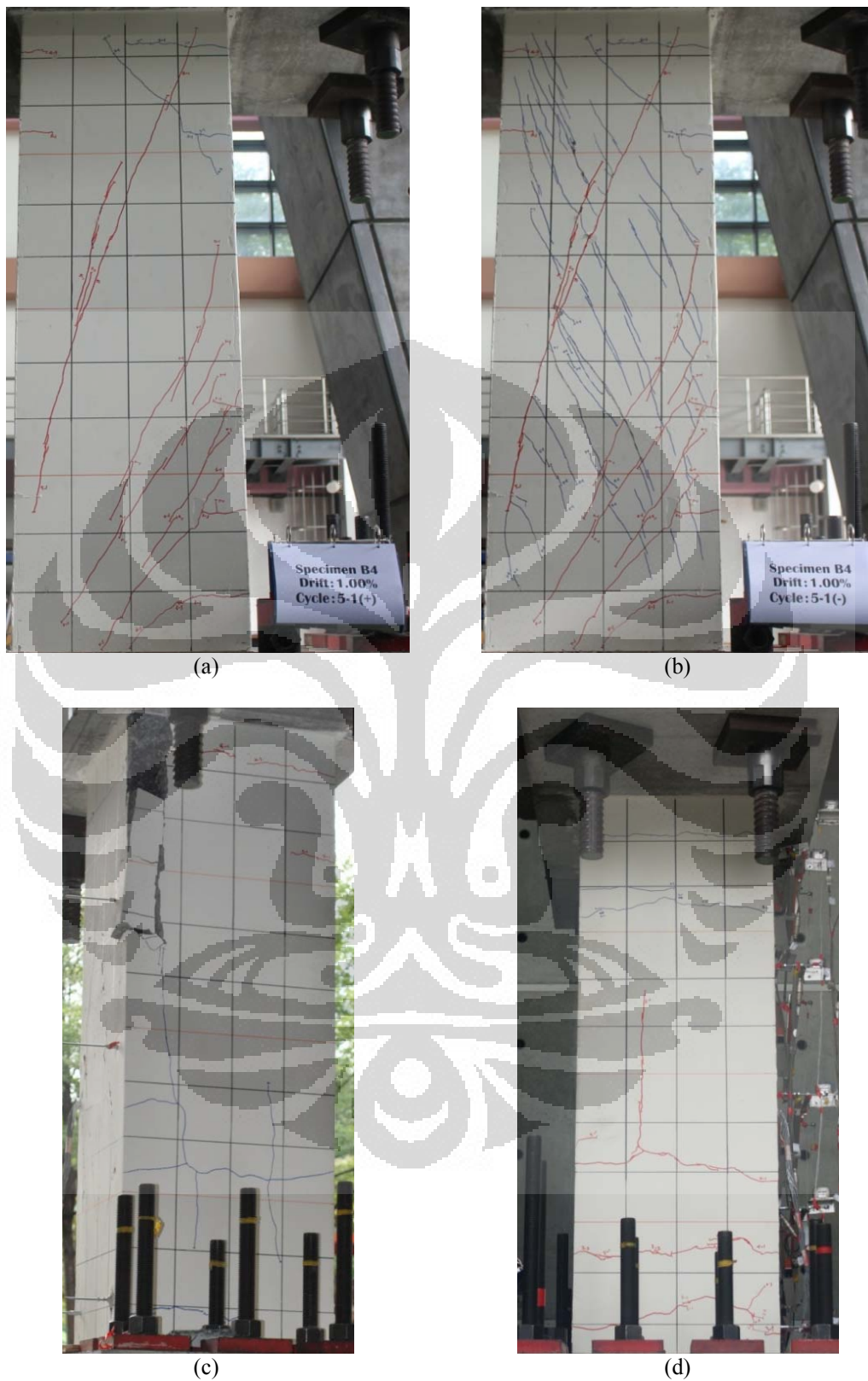
Figure 5.25 Shear crack of column B4 (1.0% drift ratio).
(a) Positive direction in first cycle (west side); (b) Negative direction in first cycle (west side); (c) vertical crack (north side); (d) vertical crack (south side).

At the negative direction stage of the first cycle, as the specimen was laterally forced on the opposite direction, shear crack (width crack of 1.2 mm) appeared perpendicular to the first one. The number of shear cracks increased as the number and magnitude of the displacement cycle increased. Furthermore, some vertical minor cracks occurred in north side. After this stage, all the measurement tools attached to the column were uninstalled. Until the third cycle of 1.00 % drift, there is no significant amount of spalled concrete. The test was stopped at the third cycle of 1.50 % drift ratio with the condition noticed almost the cover concrete at mid-height spalled after an explosive sound was heard.

Figure 5.25 shows the hysteretic loop of column B4. This figure noted several important points as summarized in table below 5.7. The maximum strain of the transverse reinforcement occurred at the first cycle of 1.00 % drift ratio, which is also at the same cycle of the maximum strength. The first shear crack coincided to the maximum lateral strength in negative direction.

Table 5.7 Important points of column B4

Points	Displacement (mm)	Lateral load (kN)	Level of drift ratio
First flexural crack	1.92	631.79	Cycle 1-1 (0.25 %)
	-2.10	-996.22	Cycle 1-1 (0.25 %)
First shear crack	7.98	2068.05	Cycle 4-1 (0.75 %)
	-7.20	-2216.27	Cycle 4-1 (0.75 %)
Maximum strength	11.58	2443.18	Cycle 5-1 (1.00 %)
	-7.20	-2216.27	Cycle 4-1 (0.75 %)
Loss lateral strength	23.37	1353.36	Cycle 6-1 (1.50 %)
	-13.08	-1817.91	Cycle 5-1 (1.00 %)
Explosive sound	11.58	2443.18	Cycle 5-1 (1.00 %)
Max strain of hoop	-9.45	-1765.45	Cycle 5-1 (1.00 %)
20% drop of lateral strength	16.01	2033.40	After Cycle 5-1 (1.00 %)
	-13.83	-1773.02	After Cycle 4-1 (0.75 %)

Figure 5.27 depicts that three envelopes reached up to 1.50 % drift ratio.
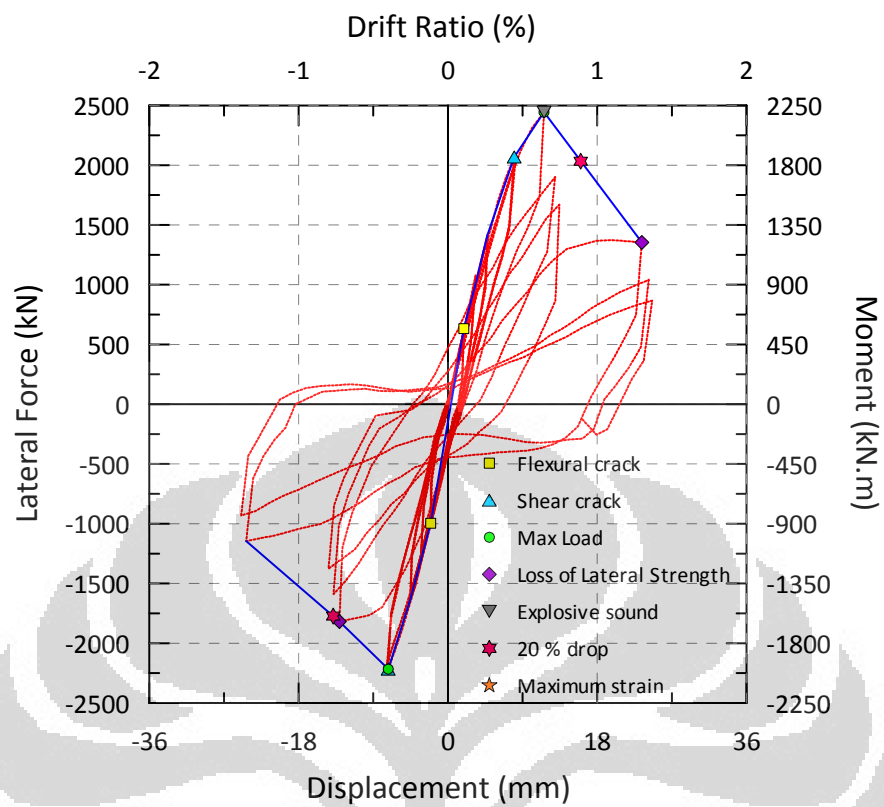
Figure 5.26 Lateral load – Displacement relationship for column B4
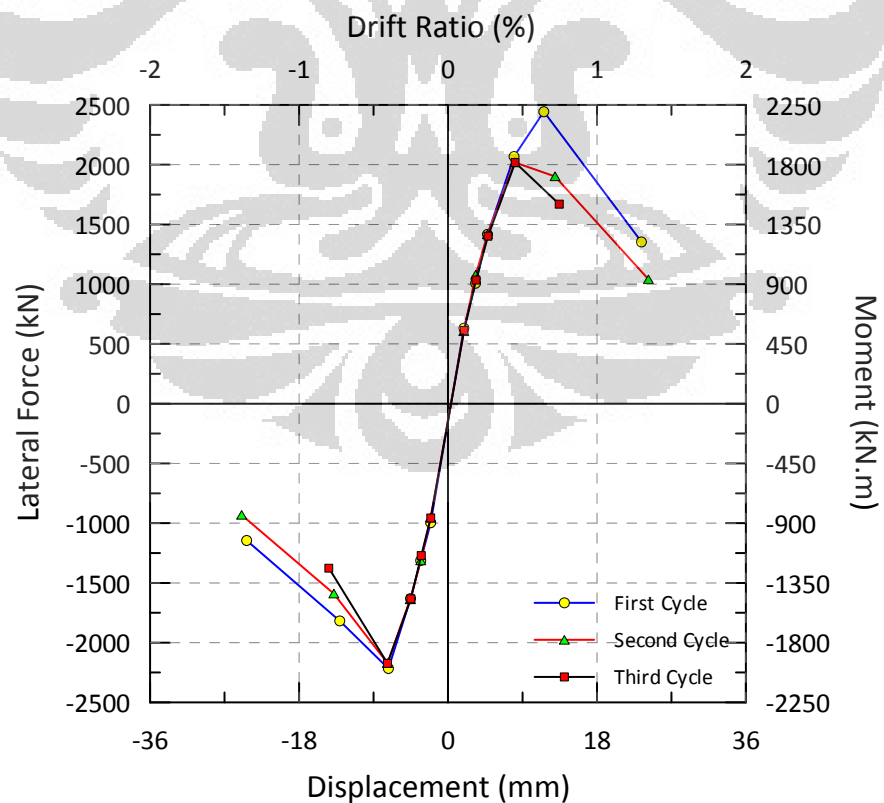
Figure 5.27 Envelope of column B4.

Figure 5.28 below indicates the location of the strain gauge and the strain reading of the reliable strain gauge (red color) during the minimum strength cycle 4-1. The black color means unreliable strain reading or malfunction of the strain gauge. From this figure can be clearly seen that small cracks on the top and the bottom of the column did not pass near the strain gauges. Strain reading in the second, the third and the fourth level are mostly very small. This condition could be happened because the crack only appeared on the top and the bottom of the column. No reliable strain reading installed in transverse reinforcement indicated a yielding of the hoops.
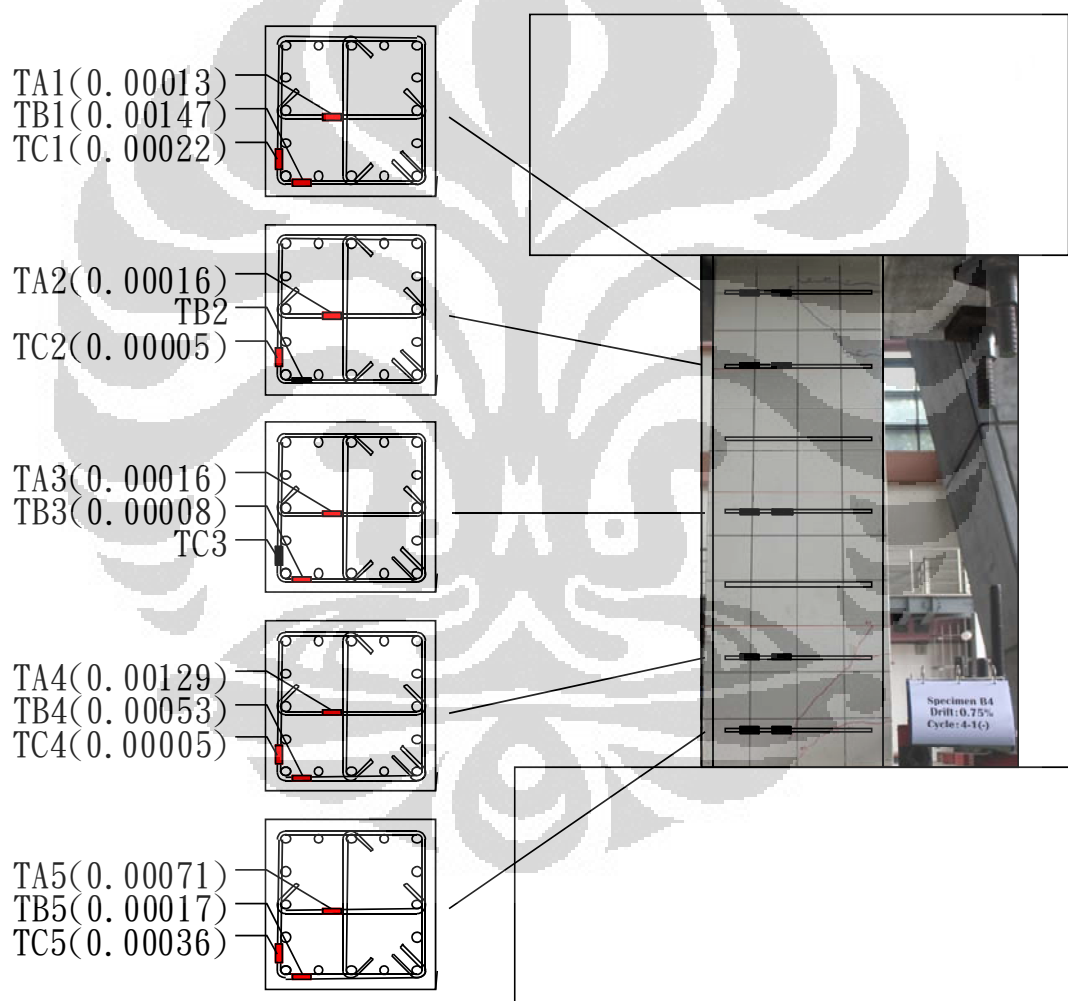
Figure 5.28 Strain reading and crack pattern of column B4 at the peak/maximum strength (negative directions).

The location of the strain gauge and the strain reading of the reliable strain gauge during the maximum strength cycle 5-1 could be seen in the figure 5.29 below. No

reliable strain reading installed in transverse reinforcement indicated a yielding of the hoops.
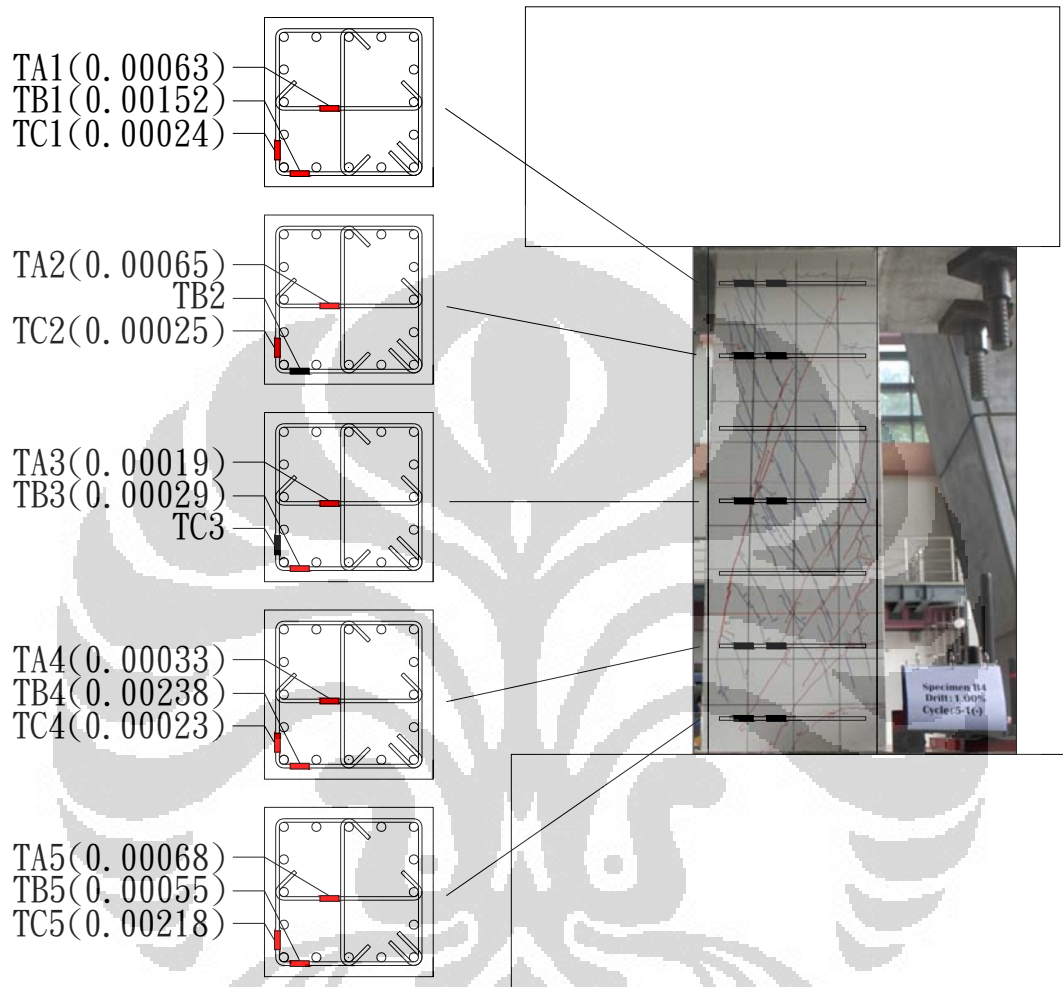
Figure 5.29 Strain reading and crack pattern of column B4 at the peak/maximum strength (positive directions).

Bending of the longitudinal reinforcement appeared as the failure of transverse reinforcement occurred as shown in figure 5.30. Furthermore, some part of concrete inside the reinforcement was broken to pieces.

Figure 5.30 Final stage of column B4 (1.00 % drift ratio). (a) West side; (b) East side; (c) Failure of transverse reinforcement south side; (d) Buckling of lateral reinforcement at the upper of the column north-west side.

5.4.2.   Column S

There are two columns of specimen S. The first column has 125 mm of transverse reinforcement vertical strength while the second column has 180 mm. Both of columns were subjected to low axial load ratio (10 %).

5.3.2.1. Column S1

Specimen S1 was subjected to constant compressive axial load of 4232.493 kN

$(0.1\, f'_{c}\, A_{g}$ where f'_{c} = the concrete compressive strength and A_{g} is the gross cross-sectional area) and cyclic increments of lateral displacement.

During the initial displacement cycles of 0.25 % drift ratio, the flexural cracks (width of less than 0.05 mm) started to develop on the edge of the column in south-west side (15-60 cm long). The width of the cracks became larger as 0.15 mm for 0.375 % and 0.50 % drift ratio. The number of the cracks increased as the number and magnitude of the displacement cycle increased.
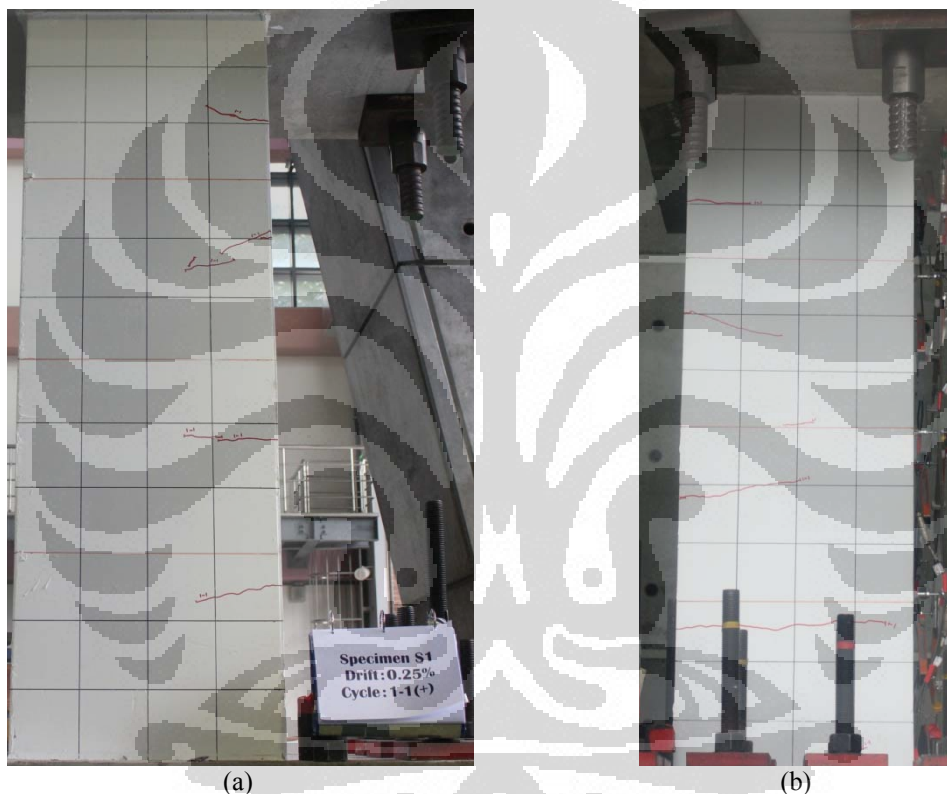
(a)   (b)
Figure 5.31 Flexural cracks during the initial displacements.
(a) First flexural crack in west side; (b) First flexural crack in south side.

Shear cracks started to develop at the first cycle negative direction of 0.50 % drift ratio (width crack of 0.05 mm) and the cracking sound was heard. The initial shear cracks developed in the mid-height of the column continued from the flexural crack with crack angle approximately 45° formed flexural-shear crack pattern as shown in figure 5.32 below. The number and the length of the shear cracks increased as the number and magnitude of the displacement cycle increased.

(a)   (b)
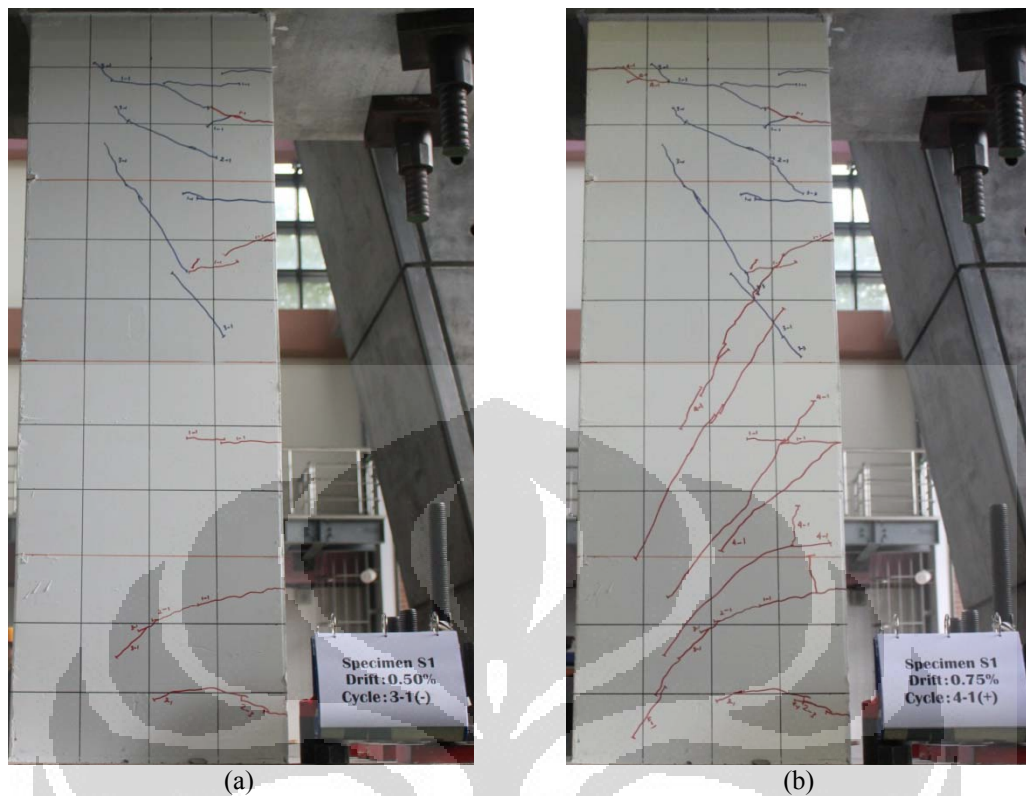
Figure 5.32 Crack on the west side of column S1.
(a) First shear crack; (b) Appearance of vertical minor cracks.

At the first cycle of 0.75 % drift ratio, 0.05 mm vertical minor cracks appeared in west side. At the negative direction stage of this cycle, as the specimen was laterally forced on the opposite direction, shear crack (width crack of 0.05 mm) appeared perpendicular to the first one. The number of flexure and shear cracks increased as the number and magnitude of the displacement cycle increased. Cover concrete started to spall of in the first cycle of 1.00 % drift ratio. Until the end of 1.50 % drift ratio, the maximum width crack appeared was 0.15 mm.

At the beginning of the first cycle of 2.00 % drift ratio, cover concrete in mid-height of column, precisely in the intersection of shear crack, spalled as the increasing of the number of cracks and all the measurement tools attached to the column were uninstalled. Moreover, in the negative direction of the first cycle, cover concrete at the edge of north-west side spalled in crooked pattern. At the third cycle, almost 30% of the cover concrete spalled, therefore, in the west side multi-spiral transverse reinforcement appeared.
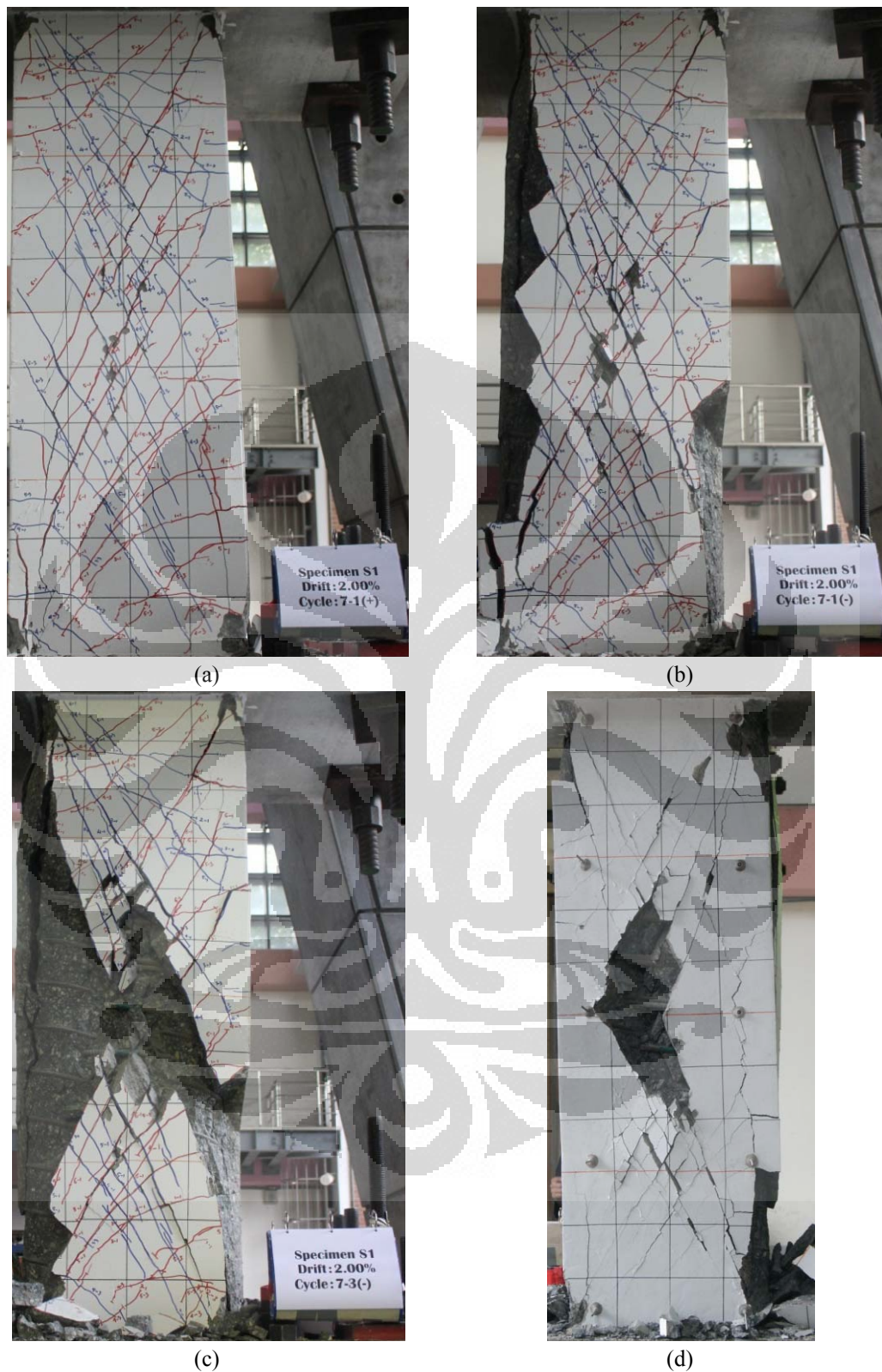
Figure 5.33 Shear crack of Column S1 (2.00 % drift ratio).
(a) Positive direction at the first cycle (west side); (b) Negative direction at the first cycle (west side),
(c) At the end of 2.00 % (west side); (c) At the end of 2.00 % (east side).

At the beginning of the first cycle of 3.00 %, the concrete inside the big spiral of the column started to spall and create a cavity in the mid-height of column. At the same time, failure of the large spiral transverse reinforcement occurred.

Figure 5.34 First Cycle at 3.00 % of drift ratio column S1 (west side).

The test was stopped at the third cycle of 4.00 % drift ratio with the condition noticed almost the cover concrete at mid-height spalled after an explosive sound was heard. Failure of transverse reinforcement occurred. Furthermore, some part of concrete inside the large spiral transverse reinforcement was broken to pieces. On the other hand, concrete inside the small transverse reinforcement did not spall.

Figure 5.35 shows the hysteretic loop of Column S1. This figure noted several important points that indicate when the flexural and shear crack started to develop, maximum strength, loss of lateral strength, first yield of the transverse reinforcement, big explosive sound and also 20% drop of ultimate strength which are summarized in table 5.8 below. The first yield of the transverse reinforcement occurred at the beginning of the first cycle of 1.50 % drift ratio, which is also the maximum lateral

strength (positive load direction). The first shear crack coincided to the maximum lateral strength in negative direction.

Table 5.8 Important points of specimen S1

Points	Displacement (mm)	Lateral load (kN)	Level of drift ratio
First flexural crack	1.99	464.07	Cycle 1-1 (0.25 %)
	-1.93	-838.76	Cycle 1-1 (0.25 %)
First shear crack	4.84	1081.28	Cycle 3-1 (0.50 %)
	-4.74	-1360.05	Cycle 3-1 (0.50 %)
Maximum strength	19.84	2254.24	Cycle 6-1 (1.50 %)
	-19.46	-2241.56	Cycle 6-1 (1.50 %)
Loss lateral strength	29.75	2178.03	Cycle 7-1 (2.00 %)
	-31.21	-1429.60	Cycle 7-1 (2.00 %)
Explosive sound	-11.81	-1934.93	Cycle 5-1 (1.00 %)
1st Yield of hoop	19.84	2254.24	Cycle 6-1 (1.50 %)
20% drop of lateral strength	37.67	1803.39	After Cycle 6-1 (1.50 %)
	-29.38	-1793.25	After Cycle 6-1 (1.50 %)

Figure 5.36 depicts the envelopes for each cycle. All three cycles reached up to 3.00 % drift ratio.
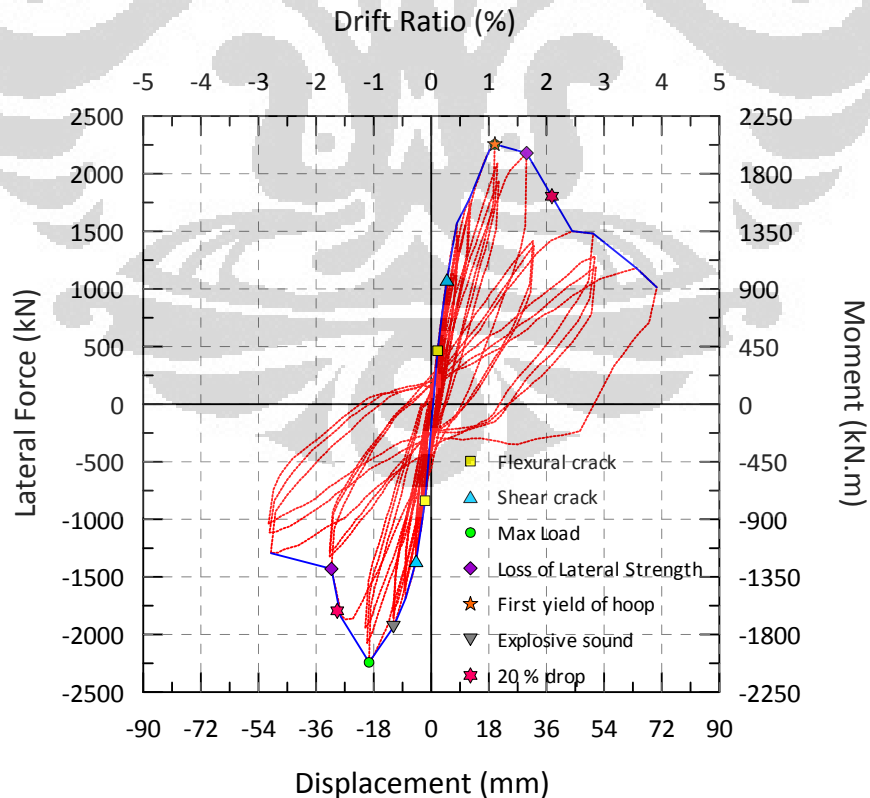
Figure 5.35 Lateral load – Displacement relationship for column S1
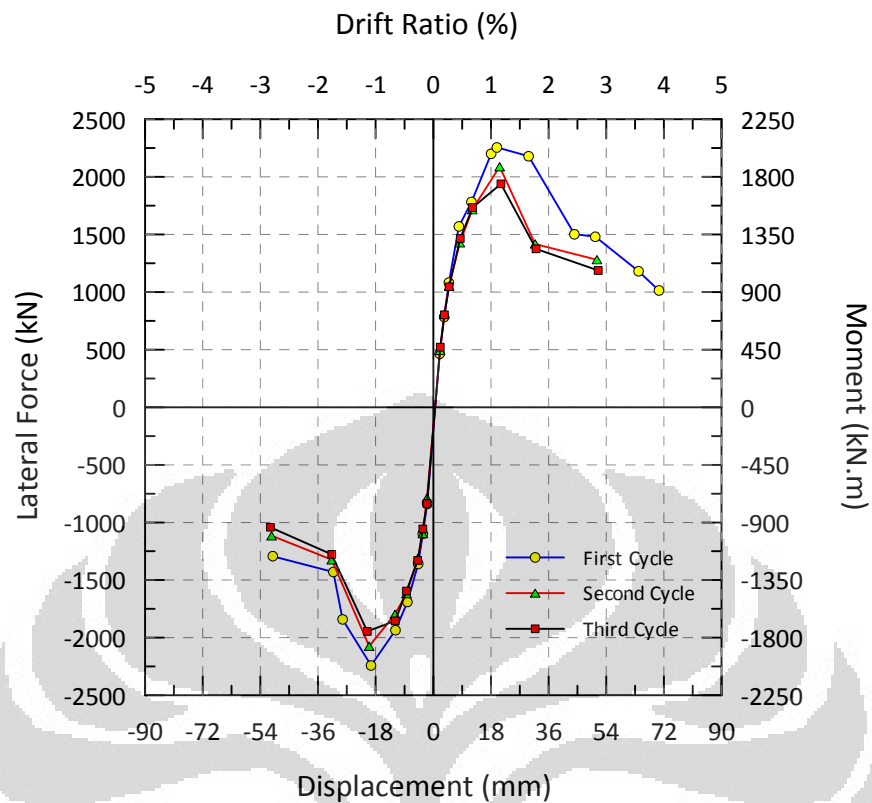
Figure 5.36 Envelope of column S1.

Figure 5.37 below indicates the location of the strain gauge during the maximum strength, cycle 6-1 which is also the first yield of the transverse reinforcement. All of the thirteen strain gauges worked well during the experiment. From this figure could be clearly seen that a lot of cracks on the bottom of the column passed near the strain gauges. As shown in figure below, two strain gauges were attached on the longitudinal reinforcement and the other eleven were on the large spiral. Nine of eleven strain gauges on the large spiral reinforcement already reached the yield point at this drift level.

Five strain gauges
at large spiral

Two strain
gauges at
longitudinal
reinforcement

Six strain gauges at
large spiral

Range of
strain gauges

Specimen S1
Drift: 1.50%
Cycle: 6-1(+)

No.	Strain reading
1	0.005135
2	0.005159
3	0.005383
4	0.003033
5	0.005522
6	0.005099
7	0.005220
8	0.003649
9	0.004522
10	0.006411
11	0.009776
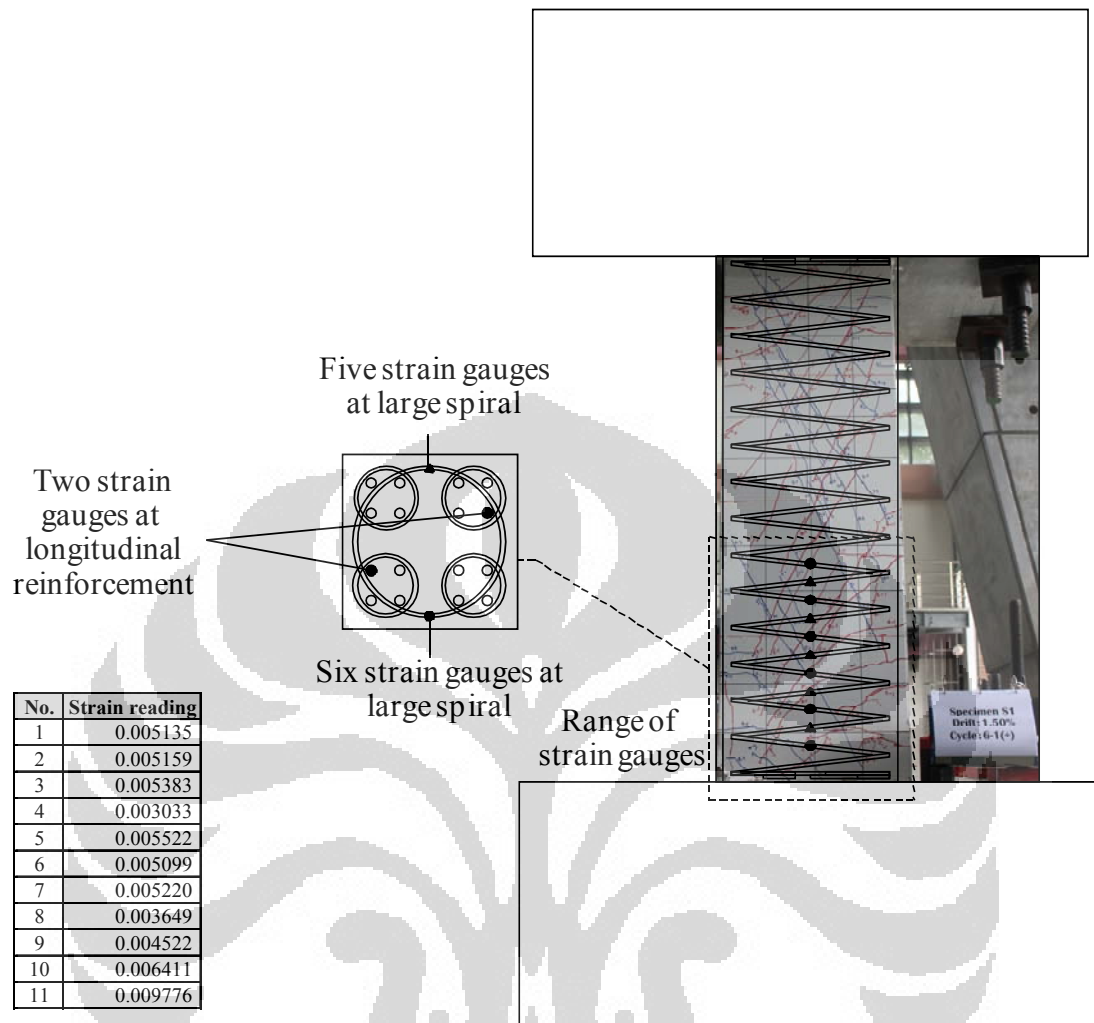
Figure 5.37 Strain reading and crack pattern of column S1 at the peak/maximum strength (positive directions).

Bending of the longitudinal reinforcement appeared as the failure of transverse reinforcement occurred as shown in figure 5.30. Furthermore, some part of concrete inside the reinforcement was broken to pieces.

Universitas Indonesia

<div align="center">(a)</div>

<div align="center">(b)</div>

<div align="center">(c)</div>

<div align="center">(d)</div>

Figure 5.38 Final stage of Column S1 (4.00 % drift ratio).
(a) West side; (b) East side; (c) Failure of large spiral transverse reinforcement west side; (d) Failure of large spiral transverse reinforcement (mid-height of the column east side).

5.3.2.2. Column S2

Specimen S2 was subjected to constant compressive axial load of 4232.49 kN (0.1 $f'_c A_g$ where f'_c = the concrete compressive strength and A_g is the gross cross-sectional area) and cyclic increments of lateral displacement.

<div align="right">Universitas Indonesia</div>

During the initial displacement cycles of 0.25 % drift ratio, the flexural crack (width of less than 0.05 mm) started to develop on the bottom of the column in west side (15 cm long). Then, at the same drift ratio in negative direction, the same flexural crack appeared in south side (40 cm long). At this displacement level, no crack was found around the mid-height region of the column. The number and length of the cracks increased as the number and magnitude of the displacement cycle increased.

(a)   (b)
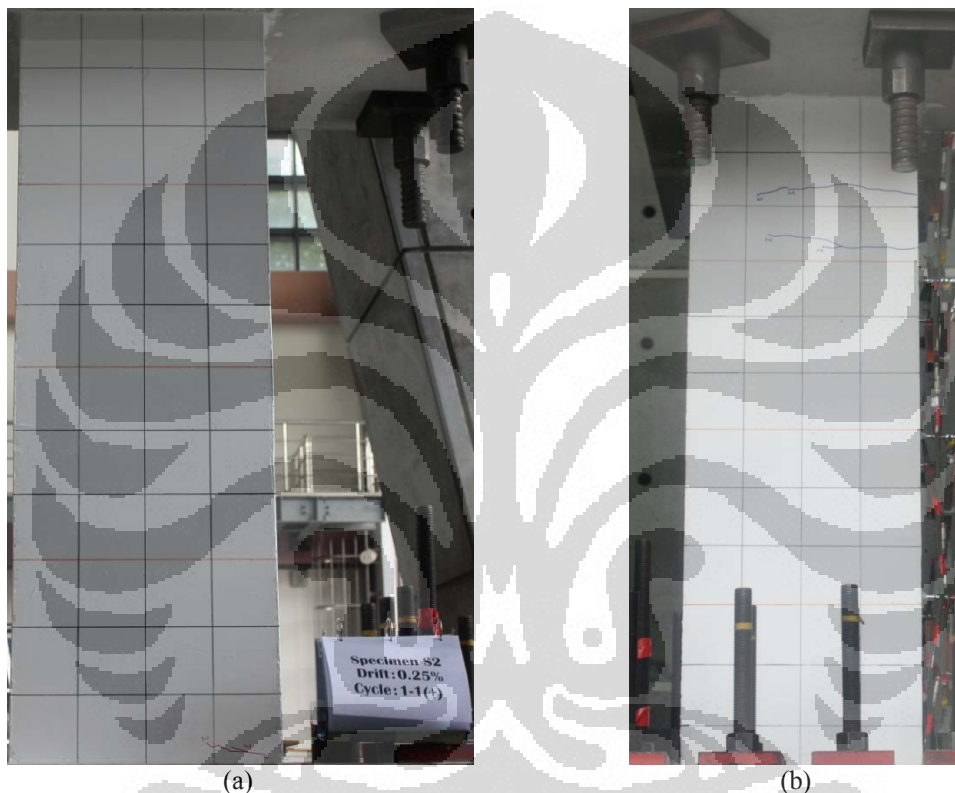
Figure 5.39 Flexural cracks of column S2 during the initial displacement.
(a) First flexural crack in west side; (b) First flexural crack in south side.

Shear cracks started to develop at the first cycle of 0.75 % drift ratio (width crack of 0.05 mm) and the cracking sound was heard simultaneously. The initial shear cracks developed in the mid-height of the column continued from the flexural crack with crack angle approximately 45° formed flexural-shear crack pattern. In negative direction, shear crack appeared in the upper part of the column. The number of the shear cracks increased as the number and magnitude of the displacement cycle increased. The shear cracks produced from two direction of loading intersected each other and initiated the spalling of the cover concrete.

Universitas Indonesia
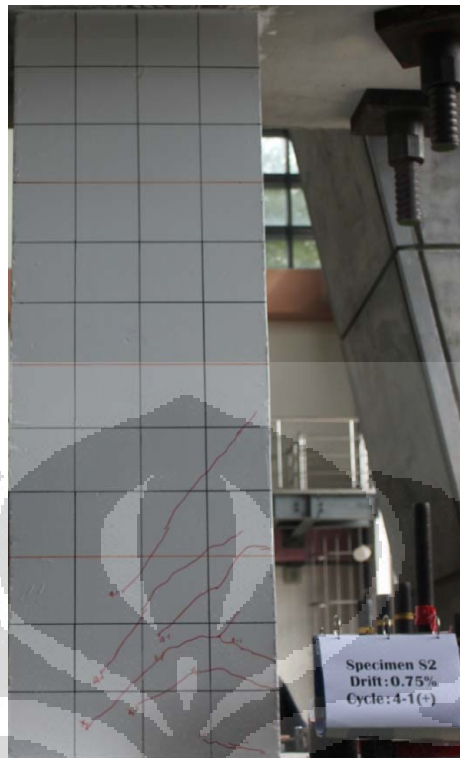
Figure 5.40 First shear crack (west side) column S2.

In the first cycle of 1.00 % drift ratio (positive direction), a hard cracking sound was heard simultaneously with the developing of some diagonal shear cracks from the right hand of upper part to the left hand of bottom part in the mid-height of column (width shear crack maximum 0.30 mm). Moreover, at the negative direction stage of this cycle, as the specimen was laterally forced on the opposite direction, shear crack (width crack of 0.10 mm) appeared perpendicular to the first one. The number of flexure and shear cracks increased as the number and magnitude of the displacement cycle increased.

Cover concrete started to spall of at the first cycle of 1.50 % drift ratio (see figure 5.42). All the measurements tools were uninstalled, except two LVDT measuring the upper and bottom part of column. Shear cracks also appeared in the east side of column. Then, cover concrete in mid-height of column, precisely at the intersection of shear crack, spalled as the increasing of the number of cracks. At the end of the last cycle of 2.00 % drift ratio, cover concrete in the bottom of column, precisely in the south side, spalled as the increasing of the number of cracks.

(a)   (b)
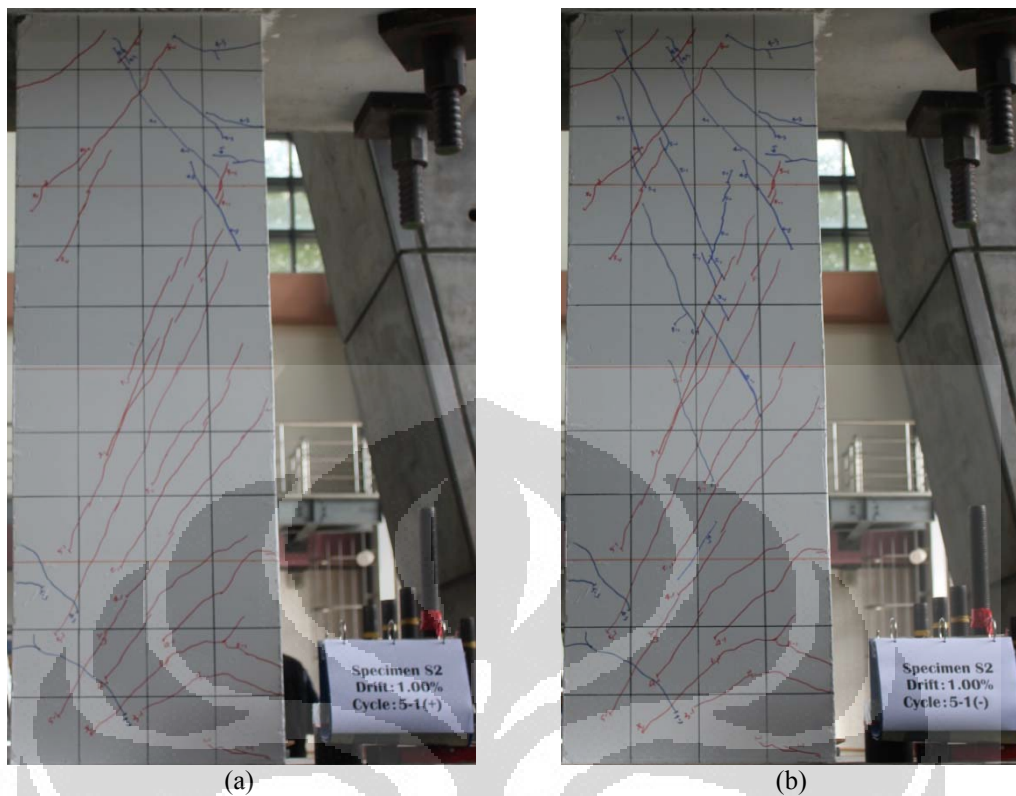
Figure 5.41 Shear crack of column S2 (1.00 % drift ratio, west side).
(a) Positive direction in first cycle; (b) Negative direction in first cycle.

(a)   (b)
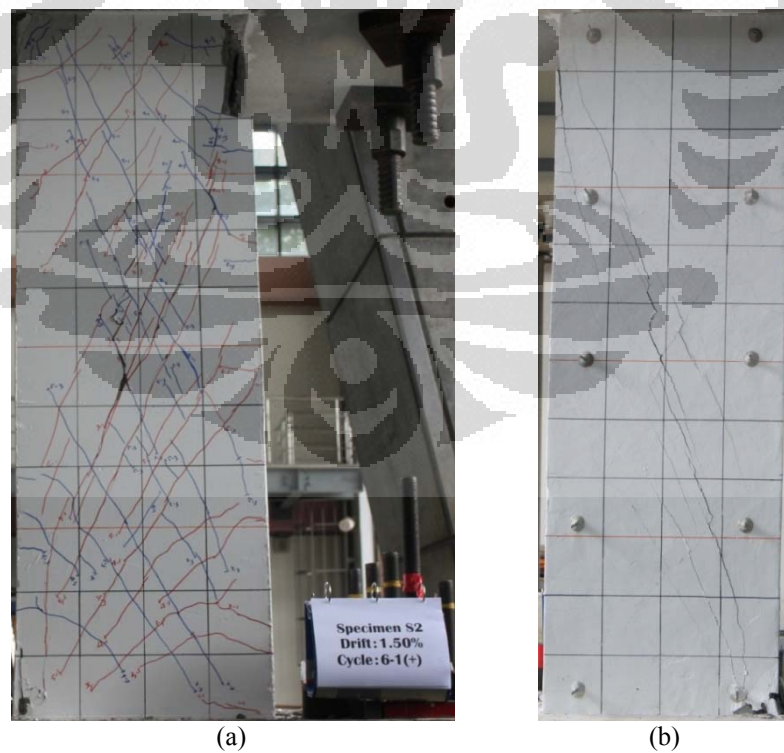
Figure 5.42 Shear crack of column S2 (1.50 % drift ratio).
(a) Spall of concrete cover in west side; (b) shear crack appeared in east side.

(a)　　　　　　　　　　　　　　　　　　　　　(b)
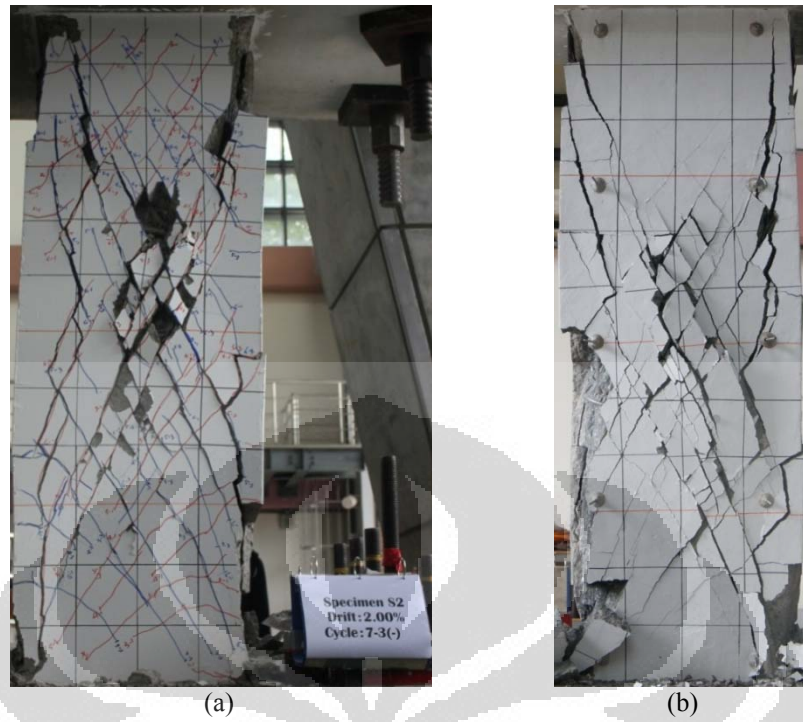
Figure 5.43 Shear crack of Column S2
(a) Third cycle (2.00 % drift ratio west side); (b) Third cycle (2.00 % drift ratio east side).
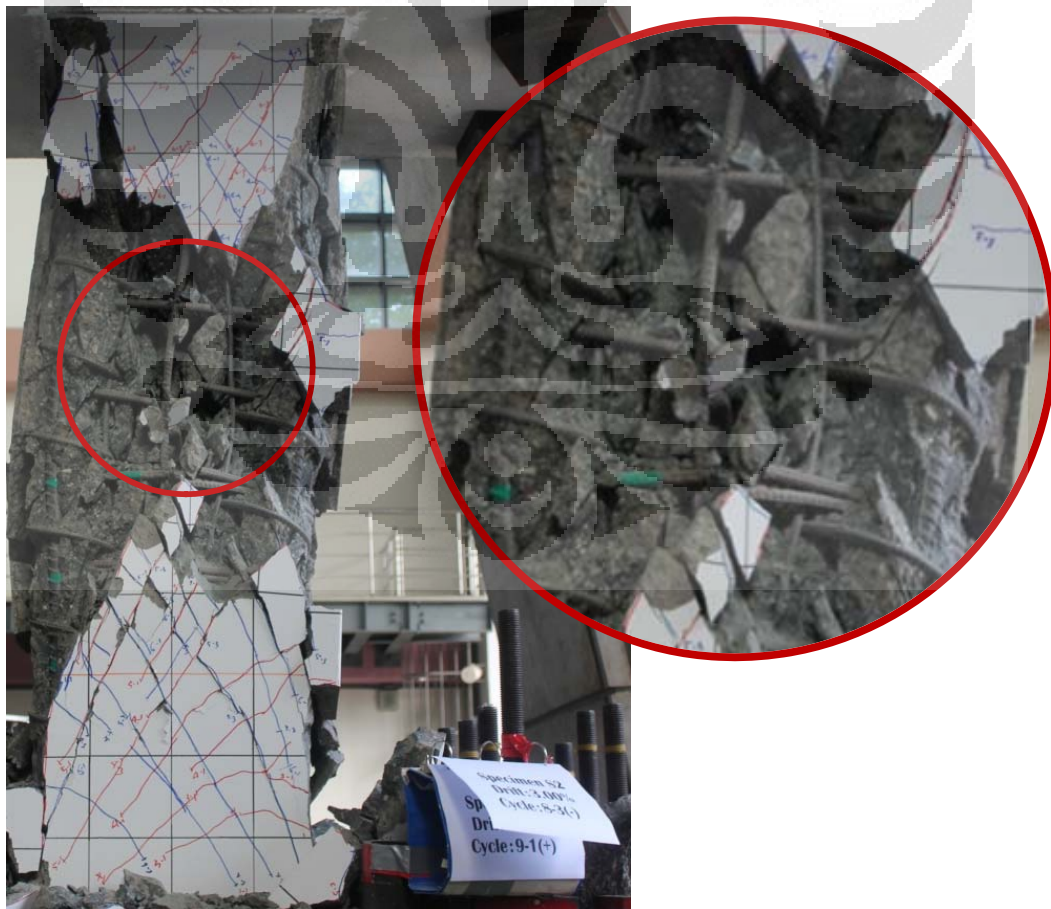
Figure 5.44 Third cycle of 3.00 % of drift ratio column S2 (west side).

Moreover, at 3.00 % of drift ratio, around 50 % of all the cover concrete spalled, therefore, in the west side multi-spiral transverse reinforcement appeared. The concrete inside the big spiral of the column started to spall and create a cavity in the mid-height of column. At the same time, failure of the large spiral transverse reinforcement occurred. Longitudinal reinforcement bent easily that caused more spalling off the concrete. The test was stopped at the first cycle of 4.00 % drift ratio with the condition noticed almost the cover concrete at mid-height spalled.

Figure 5.45 shows the hysteretic loop of Column S2. This figure noted several important points that indicate when the flexural and shear crack started to develop, maximum strength, loss of lateral strength, first yield of the transverse reinforcement, big explosive sound and also 20% drop of ultimate strength. Table 5.9 below shows the summary of these seven points. The first yield of the transverse reinforcement occurred at the beginning of the first cycle of 1.00 % drift ratio, which is also the same time of the explosive sound during the test. Figure 5.46 depicts the envelopes for each cycle. The first cycle was up to 4.00 % of drift ratio, but the other two were only up to 3.00 % drift ratio.
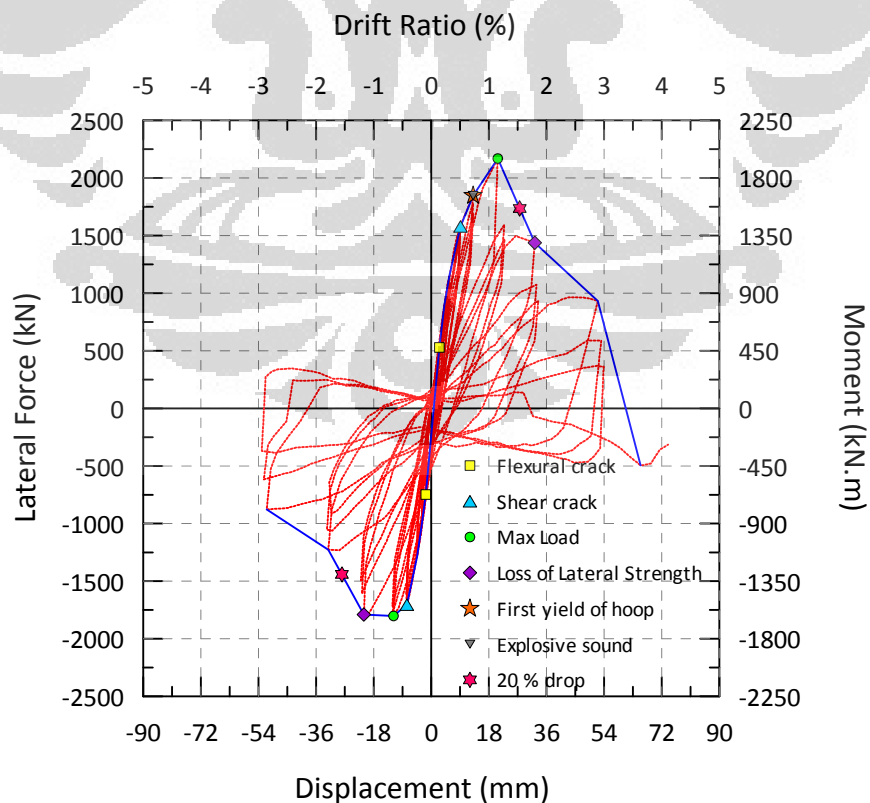
Figure 5.45 Lateral load – Displacement relationship for column S2

Universitas Indonesia
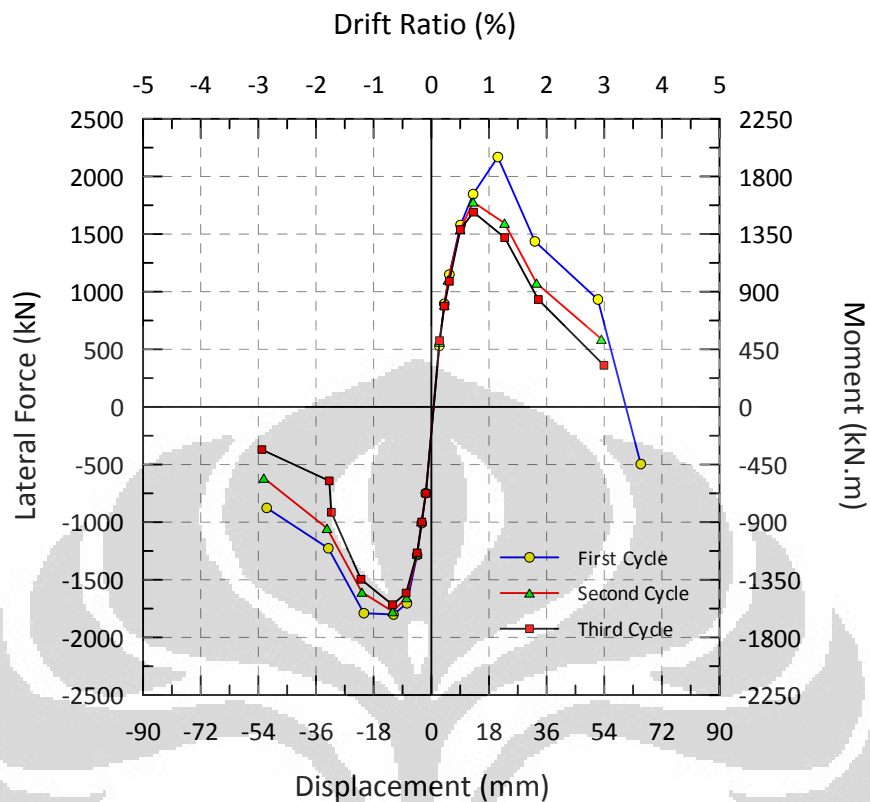
Drift Ratio (%)

Figure 5.46 Envelope of column S2.

Table 5.9 Important points of specimen S2.

Points	Displacement (mm)	Lateral load (kN)	Level of drift ratio
First flexural crack	2.50	529.16	Cycle 1-1 (0.25 %)
	-1.74	-748.17	Cycle 1-1 (0.25 %)
First fhear crack	9.12	1578.64	Cycle 4-1 (0.75 %)
	-7.61	-1703.84	Cycle 4-1 (0.75 %)
Maximum strength	20.77	2168.57	Cycle 6-1 (1.50 %)
	-11.80	-1801.51	Cycle 5-1 (1.00 %)
Loss lateral strength	32.33	1436.46	Cycle 7-1 (2.00 %)
	-21.06	-1789.57	Cycle 6-1 (1.50 %)
Explosive sound	13.05	1846.64	Cycle 5-1 (1.00 %)
1st Yield of hoop	13.05	1846.64	Cycle 5-1 (1.00 %)
20% drop of lateral strength	27.62	1734.85	After Cycle 6-1 (1.50 %)
	-27.93	-1441.21	After Cycle 5-1 (1.00 %)

Figure 5.47 below depicts the location of the strain gauge during the first yield of hoop, at cycle 5-1. Ten of eleven strain gauges worked well during the experiment. Two of these ten strain gauges were attached on longitudinal reinforcement. From

this figure could be clearly seen that a lot of cracks on the bottom of the column passed near the strain gauges, most of them are the red crack, which means the crack that appeared at positive loading direction. No strain reading from longitudinal reinforcement indicated yielding of the bar.
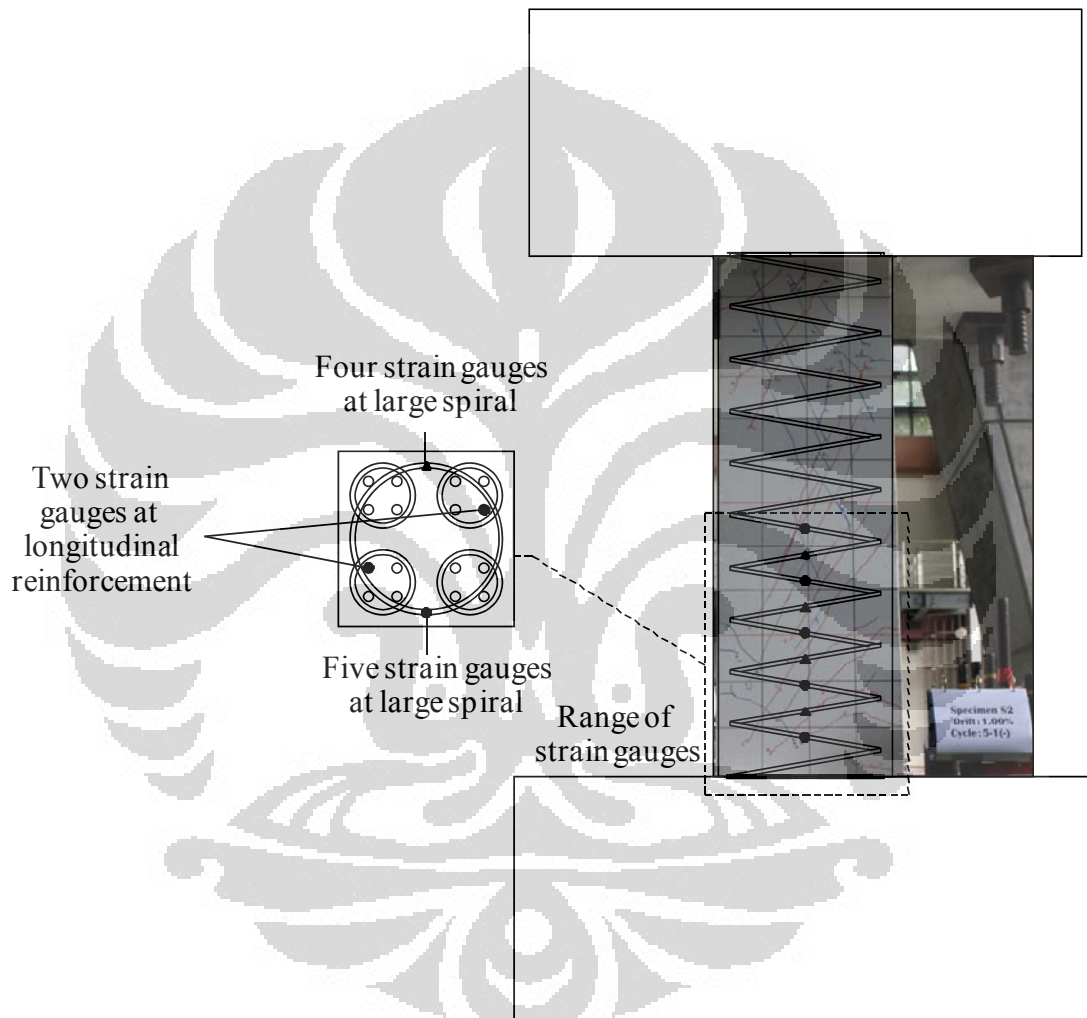
Figure 5.47 Strain reading and crack pattern of column S2 at the first yield of hoop, cycle 5-1 (positive direction).

Figure 5.48 below indicates the location of the strain gauge at the maximum strength of column S2, precisely at cycle 5-1. From this figure could be clearly seen that a lot of cracks on the bottom of the column passed through the strain gauges. Strain reading from longitudinal reinforcement did not indicate yielding but five of eight reliable strain gauges attached on spiral reinforcement reached yield point.

Figure 5.49 shows the condition of column S2 at the final stage. Some part of concrete inside the large spiral transverse reinforcement was broken to pieces including the concrete inside the small transverse reinforcement.

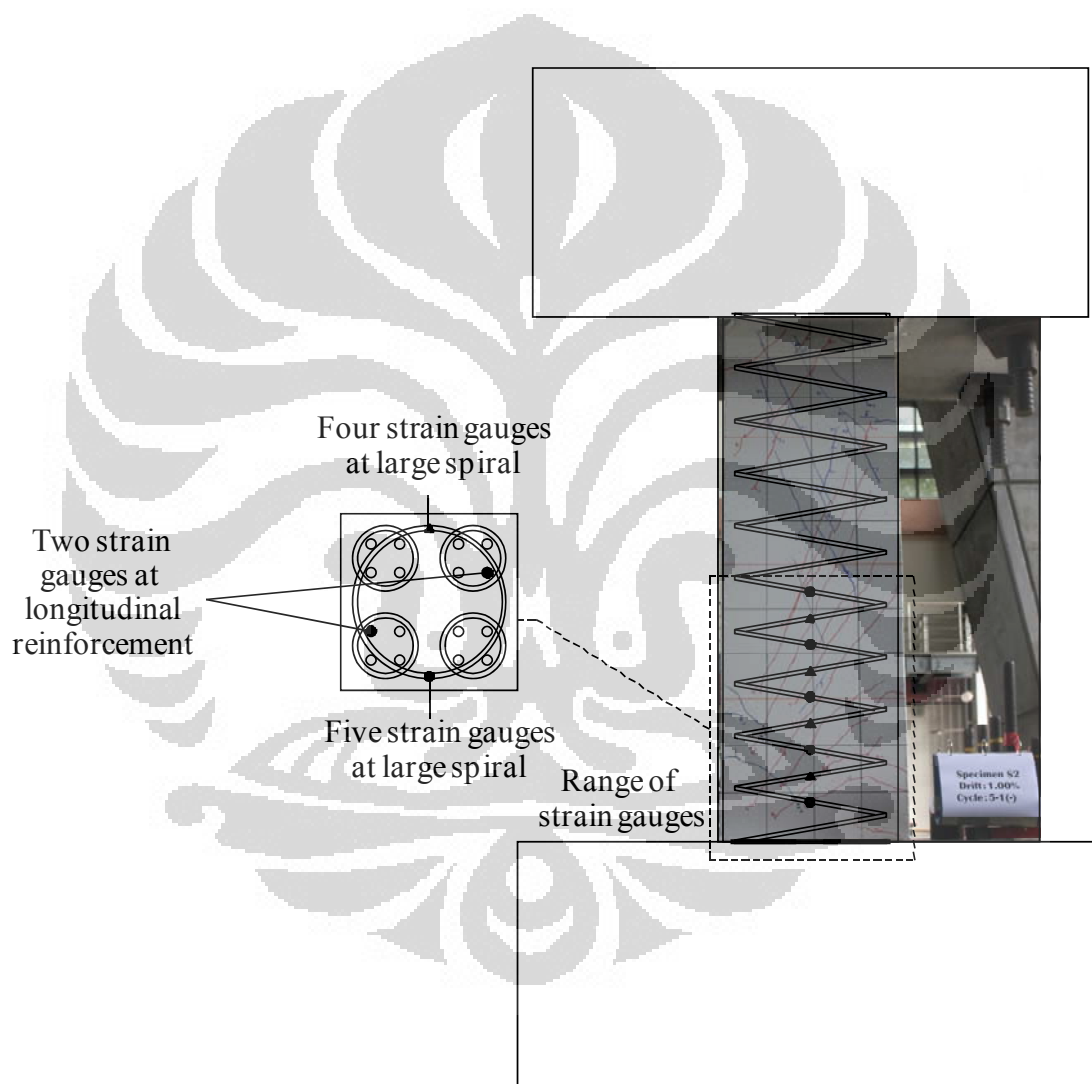**Figure 5.48** Strain reading and crack pattern of column S2 at the maximum strength of column, cycle 6-1 (positive direction).

(a)

(b)

(c)

(d)

Figure 5.49 Final stage of column S2 (4.00 % drift ratio).
(a) West side; (b) East side; (c) South-east side; (d) Failure of large spiral transverse reinforcement at the mid-height of the column west side.

5.4. TEST RESULT COMPARISONS

Figure 5.50 up to 5.53 show the comparison hysteretic loops and envelope of all tested specimens. Six specimens are separated in two different curves, based on its type. Specimen type B has two parameters used in four tested columns, such as: concrete compressive strength (f'_c) and spacing of the transverse reinforcement (*s*). Specimen type S has one parameter in two tested columns, spacing of the transverse reinforcement. Table below shows the summary of the parameters for six specimens.

Table 5.10. Summary of parameters and test results for six specimens.

Specimen	f'_c (MPa)		spacing *s* (mm)	Shear strength Experiment (kN)
	Design	Actual		
B1	70	80.55	450	2184.94
B2	100	114.10	450	2202.54
B3	70	112.85	260	2374.04
B4	100	121.04	260	2443.18
S1	100	117.57	125	2254.24
S2	100	117.57	180	2168.57

It could be clearly seen in Table 5.10 that specimen B1 has the lowest concrete compressive strength (f'_c), 80.55 MPa. The gap of f'_c do not affect significantly to the shear strength of column (the gap was less than 100 kN). On the other hand, the gap of spacing *s* affects up to around 200 kN. Column B1 and B2 that have same spacing of the hoops but different f'_c, give almost same shear strength although the gap for f'_c is quite large. The shear strength of B1 and B2 are 2184.94 kN and 2202.547 kN, respectively. The same thing was also happened in column B3 and B4 due to lack of gap for f'_c. On the other hand, the shear strength of column B1, that have similar f'_c but larger spacing of the hoops, was smaller than column B3 that has more dense hoops. The shear strength of B1 and B3 are 2184.94 kN and 2374.04 kN, respectively. This condition could also be seen for column B2 and B4; S1 and S2.

5.4.1. Test result comparison of type B specimens
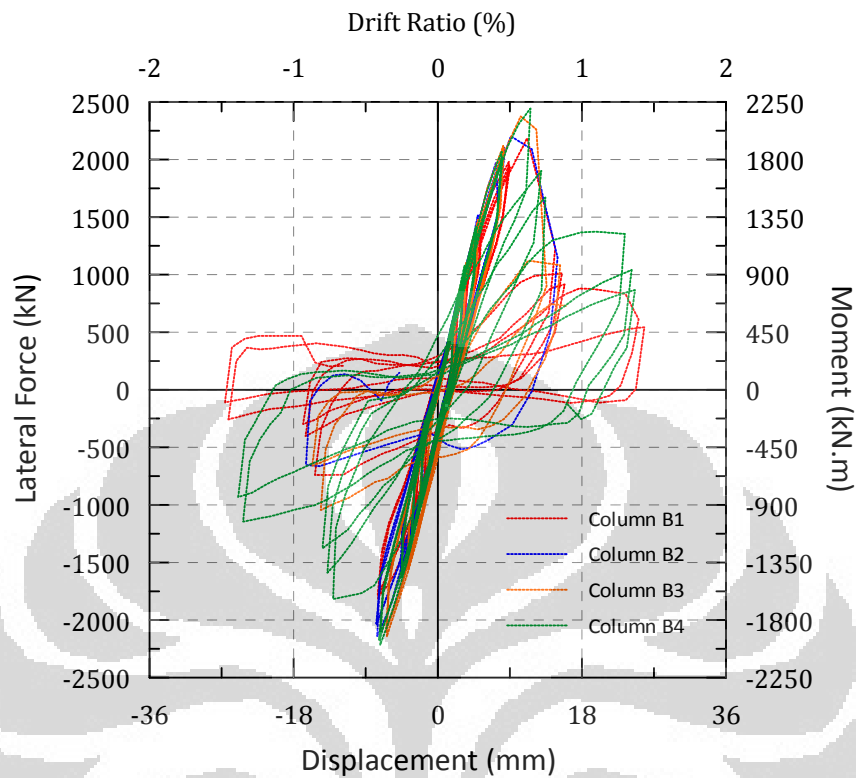
Figure 5.50 Hysteretic loops of four type B specimens.
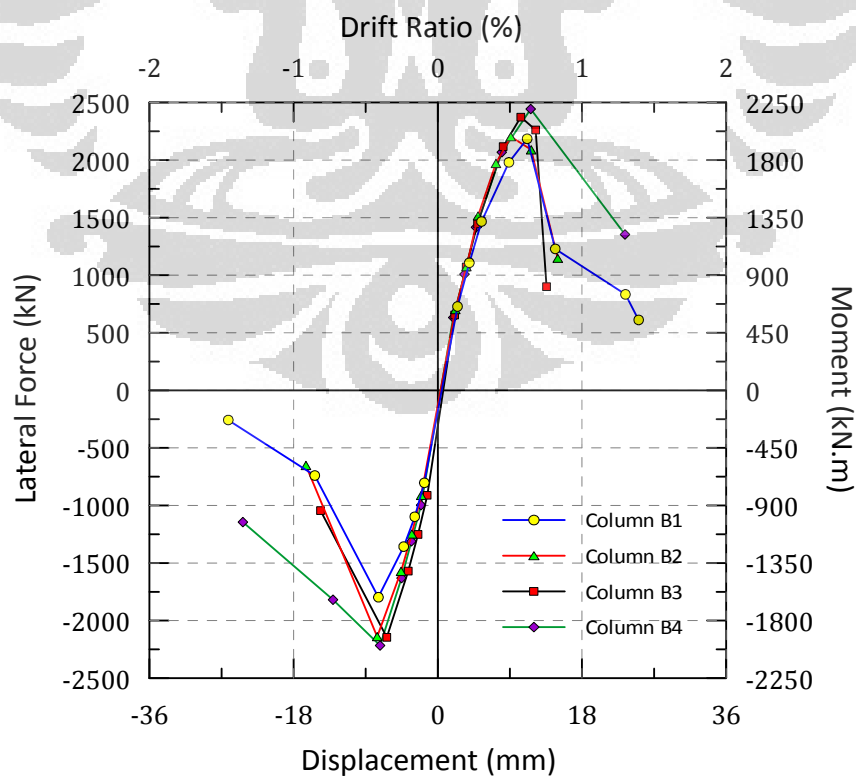
Figure 5.51 Envelope of four type B specimens.

5.4.2. Test result comparison of type S specimens

Drift Ratio (%)
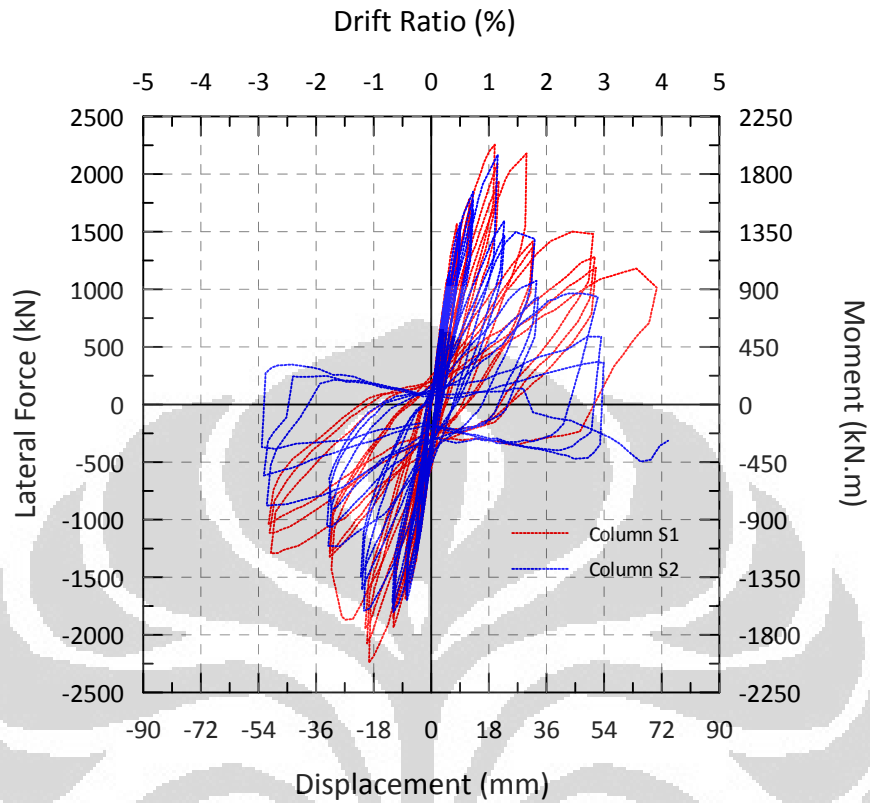
Figure 5.52 Hysteretic Loops of two type S specimens (Multi-spiral).

Drift Ratio (%)
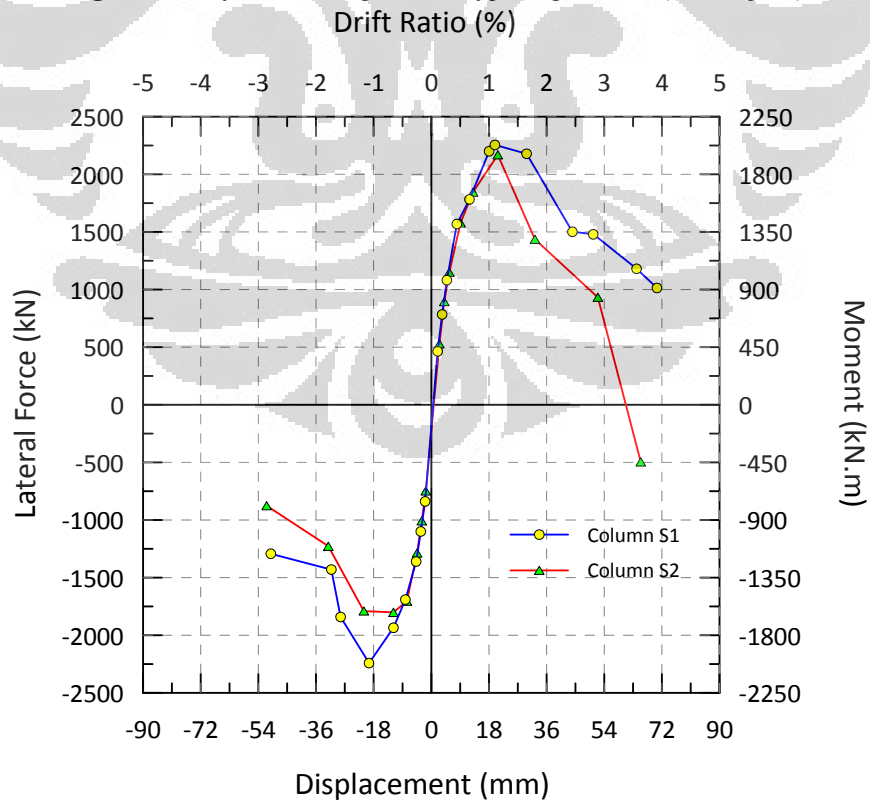
Figure 5.53 Envelope of two specimens type S (Multi-spiral).

5.5. OBSERVATION DURING THE TEST

5.5.1. Critical Crack Angle

Figure 5.54, 5.55 and 5.56 below show the crack angle measured from all specimens.

(a) Column A1   (b) Column A2

(c) Column A3   (d) Column A4
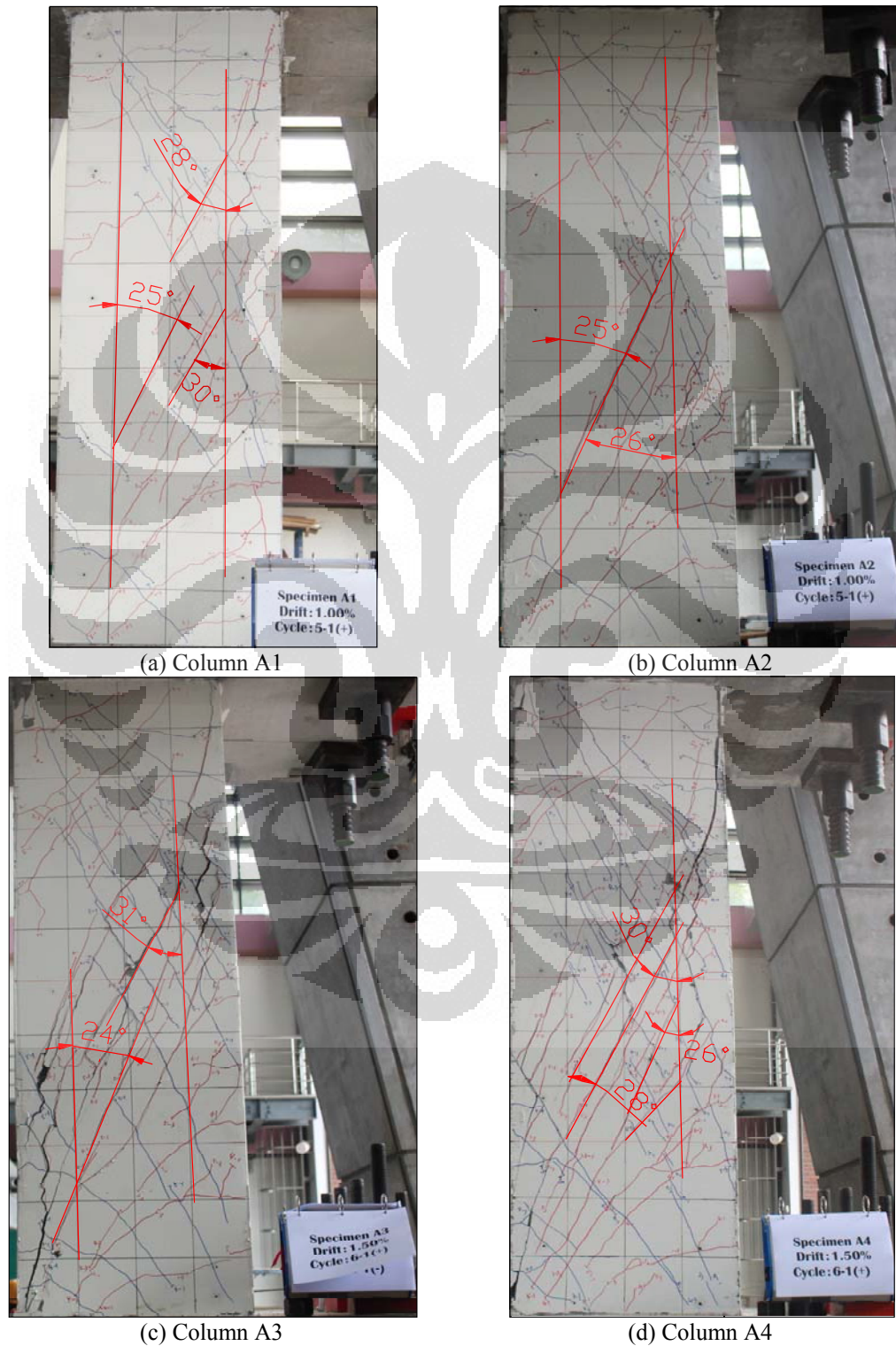
Figure 5.54 Crack angle of specimens A

(a) Column B1

(b) Column B2

(c) Column B3

(d) Column B4
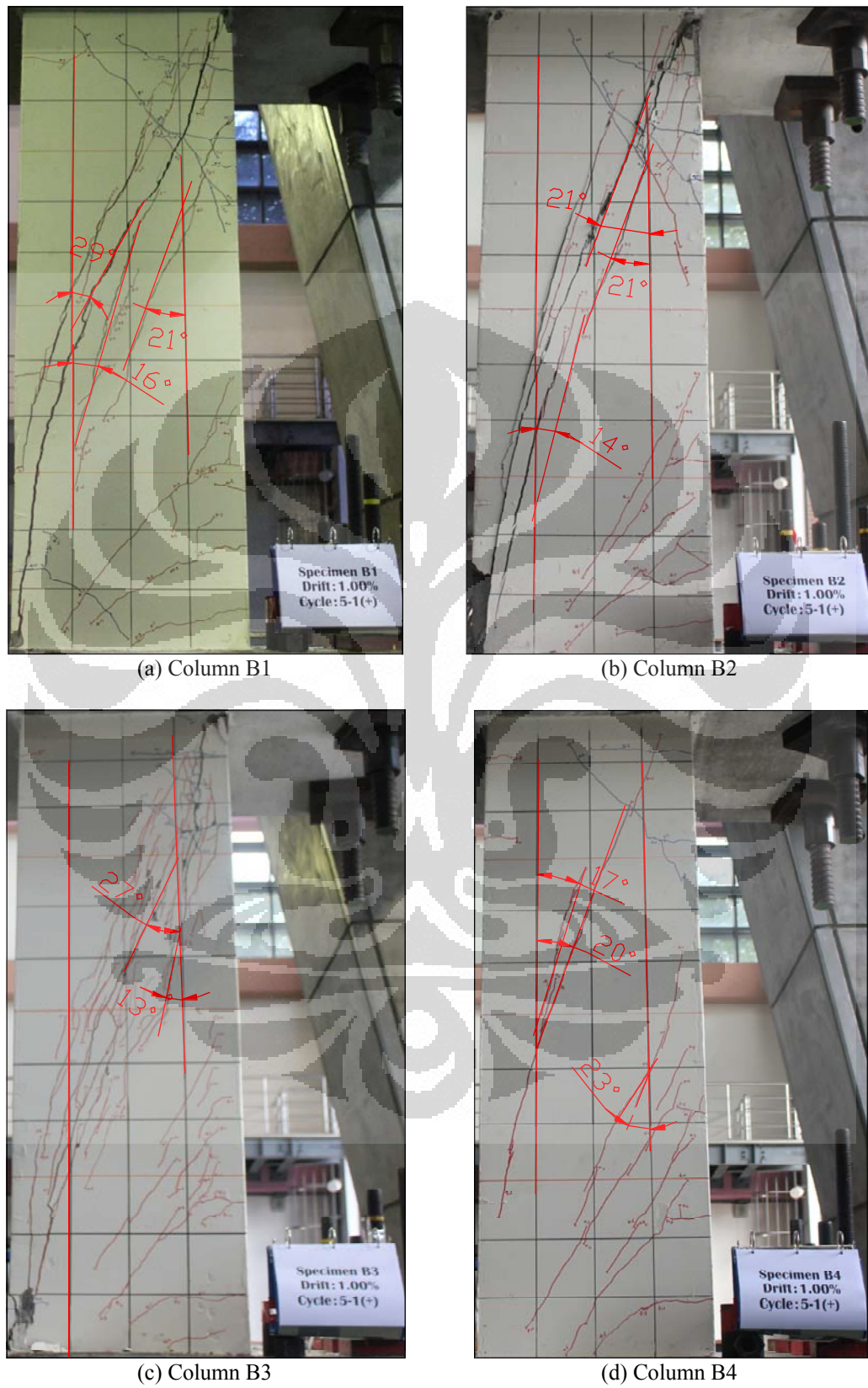
Figure 5.55 Crack angle of specimens B
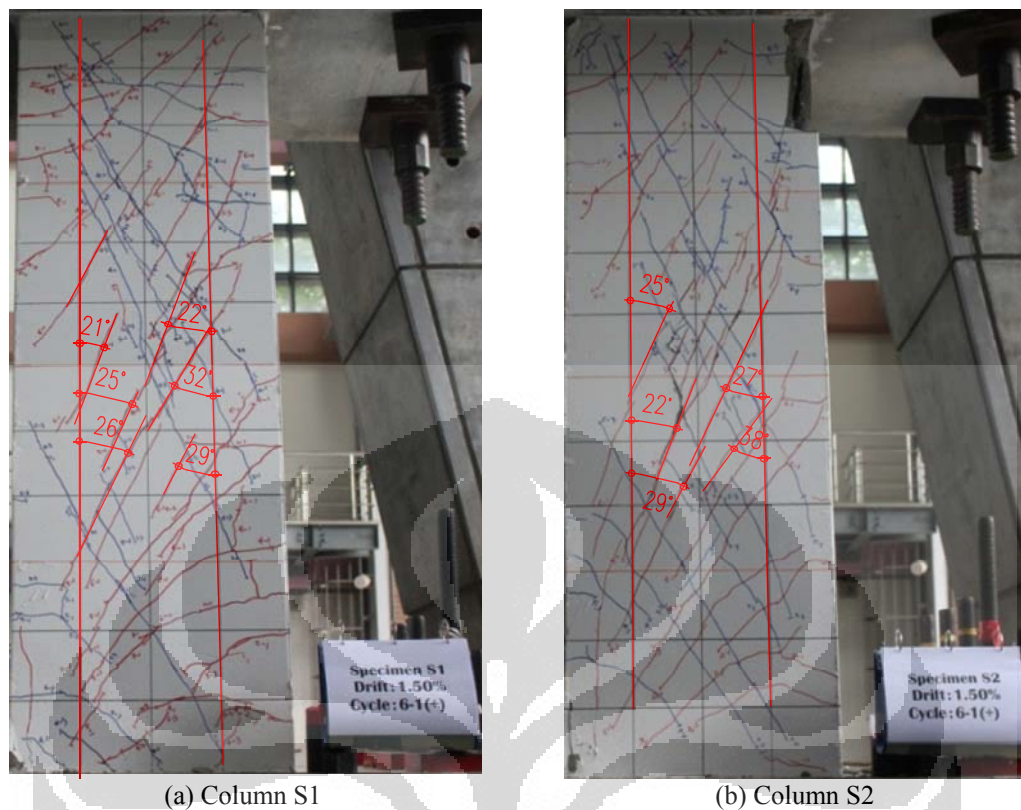
(a) Column S1   (b) Column S2
Figure 5.56 Crack angle of specimens S

Some codes, provisions and researchers (Sezen, Aschheim & Moehle and Kowinski) adopt 45º of the critical crack angle in their models. Other researchers (Priestley et.al., Kowalsky and Xiao & Martirossyan) proposed 30º of critical crack angle in their proposed equations.

AASHTO LRFD 2007[19] provided table that can be used to calculate the critical crack angle as the contribution of the axial compression shown in Table 2.8. The critical crack angle (θ) is based on calculating the stresses that can be transmitted across diagonally cracked concrete that contains at least the minimum amount of transverse reinforcement required for crack control. On the other hand, Elwood and Moehle[23] proposed an equation (Chapter 2 part 2.3.6) to calculate the critical crack angle based on the experimental result.

Crack angle from test result were varies from 13º to 32º as shown in Figure 5.54, 5.55 and 5.56. The crack angle was measured by observing the dominant diagonal shear crack that occurred during the test. Based on the experimental result, the axial compression affects the developing critical crack angle. The 45º crack angle used by codes and also 30º crack angle proposed by several shear models were relatively

constant to any applied axial load.

Table 5.11 shows the comparison crack angle obtained from the experimental result to the crack angle proposed by ASSHTO LRFD 2007[19] and also Elwood & Moehle[23]. Also test result of specimen A (subjected to 10% axial load ratio) is included (Dimas Pramudya Kurniawan[28]).

Table 5.11 Comparison of crack angle

| Specimen | Axial Load Ratio | Critical Crack Angle (°) | | | AASHTO LRFD | Elwood & Moehle |
| | | Test Result | | | | |
		Min	Average	Max		
A1	10%	24.00	26.75	30.00	28.00	31.84
A2		24.00	25.00	26.00	26.90	31.75
A3		22.00	24.60	31.00	28.00	31.80
A4		26.00	28.60	30.00	26.90	31.72
B1	20%	16.00	23.00	29.00	28.00	28.57
B2		14.00	18.50	21.00	26.90	28.35
B3		13.00	21.40	27.00	26.90	28.36
B4		17.00	20.00	23.00	26.90	28.26
S1	10%	21.00	25.83	32.00	25.90	31.49
S2		22.00	26.67	34.00	25.90	31.49

Since the crack angles from the test results are equal or smaller than 30° (for A and B series) and the crack angles from Elwood & Moehle are larger than 30°, that means the crack angle of 30° can be used. Higher the crack angle used in calculation means more conservative of nominal shear strength. Using crack angle of 30° is relatively constant for any applied axial load. The tested columns were applied 10 % axial load ratio for column A and S moreover, four type B columns were subjected to 20 % axial load ratio. Based on experimental results, it could be concluded that higher axial load ratio, smaller the cracking angle appeared. It is obvious from the table that Elwood and Moehle give the same conclusion as the experimental results.

5.5.2. Aggregate Interlock

As explained before, specimens were designed using High-Strength Concrete (f'_c up to 121.04 MPa). Concrete shear strength contribution consists of three important terms, such as: compression zone mechanism, aggregate interlock, and dowel action.

Strength of normal concrete is smaller than the aggregate so the cracks generally show the failure of mortar. In high-strength concrete, the crack shows the failure of aggregates since the strength of the mortar is the same as or larger than the strength of the aggregates. Experimental results show the condition of cutting through aggregate of the columns (Figure 5.57).

Figure 5.57 Cutting through the aggregate.

When crack initiates and passes through the longitudinal reinforcement, dowel action, aggregate interlock and compression zone mechanism are created. It was predicted that these three mechanisms contribute to shear resistance during the development of the crack. As the crack is getting larger, the compression zone decreases and V_c (concrete shear strength contribution) will be reduced. Thus, the shear strength of the column is drop. However, Park et.al[29] stated that nowadays several researchers such as Zararis-Papadakis and Kotsovos-Pavlovic proposed not to consider aggregate interlock along the crack surfaces and dowel action of longitudinal reinforcement. Since the compression zone of intact concrete prevents shear-slip of the crack surfaces, these two mechanisms do not significantly contribute to the shear strength of the structural member. Stated differently, these two mechanisms will not appear as long as the compression zone still exists. In order to design conservatively, the shear resistance was assumed to be provided mainly by the compression zone of the intact concrete.

5.6. MAXIMUM STRESS OF TRANSVERSE REINFORCEMENT

Experimental results indicate that reliable strain reading from column B1, B3 and B4 did not reach the yield point of hoop. On the other hand the rest of the specimen (B2, S1 and S2) indicated the yielding point of hoop. Moreover, column B2 reached the yield point after passed the maximum/peak strength and maximum shear strength of column S1 and S2 occurred at the same time with their yield point. Based on this condition, the actual stresses in the hoop at the maximum strength (peak point) of column are smaller than the yield point of the transverse reinforcement. Although most of nominal shear strength obtained from codes and guidelines give a result smaller than 1.00 (means they perform well, see Table 3.2 and 3.3), the limitation of the maximum stress at peak point of transverse reinforcement is needed since the behavior of columns show this condition. The limitation is not only useful for the design but also important to understand the behavior of structure member specially column with high strength steel and concrete.

The New RC equation mentioned in Chapter 2, limits the maximum stress of hoops by the following equation $f_{yt} \leq 125\sqrt{\nu_0 f'_c}$ where ν_0 and f'_c are the effective concrete factor and concrete compressive strength, respectively. Table 5.12 below shows the yield and actual stress of transverse reinforcement and current code limitation, data of type A specimen obtained from Dimas Pramudya Kurniawan[28].

Table 5.12 Yield & Actual Stress of Transverse Reinforcement and Current Code Limitation

Specimen	f_{yt} (MPa)	Maximum Hoop Stress at Peak Point (MPa)	Maximum Stress (MPa)	
			ACI 318-08	New RC Equation
A1	862	638.80	550	807.33
A2	862	548.00	550	837.30
A3	862	839.60	550	819.94
A4	862	-	550	847.86
B1	862	683.59	550	862.00
B2	862	525.09	550	862.00
B3	862	-	550	862.00
B4	862	563.40	550	862.00
S1	862	865.86	550	862.00
S2	862	865.86	550	862.00

The maximum stress of the hoops obtained from New RC equations for type A

specimens are quite close to the yield stress of transverse reinforcement. Moreover, type B and S specimens have the same value as the yield stress. Most of the actual stress of the hoops at the peak point is lower than yield stress and the limitation of New RC equation. Only one strain reading from specimen A3 passed the yield point. The limitation of the ACI 318-08[14] is conservative compare to the actual stress of the test results. It has 550 MPa (for welded deformed wire reinforcement) which is close enough to some values of strain reading maximum hoop stress.

Only six of eight columns (type A and B) gave the reliable strain reading. They give the average value of 633.08 MPa and standard deviation of 117.47 MPa. Although this average value seems good enough, more conservative value is apparently more considered for the design. Based on ACI 318-08, it is proposed that the design value for the maximum hoop stress is 550 MPa.

Furthermore, a normal distribution analysis of these six strain reading was performed. Using the average value of 633.08 MPa, standard deviation of 117.47 MPa and random value of $z = \pm 3$, normal distribution (PDF and CDF) graph as shown in Figure 5.58 obtained.
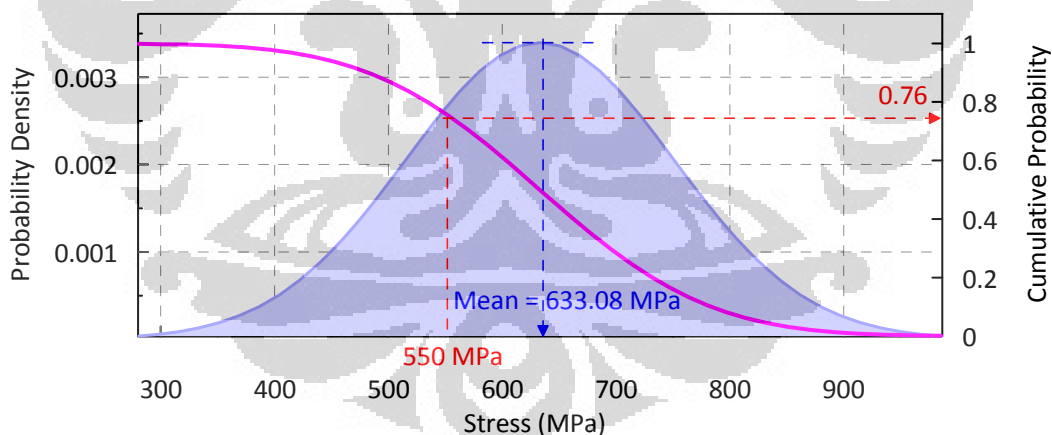

Figure 5.58 Probability Density Function (PDF) and Cumulative Density Function (CDF) of stress at hoops from strain reading of A & B columns.

From the Cumulative Density Function (CDF) as shown in Figure 5.58 above, it is obvious that at 550 MPa of stress, 0.76 or 76% of exceedance probability occur. Seventy six percent of exceedance probability (P76) means there is a possibility of 24% that the P76 level will not be reached. On the other words, 24 from 100 events will not reach the design value of 550 MPa.

From Table 5.12, specimen S1 and S2 reached yield of hoops which is also the same

prediction from New RC equation. As explained before, most of the strain gauges type S specimens worked well. The maximum hoops stress of multi-spiral specimens passed the yield point. This condition means that during the design, it is possible to use the yield value of transverse reinforcement.

5.7. DRIFT RATIO AND STRESS OF TRANSVERSE REINFORCEMENT

(a) Drift ratio less than 0.50%

(b) 0.50-0.59 % of drift ratio

(c) 0.60-0.69 % of drift ratio

(d) 0.70-0.79 % of drift ratio

(e) 0.80-0.99 % of drift ratio

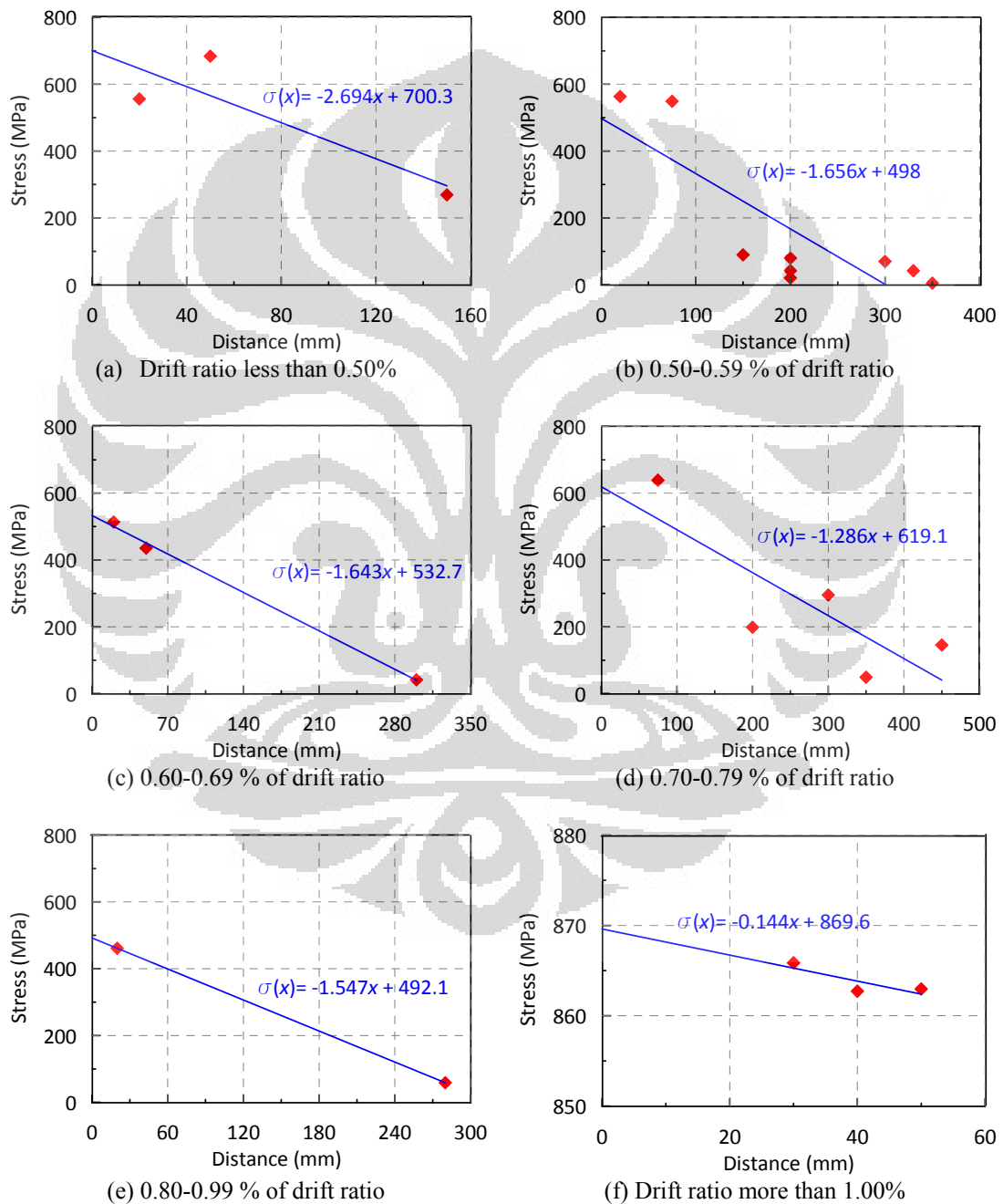(f) Drift ratio more than 1.00%

Figure 5.59 Distance vs. Stress at hoops for different level of drift ratio.

Universitas Indonesia

Observation on type A and B columns during experimental shows that crack did not appear and pass the hoops exactly where the strain gauges attached. More study from test results indicates that closer the strain gauges position to the crack, higher the accuracy of strain gauges reading. In other words, the measurement of strain gauges will be very important at zero distance from the closer cracked (or exactly at crack). Figure 5.59 in previous page shows the relationship between distance and stress at transverse reinforcement from six different drift ratios. Since the stress will reach higher value at smaller distance to the crack, it is reasonable to relate this relationship linearly as marked in blue line for each graph in this figure.

Furthermore, linear relationship gives the stress of the hoop at zero distance to crack. It is observable that the higher drift level, the higher of stress that could be reached by the hoops. Figure 5.60 below gives the idea of this condition. Five red squares show the approximation value of hoop stress at the crack for five different drift levels. Linear relationship of drift ratio and stress of hoops at crack is shown in blue line. The intersection point with yield stress of hoops ($(\sigma_y)_{design} = 785$ MPa) demonstrates that at around 0.95% drift ratio, the yield point of hoop stress will be reached.
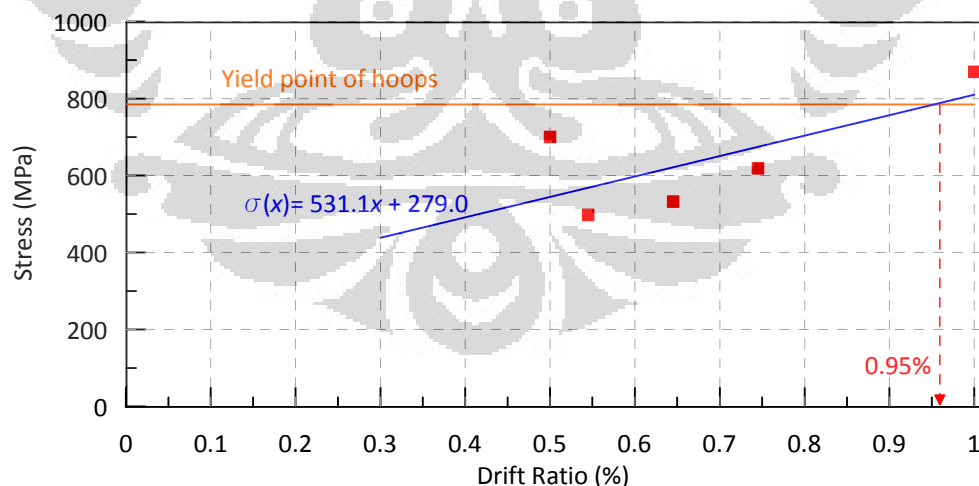

Figure 5.60 Drift ratio vs. Stress at hoops for different level of drift ratio.

Previous explanation gives an idea about relationship between drift ratio and stress of hoops. In the future research, it is reasonable to consider the drift ratio in order to predict the nominal shear strength of concrete. Two figures in this part show the

relationship to the stress of hoops from two types of specimens which were loaded by low axial load ratio (10% for type A columns and 20% for type B columns). So, it will be important to consider the axial load ratio and its effect to relationship of drift ratio and hoops yield stress.

5.8. SHEAR STRAIN, CURVATURE AND DISPLACEMENT

Measurement of displacement and rotation of columns was performed by the instrumentation that consists of LVDT, rotation gauges (tilt meter) and NDI image system. Figure 5.61 shows the configuration and illustration of the LVDT deformation due to shear force. The diagonal LVDT will deform such a manner where γ is shear strain and Δ_s is shear displacement.
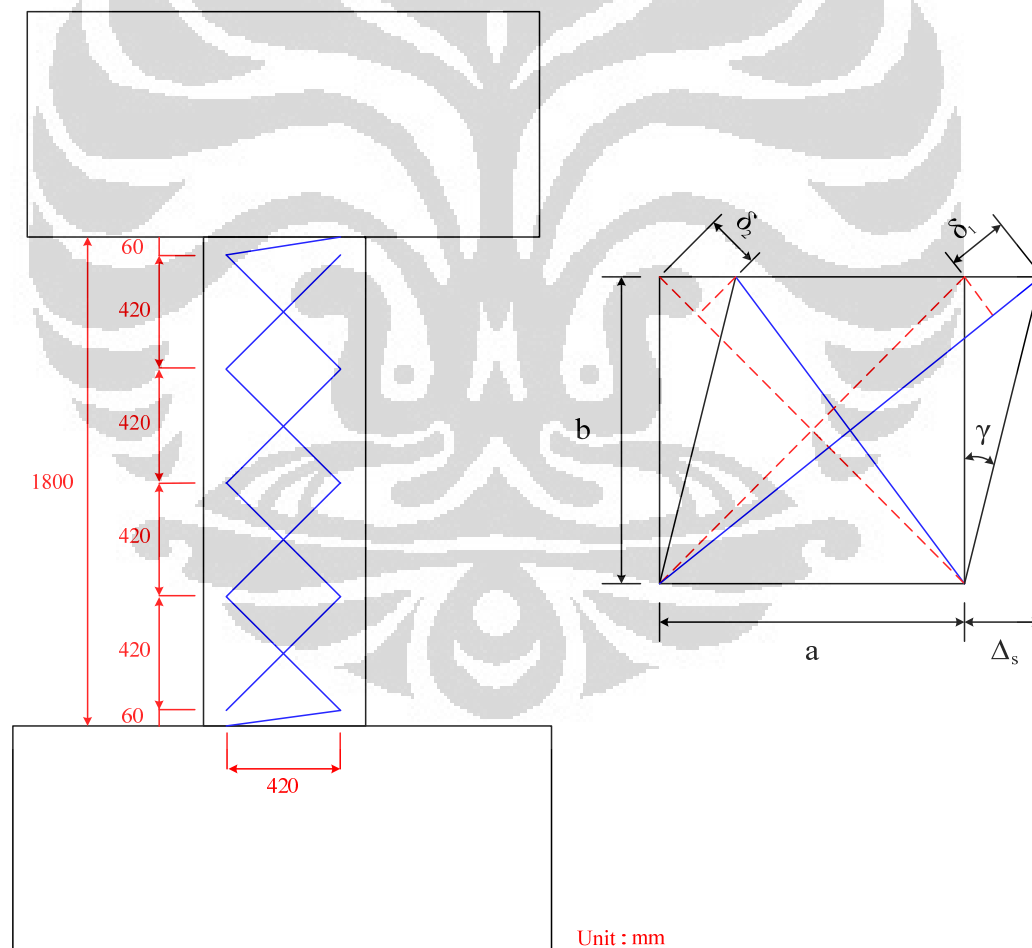

Figure 5.61 Shear strain and shear displacement of the column

The following equations explain how the shear strain (γ) and shear displacement (Δ_s) were derived. At the end of derivation, it could be seen that shear displacement can be obtained as one of the component of column displacement. Some part of the equation (5.3) will be neglected since the value is small compared to other components.

$$\sqrt{(a + \gamma b)^2 + b^2} = \sqrt{a^2 + b^2} + \frac{\delta_1 + \delta_2}{2} \tag{5.1}$$

$$(a + \gamma b)^2 + b^2 = \left(\sqrt{a^2 + b^2} + \frac{\delta_1 + \delta_2}{2}\right)^2 \tag{5.2}$$

$$a^2 + 2a\gamma b + (\gamma b)^2 + b^2 = a^2 + b^2 + 2\sqrt{a^2 + b^2}\delta_{ave} + \delta_{ave}^2 \tag{5.3}$$

Where:

$$\delta_{ave} = \frac{\delta_1 + \delta_2}{2} \tag{5.4}$$

Shear strain(γ) can be obtain from the following equation

$$2a\gamma b = 2\sqrt{a^2 + b^2}\left(\frac{\delta_1 + \delta_2}{2}\right) \tag{5.5}$$

$$\gamma = \frac{\sqrt{a^2 + b^2}(\delta_1 + \delta_2)}{2ab} \tag{5.6}$$

And shear displacement (Δ_s) can be obtain from the following equation

$$\Delta_s = \gamma b \tag{5.7}$$

Flexural displacement will also be discussed in this part including the theoretical background of attached instrumentation, such as LVDT, rotation gauge and image measurement that were installed in the specimens. Figure 5.62 illustrated the curvature and rotation of the column due to flexure. The following equations explain how curvature $(\emptyset)$ and flexural displacement (Δ_f) were derived. As the specimens are restrained in two points, double curvature will be obtained from this experiment.
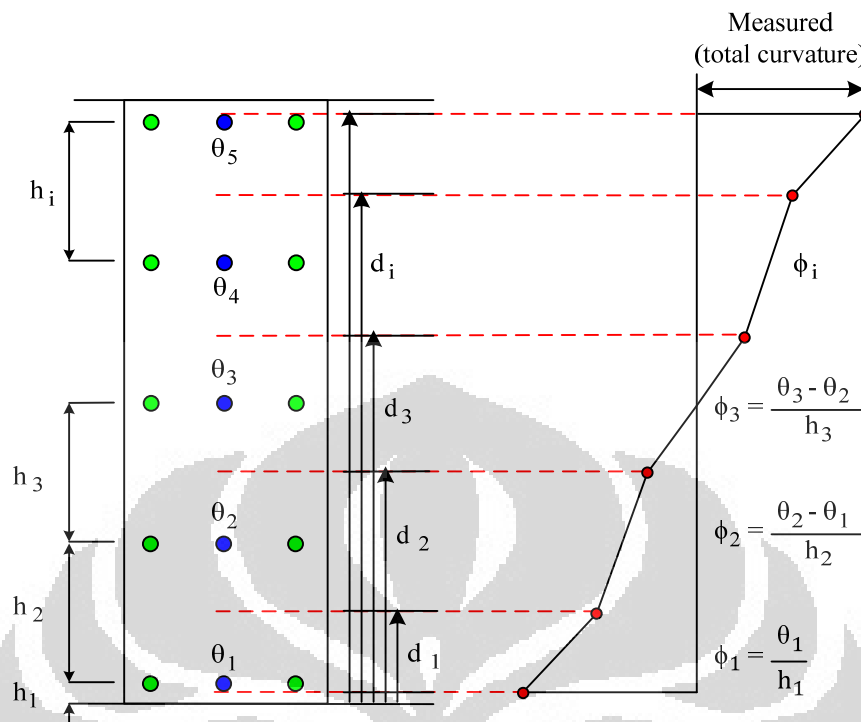
Figure 5.62 Rotation and curvature of the column

As illustrated in Figure 5.62 the curvature of the column can be obtained from

$$\phi_i = \frac{\theta_{i+1} - \theta_i}{h_i} \tag{5.8}$$

And the flexural displacement can be obtained from following equation

$$\Delta_f = \phi_i d_i h_i \tag{5.9}$$

5.8.1. Shear strain of the specimens

Figures 5.63 to Figure 5.68 show the Average Shear Strain (γ_{ave}) vs. Percentage of Column Height (%) relationships of all specimens obtained from the instrumentation.

5.8.2. Curvature of the specimens

Average Curvature (ϕ_{ave}) vs. Percentage of Column Height (%) relationships all specimens obtained from the instrumentation are shown in Figure 5.69 to Figure 5.74.

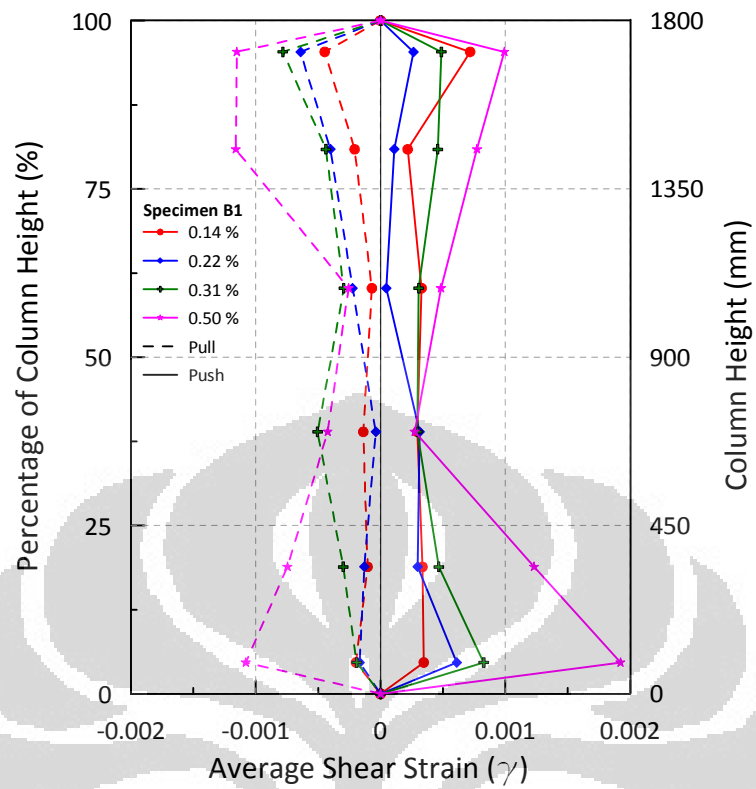**Figure 5.63** Average shear strain (γ) over the height of column B1 up to 0.75% drift ratio
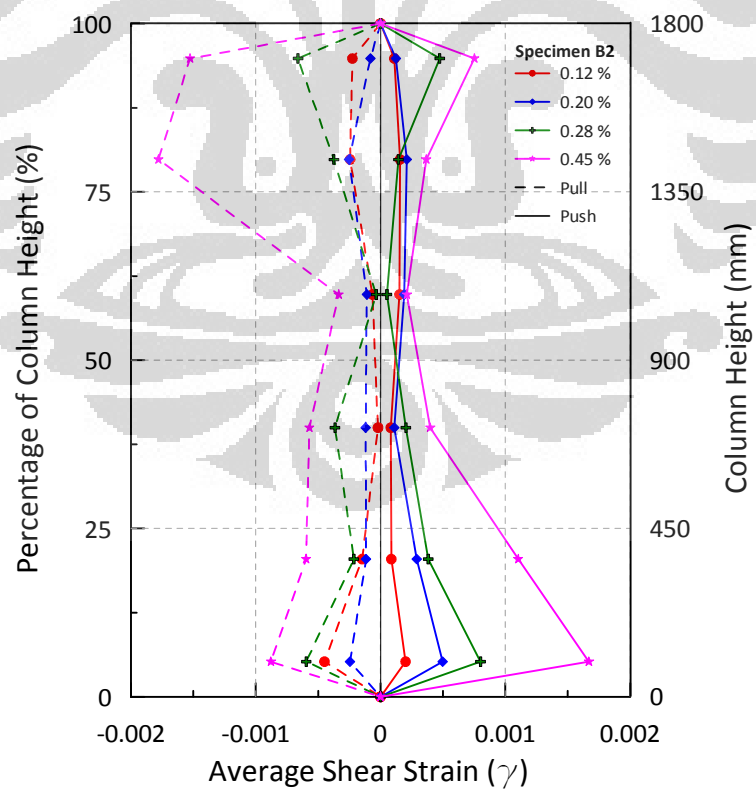

Figure 5.64 Average shear strain (γ) over the height of column B2 up to 0.75% drift ratio

Figure 5.65 Average shear strain (γ) over the height of column B3 up to 0.75% drift ratio

Figure 5.66 Average shear strain (γ) over the height of column B4 up to 0.75% drift ratio
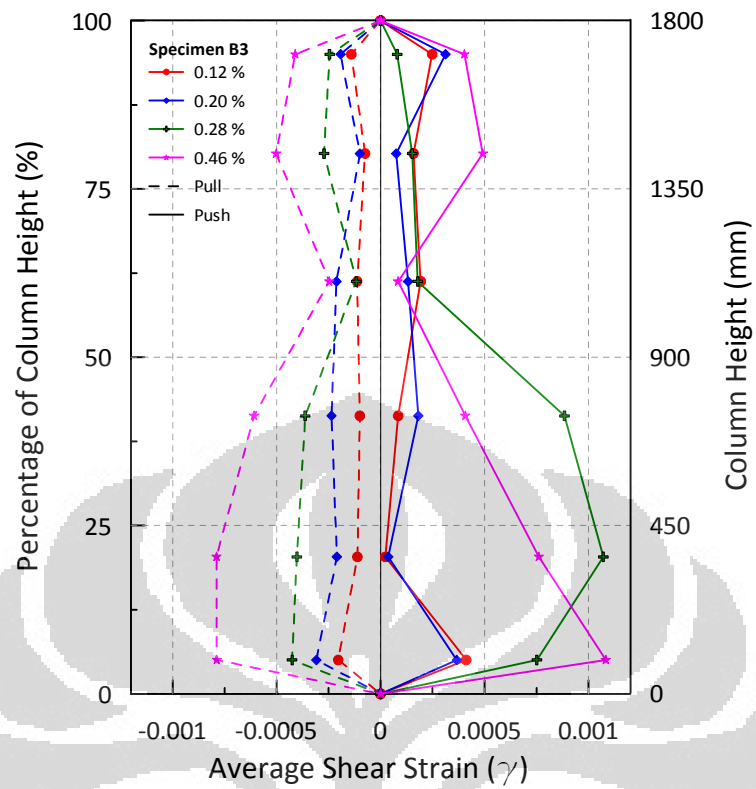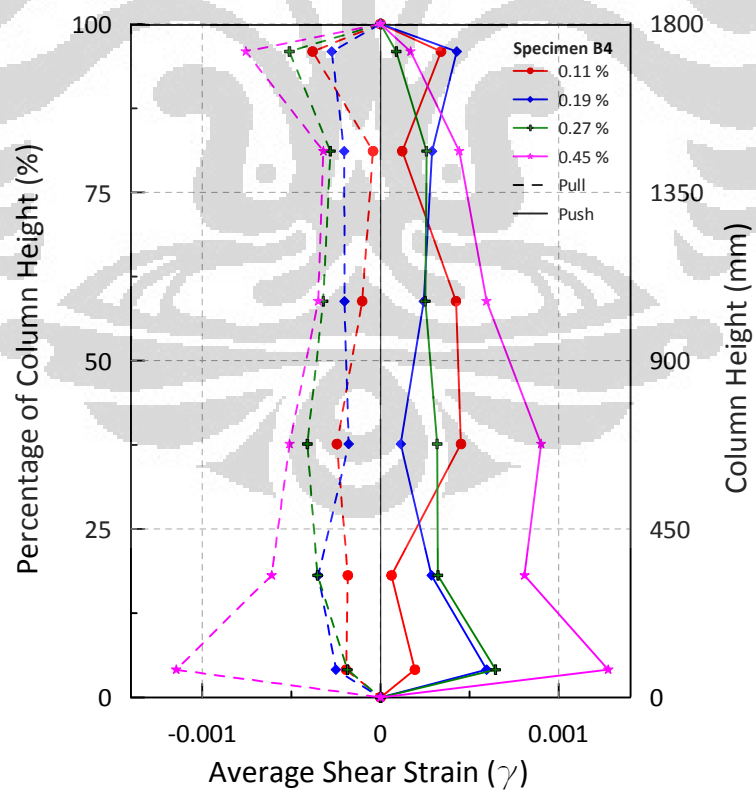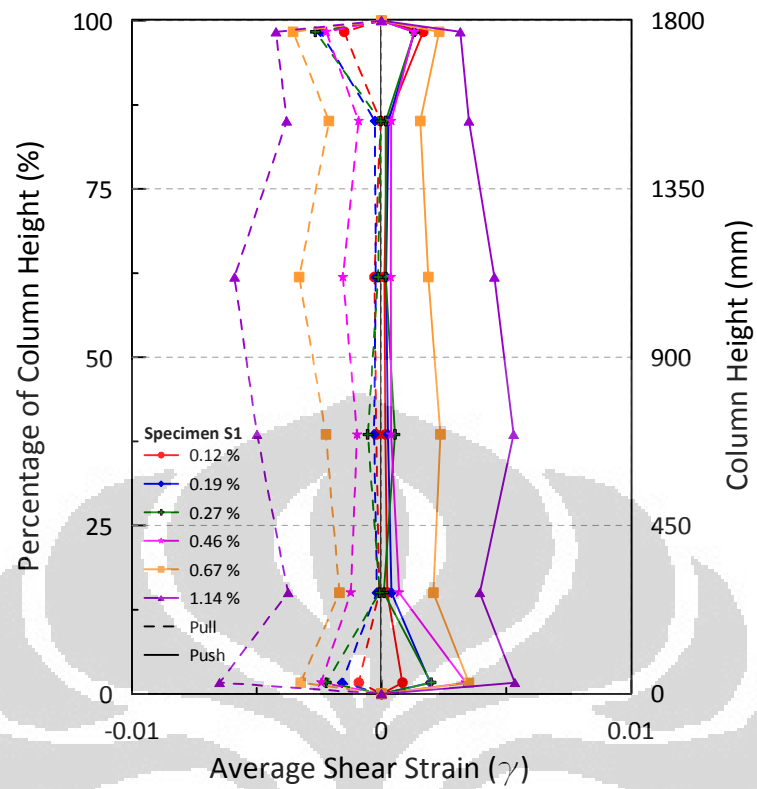
Figure 5.67 Average shear strain (γ) over the height of column S1 up to 1.50% drift ratio

Figure 5.68 Average shear strain (γ) over the height of column S2 up to 2.00% drift ratio

Universitas Indonesia

Figure 5.69 Average curvature over the height of column B1 up to 0.75% drift ratio

Figure 5.70 Average curvature over the height of column B2 up to 0.75% drift ratio

Figure 5.71 Average curvature over the height of column B3 up to 0.75% drift ratio.

Figure 5.72 Average curvature over the height of column B4 up to 0.75% drift ratio
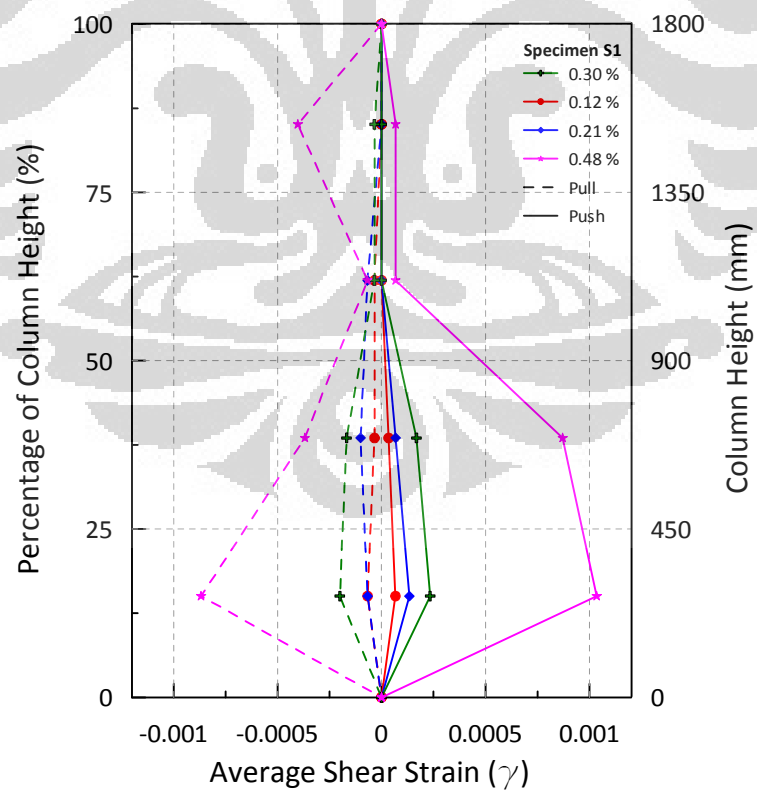
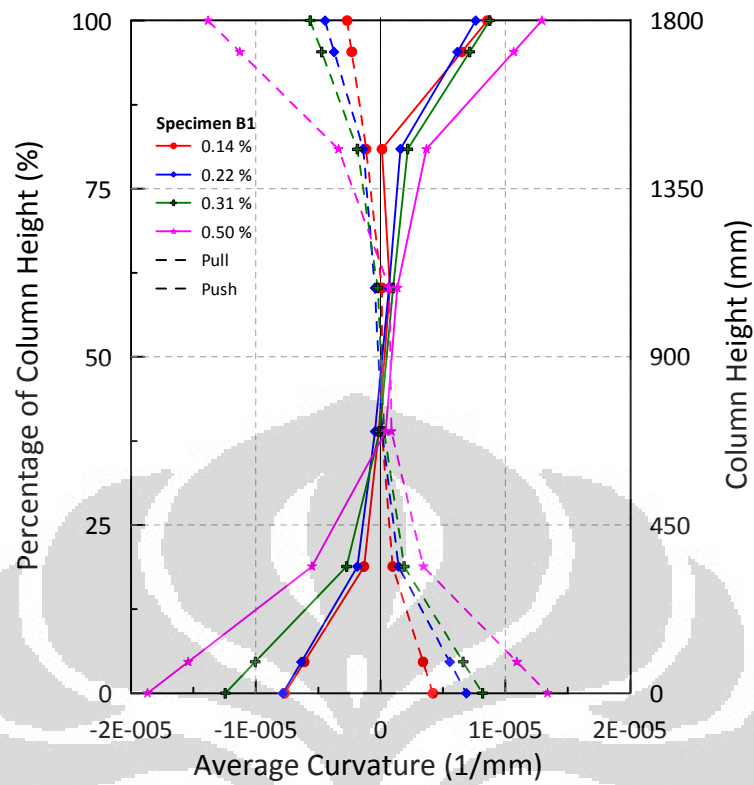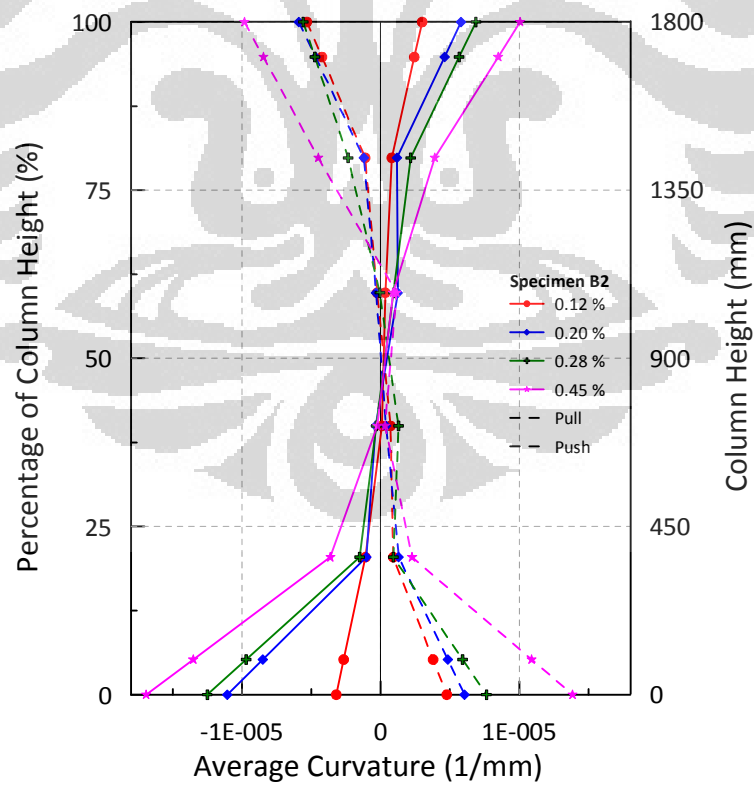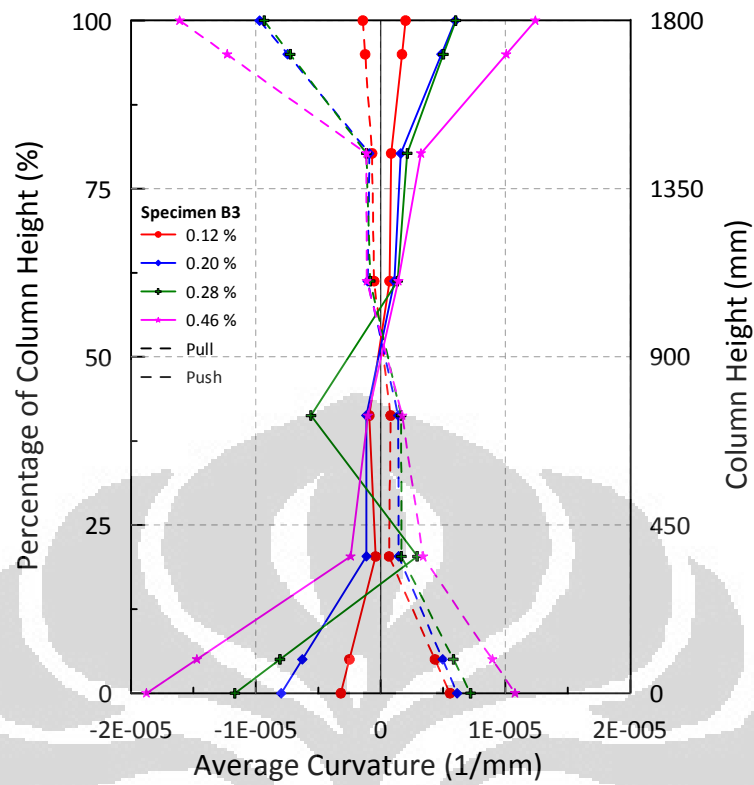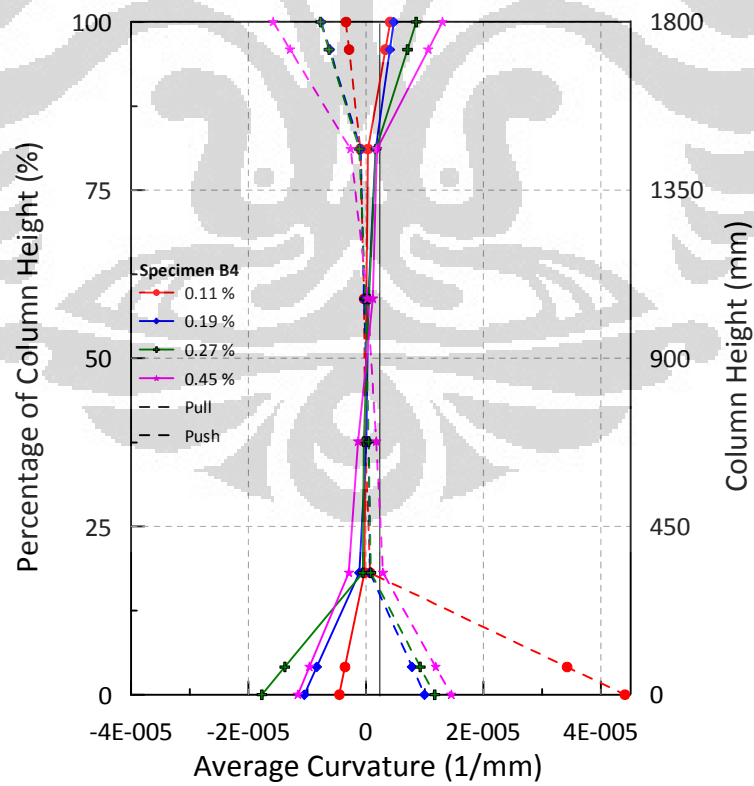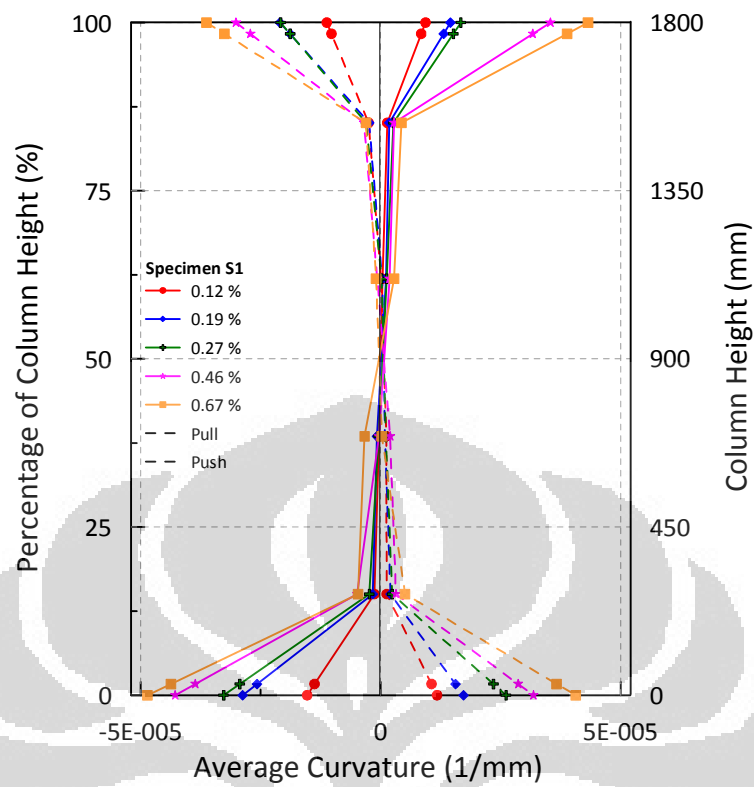Universitas Indonesia

Figure 5.73 Average curvature over the height of column S1 up to 1.00% drift ratio

Figure 5.74 Average curvature over the height of column S2 up to 2.00% drift ratio
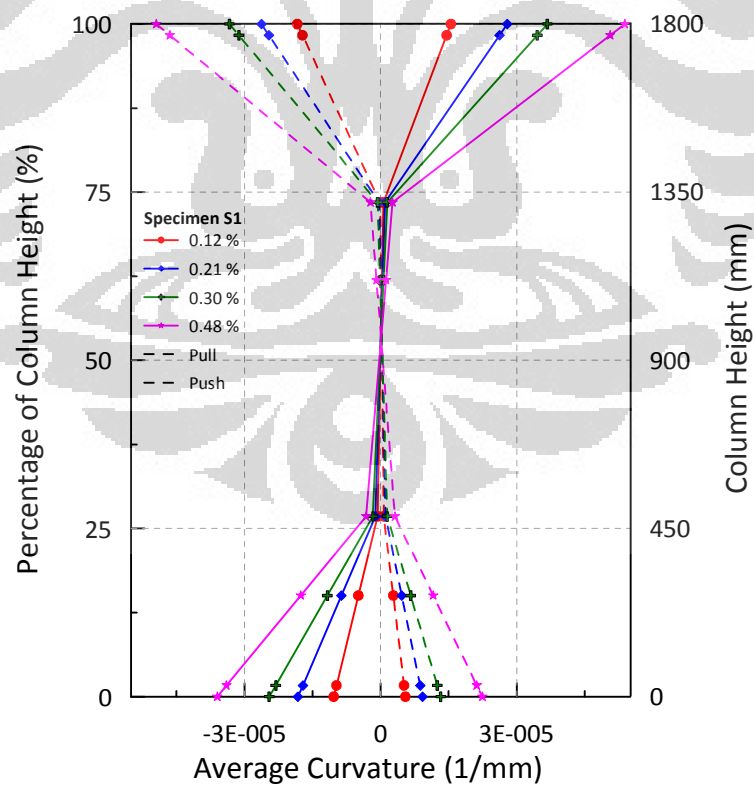
Universitas Indonesia

5.8.3. Displacement of the specimens

Measured displacement obtained from instrumentation (LVDT, tilt meter and NDI image system) of the specimens could be seen in the next eighteen figures. Two parts separate type B and S specimens. Each specimen has three different graphs. Based on analysis and observation, there are three component of displacement of each column, flexure and slip displacement, shear displacement and displacement as the effect of block rotation. Block is considered as rigid component in foundation and upper part of columns.

Figure 5.75, 5.78, 5.81, 5.84, 5.87 and 5.90 depicts the displacement vs. time step of each column. The contribution of three different components, such as shear, flexure-slip and the block rotation are represented in yellow, red and green color respectively.

The second figure shows the stacked column chart illustrating the percentage of each displacement component. As mentioned in part 4.3, there are three cycles for each drift level, therefore in this figure, three number represents one level of drift ratio in positive and negative loading direction. At the beginning, shear displacement took a large portion of measured displacement. In part 5.3, it was mentioned that shear cracked started to propagate in these four type B columns at 0.75% drift ratio. Figure 5.76, 5.79, 5.82 and 5.85 depicts obviously that shear dominates the displacement contribution after passing the cycle 12 (0.75% drift ratio). Apparently, when shear crack started to develop, columns under compression and lateral loading resisted the shear transfer. While the cracks were getting larger and specimen reached its peak strength, the shear displacement enlarged. The flexural and slip contribution decrease while the shear contribution increases significantly. Two type S columns do not have the leap value of shear displacement. It increases gradually until the end of experiment (Figure 5.88 and 5.91).

The percentage of measured displacement components vs. drift ratio of all specimens could be seen in Figure 5.77, 5.80, 5.83 and 5.86. The displacement from the first cycle of each drift ratio were used and plotted. Shear displacement took a large portion of the measured displacement at the end of experiment.

Universitas Indonesia

5.8.3.1. Type B Columns

Figure 5.75 Measured Displacement vs. Time Step of Column B1

Figure 5.76 Percentage of Measured Displacement vs. Cycle of Column B1

Figure 5.77 Percentage of Measured Displacement Component vs. Drift Ratio of Column B1

Universitas Indonesia

Figure 5.78 Measured Displacement vs. Time Step of Column B2

Figure 5.79 Percentage of Measured Displacement vs. Cycle of Column B2

Figure 5.80 Percentage of Measured Displacement Component vs. Drift Ratio of Column B2

Figure 5.81 Measured Displacement vs. Time Step of Column B3

Figure 5.82 Percentage of Measured Displacement vs. Cycle of Column B3

Figure 5.83 Percentage of Measured Displacement Component vs. Drift Ratio of Column B3

Figure 5.84 Measured Displacement vs. Time Step of Column B4

Figure 5.85 Percentage of Measured Displacement vs. Cycle of Column B4

Figure 5.86 Percentage of Measured Displacement Component vs. Drift Ratio of Column B4
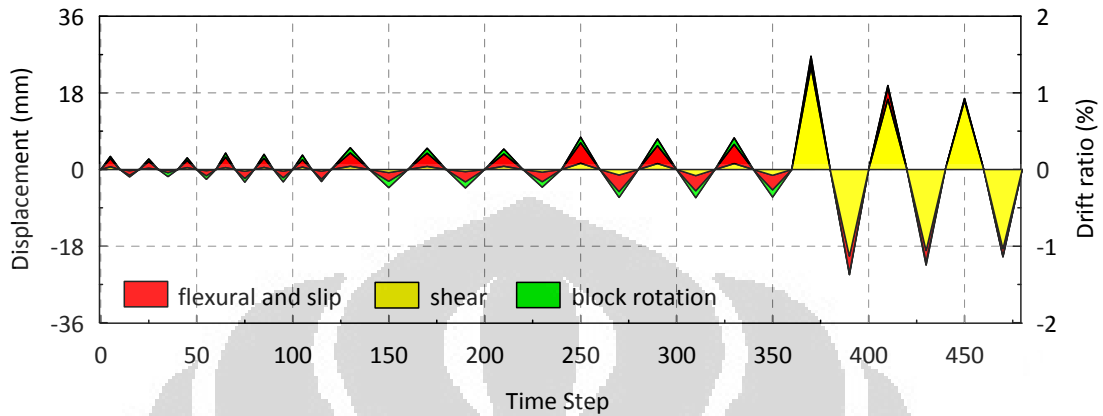
5.8.3.2. Type S Columns
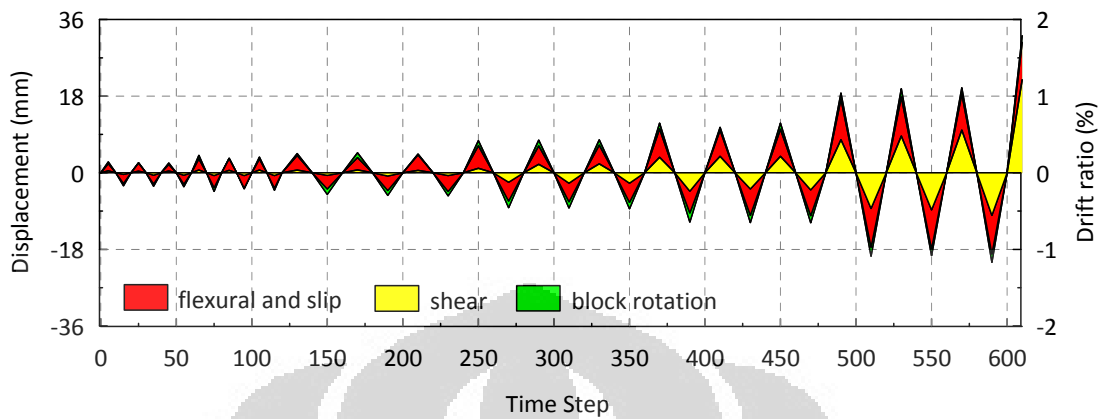
Figure 5.87 Measured Displacement vs. Time Step of Column S1
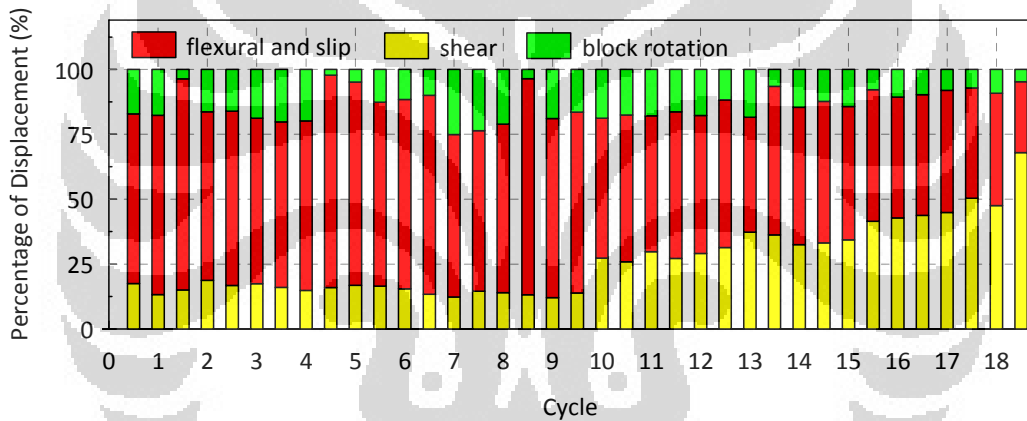
Figure 5.88 Percentage of Measured Displacement vs. Cycle of Column S1
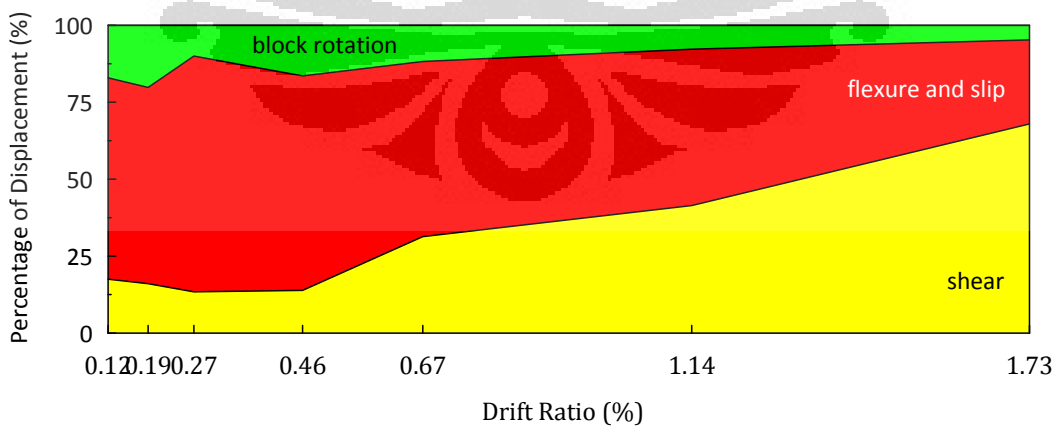
Figure 5.89 Percentage of Measured Displacement Component vs. Drift Ratio of Column S1

Universitas Indonesia
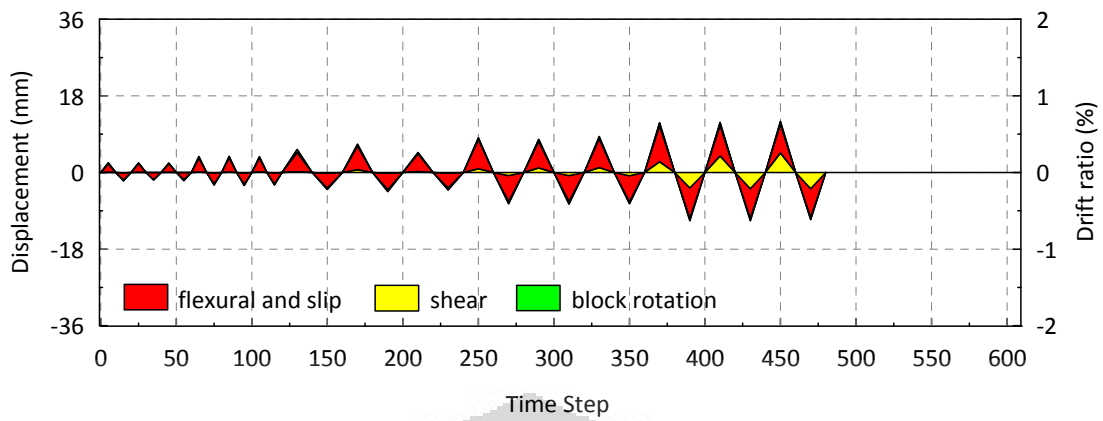
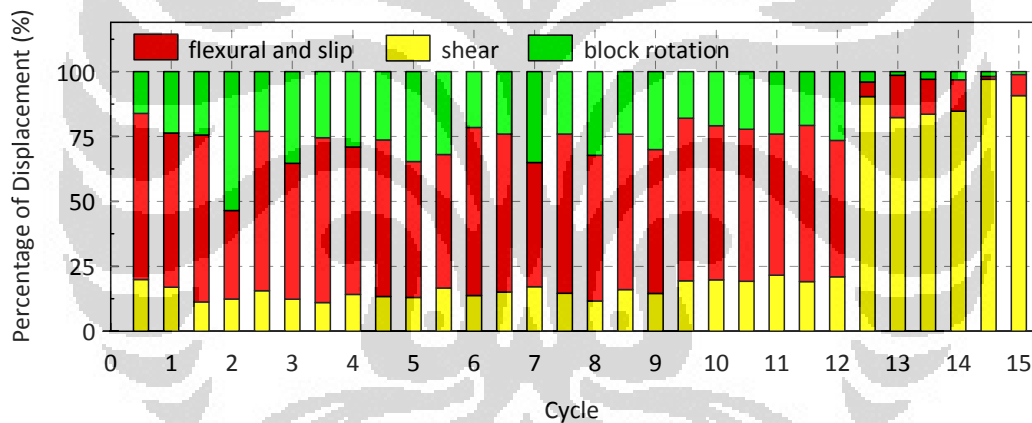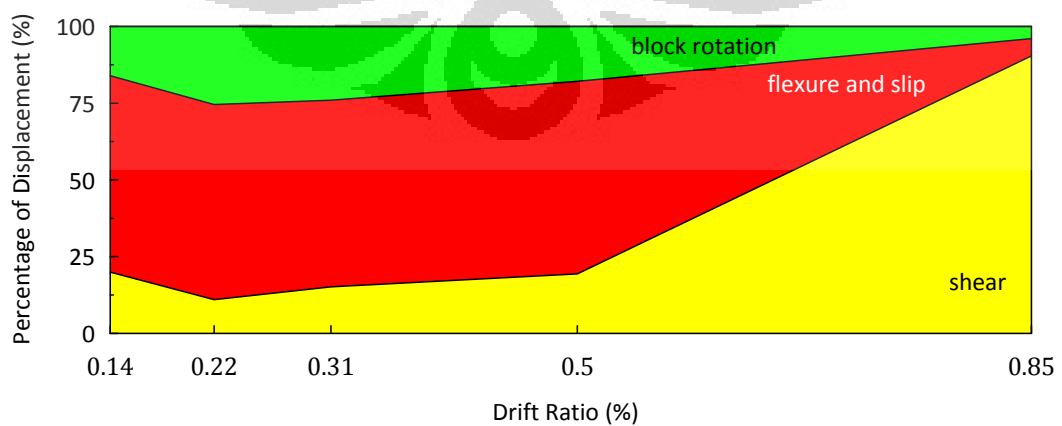**Figure 5.90** Measured Displacement vs. Time Step of Column S2
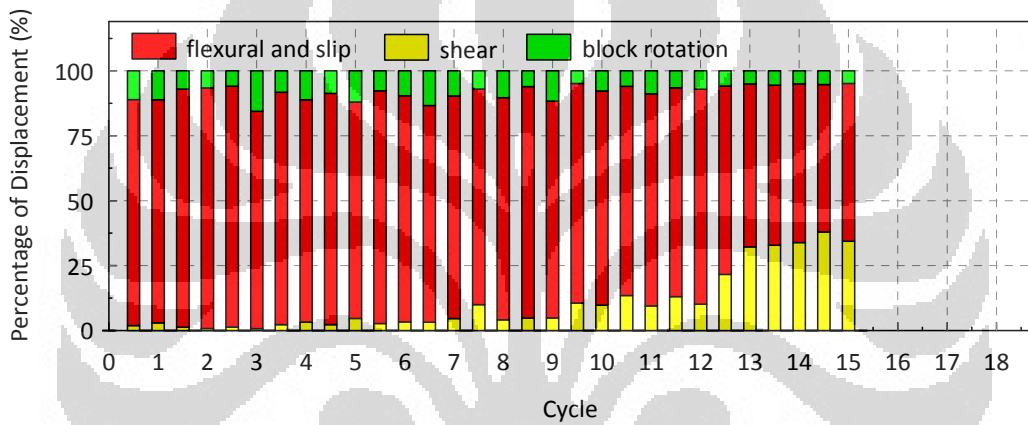
Figure 5.91 Percentage of Measured Displacement vs. Cycle of Column S2
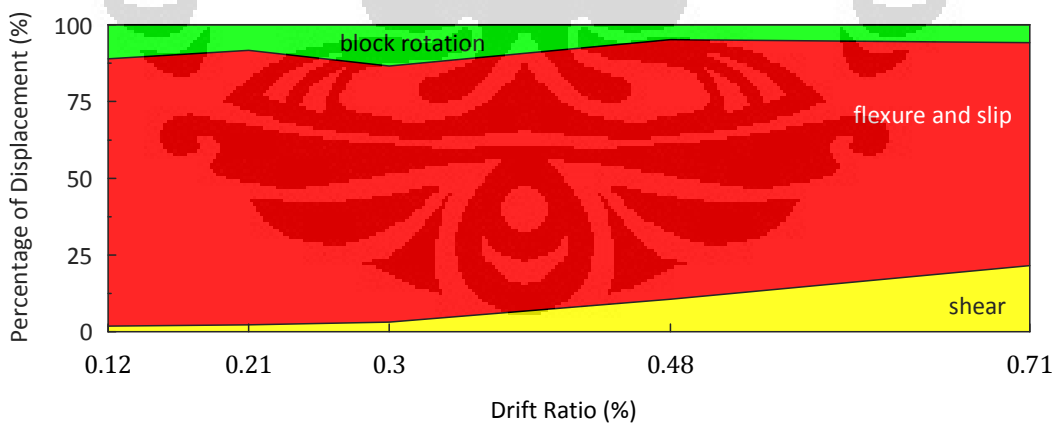
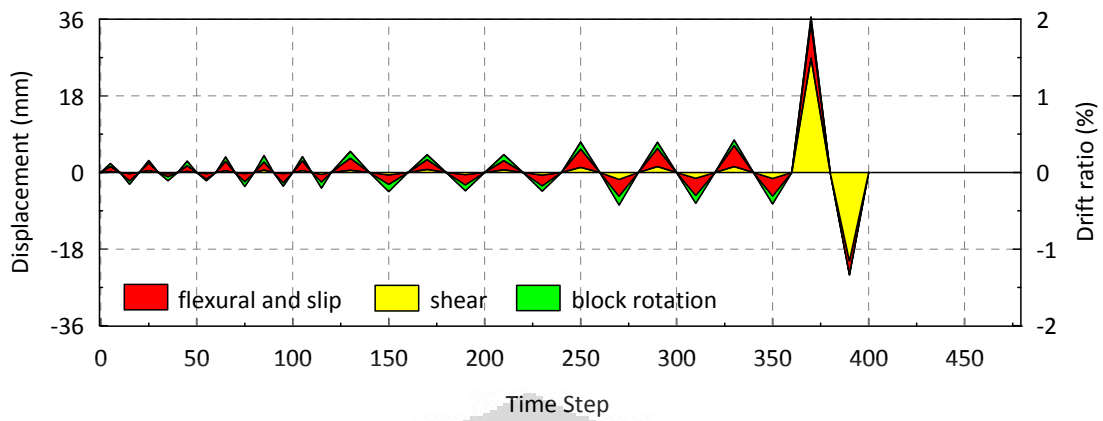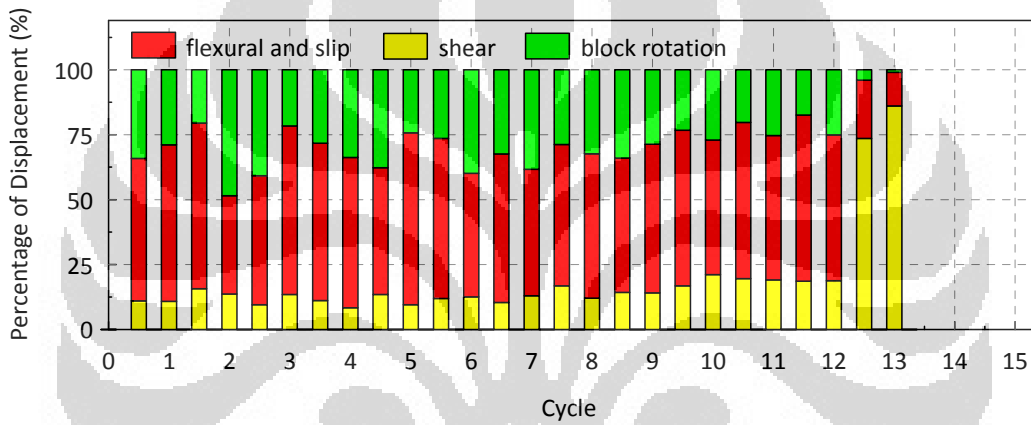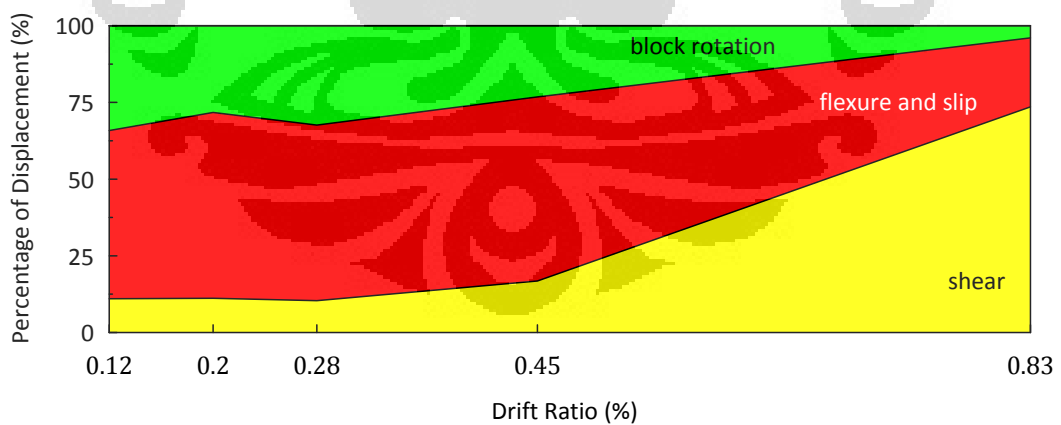**Figure 5.92** Percentage of Measured Displacement Component vs. Drift Ratio of Column S2
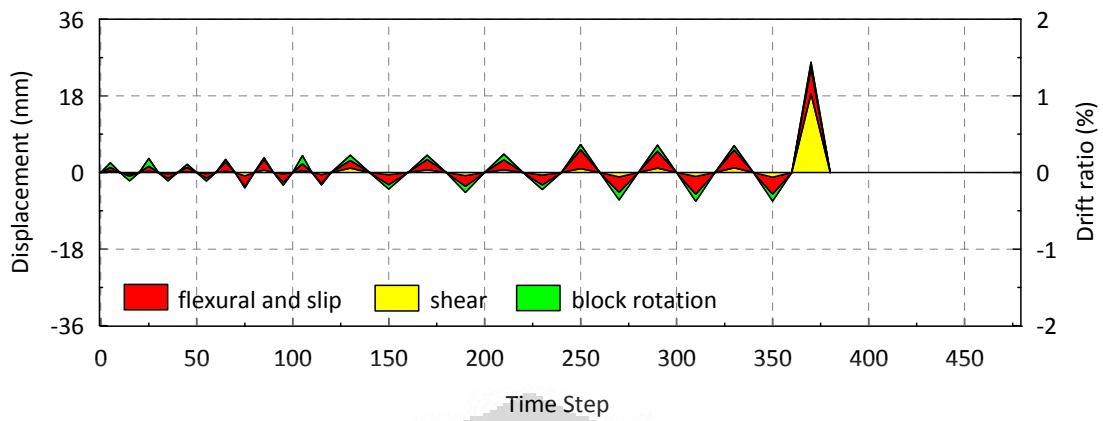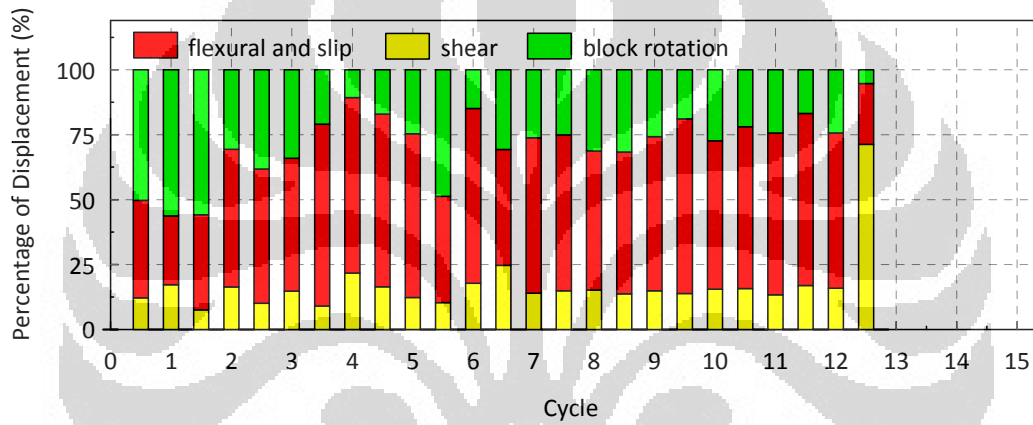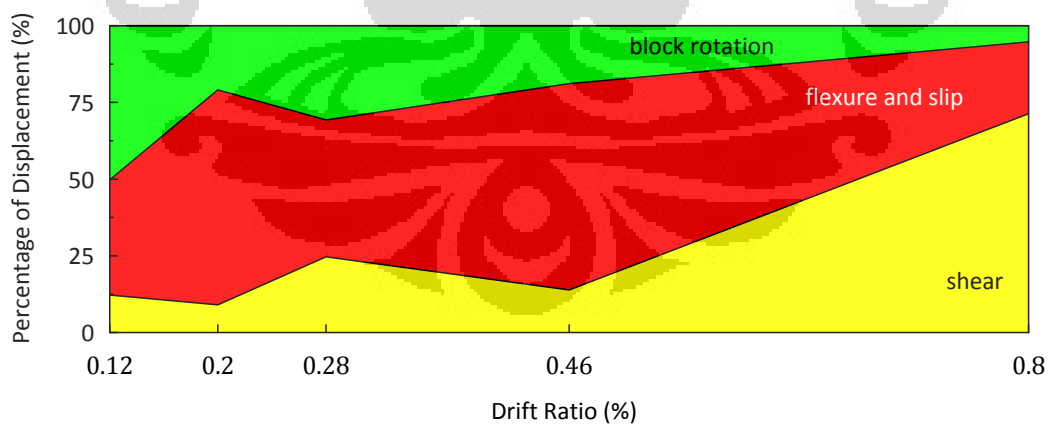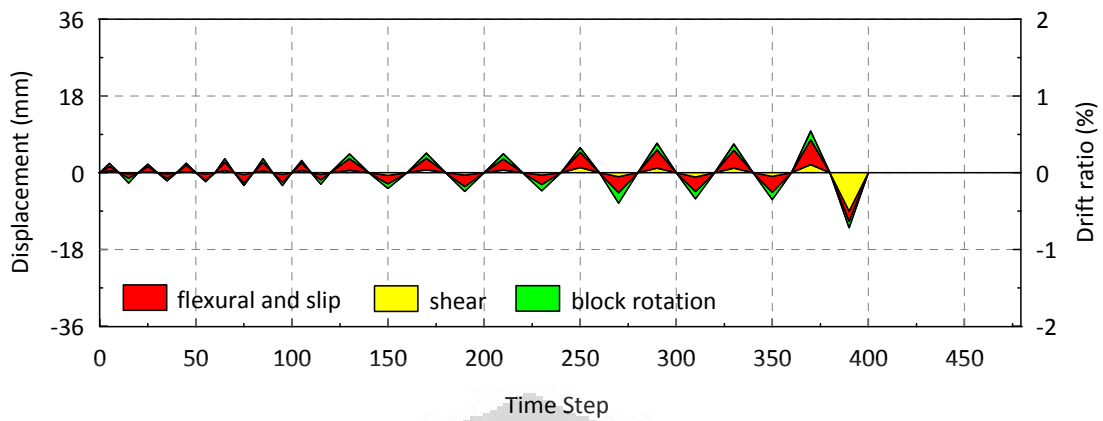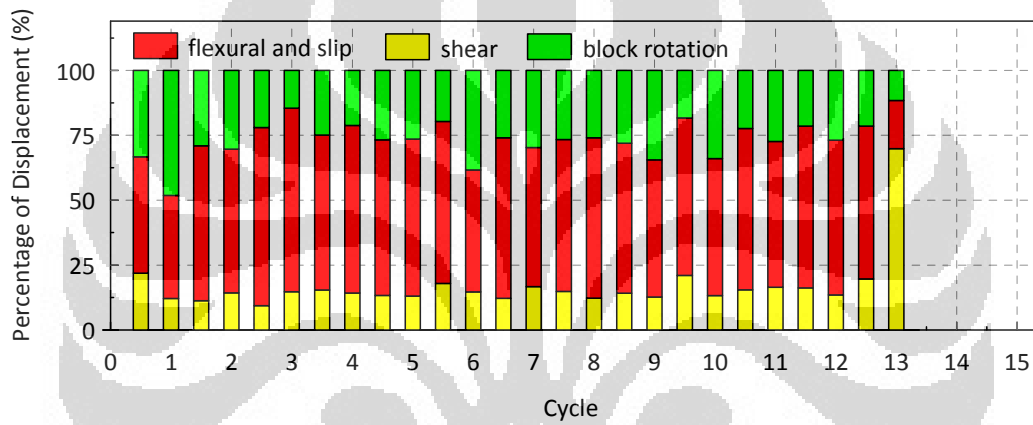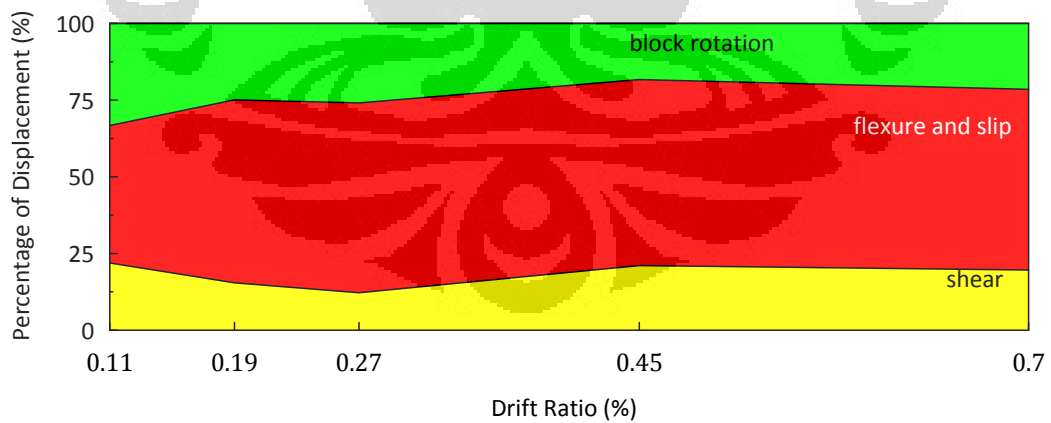
5.9. TOTAL AND MEASURED DISPLACEMENT

Total and measured displacement obtained will be compared in this part. Each specimen is illustrated in six different graphs. One additional component, error as a result from this comparison, is added.

Figure 5.93 to 5.110 show Comparison of Total and Measured Displacement vs. Cycle; Total Displacement Components vs. Time Step; Comparison of Total and Measured Displacement vs. Time Step.

Measured displacement which was obtained from instrumentation is mostly smaller than the total displacement at the beginning of experiment. Moreover, after passing 0.75% drift ratio, the measured displacement is increasing. The second and the third figures of each columns show the significance increase of shear displacement. The red color represents the total displacement and the yellow color represents measured displacement (instrumentation).

The following figures show the percentage of the total displacement components, the red, yellow, green and blue colors represent flexural and slip displacement, shear displacement, block rotation and other/error, respectively. The other /error component took 0.5-38 % of the total displacement. The rotation of the top and bottom block and also the reading of the instrumentation can caused the error component since the largest portion of error occurred in the small drift ratio. When the drift ratio was getting larger the error will be reduced as shown in the following figures.

The sixth figure for each specimen (Figure 5.95, 5.98, 5.101, 5.104, 5.107 and 5.110) shows the percentage of total displacement components vs. drift ratio of all specimens. The displacement from the first cycle of each drift ratio were used and plotted. It can be seen from those figures that the shear displacement took a larger portion of the total displacement when the drift ratio increased.

5.9.1. Type B Columns

Figure 5.93 Comparison of Total and Measured Displacement vs. Cycle of Column B1

Figure 5.94 Total Displacement Components vs. Time Step of Column B1

Figure 5.95 Percentage of Total Displacement Components vs. Cycle of Column B1

Figure 5.96 Comparison of Total and Measured Displacement vs. Cycle of Column B2

Figure 5.97 Total Displacement Components vs. Time Step of Column B2
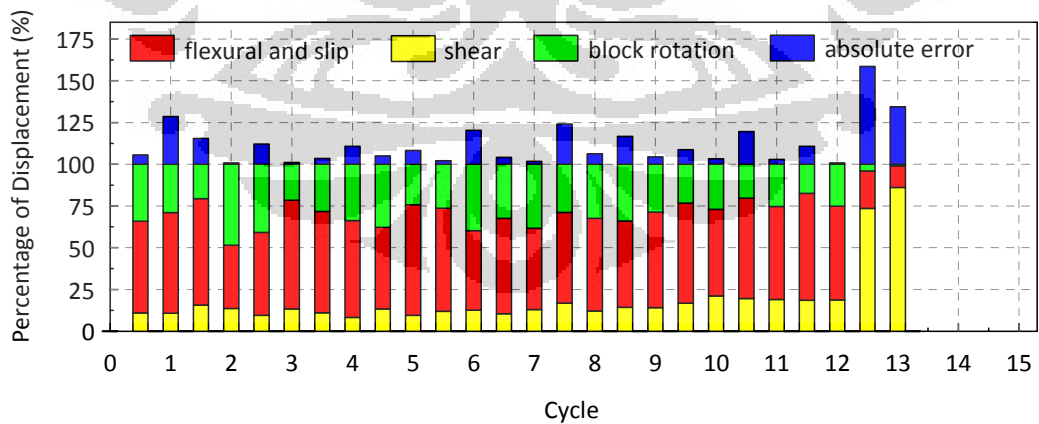
Figure 5.98 Percentage of Total Displacement Components vs. Cycle of Column B2
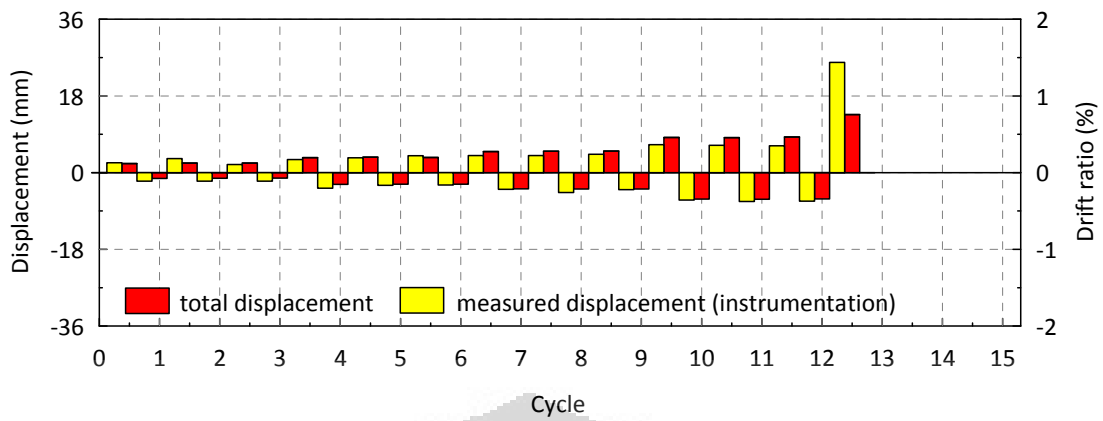
Figure 5.99 Comparison of Total and Measured Displacement vs. Cycle of Column B3
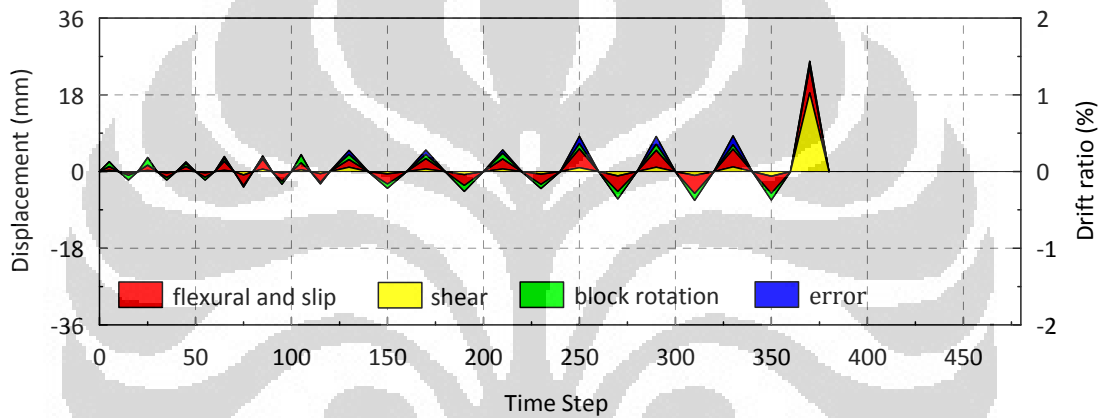
Figure 5.100 Total Displacement Components vs. Time Step of Column B3
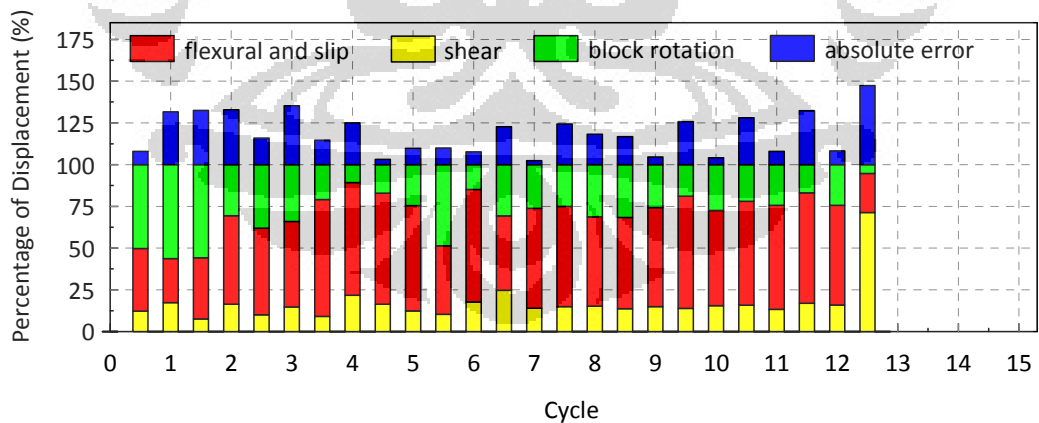
Figure 5.101 Percentage of Total Displacement Components vs. Cycle of Column B3

Universitas Indonesia
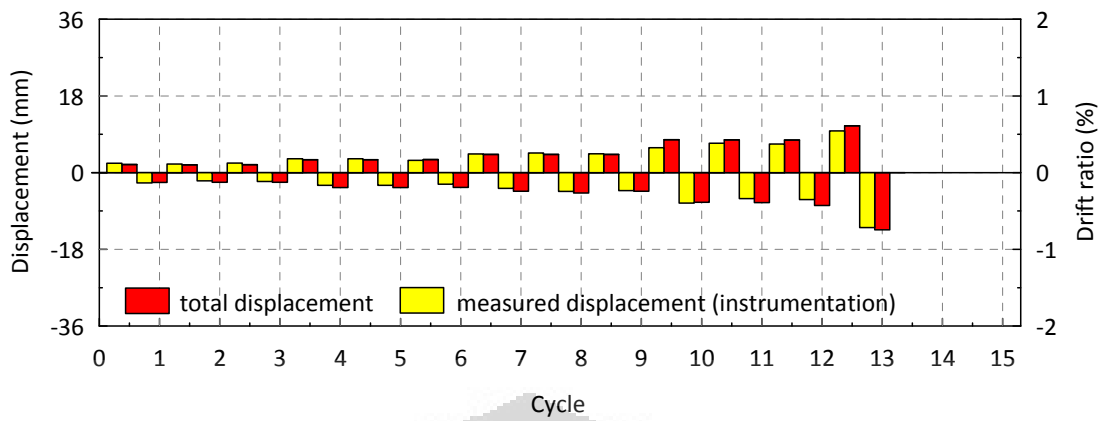
Figure 5.102 Comparison of Total and Measured Displacement vs. Cycle of Column B4
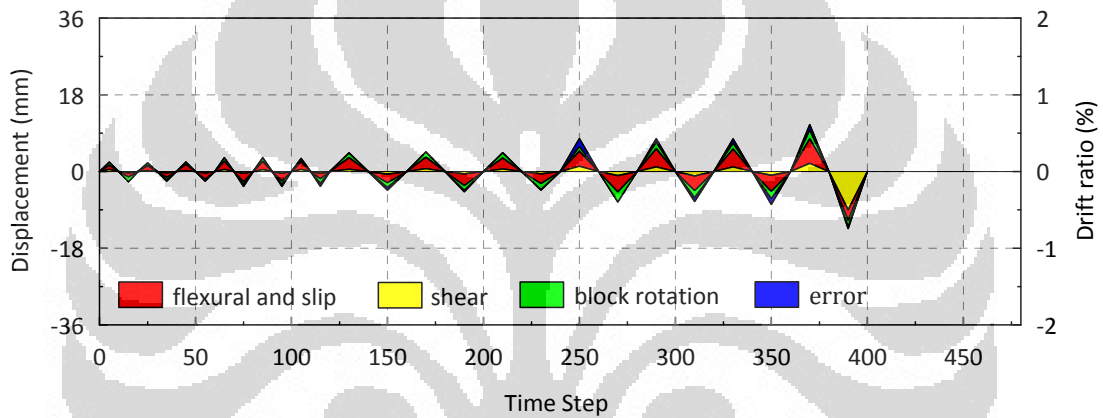
Figure 5.103 Total Displacement Components vs. Time Step of Column B4
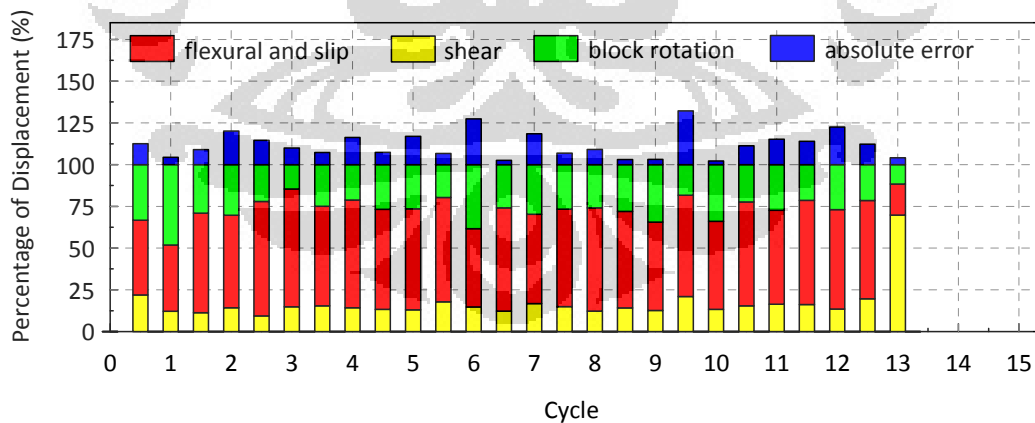
Figure 5.104 Percentage of Total Displacement Components vs. Cycle of Column B4

Universitas Indonesia

5.9.2. Type S Columns
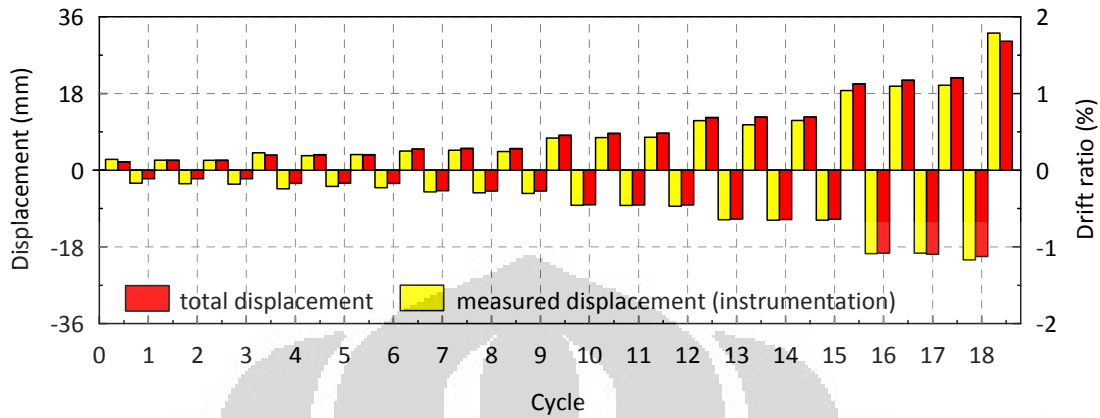
Figure 5.105 Comparison of Total and Measured Displacement vs. Cycle of Column S1
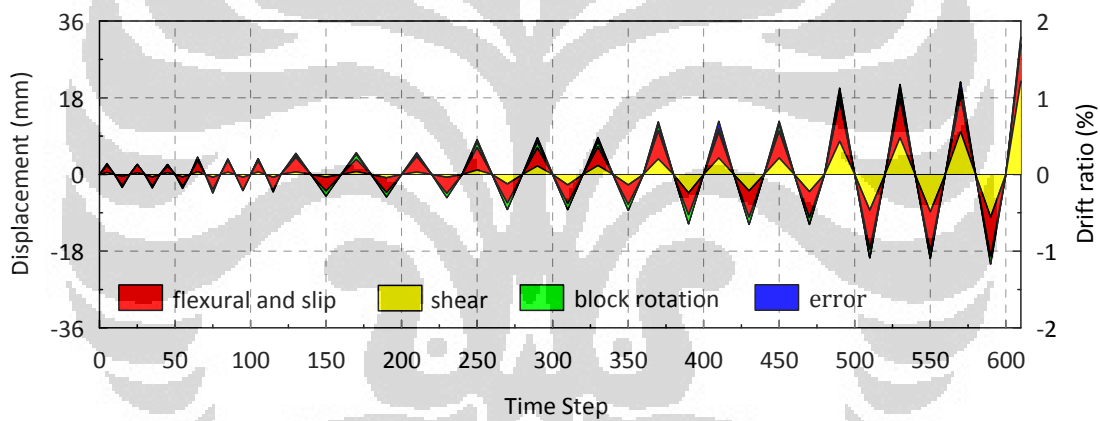
Figure 5.106 Total Displacement Components vs. Time Step of Column S1
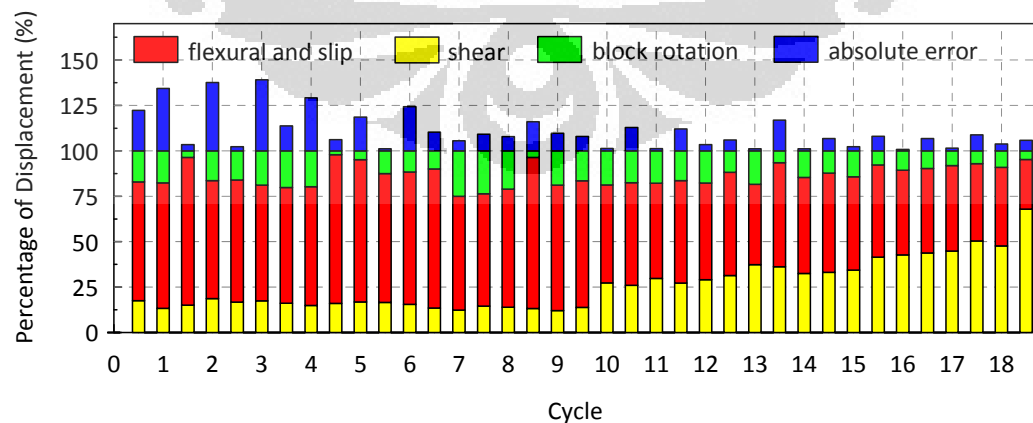
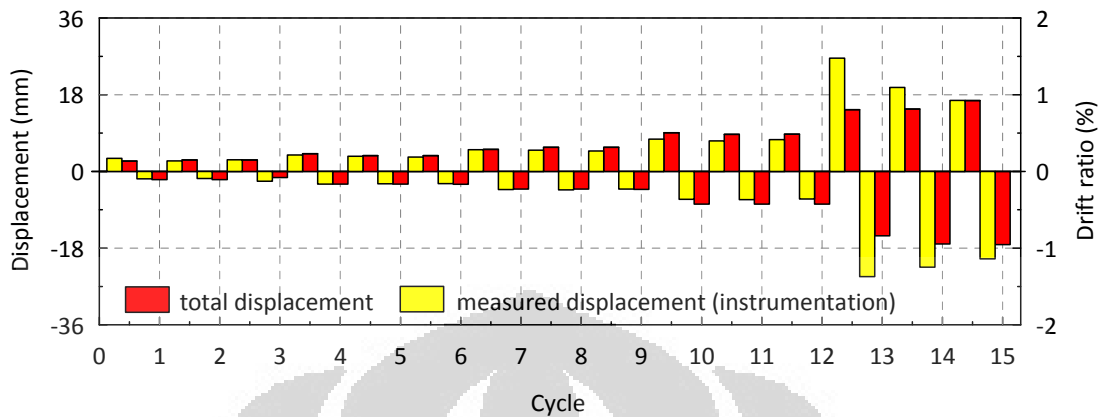**Figure 5.107** Percentage of Total Displacement Components vs. Cycle of Column S1
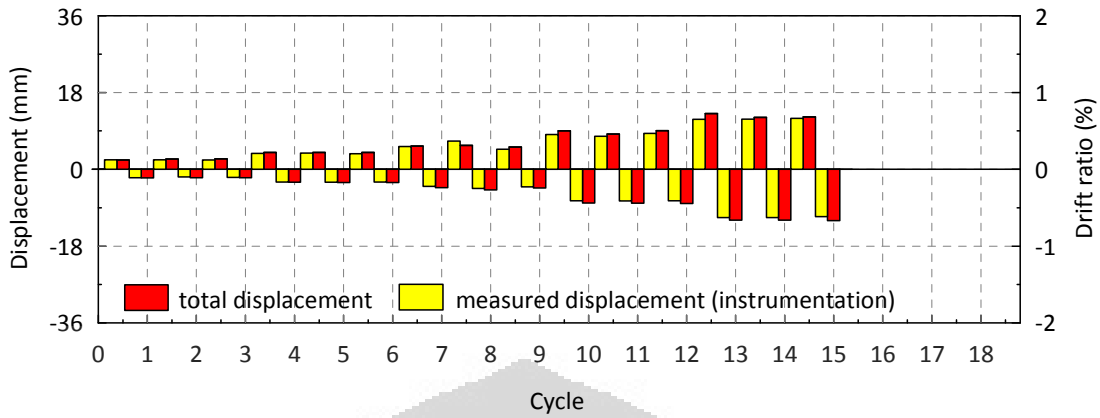
Figure 5.108 Comparison of Total and Measured Displacement vs. Cycle of Column S2
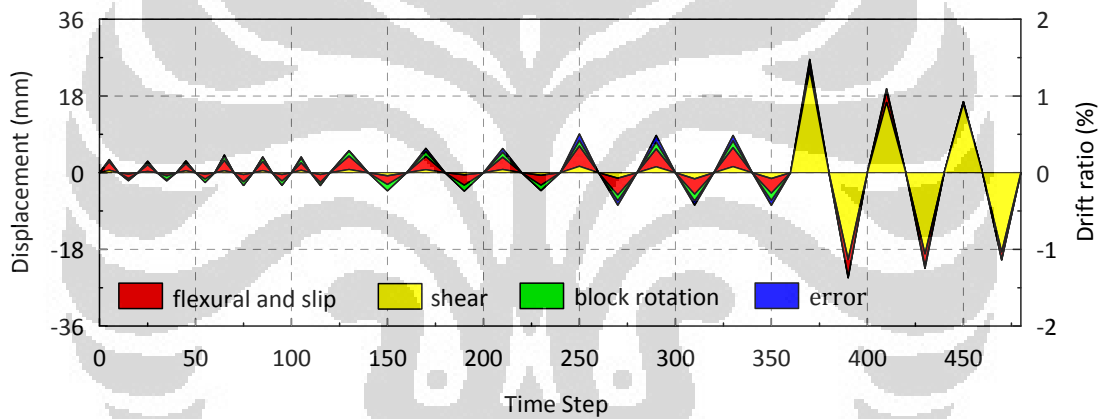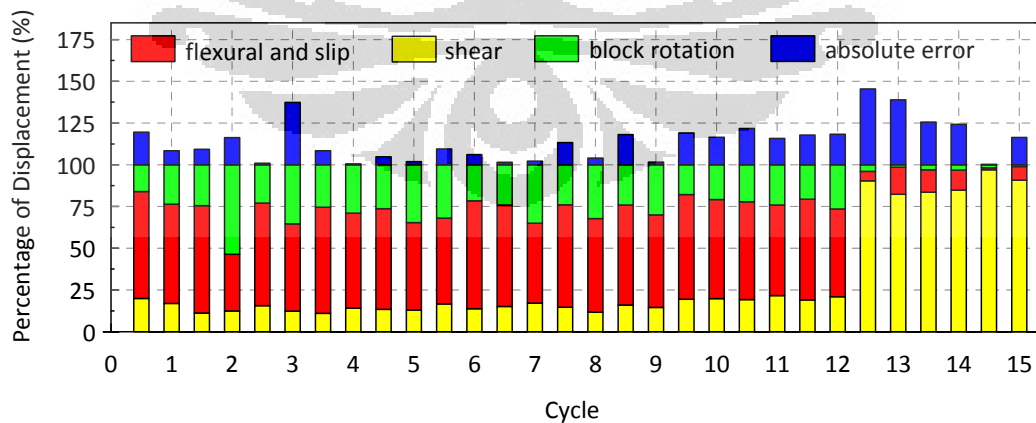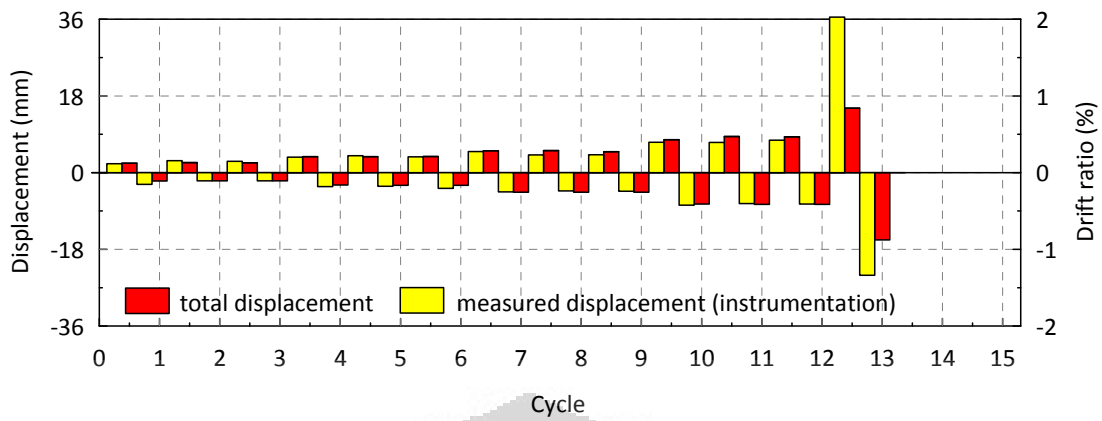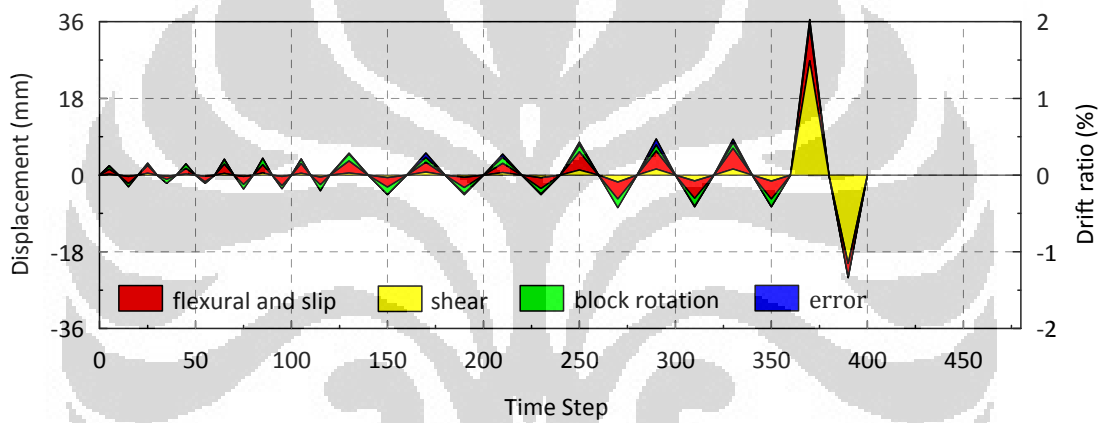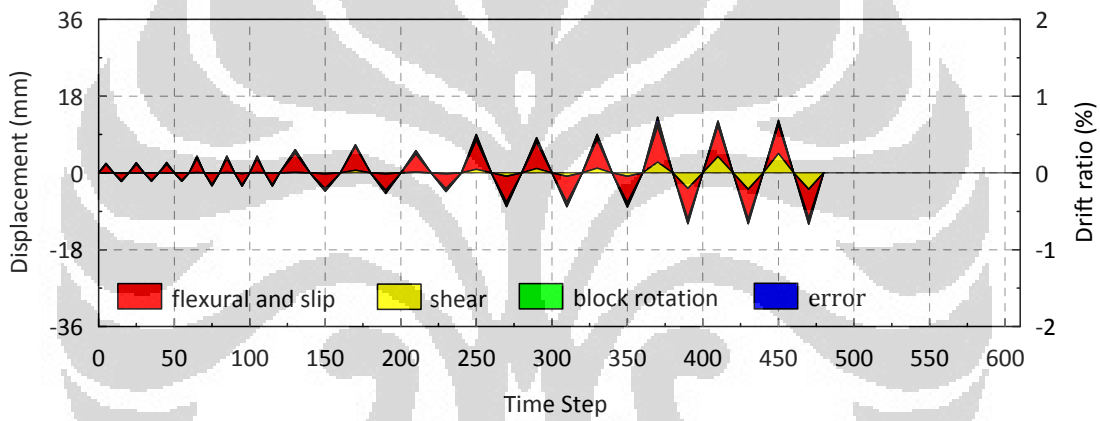

Figure 5.109 Total Displacement Components vs. Time Step of Column S2
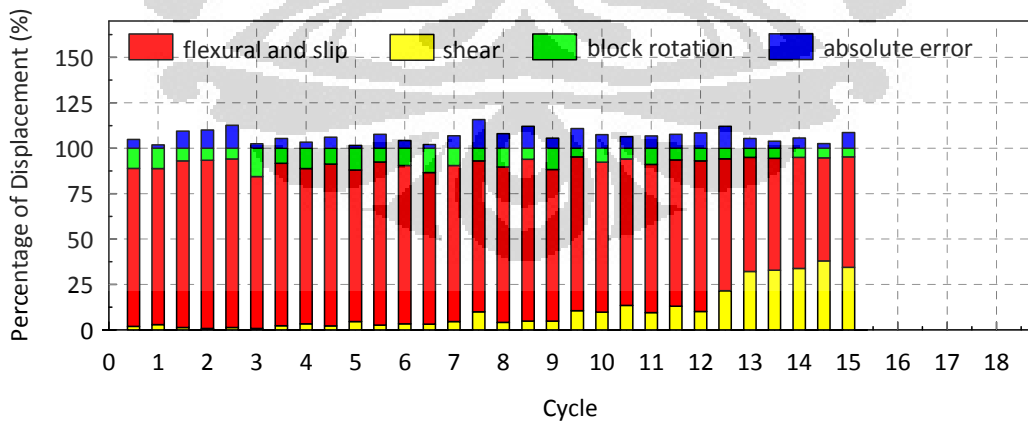
Figure 5.110 Percentage of Total Displacement Components vs. Cycle of Column S2

Universitas Indonesia

5.10. EFFECT OF AXIAL LOAD RATIO

As mentioned before, this research is the persistence of the previous study performed by Kurniwawan[28]. A part from the addition of multi-spiral specimens, the difference between this and the previous research is the applied axial load ratio to the specimens. Specimen A (Kurniwawan[28]) was subjected to 10% axial load ratio meanwhile specimen B was subjected to 20% axial load ratio. In this part, the consequence of 10% additional of axial load ratio to lateral strength and stiffness; also strain gauges reading of longitudinal reinforcement, will be discussed.

5.10.1. Lateral strength and secant lateral stiffness

Linbeck[30] stated that lateral stiffness of reinforced concrete column was found to be profoundly influenced by axial load. In his research, four double curvature columns were subjected to axial and compression load. One of the column, named- I-HA was subjected to cyclic axial compression and lateral load. Test result show that specimen behavior was sensitive to maximum axial compression experienced during testing. When axial loads exceed balanced axial load lateral stiffness quickly degraded and lateral capacity of the column dropped well below ultimate. When axial load kept below balanced point, lateral stiffness did not degrade as quickly and lateral capacity of the column was maintained near ultimate capacity. Linbeck defined the secant stiffness as the ratio of lateral load (kips) and drift (in).

Column A1 and B1 have the same specific design as mentioned in Table 5.1. Test result of type A and B column show that the shear strength of column with 20% is larger than the shear strength of column with 10% axial load ratio. It is reasonable to consider the lateral stiffness since the peak strength of each column occurred at different displacement. If the same definition of secant lateral stiffness by Linbeck is used, the following table shows the increasing of this term as the increasing of axial load ratio.

Displacement in the third column of Table 5.13 is the actual position of column when it reached its maximum lateral strength. As shown in the table, secant lateral stiffness of type B columns is larger than the value of type A columns. Since the axial compression load higher, the lateral load needed higher to move the column to certain value of displacement.

Table 5.13 Experimental Result (The data of Type A specimen obtained from Kurniwawan[28])

Specimen	Axial Load Ratio	f'_c (MPa)	Experiment (kN)	Displacement (mm)	Secant lateral stiffness (10^8 N/mm)
A1		92.47	1615.44	9.55	1.69
A2	10%	103.15	1632.41	10.03	1.63
A3		96.87	1789.59	13.79	1.30
A4		107.10	1832.35	14.22	1.29
B1		98.95	2184.94	11.16	1.96
B2	20%	114.10	2202.54	9.12	2.42
B3		112.85	2374.04	10.36	2.29
B4		121.04	2443.18	11.58	2.11

5.10.2. Strain reading of longitudinal reinforcement

As mention in part 4.1, strain gauges were also attached on longitudinal reinforcement. Plot of strain gauges could be found in Appendix C Strain Reading. In order to evaluate, two reliable strain reading from two different specimens are compared. Figure 5.111 below shows the comparison between strain reading from specimen A3 and B3 which are designed with the same concrete compressive strength. As the axial compression loading is getting higher, the strain of the longitudinal reinforcement is getting lower. Figure 5.111 shows this condition.

(a)   (b)
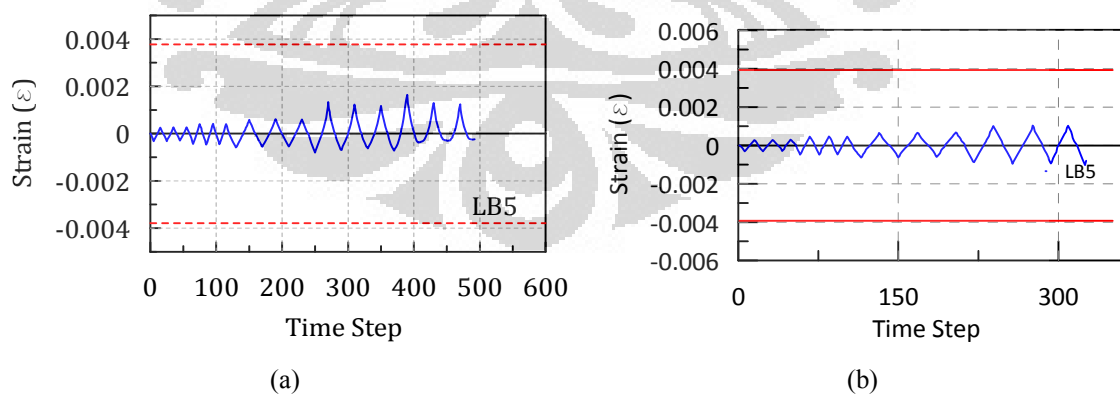
Figure 5.111 Comparison of strain reading
(a) Specimen A3 (10 % axial load ratio); (b) Specimen B3 (10 % axial load ratio)

CHAPTER VI
COMPARISON OF TEST RESULTS AND SHEAR PREDICTION

6.1. YIELD STRESS OF TRANSVERSE REINFORCEMENT

Tables 6.1 and 6.2 show the comparison and ratio of test result shear strength predictions with yield stress of transverse reinforcement (862 MPa). From those tables, it can be seen that almost all of the shear predictions from the codes, provisions and guidelines are smaller than the test result and give the ratio smaller than 1.00. All of the shear prediction from shear equations proposed by researchers are larger than test result and have ratio larger than 1.00.

Shear predictions of New RC give the ratio of V_n/V larger than 1.00. The ratio of 1.00 for column B3 is actually 0.99973 meanwhile for B4, the ratio reached 1.0032. Shear predictions of ACI 318 simplified equation and Caltrans of Specimen S1 are also larger than 1.00.

The predictions by shear models proposed by researchers are higher than the test results. The ratio V_n/V of those models varies from 1.08 to 1.80 as shown in Table 6.2. Further observation related to those shear models is needed since those models were derived from experimental data that most of them are using normal strength material and also most of them have inelastic shear failure mechanism rather than elastic shear failure.

The actual stresses in the hoop at the maximum strength (peak point) are smaller than the yield point of the transverse reinforcement. The yield point was used in the calculation that shown in the Tables 6.1 and 6.2 and also in the following figures. Although the yield point was used, the codes and provisions generally still perform well.

Figures 6.1 to 6.8 show the shear strength vs. drift ratio of the test result and also the shear strength predictions from several shear equations. Since the shear failure that occurred is elastic shear, the following figures cannot capture the degradation of the shear strength as used by several shear models. The degradation of shear strength was related to the displacement ductility. In elastic shear case, the shear failure occurs before the yielding of longitudinal bars. That means the displacement ductility is smaller than 1.00.

Table 6.1 Comparison of test results and shear strength predictions with yield stress of transverse reinforcement

Specimen	Test Result V (kN)	Shear Strength V_n (kN)												
		ACI 318 simplified	ACI 318 detailed	ACI - 426	AIJ 1990	AIJ 1999	New RC	AASHTO	CALTRANS	Aschheim & Moehle	Priestley	Kowalsky	Sezen	Xiao Martirossyan
B1	2184.94	1571.75	1150.41	1191.58	1649.00	1309.74	1920.57	1092.44	1315.91	2162.71	2736.18	2864.71	2490.59	2391.23
B2	2202.54	1776.81	1231.60	1251.97	1754.80	1415.53	2068.69	1172.77	1385.93	2559.49	2994.73	3154.89	2713.71	2653.16
B3	2374.04	2025.82	1480.19	1651.09	2175.00	1847.12	2373.40	1642.20	1646.56	2637.43	3400.76	3364.13	2931.19	2798.53
B4	2443.18	2139.84	1524.87	1686.81	2230.47	1902.59	2451.06	1660.21	1682.55	2856.98	3576.97	3543.99	3076.70	2987.52
S1	2254.24	1445.10	1127.11	1297.01	1826.25	1797.34	1924.24	1598.97	1522.21	1821.95	2995.60	3098.00	2309.34	2301.17
S2	2168.57	1296.88	978.80	1148.79	1472.67	1566.37	1581.61	1293.56	1373.99	1828.41	2668.20	2867.18	2185.31	2193.45
Considering small spiral														
S1	2254.24	2225.12	1907.13	2077.02	2289.99	2012.94	2387.98	1822.64	2302.23	2601.97	3775.62	3878.02	2699.35	3081.19
S2	2168.57	1881.89	1563.81	1733.80	1794.72	1716.09	1903.66	1529.92	1959.00	2413.43	3253.21	3452.19	2477.82	2778.46

Table 6.2 Ratio of test results and shear strength predictions with yield stress of transverse reinforcement

Specimen	Test Result V (kN)	Ratio of Shear Strength Prediction & Test Result (V_n/V)												
		ACI 318 simplified	ACI 318 detailed	ACI - 426	AIJ 1990	AIJ 1999	New RC	AASHTO	CALTRANS	Aschheim & Moehle	Priestley	Kowalsky	Sezen	Xiao Martirossyan
B1	2184.94	0.72	0.53	0.55	0.75	0.60	0.88	0.50	0.60	0.99	1.25	1.31	1.14	1.09
B2	2202.54	0.81	0.56	0.57	0.80	0.64	0.94	0.53	0.63	1.16	1.36	1.43	1.23	1.20
B3	2374.04	0.85	0.62	0.70	0.92	0.78	1.00	0.69	0.69	1.11	1.43	1.42	1.23	1.18
B4	2443.18	0.88	0.62	0.69	0.91	0.78	1.00	0.68	0.69	1.17	1.46	1.45	1.26	1.22
S1	2254.24	0.64	0.50	0.58	0.81	0.80	0.85	0.71	0.68	0.81	1.33	1.37	1.02	1.02
S2	2168.57	0.60	0.45	0.53	0.68	0.72	0.73	0.60	0.63	0.84	1.23	1.32	1.01	1.01
Considering small spiral														
S1	2254.24	0.99	0.85	0.92	1.02	0.89	1.06	0.81	1.02	1.15	1.67	1.72	1.20	1.37
S2	2168.57	0.87	0.72	0.80	0.83	0.79	0.88	0.71	0.90	1.11	1.50	1.59	1.14	1.28

Universitas Indonesia
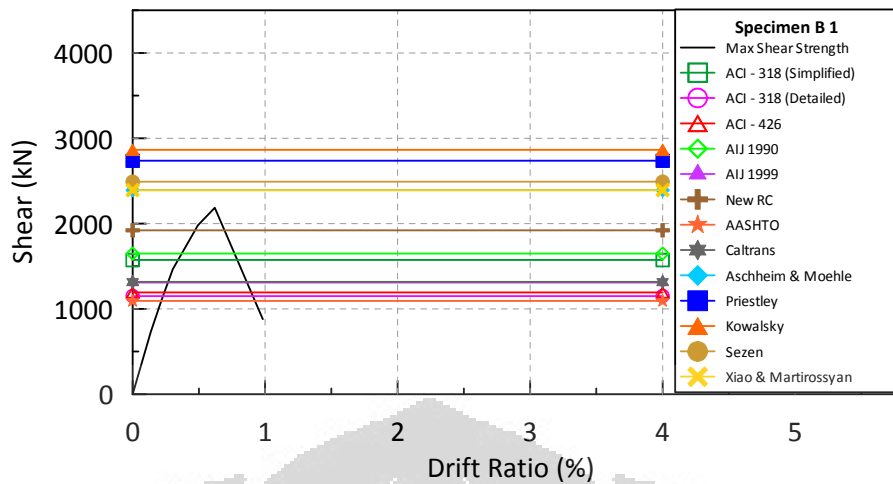
Figure 6.1 Drift ratio vs. shear strength prediction of Column B1 (yield stress of hoop)
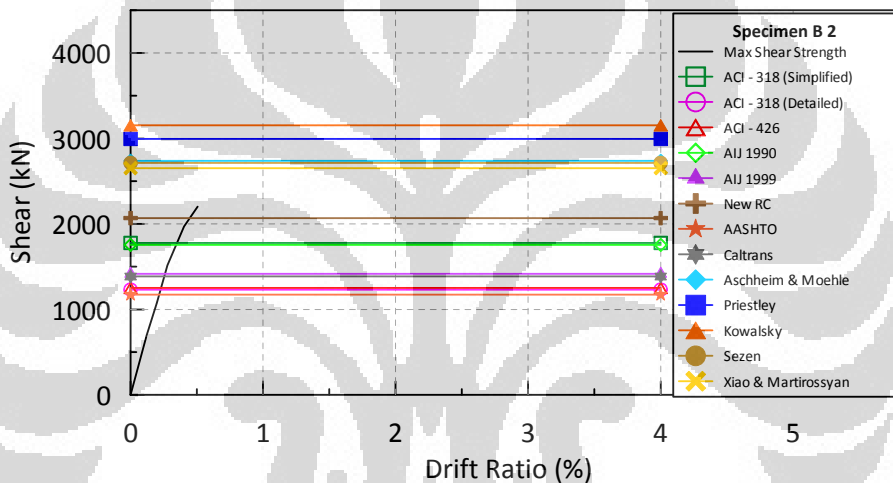
Figure 6.2 Drift ratio vs. shear strength prediction of Column B2 (yield stress of hoop)
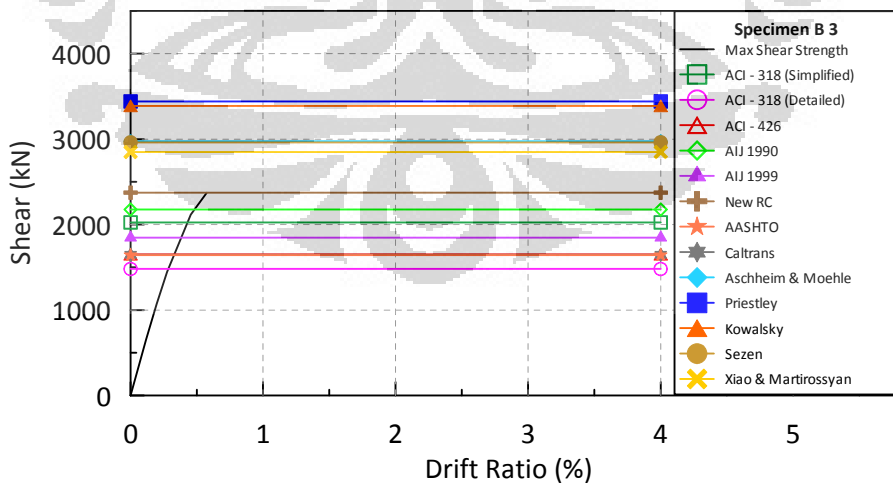
Figure 6.3 Drift ratio vs. shear strength prediction of Column B3 (yield stress of hoop)

Universitas Indonesia
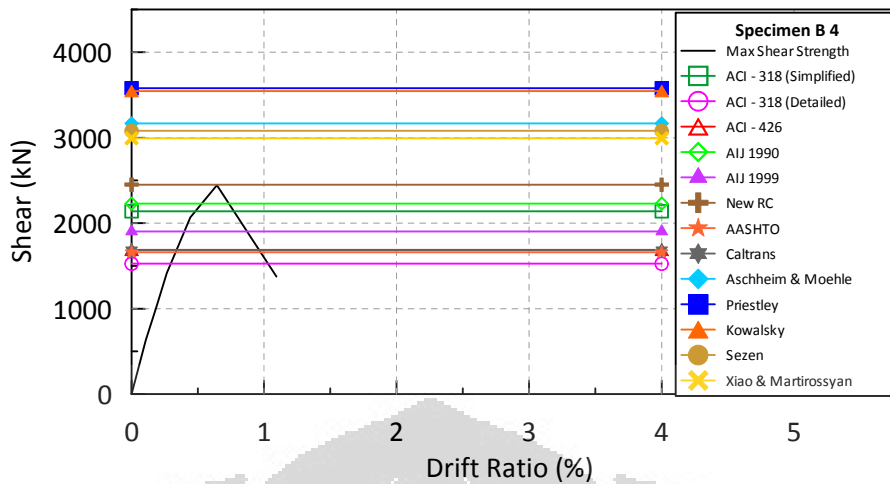
Figure 6.4 Drift ratio vs. shear strength prediction of Column B4 (yield stress of hoop)
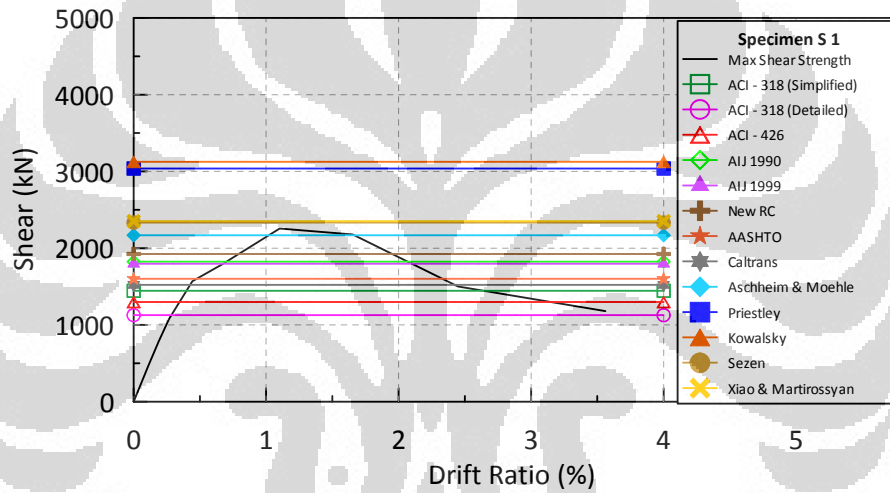
Figure 6.5 Drift ratio vs. shear strength prediction of Column S1 (yield stress of hoop)
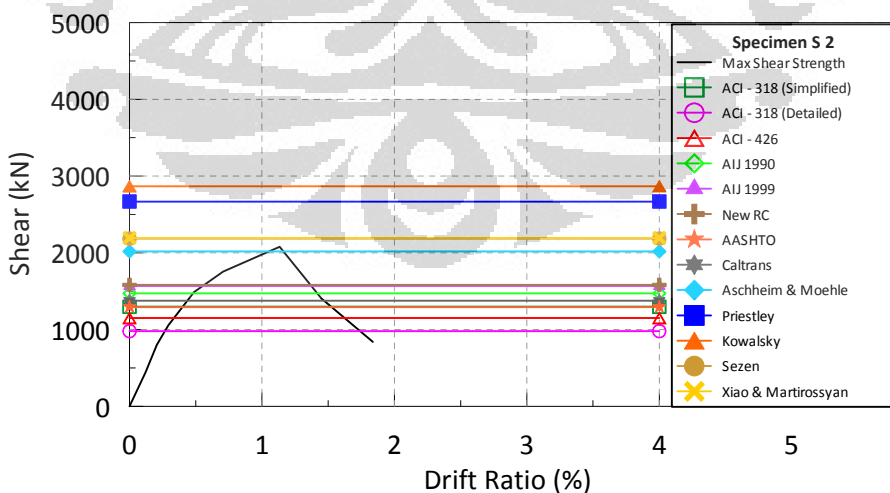
Figure 6.6 Drift ratio vs. shear strength prediction of Column S2 (yield stress of hoop)
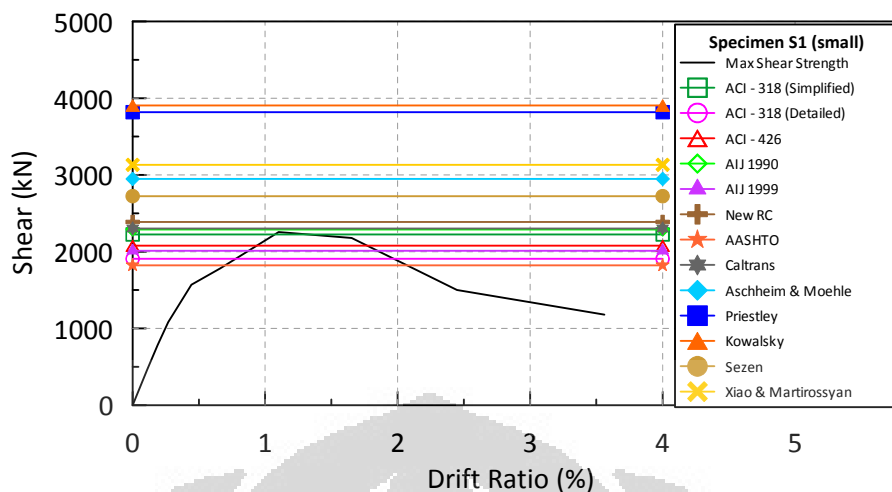
Figure 6.7 Drift ratio vs. shear strength prediction of Column S1 considering small spiral (yield stress of hoop)
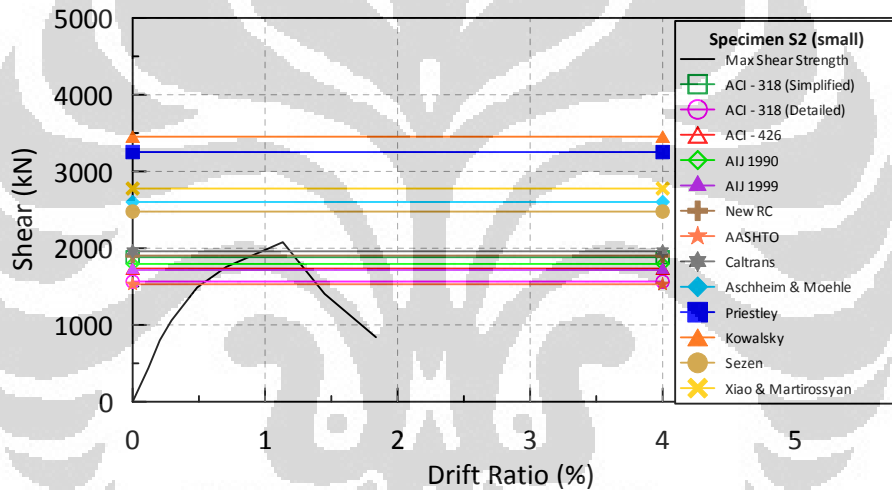
Figure 6.8 Drift ratio vs. shear strength prediction of Column S2 considering small spiral (yield stress of hoop)

6.2. ACI 318-08 LIMIT STRESS OF TRANSVERSE REINFORCEMENT

The comparison and ratio of test result shear strength predictions with limit stress of transverse reinforcement from ACI 318R-08 at maximum strength and using the original model of critical crack angle are shown respectively in Table 6.3 and 6.4 below. In this part, the result from previous research (Kurniawan[28]) is included. From those tables, it can be seen that all of the shear predictions from the codes, provisions and guidelines are smaller than the test result and give the ratio smaller than 1.00. All of the shear prediction from shear equations proposed by researchers are larger than test result and have ratio larger than 1.00.

As stated in ACI 318-08[14] that the values of f_y and f_{yt} used in design of shear reinforcement shall not exceed 420 MPa, except the value shall not exceed 550 MPa for welded deformed wire reinforcement. The design requirement from ACI 318R-08 is more conservative compared to the actual stresses of the hoops. The limit design by ACI 318R-08 was used in the calculation. The shear predictions by the codes and provisions perform well since the result is more conservative.

The predictions of shear models proposed by researchers are higher than the test results. The ratio V_n/V of those models varies from 0.73 to 1.59 as shown in Table 6.4.
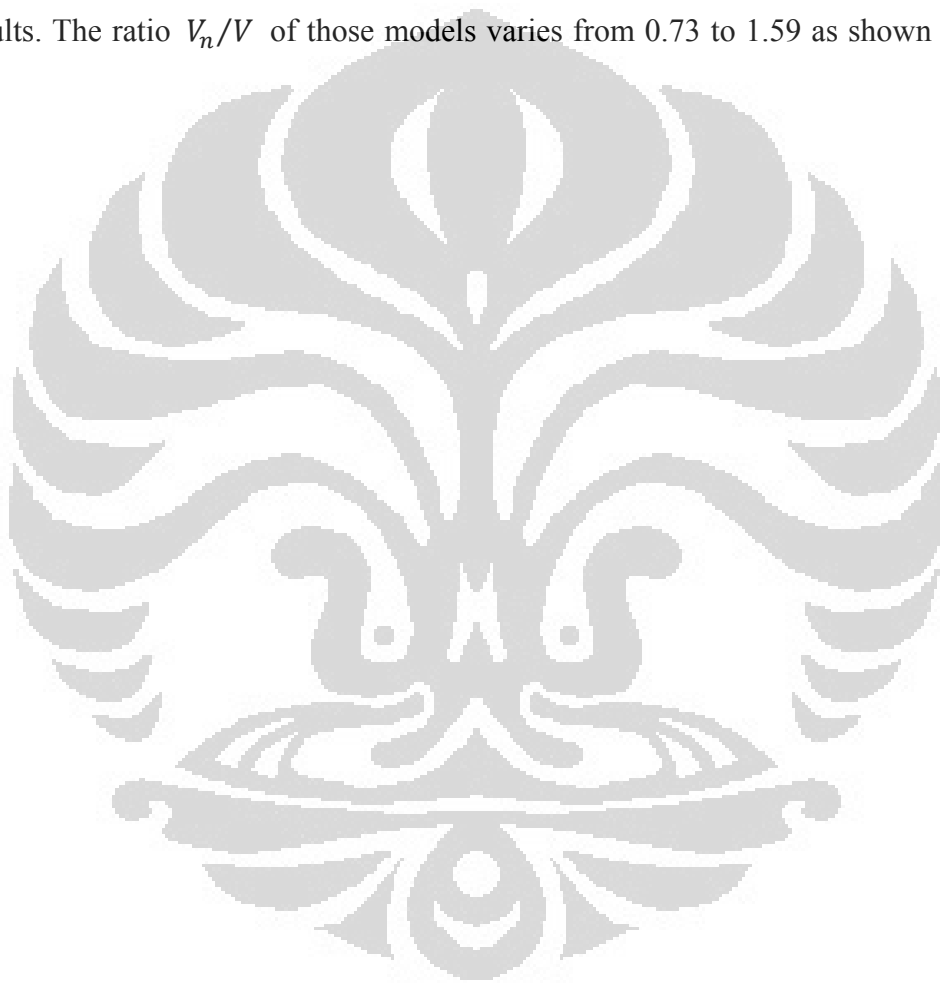
Table 6.3 Comparison of test results and shear strength predictions with Limit Stress from ACI 318-08

Specimen	Test Result V (kN)	Shear Strength V_n (kN)												
		ACI 318 simplified	ACI 318 detailed	ACI - 426	AIJ 1990	AIJ 1999	New RC	AASHTO	CALTRANS	Aschheim & Moehle	Priestley	Kowalsky	Sezen	Xiao Martirossyan
A1	1615.44	986.61	832.04	842.35	1389.72	1173.25	1546.28	818.16	1141.79	1361.01	1925.72	2197.79	1796.45	1715.34
A2	1632.41	1064.67	860.94	875.28	1466.50	1250.03	1638.42	875.84	1192.99	1528.44	2058.11	2354.58	1914.93	1849.33
A3	1789.59	1181.13	1008.14	1117.59	1695.23	1486.03	1824.18	1104.30	1325.46	1423.98	2191.82	2411.25	1959.76	1805.94
A4	1832.35	1254.62	1035.16	1151.63	1767.75	1558.55	1911.21	1173.98	1372.70	1600.39	2374.80	2600.10	2101.35	2006.62
B1	2184.94	1439.84	1018.50	1059.67	1436.66	1220.19	1763.74	869.16	1184.00	2030.81	2504.66	2737.03	2358.69	2284.56
B2	2202.54	1644.97	1099.76	1120.13	1542.46	1325.99	1911.85	938.89	1254.09	2427.65	2763.21	3026.86	2581.88	2545.27
B3	2374.04	1797.63	1251.99	1422.89	1807.48	1598.28	2101.96	1237.38	1418.36	2409.23	3000.05	3142.60	2705.37	2611.98
B4	2443.18	1911.74	1296.76	1458.70	1862.95	1653.75	2179.62	1255.55	1454.44	2628.87	3176.27	3321.98	2848.82	2799.83
S1	2254.24	1269.52	951.53	1121.43	1407.42	1666.27	1518.38	1215.83	1346.63	1646.38	2559.20	2793.90	2135.58	2112.21
S2	2168.57	1174.95	856.87	1026.86	1181.82	1495.62	1299.77	1020.96	1252.06	1706.49	2365.14	2655.99	2063.38	2062.23
Considering small spiral														
S1	2254.24	2049.54	1731.55	1901.45	1871.16	1938.51	1982.12	1439.49	2126.65	2426.39	3339.21	3573.91	2525.59	2892.23
S2	2168.57	1759.96	1441.88	1611.87	1503.86	1664.40	1621.81	1257.32	1837.07	2291.50	2950.15	3241.00	2355.89	2647.24

Universitas Indonesia

Table 6.4 Ratio of test results and shear strength predictions with Limit Stress from ACI 318-08

Specimen	Test Result V (kN)	Ratio of Shear Strength Prediction & Test Result (V_n/V)												
		ACI 318 simplified	ACI 318 detailed	ACI - 426	AIJ 1990	AIJ 1999	New RC	AASHTO	CALTRANS	Aschheim & Moehle	Priestley	Kowalsky	Sezen	Xiao Martirossyan
A1	1615.44	0.61	0.52	0.52	0.86	0.73	0.96	0.51	0.71	0.84	1.19	1.36	1.11	1.06
A2	1632.41	0.65	0.53	0.54	0.90	0.77	1.00	0.54	0.73	0.94	1.26	1.44	1.17	1.13
A3	1789.59	0.66	0.56	0.62	0.95	0.83	1.02	0.62	0.74	0.80	1.22	1.35	1.10	1.01
A4	1832.35	0.68	0.56	0.63	0.96	0.85	1.04	0.64	0.75	0.87	1.30	1.42	1.15	1.10
B1	2184.94	0.66	0.47	0.48	0.66	0.56	0.81	0.40	0.54	0.93	1.15	1.25	1.08	1.05
B2	2202.54	0.75	0.50	0.51	0.70	0.60	0.87	0.43	0.57	1.10	1.25	1.37	1.17	1.16
B3	2374.04	0.76	0.53	0.60	0.76	0.67	0.89	0.52	0.60	1.01	1.26	1.32	1.14	1.10
B4	2443.18	0.78	0.53	0.60	0.76	0.68	0.89	0.51	0.60	1.08	1.30	1.36	1.17	1.15
S1	2254.24	0.56	0.42	0.50	0.62	0.74	0.67	0.54	0.60	0.73	1.14	1.24	0.95	0.94
S2	2168.57	0.54	0.40	0.47	0.54	0.69	0.60	0.47	0.58	0.79	1.09	1.22	0.95	0.95
Considering Small														
S1	2254.24	0.91	0.77	0.84	0.83	0.86	0.88	0.64	0.94	1.08	1.48	1.59	1.12	1.28
S2	2168.57	0.81	0.66	0.74	0.69	0.77	0.75	0.58	0.85	1.06	1.36	1.49	1.09	1.22

Figures 6.9 to 6.16 show the shear strength vs. drift ratio of the test result and also the shear strength predictions from several shear equations.
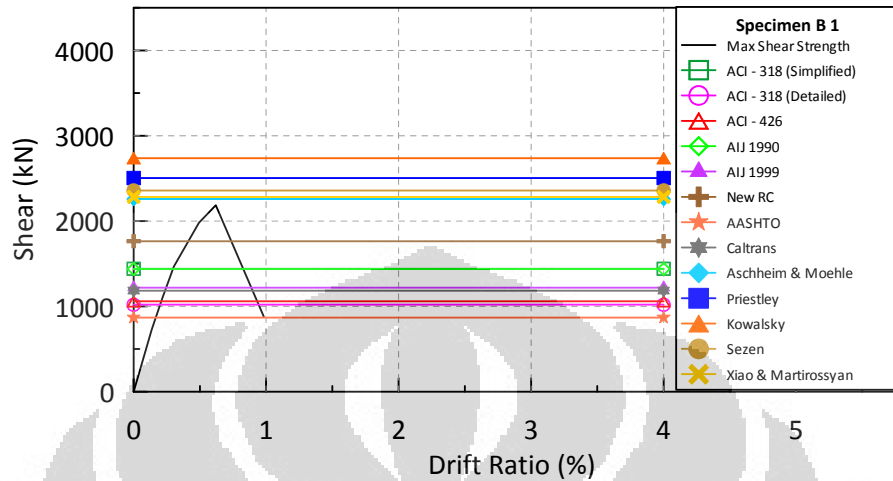
Figure 6.9 Drift ratio vs. shear strength prediction of Column B1 (Limit Stress ACI318-08)
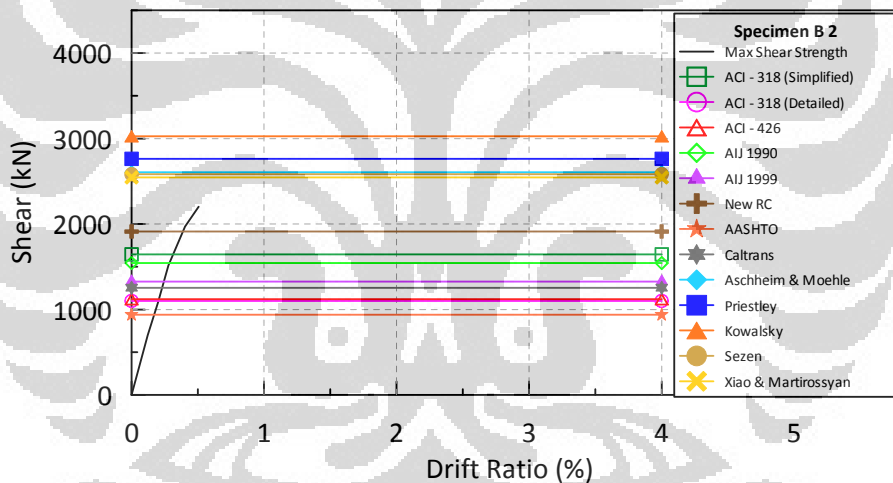
**Figure 6.10** Drift ratio vs. shear strength prediction of Column B2 (Limit Stress ACI318-08)
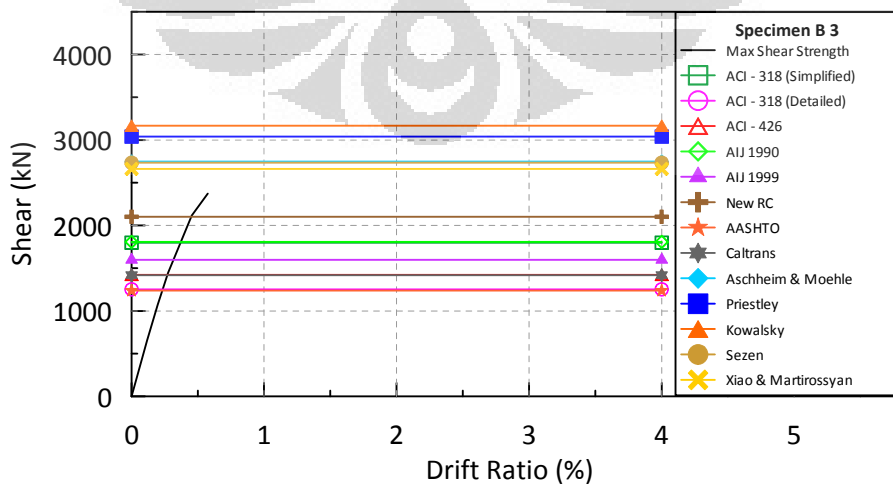
Figure 6.11 Drift ratio vs. shear strength prediction of Column B3 (Limit Stress ACI318-08)

Universitas Indonesia
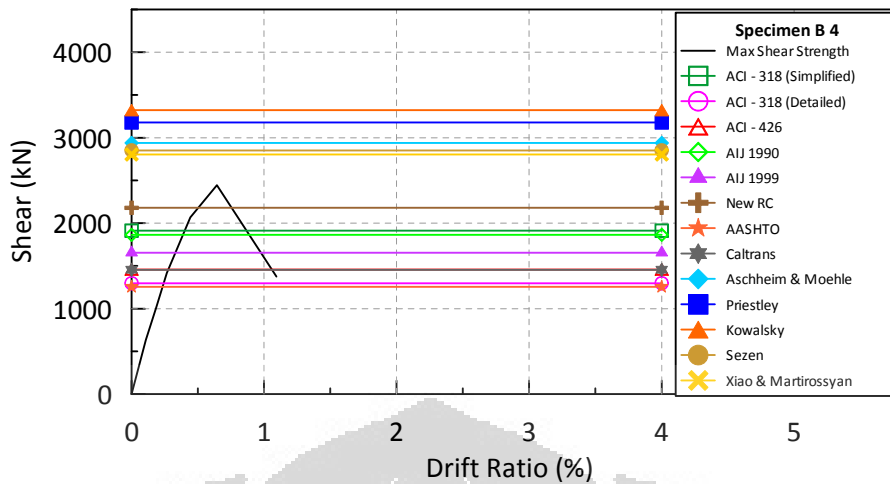
Figure 6.12 Drift ratio vs. shear strength prediction of Column B4 (Limit Stress ACI318-08)
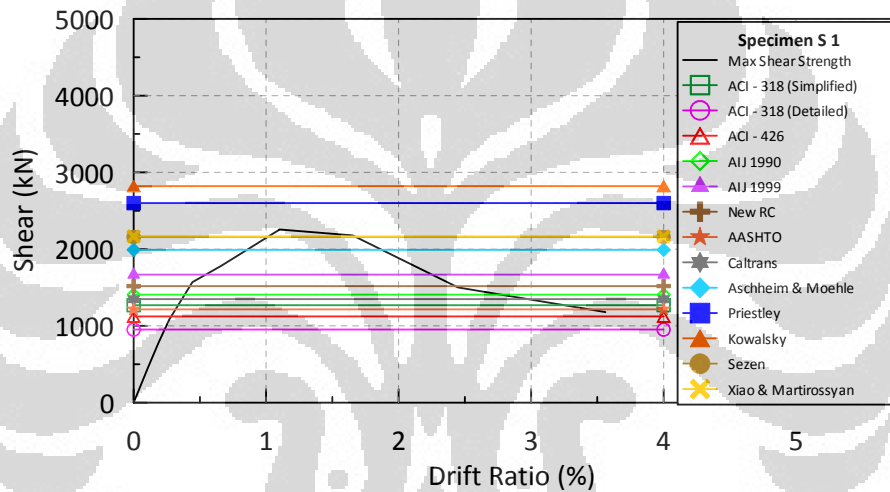
Figure 6.13 Drift ratio vs. shear strength prediction of Column S1 (Limit Stress ACI318-08)
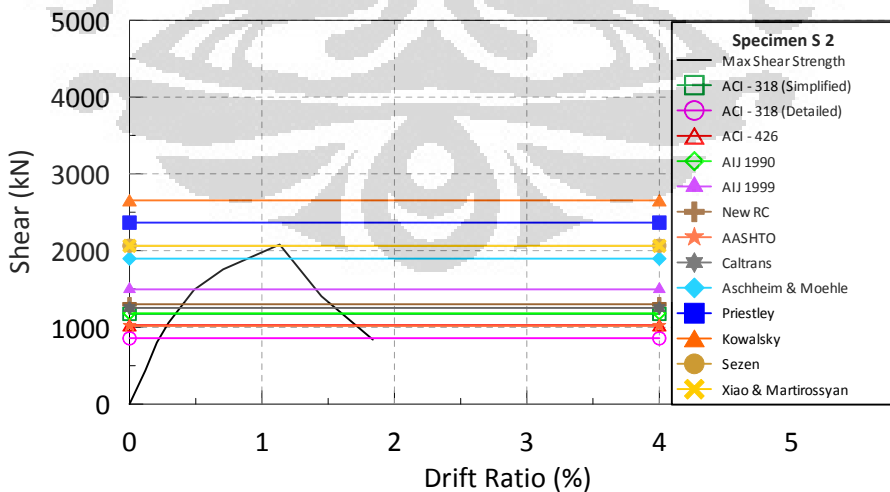
Figure 6.14 Drift ratio vs. shear strength prediction of Column S2 (Limit Stress ACI318-08)

Universitas Indonesia
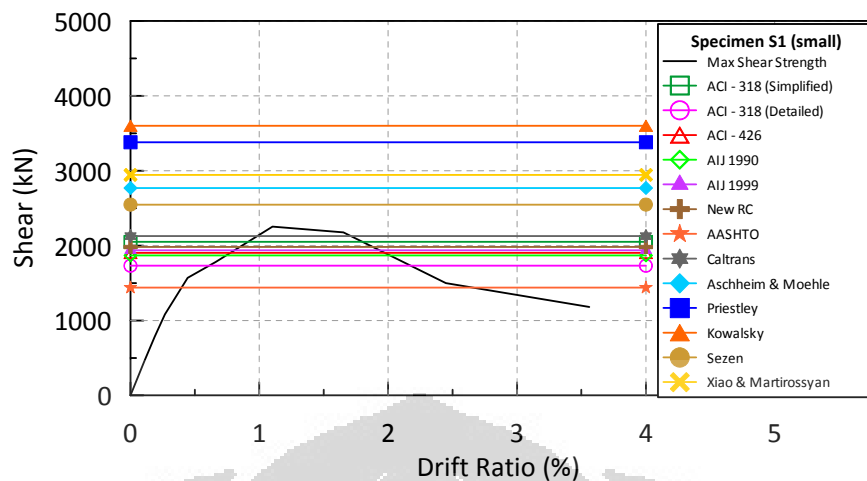
Figure 6.15 Drift ratio vs. shear strength prediction of Column S1 considering small spiral (Limit Stress ACI318-08)
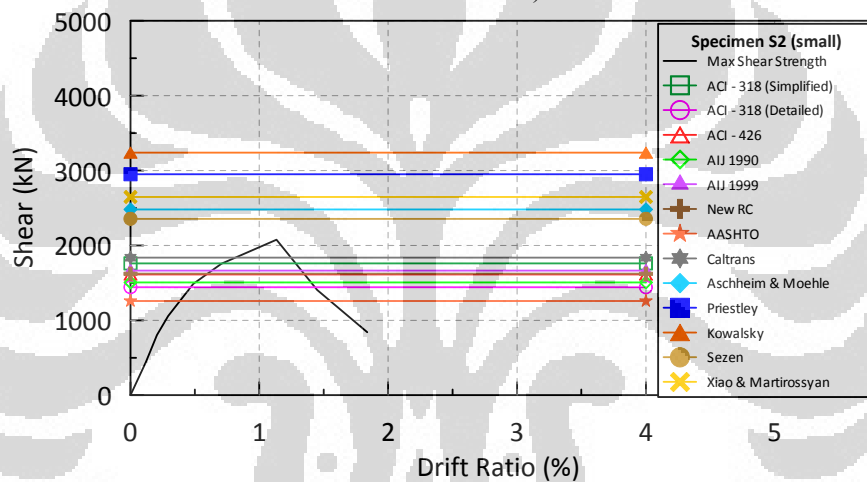
Figure 6.16 Drift ratio vs. shear strength prediction of Column S2 considering small spiral (Limit Stress ACI318-08)

6.3. TRANSVERSE REINFORCEMENT STRESS FROM PREDICTION MODEL

The comparison and ratio of test result shear strength predictions with limit from prediction model and using the original critical crack angle model are shown respectively in Table 6.5 and 6.6 below. In this part, the result from previous research (Kurniawan[28]) is included. From those tables, it can be seen that some of the shear predictions from the codes, provisions and guidelines are larger than the test result (ratio > 1.00), precisely for specimen S1 when small spiral are considered. The rest of the calculation performs well (ratio < 1.00). Shear strength calculation proposed by some researchers shows the higher ratio. The ratio V_n/V of those models varies from 0.79 to 1.69 as shown in Table 6.6.

Table 6.5 Comparison of test results and shear strength predictions (prediction model)

Specimen	Test Result V (kN)	Shear Strength V_n (kN)												
		ACI 318 simplified	ACI 318 detailed	ACI - 426	AIJ 1990	AIJ 1999	New RC	AASHTO	CALTRANS	Aschheim & Moehle	Priestley	Kowalsky	Sezen	Xiao Martirossyan
A1	1615.44	990.96	836.39	846.70	1397.06	1176.35	1552.71	825.55	1146.14	1365.36	1933.72	2203.25	1800.80	1719.21
A2	1632.41	1074.72	870.99	885.33	1483.47	1253.12	1653.28	893.77	1203.03	1538.49	2076.61	2367.29	1924.98	1858.37
A3	1789.59	1276.01	1103.03	1212.48	1855.29	1494.62	1964.35	1265.67	1420.35	1518.87	2366.34	2530.59	2052.36	1890.72
A4	1832.35	1358.08	1138.62	1255.09	1942.83	1567.15	2064.54	1358.97	1476.15	1703.85	2565.69	2731.91	2203.92	2100.28
B1	2184.94	1464.48	1043.14	1084.31	1476.33	1223.28	1793.04	910.87	1208.64	2055.45	2547.91	2760.88	2383.33	2304.49
B2	2202.54	1643.03	1097.82	1118.18	1539.33	1329.08	1909.54	935.44	1252.15	2425.71	2759.80	3024.97	2579.94	2543.68
B3	2374.04	1822.99	1277.36	1448.25	1848.33	1606.87	2132.13	1282.37	1443.73	2434.59	3044.59	3167.22	2730.47	2632.71
B4	2443.18	1963.41	1348.43	1510.37	1946.20	1662.35	2241.11	1347.21	1506.11	2680.54	3267.04	3372.27	2900.44	2842.34
S1	2254.24	1401.77	1083.78	1253.68	1722.88	1778.97	1824.07	1504.41	1478.88	1778.62	2887.90	3022.95	2266.46	2254.54
S2	2168.57	1266.79	948.71	1118.69	1400.89	1553.61	1512.06	1226.28	1343.90	1798.32	2593.40	2815.06	2155.22	2161.06
Considering small spiral														
S1	2254.24	2181.79	1863.80	2033.69	2186.62	1994.57	2287.81	1728.08	2258.89	2558.64	3667.91	3802.97	2656.47	3034.55
S2	2168.57	1851.80	1533.72	1703.71	1722.94	1703.33	1834.10	1462.64	1928.91	2383.34	3178.42	3400.07	2447.73	2746.08

Universitas Indonesia

Table 6.6 Ratio of test results and shear strength predictions (prediction model)

Specimen	Test Result V (kN)	Ratio of Shear Strength Prediction & Test Result (V_n/V)												
		ACI 318 simplified	ACI 318 detailed	ACI - 426	AIJ 1990	AIJ 1999	New RC	AASHTO	CALTRANS	Aschheim & Moehle	Priestley	Kowalsky	Sezen	Xiao Martirossyan
A1	1615.44	0.61	0.52	0.52	0.86	0.73	0.96	0.51	0.71	0.85	1.20	1.36	1.11	1.06
A2	1632.41	0.66	0.53	0.54	0.91	0.77	1.01	0.55	0.74	0.94	1.27	1.45	1.18	1.14
A3	1789.59	0.71	0.62	0.68	1.04	0.84	1.10	0.71	0.79	0.85	1.32	1.41	1.15	1.06
A4	1832.35	0.74	0.62	0.68	1.06	0.86	1.13	0.74	0.81	0.93	1.40	1.49	1.20	1.15
B1	2184.94	0.67	0.48	0.50	0.68	0.56	0.82	0.42	0.55	0.94	1.17	1.26	1.09	1.05
B2	2202.54	0.75	0.50	0.51	0.70	0.60	0.87	0.42	0.57	1.10	1.25	1.37	1.17	1.15
B3	2374.04	0.77	0.54	0.61	0.78	0.68	0.90	0.54	0.61	1.03	1.28	1.33	1.15	1.11
B4	2443.18	0.80	0.55	0.62	0.80	0.68	0.92	0.55	0.62	1.10	1.34	1.38	1.19	1.16
S1	2254.24	0.62	0.48	0.56	0.76	0.79	0.81	0.67	0.66	0.79	1.28	1.34	1.01	1.00
S2	2168.57	0.58	0.44	0.52	0.65	0.72	0.70	0.57	0.62	0.83	1.20	1.30	0.99	1.00
Considering Small														
S1	2254.24	0.97	0.83	0.90	0.97	0.88	1.01	0.77	1.00	1.14	1.63	1.69	1.18	1.35
S2	2168.57	0.85	0.71	0.79	0.79	0.79	0.85	0.67	0.89	1.10	1.47	1.57	1.13	1.27

Universitas Indonesia

Multi-spiral specimens were subjected to 10% axial load ratio (same as the A series specimens). In Table 6.6, it can be seen that without considering small spiral, the ratio of shear strength are around the same range as A series columns even the difference ratio between them around 0.10. On the other hand when small spiral contribution is considered, the ratio obtained is much larger. This condition gives an idea that the contribution from small spiral reinforcement exists but it is not as higher as calculated.

Figures 6.17 to 6.24 show the shear strength vs. drift ratio of the test result and also the shear strength predictions from several shear equations.

Figure 6.17 Drift ratio vs. shear strength prediction of Column B1 (prediction)

Figure 6.18 Drift ratio vs. shear strength prediction of Column B2 (prediction)

Figure 6.19 Drift ratio vs. shear strength prediction of Column B3 (prediction)

Figure 6.20 Drift ratio vs. shear strength prediction of Column B4 (prediction)

Figure 6.21 Drift ratio vs. shear strength prediction of Column S1 (prediction)
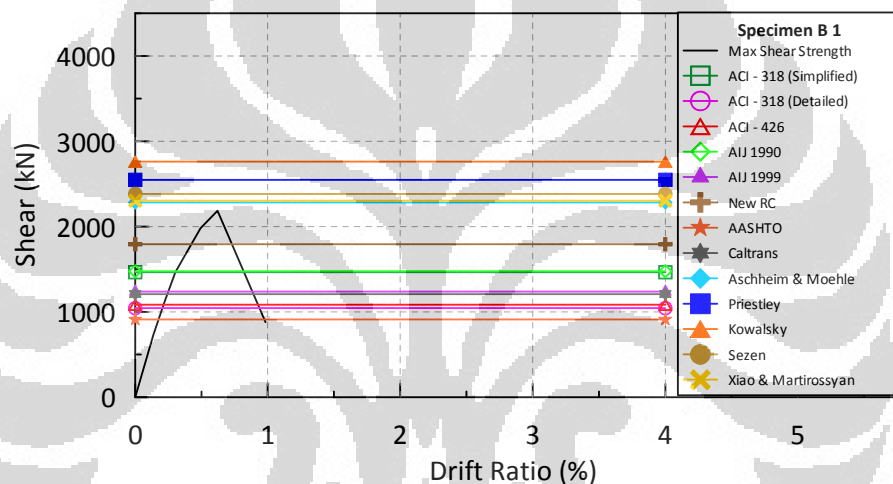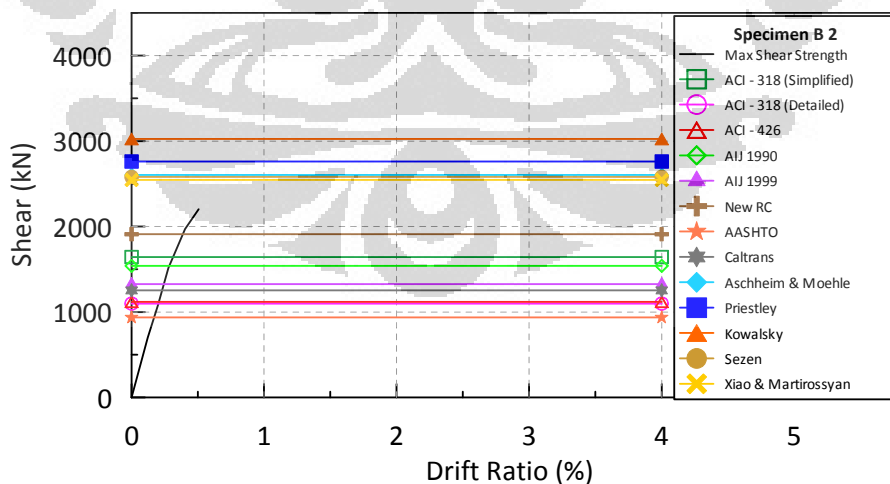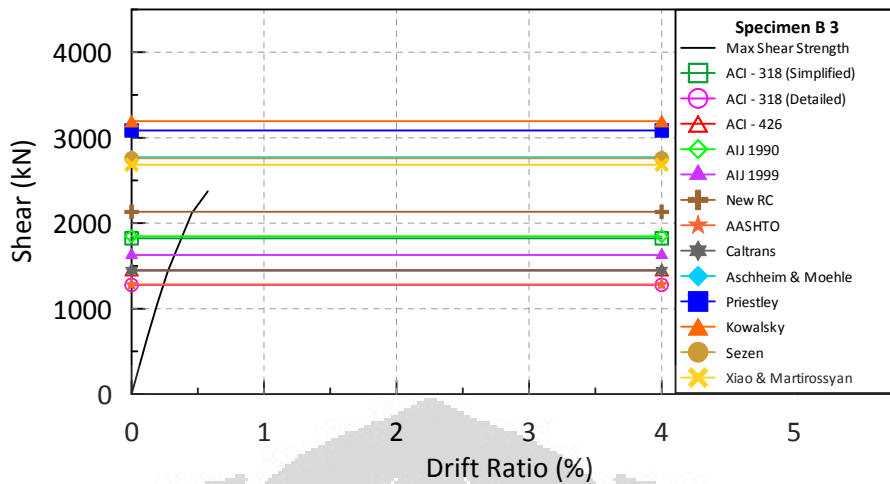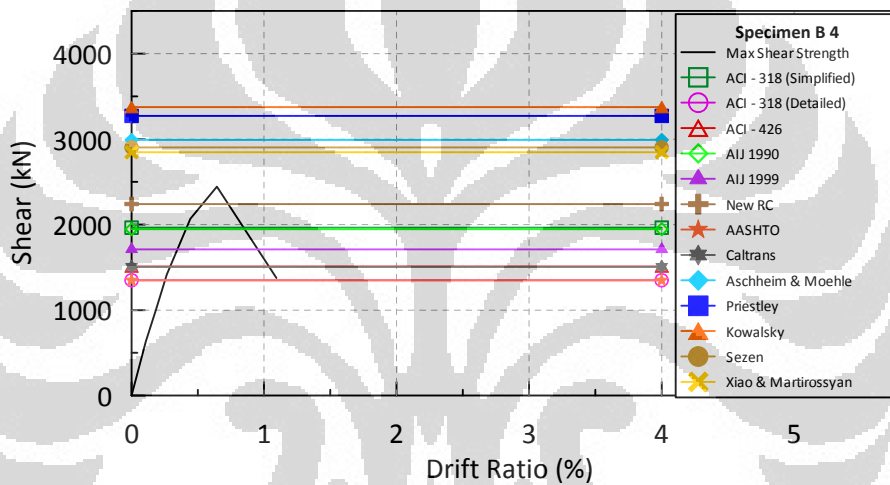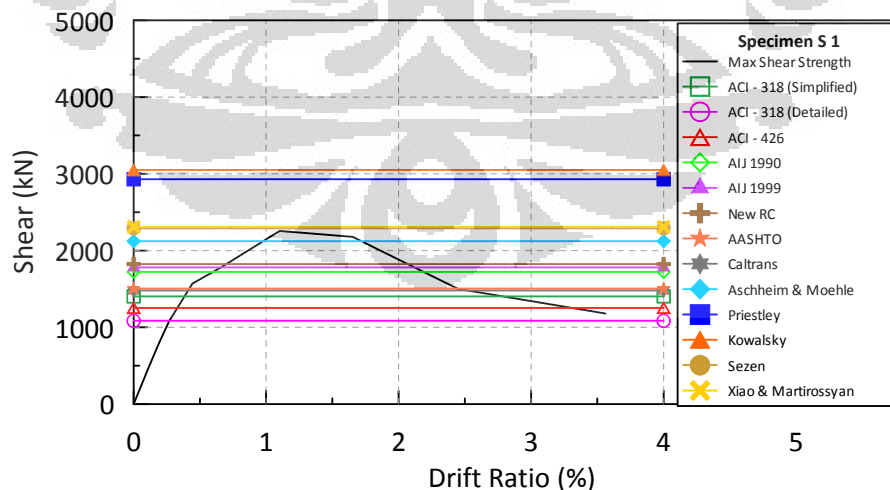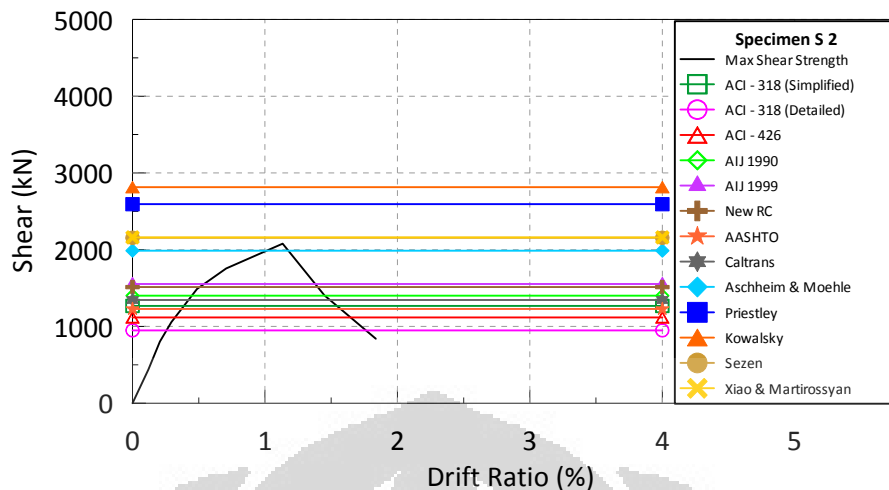
Figure 6.22 Drift ratio vs. shear strength prediction of Column S2 (prediction)
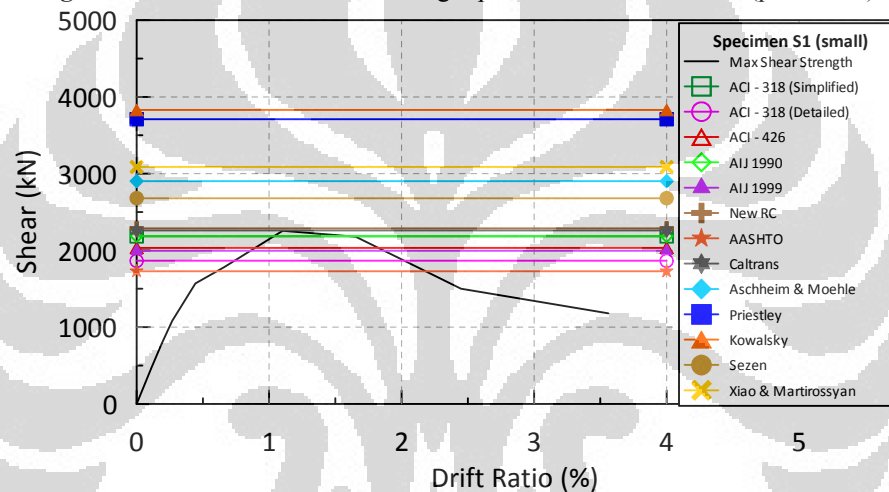

Figure 6.23 Drift ratio vs. shear strength prediction of Column S1 considering small spiral (prediction)
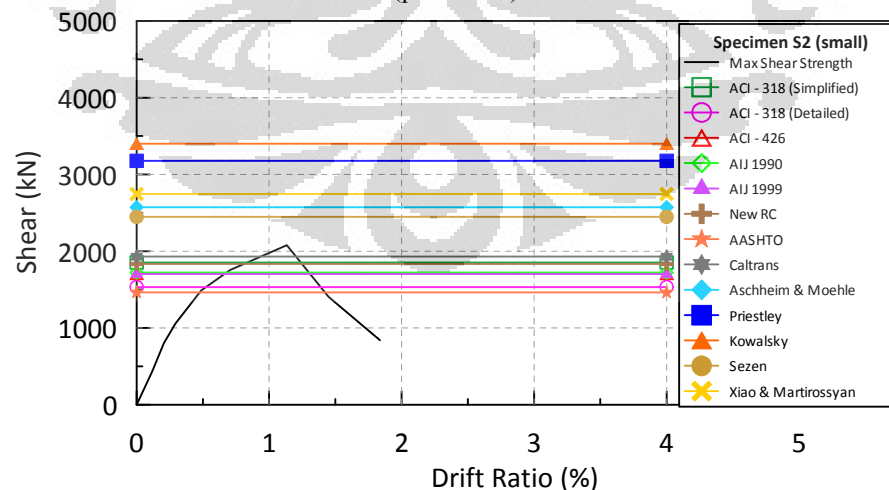

Figure 6.24 Drift ratio vs. shear strength prediction of Column S2 considering small spiral (prediction)

According to Table 6.5 and 6.6, there are some important notes from ACI 318 and

Japanese codes. ACI 318-08 captures axial load effect better than Japanese codes. It could be seen clearly from table 6.6 that for specimen A and B series, ACI 318 shows that the higher the axial load, the higher the ratio of V_n/V. On the other hand, from Japanese codes, ratio V_n/V of B series is lower than A series. As mentioned in chapter 2, equation 2.24 and 2.25 (for ACI 318); equation 2.33 (AIJ 1990); equation 2.41, 2.42, 2.43, 2.44 (AIJ 1999) and equation 2.52 (New RC), it could be seen that only New RC equation considers axial load ratio in its calculation. Furthermore, the consideration of axial load ratio in New RC seems contrary to the effect from ACI equations. Below, the equation 2.54 from chapter 2 shows the part of New RC equations that use the axial load ratio. In order to calculate $cot\ \phi$ there are three different formulas. In this research, all of the calculation depends to the first formula, the one that considers axial load ratio n. The higher the n value, the lower the $cot\ \phi$ means the larger of ϕ (crack angle). So, the crack angle becomes larger as the axial load becomes higher. This condition is contrary to the experimental result and ACI calculation.

$$cot\ \phi = min\left(2.0 - 3n - 50R_p, \frac{j_t}{2\alpha D}, \sqrt{\frac{\nu f'_c}{\rho_w f_{yt}} - 1}\right) \qquad (2.54)$$

Table 6.7 shows the comparison of test results and shear strength predictions using design value of concrete compressive strength (f'_c). It could be seen that the higher n value, the lower the $cot\ \phi$. Moreover, from specimen A1-A3 and B1-B3, the increasing of axial load ratio augments the V_n. However the augmentation of shear from experimental result is higher. This condition affects the lower ratio of V_n/V as shown in Table 6.6.

Table 6.7 Comparison of test results and shear-strength predictions using design value of concrete compressive strength (New RC equation)

Specimen	f'_c (MPa)	spacing (mm)	n	Selected cot ϕ	V_n (kN)
A1	70	450	0.1	1.7	1450.646
A3	70	260	0.1	1.7	1771.117
B1	70	450	0.2	1.4	1580.29
B3	70	260	0.2	1.4	1872.23

Regarding to three Japanese codes, for specimen A series using AIJ 1990 and New RC (1993) equations, the ratio larger than 1.00. This condition shows that the nominal shear strength calculation is not conservative.

Among three Japanese codes, AIJ 1999 performed well, means give conservative value. In this part AIJ 1990 and 1999 will be examined. Equation 2.33 from AIJ 1990 can be written as follow.

$$V_{u-AIJ\ 1990} = \rho_w f_{yt} b j_t \cot\phi + (vf'_c - vf'_c\beta)\frac{bD}{2}\tan\theta \qquad (6.1)$$

AIJ 1999 has 3 equations to be considered to calculate the lowest value of shear strength. In this case, all of the specimens use the first equation (equation 2.42) as shown below.

$$V_{u1} = \rho_w f_{yt} b_e j_e \cot\phi + \left(vf'_c - \frac{5\rho_w f_{yt}}{\lambda}\right)\frac{bD}{2}\tan\theta \qquad (6.2)$$

As shown in these two equations, one part from arch action gives the different value. The diminution of arch action from AIJ 1999 (equation 6.2) is larger than the diminution of arch action from AIJ 1990. This condition is the reason why the AIJ 1999 gave better value than AIJ 1990.

Small spirals contribute to the shear strength formulation, precisely in steel contribution. Table 6.6 shows that when the calculation considers the small spirals, shear strength calculation is overestimated. ACI 318-08[14] provides development length as the attainable average bond stress over the length of embedment of the reinforcement. Development lengths are required because of the tendency of highly stressed bars to split relatively thin sections of restraining concrete. A single bar embedded in a mass of concrete should not require as great a development length; although a row of bars, even in mass concrete, can create a weakened plane with longitudinal splitting along the plane of the bars.

Half of small spiral is considered as development length (l_{dh}) as a crack can passed through the transverse reinforcement. The value l_{dh} should be larger than 150 mm

(ACI 318-08[14]). As the diameter of small spiral is 220 mm, its half gives 110 mm. This insufficient development length can be the reason why the consideration of all small spirals gave an overestimation value. It could be concluded that, small spirals contribute partially to shear strength calculation.

More explanation about multi-spiral column (S series) will be discussed based on Table 6.8 in the next page. S series specimens were subjected under 10% axial load ratio which is the same condition as the A series specimens, therefore, Specimen A4 and S2 will be examined. These two specimens have approximately the same value of ρ (volumetric ratio of confining steel) and concrete compressive strength. Experimental result shows a slightly different value of shear strength from both specimens. V_n/V ratio from specimen S2 shows that without small spirals is lower than the value from specimen A4. Moreover, when small spirals are considered, the ratio is higher enough. This condition shows that small spirals contribute partially to shear strength calculation.

Table 6.8 Comparison of test results and shear strength predictions using ACI 318-08 formulation and proposed yield strength formulation.

Specimen	f'_c (MPa)	Axial Load Ratio	Experiment	Volumetric ratio of confining steel (ρ)	Ratio ACI 318 simplified	Ratio ACI 318 detailed
A1	92.47		1615.44	0.00333	0.61	0.52
A2	103.15	10%	1632.41	0.00333	0.66	0.53
A3	96.87		1789.59	0.00576	0.71	0.62
A4	107.10		1832.35	0.00576	**0.74**	0.62
B1	98.95		2184.94	0.00333	0.67	0.48
B2	114.10	20%	2202.54	0.00333	0.75	0.50
B3	112.85		2374.04	0.00576	0.77	0.54
B4	121.04		2443.18	0.00576	0.80	0.55
S1	117.57	10%	2254.24	0.00799[1]	0.62	0.48
S2	117.57		2168.57	0.00555*	**0.58**	0.44
Considering Small Spiral						
S1	117.57	10%	2254.24		0.99	0.85
S2	117.57		2168.57		**0.87**	0.72

---

[1] Volumetric ratio of confining steel without considering small spirals

CHAPTER VII
CONCLUSION AND FUTURE WORK

7.1. CONCLUSION

Experiment related to elastic shear strength of column with high strength concrete and steel was performed during this research. Two types of columns were tested, columns with square hoops and columns with innovative multi-spiral reinforcement. Columns with square hoops (type B columns) were tested under 20% axial load ratio and lost their lateral strength at low drift ratio. On the other hand, columns with multi-spiral reinforcement (type S columns) were tested under 10% axial load ratio. Shear failure mechanism indicated by the developing of diagonal shear cracks occurred in all type specimens.

Spacing of transverse reinforcement is the main parameter used for all specimens. For type B specimens, another parameter used in this study is concrete compressive strength. Test results show the significant effect of different value of the spacing on shear strength. The effect of different concrete compressive strength is not large since the actual value of f'_c did not reflect a clear gap.

The strong explosive sound which was heard during the test is the sound from the developing of diagonal shear crack.

The critical crack angle predicted by Elwood and Moehle (ranging from 28.26º to 31.84º) gave the same trend as the test result (ranging from 16.50º to 28.50º) as the axial load changes. However, the difference is quite large. Experimental results show that higher axial load ratio, smaller the cracking angle appeared. This condition can be seen from specimen A1 (27.00º critical crack angle) and B1 (18.00º critical crack angle). Both were designed by the same design parameter but were subjected by different axial load ratio (10% and 20% axial load ratio for A1 and B1 respectively).

Observation during the test shows the crack cut through the aggregates. This condition reflected the decrease of the aggregate interlock resistance. If aggregate interlock resistance is an important mechanism, this will decrease the shear strength contribution from concrete. However, nowadays several researchers such as Zararis-Papadakis and Kotsovos-Pavlovic proposed not to consider aggregate

196

interlock along the crack surfaces and dowel action of longitudinal reinforcement (Park et.al[29]) in shear strength. Since the compression zone of intact concrete prevents shear-slip of the crack surfaces, these two mechanisms do not significantly contribute to the shear strength.

The stress of the transverse reinforcement at maximum lateral strength should be limited. Test result proves that the maximum strength (peak point) of column occurred first and was followed by yielding of the transverse reinforcement. It means the actual stresses in the hoop at the maximum strength (peak point) are smaller than the yield point of the transverse reinforcement. Limit stress from ACI 318 for welded deformed wire reinforcement (550 MPa) is apparently conservative.

Drift ratio and stress at hoops relationship derived from test result indicates that the stress in the stirrups augments as the increase of the drift. The intersection between the prediction line and nominal yield stress of transverse reinforcement gives 0.95% drift ratio which is the predicted time where the yield stress of hoop reached.

The ratio of test result and shear prediction provided by codes, provisions and guidelines using 550 MPa (welded deformed wire reinforcement of ACI 318) yield stress of transverse reinforcement (V_n/V) are conservative (smaller than 1.00) and performed well. On the other hand, some shear strength predictions proposed by researchers overestimated the test results.

More studies in shear prediction show that some of the nominal shear strength provided by codes, provisions and guidelines using prediction model of stress at transverse reinforcement drift ratio relationship (part 5.7) and the experimental result of critical crack angle have ratio of (V_n/V) larger than 1.00. On the other hand, using the original model of critical crack angle and the prediction model of transverse reinforcement seems to provide satisfactory results.

According to the use of prediction model of transverse reinforcement stress, ACI 318-08 captures axial load effect better than Japanese codes. Among three Japanese codes, only New RC equation considers axial load ratio in its calculation. Furthermore, the consideration of axial load ratio in New RC seems contrary to the experimental result and ACI calculation. The crack angle becomes larger as the axial load becomes higher.

AIJ 1999 performed better than AIJ 1990, means give conservative value. The diminution of arch action from AIJ 1999 is larger than the diminution of arch action from AIJ 1990.

Small spirals from innovative multi-spiral reinforcement give contribution value to the shear strength of type S columns much lower than that calculated by assuming all of the small spirals capable of developing the same stress level to resist shear as the large spirals. The insufficient development length can be the reason why the consideration of all small spirals gave an overestimation value. It could be concluded that, small spirals contribute partially to shear strength calculation.

In general, S series specimens have shear failure at higher drift ratio than A and b series. Simply because the shear strength of S series columns are higher, therefore

The effect of axial load ratio could be seen in three different terms, such as: lateral strength, secant lateral stiffness and strain reading of longitudinal reinforcement. As the axial compression is getting higher, the lateral strength is also getting higher. It is obvious that column is also getting stiffer that decreases the strain of longitudinal reinforcement. From the shear strength calculation comparing type A and B columns, it is noted that higher the axial load ratio, the higher ratio V_n/V of columns can be obtained. The shear strength value becomes less conservative as the higher axial load compression increases.

7.2. FUTURE WORK

As the sequence of previous research, this thesis already compares the effect of various parameters on the column behavior, especially for type B specimens. On the other hand, type S specimen is initiated to be researched.

Further experimental and analytical studies for specimen with square hoop are needed to investigate the following parameters.

1. Axial Load Ratio

    Some effects of axial load ratio that already mentioned in this research are lateral strength, secant lateral stiffness and strain reading of longitudinal reinforcement. However, 10 and 20% axial load ratio are categorized as low axial load ratio. Further test, such as for 30 and 40% axial load ratio is needed to know the behavior of the column under high axial load ratio. By performing all these four

axial load ratios, the complete figure of the column could be understood well.

2. Drift Ratio vs. Stress of Transverse Reinforcement

    Relationship between stress at transverse reinforcement and drift ratio is already discussed. An idea to predict the yield point of transverse reinforcement considering drift ratio will be very interesting in the future. Strain reading from type A and B specimen gave the prediction of drift where the yield of stress could appear. Further study is needed to verify the recent result of the relationship drift ratio and stress at hoops. By doing the experiment with higher axial load ratio to specimens, more data of stress in the stirrup can be obtained. Moreover, higher axial load can give other effect in strain reading of stirrups. Thus, more stress data in the stirrup could propose more reasonable model to be used in the future. Another idea to predict the stress of transverse reinforcement bar from drift ratio is generating its formulation by considering its mechanism term. There are three steps to generate this formulation. First step is finding the relationship between percentage of shear displacement relative to total displacement and the drift ratio. Either the drift ratio at max strength of column or shear displacement, both can be obtained from experimental result. Next step, from experimental result (shear displacement), width of the crack can be found. It seems reasonable that the half of this crack width is related to the value of bond-slip stress relationship. So, as the third step, slip bond relationship can give the stress of transverse reinforcement bar. In the final, the percentage of shear displacement can give the stress of transverse reinforcement bar. In order to perform this analysis, profound study in anchorage behavior of reinforcing bars and analytical bond-slip models should be performed.

REFERENCES

1. Tony C. Liu and Jenn-Chuan Chern. "Sustainable Concrete Technology – Challenge and opportunity," Presentation National Taiwan University, ROC.

2. Samuel Yen-Liang Yin, "Design and Construction Innovations for Reinforced Concrete Structures". The 3rd ACF International Conference ACF/VCA 2008.

3. Caldarone MA, "High-Strength Concrete - A Practical Guide," *Taylor & Francis*. 2008.

4. Concrete Basics. *High Performance Concrete & High Strength Concrete* Available from: http://www.concretebasics.org/articlesinfo/hpchsc.php[cited 2012 June 02]

5. Razvi S, "Confinement of Normal and High-Strength Concrete Columns," *PhD Thesis, Department of Civil Engineering, University of Ottawa*. 1995.

6. Razvi S, Saatcioglu M, "Confinement Model for High-Strength Concrete," *ASCE Journal of Structural Engineering*, V. 125, No. 3. 1999, pp. 281-9.

7. Saatcioglu M, Razvi S, "Strength and Ductility of Confined Concrete," *ASCE Journal of Structural Engineering*, V. 118, No. 6. 1992, pp. 1590-607.

8. Carrasquillo RL, Nilson AH, Slate FO, "Propoerties of High Strength Concrete Subject to Short-Term Loads " *ACI Structural Journal*, V. 78, No. 3. 1981, pp. 171-8.

9. Bechtoula H, Kono S, Watanabe F, "Seismic Performance of High-Strength Reinforced Concrete Columns," *Structural Engineering and Mechanic* V. 31, No. 6. 2009, pp. 697-716.

10. Nemati KM, Gargoni P, Noguchi T, "On Modulus of Elasticity of High-Strength Concrete," *International Conference on Construction and Building Technology* 2008.

11. Aoyama H, "Design of Modern Highrise Reinforced Concrete Structures," *Imperial College Press*. 2001.

12. Maruta M, "Shear Capacity of Reinforced Concrete Column Using High Strength Concrete," *Invited Lecture in the 8th International Symposium on Utilization of High-Strength and High-Performance Concrete, Tokyo*. October 27-29, 2008.

200

13. Samuel Yen-Liang Yin, Jui-Chen Wang, Ping-Hsiung Wang, "Development of Multi-spiral Confinements in Rectangular Columns for Construction Automation", *Journal of the Chinese Institute of Engineers* Vol. 35, No. 3. April 2012, pp. 309-320.

14. ACI Committee 318, "Building Code Requirements for Structural Concrete (ACI 318-08) and Commentary (ACI 318R-08)," American Concrete Institute, Farmington Hills, MI. 2008.

15. ACI-ASCE Committee 426, "The Shear Strength of Reinforced Concrete Members," *ACI Journal,* V. 70, No. 7. 1973, pp. 471-3

16. AIJ 1990, "Design Guidelines for Earthquake Resistant Reinforced Concrete Building Based on Ultimate Strength Concept ", Architectural Institute of Japan. 1990.

17. AIJ 1999, "Design Guidelines for Earthquake Resistant Reinforced Concrete Building Based on Inelastic Displacement Concept," Architectural Institute of Japan. 1999

18. Sezen H, "Seismic Behavior and Modeling of Reinforced Concrete Building Columns," *PhD Thesis, Departement of Civil and Enviromental Engineering, University of California, Berkeley*. 2002.

19. AASHTO LRFD, "Bridge Design Specifications 4th edition," Association of State Highway and Transportation Officials Washington, DC. 2007.

20. Priestley MJN, Verma R, Xiao Y, "Sesimic Shear Strength of Reinforced Concrete Columns," *ASCE Journal of Structural Engineering*, V. 120, No. 8. 1994, pp. 2310-29.

21. Ang, BG, Priestley MJN, Paulay T, "Seismic Shear Strength of Circular Reinforced Concrete Columns," *ACI Structural Journal,* V.86, No. 1, Jan. 1989.

22. Kowalsky MJ, Priestley MJN, "Improved Analytical Model for Shear Strength of Circular Reinforced Concrete Columns in Seismic Regions," *ACI Structural Journal,* V.97, No. 3, May-June. 2000.

23. Elwood KJ, Moehle JP, "An Axial Capacity Model for Shear-Damaged Columns," *ACI Structural Journal*, V. 102, No. 4. 2005, pp. 578-87.

24. Priestley MJN, Seible F, Calvi GM, "Seismic Design and Retrofit of Bridges,"

John Wiley & Son, Inc. 1996.

25. Kowalsky M, Priestley M, "Improved Analytical Model for Shear Strength of Circular Reinforced Concrete Columns in Seismic Regions," *ACI Structural Journal*, V. 97, No. 3. 2000, pp. 388-96.

26. Aschheim M, Moehle JP, "Shear Strength and Deformability of RC Bridge Columns Subjected to Inelastic Displacements," *UCB/EERC 92/04*. 1992, pp. 93.

27. Xiao Y, Martirossyan A, "Seismic Performance of High-Strength Concrete Columns," *ASCE Journal of Structural Engineering*, V. 124, No. 3. 1998, pp. 241-51.

28. Kurniawan, Dimas Pramudya, "Shear Behavior of Reinforced Concrete Columns with High Strength Steel and Concrete under Low Axial Load," *Master Thesis, Department of Construction Engineering, National Taiwan University of Science and Technology*. 2011.

29. Park HG, Choi KK, Wight JK, "Strain-Based Shear Strength Model for Slender Beams without Web Reinforcement", *ACI Structural Journal November-December 2006*.

30. Leo Edward Linbeck, "Behavior of Reinforced Concrete Columns Subjected to Lateral and Axial Load Reversals", *Master thesis, University of Texas at Austin*, 1987.

31. ACI ITG-4.3R-07, "Specification for High-Strength Concrete in Moderate to High Seismic Applications," American Concrete Institute 2007, pp. 10.
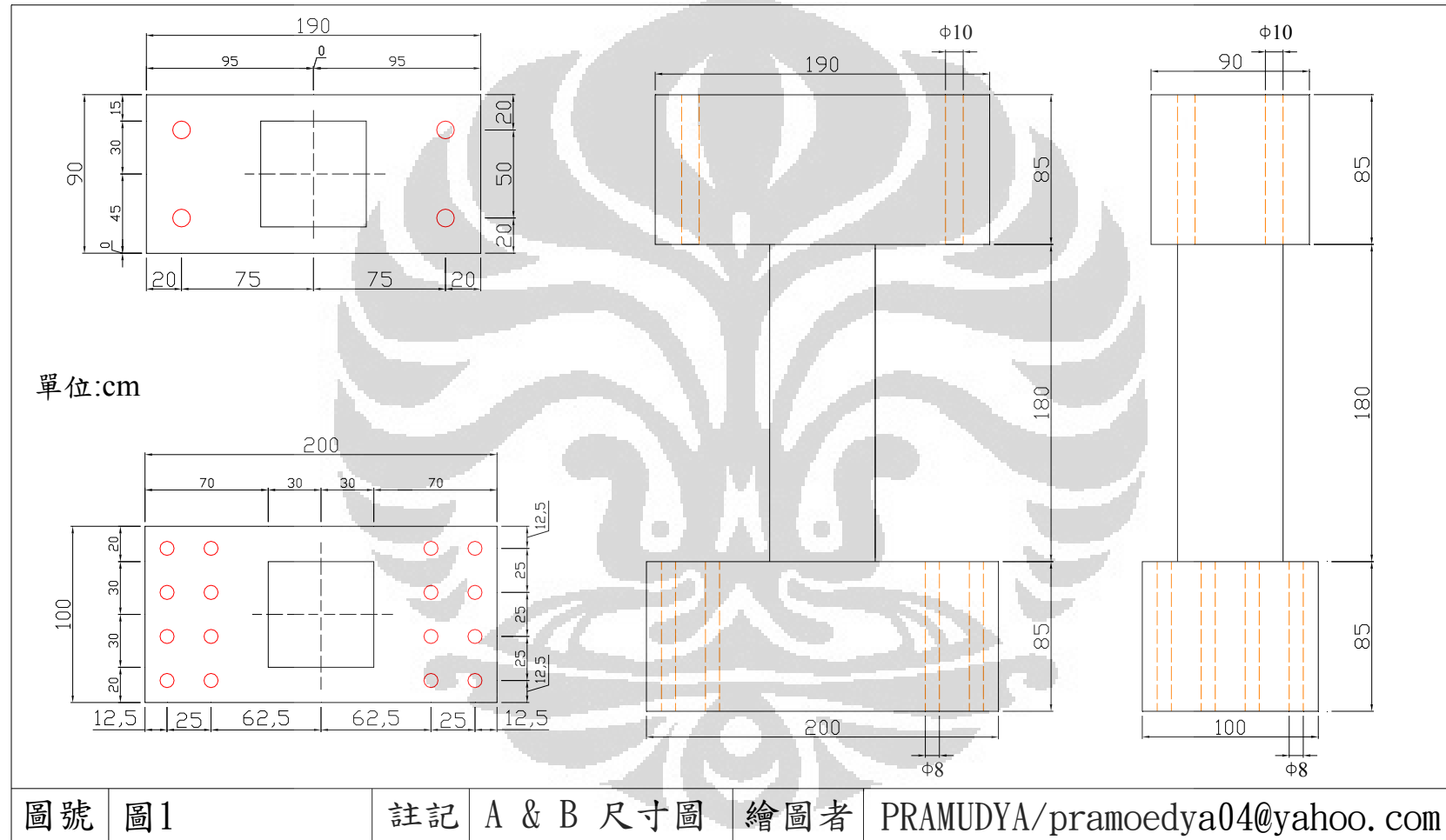
Figure A.1 Dimension of the specimens
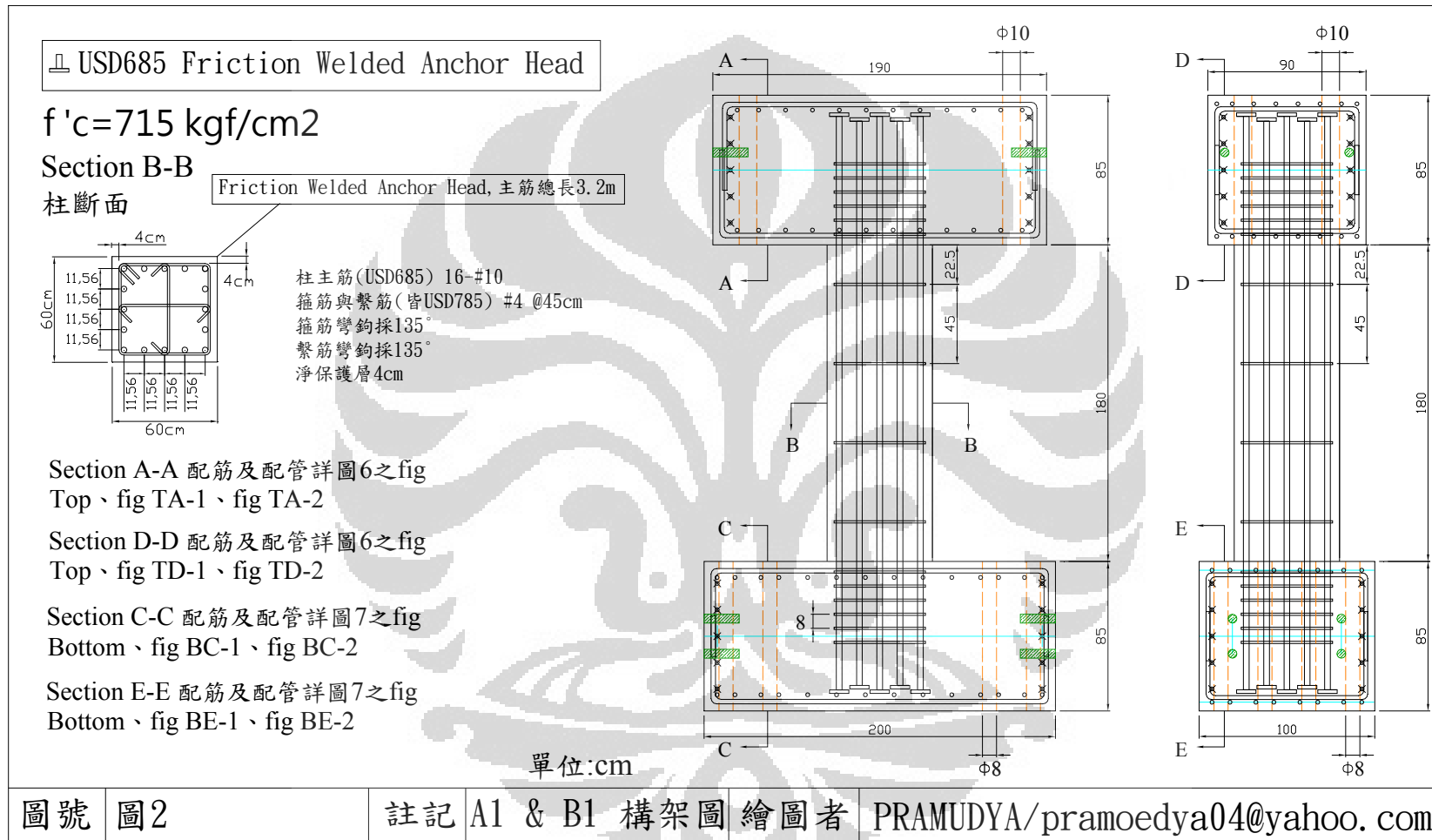
Figure A.2 Reinforcement detail of Column A-1

⊥USD685 Friction Welded Anchor Head

f'c=1020 kgf/cm2

Section B-B
柱斷面

Friction Welded Anchor Head, 主筋總長3.2m

柱主筋(USD685) 16-#10
箍筋與繫筋(皆USD785) #4 @45cm
箍筋彎鉤採135°
繫筋彎鉤採135°
淨保護層4cm

Section A-A 配筋及配管詳圖6之fig
Top、fig TA-1、fig TA-2

Section D-D 配筋及配管詳圖6之fig
Top、fig TD-1、fig TD-2

Section C-C 配筋及配管詳圖7之fig
Bottom、fig BC-1、fig BC-2

Section E-E 配筋及配管詳圖7之fig
Bottom、fig BE-1、fig BE-2

單位:cm

| 圖號 | 圖3 | 註記 | A2 & B2 構架圖 | 繪圖者 | PRAMUDYA/pramoedya04@yahoo.com |

Figure A.3 Reinforcement detail of Column A-2

205
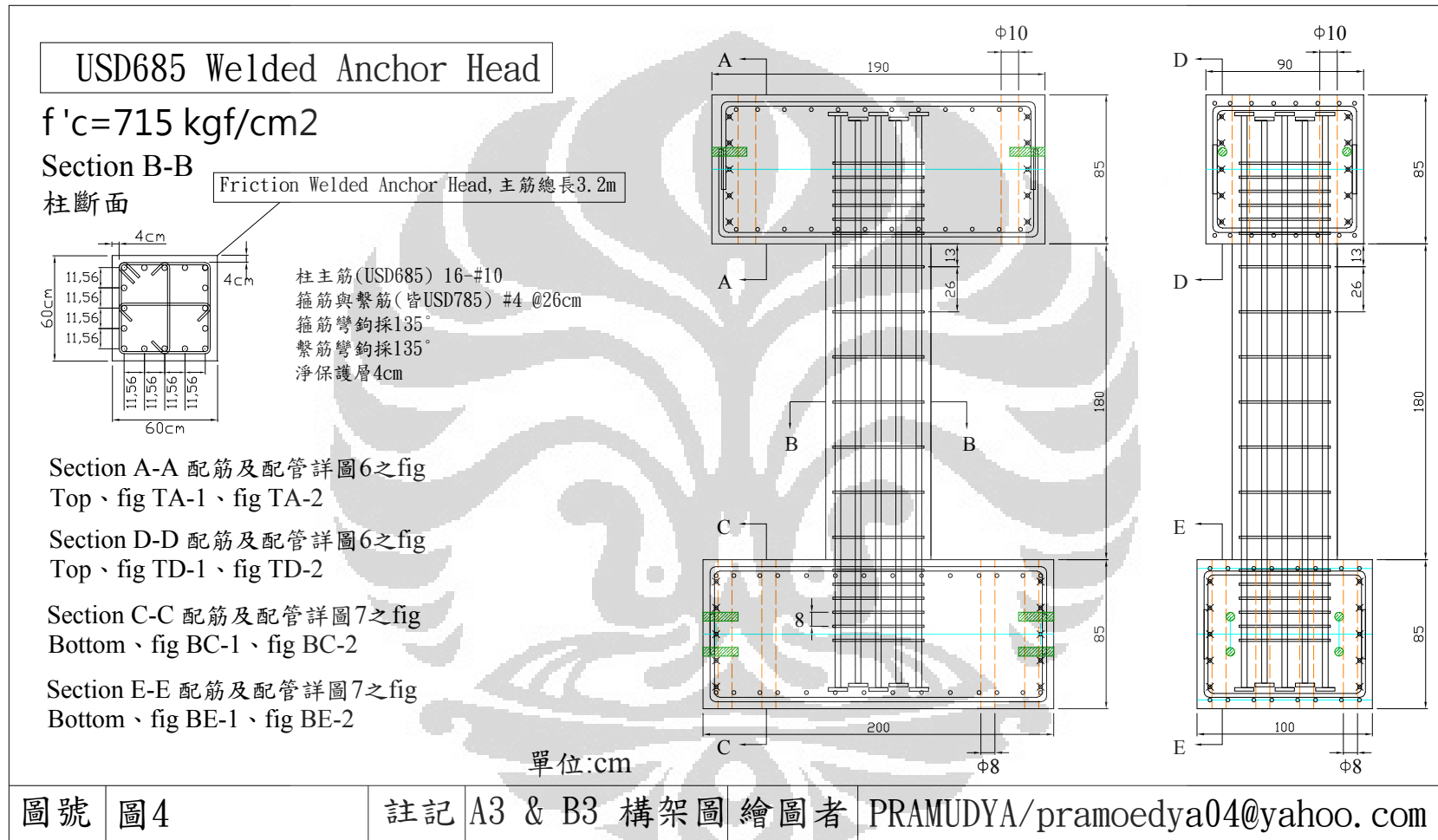
Figure A.4 Reinforcement detail of Column A-3

⊥ USD685 Friction Welded Anchor Head

f'c=1020 kgf/cm2

Section B-B
柱斷面

Friction Welded Anchor Head, 主筋總長3.2m

柱主筋(USD685) 16-#10
箍筋與繫筋(皆USD785) #4 @26cm
箍筋彎鉤採135°
繫筋彎鉤採135°
淨保護層4cm

Section A-A 配筋及配管詳圖6之fig
Top、fig TA-1、fig TA-2

Section D-D 配筋及配管詳圖6之fig
Top、fig TD-1、fig TD-2

Section C-C 配筋及配管詳圖7之fig
Bottom、fig BC-1、fig BC-2

Section E-E 配筋及配管詳圖7之fig
Bottom、fig BE-1、fig BE-2

單位:cm

圖號 | 圖5 | 註記 | A4 & B4 構架圖 | 繪圖者 | PRAMUDYA/pramoedya04@yahoo.com

Figure A.5 Reinforcement detail of Column A-4

207
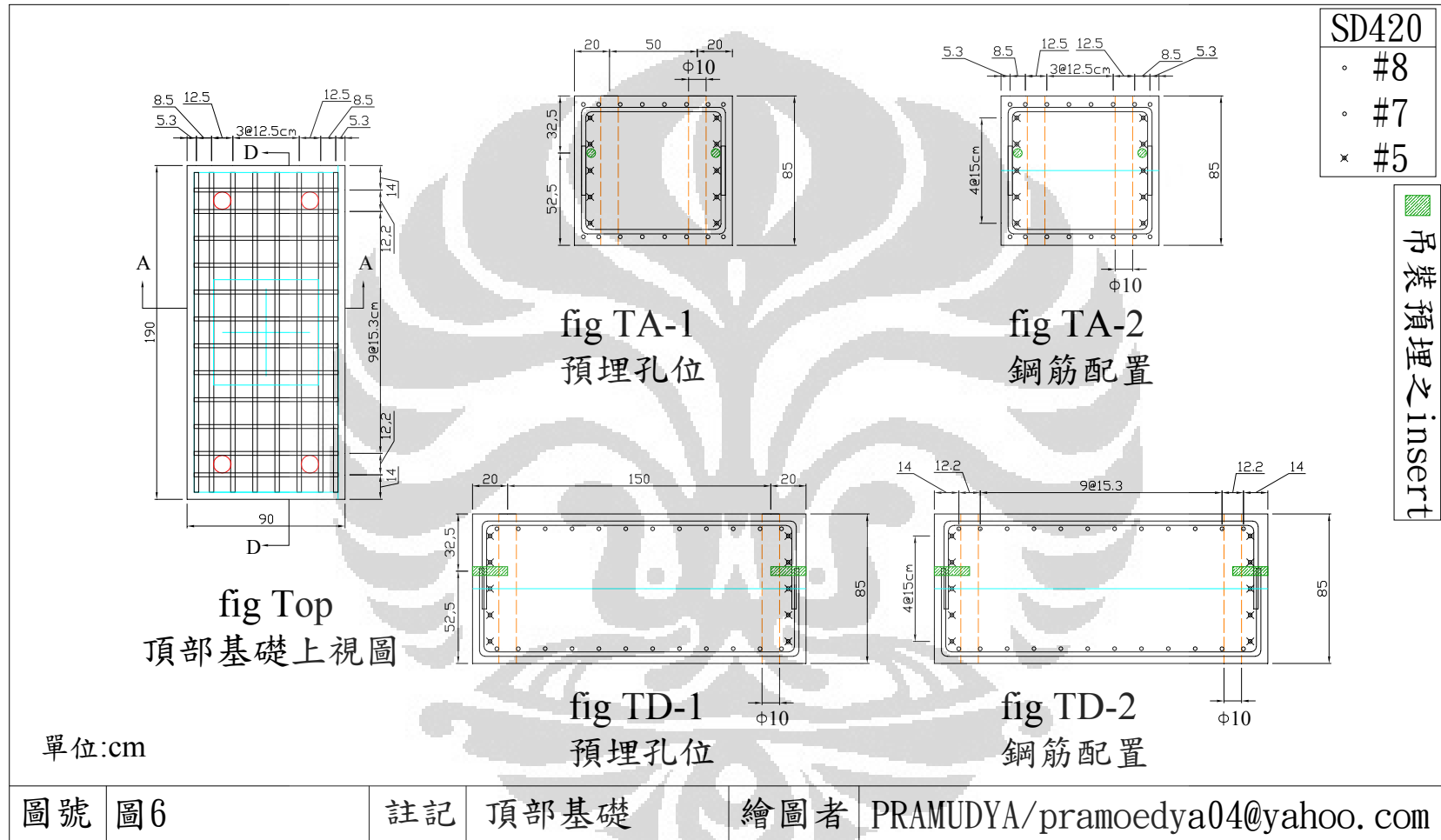
Figure A.6 Reinforcement detail of top block
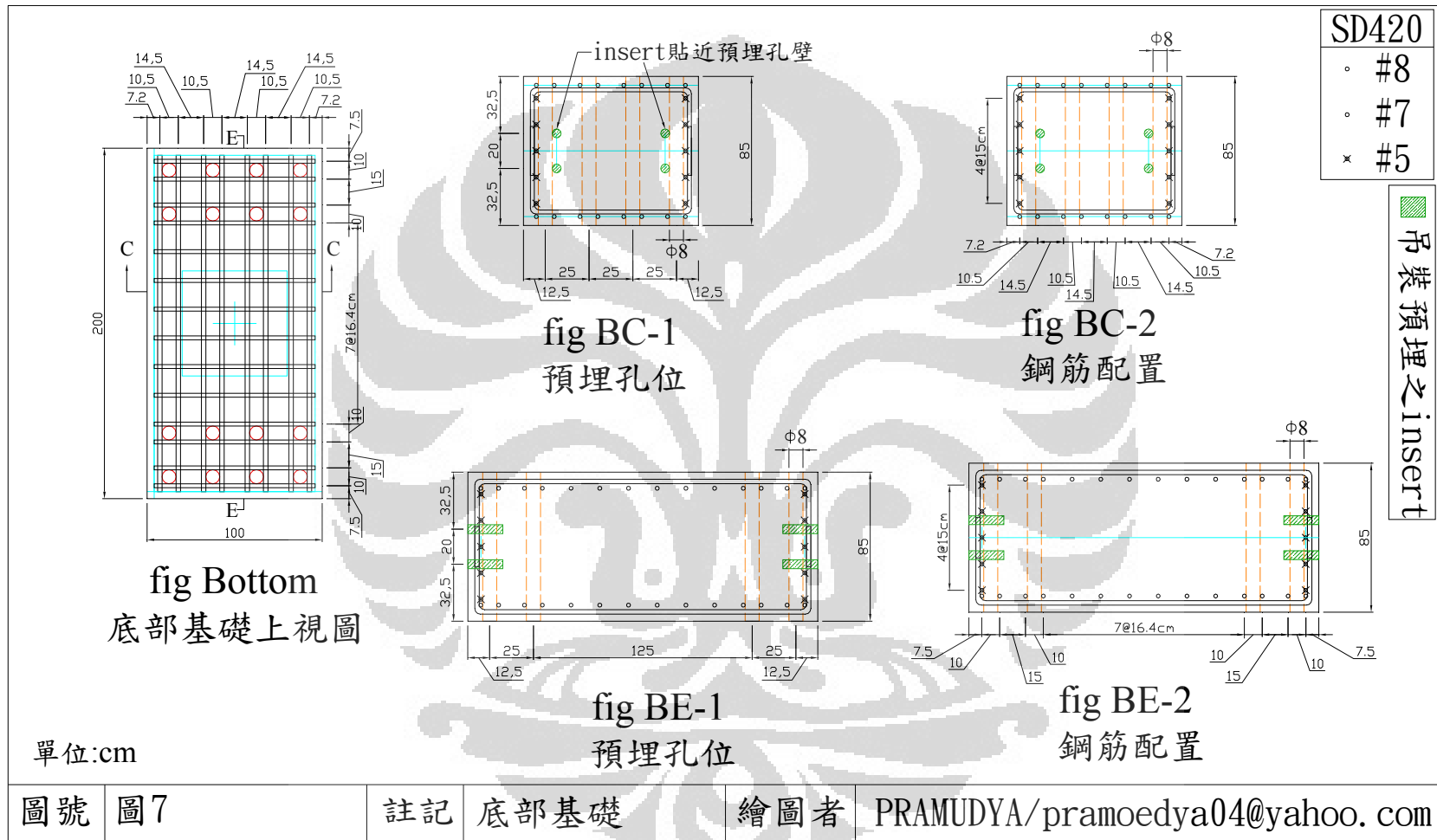
Figure A.7 Reinforcement detail of bottom block
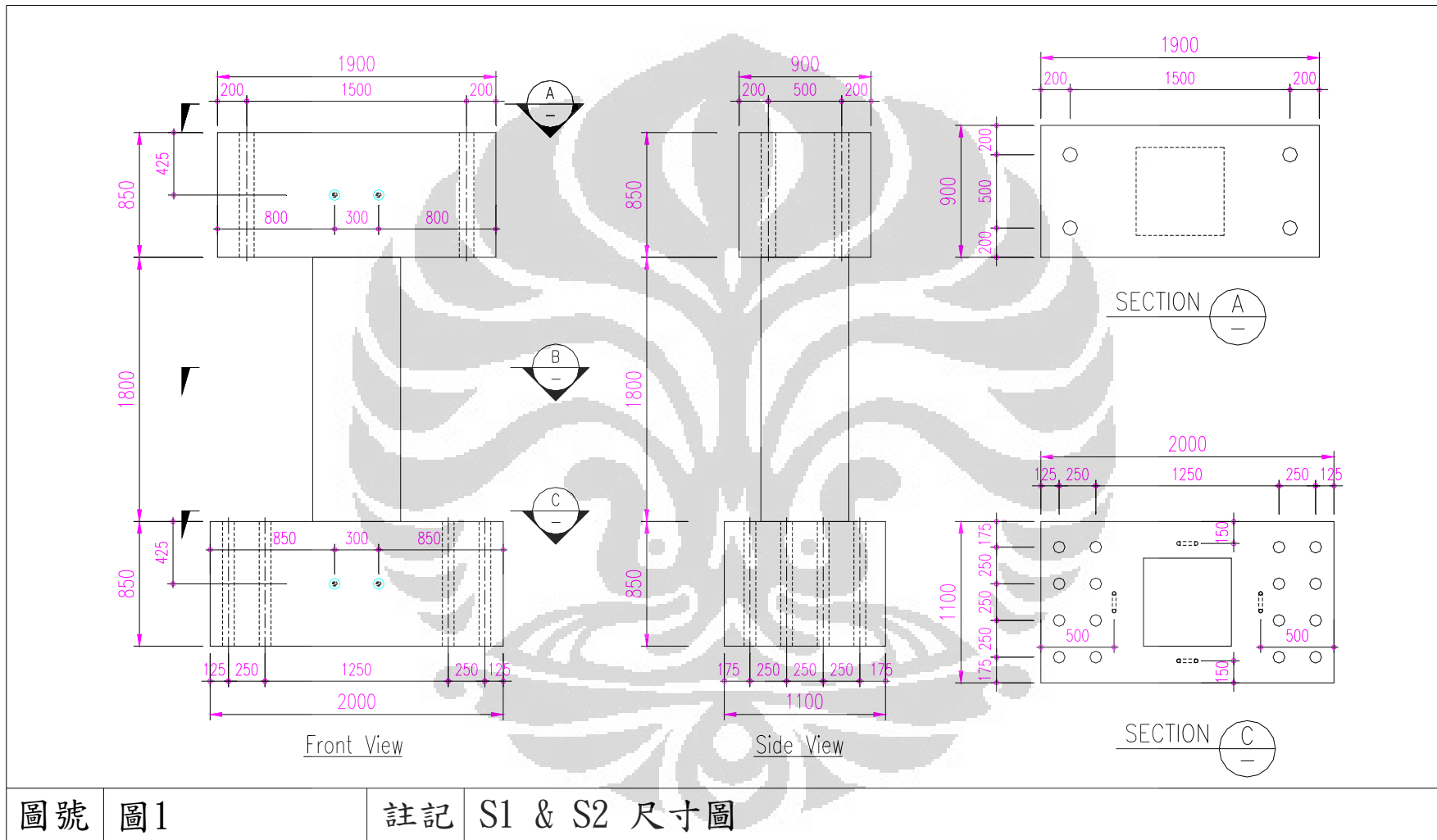
Figure A.8 Dimension of the specimens

210
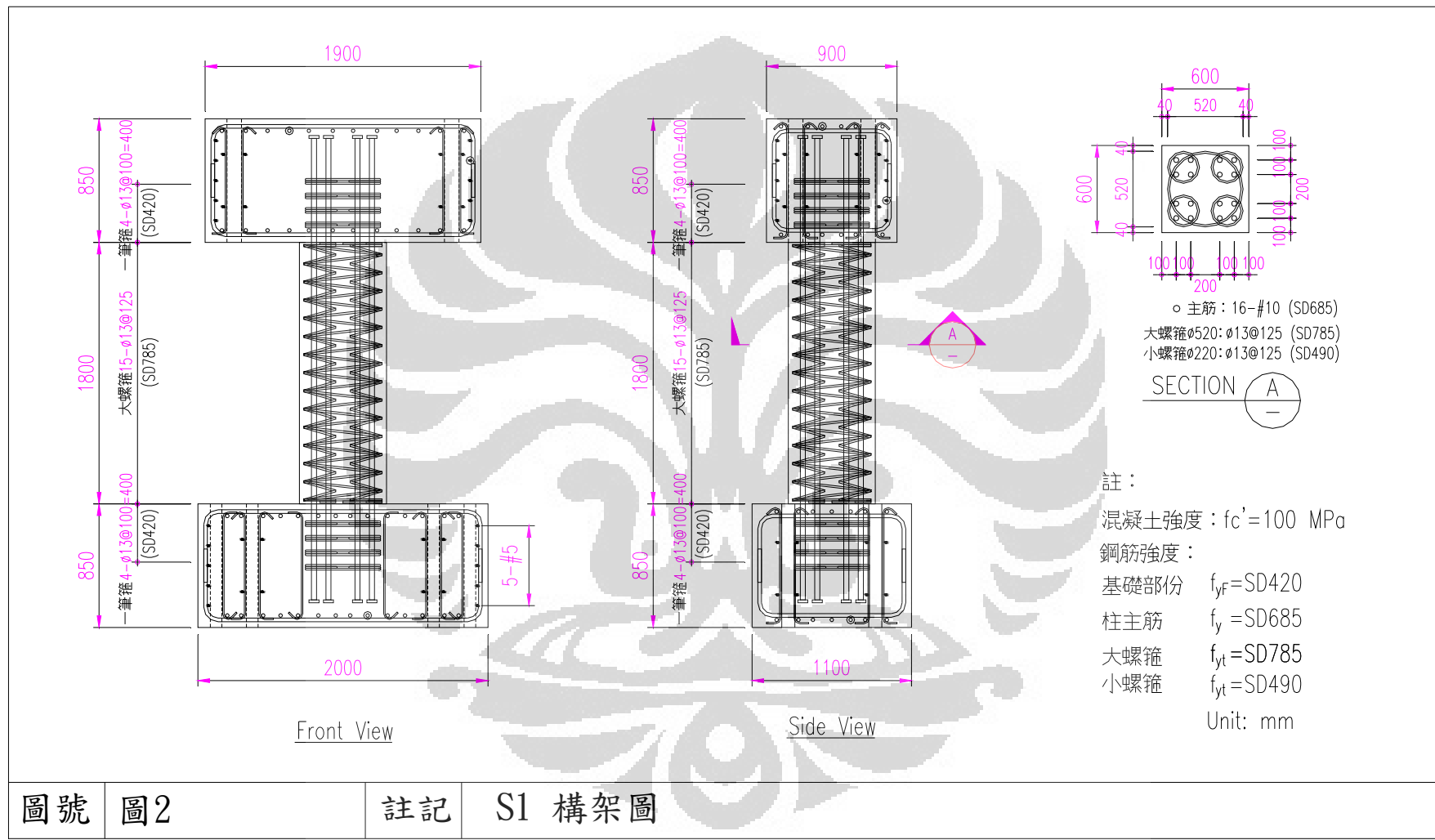
Figure A.9 Reinforcement detail of Column S1
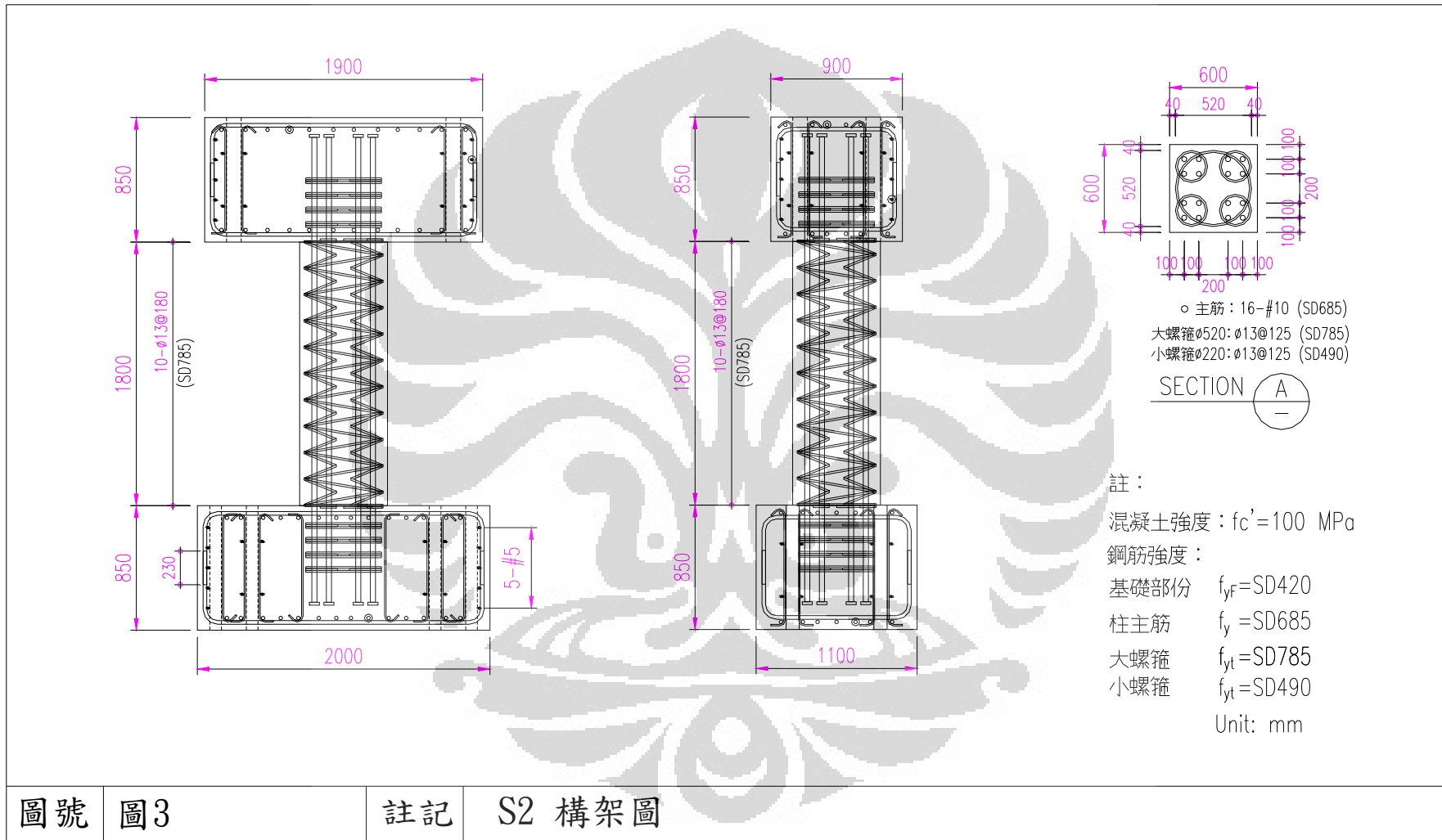
Figure A.10 Reinforcement detail of Column S2

APPENDIX B FRICTION AND AXIAL FORCE
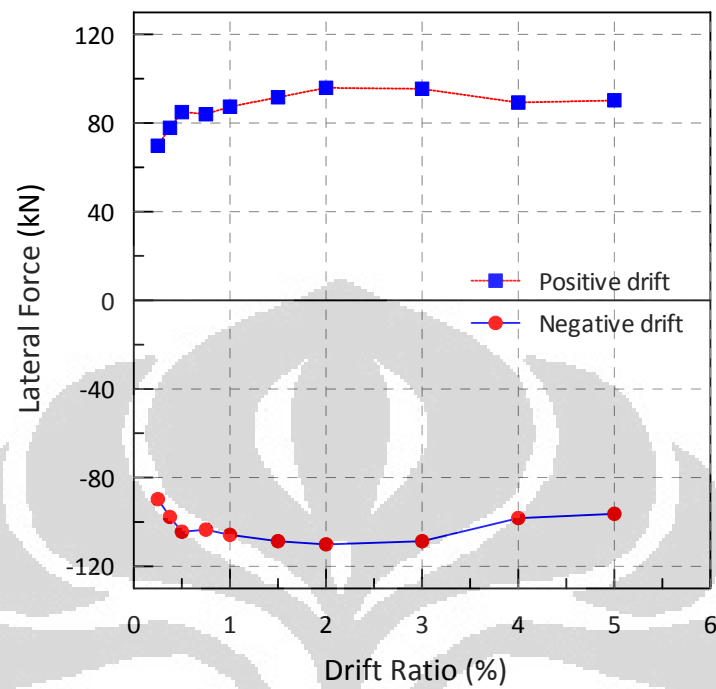
Figure B.1 Friction force of type B specimens
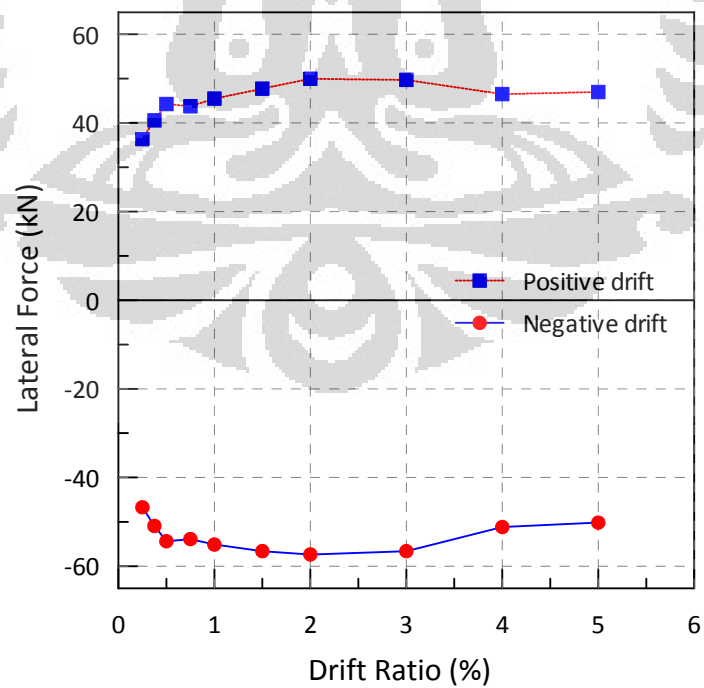
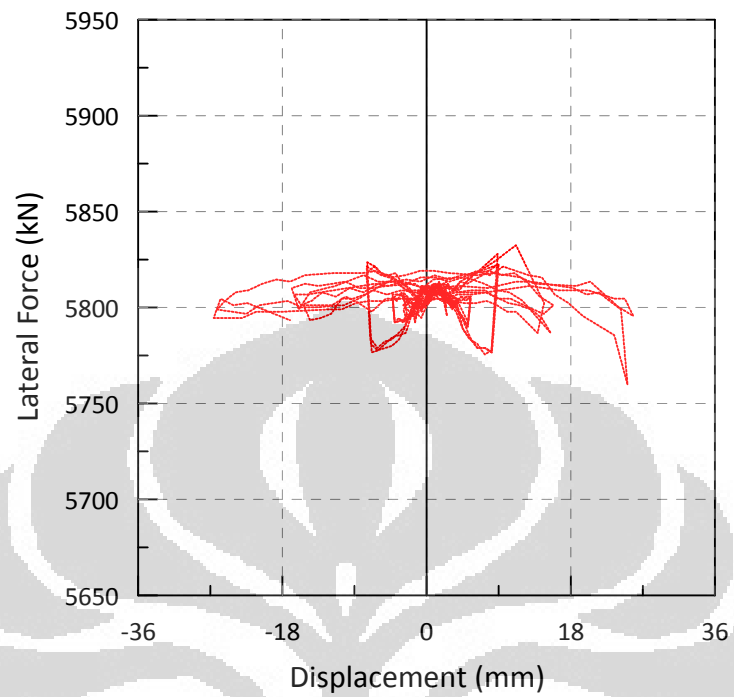**Figure B.2** Friction force of type S specimens
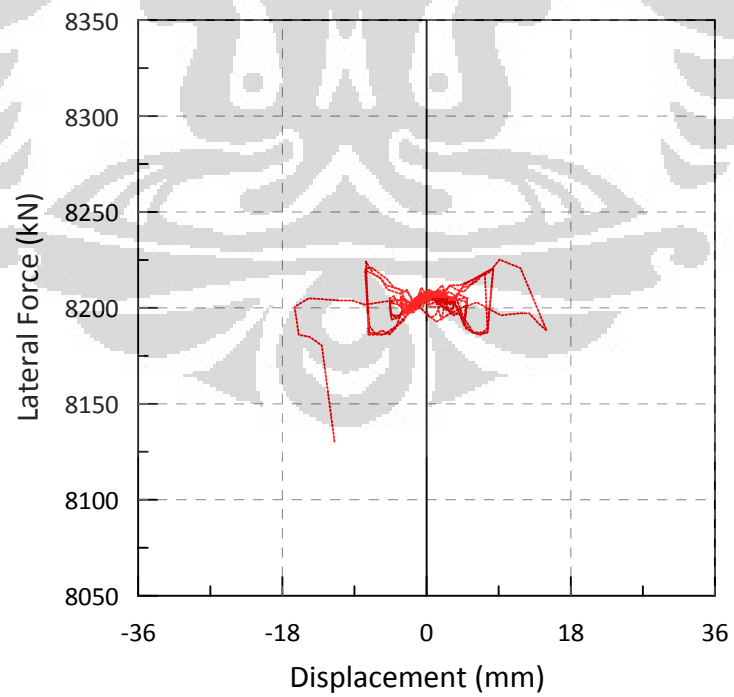
Figure B.3 Applied axial load of Column B1

Figure B.4 Applied axial load of Column B2
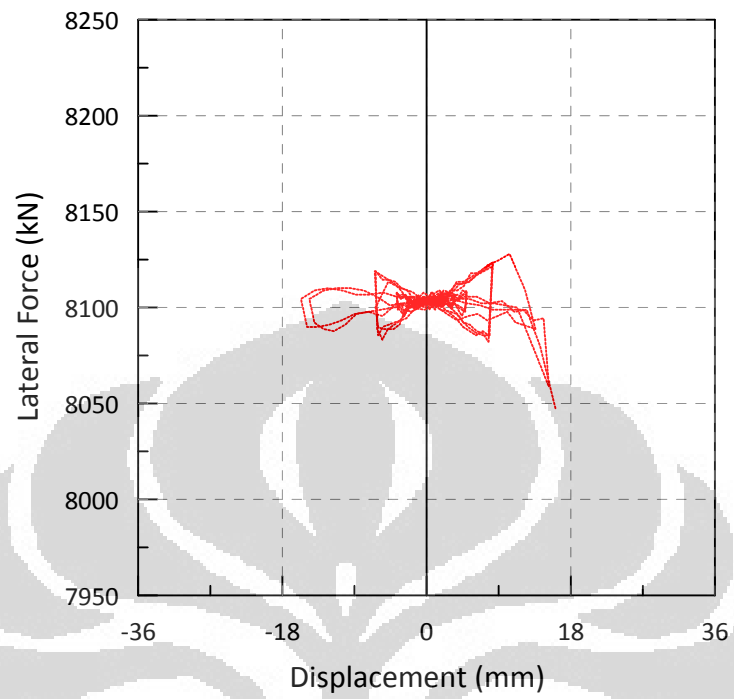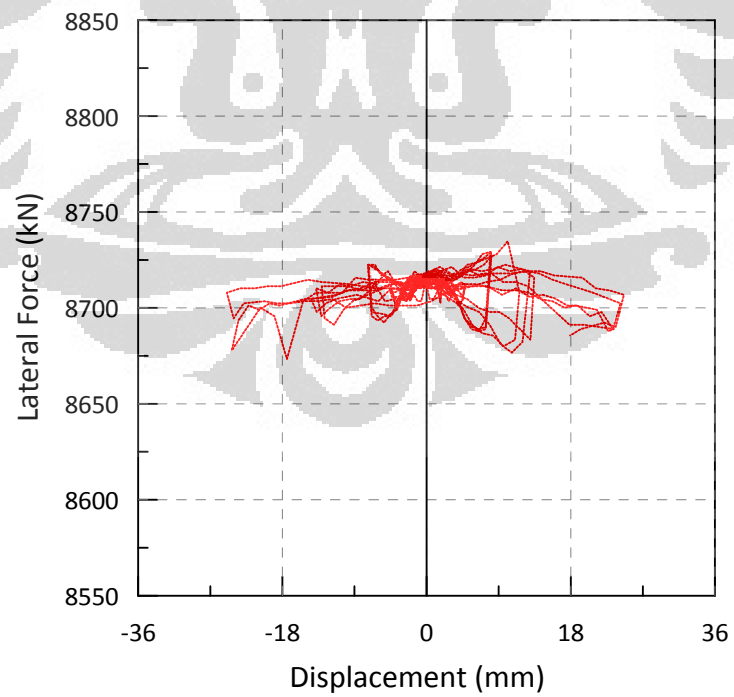
Figure B.5 Applied axial load of Column B3
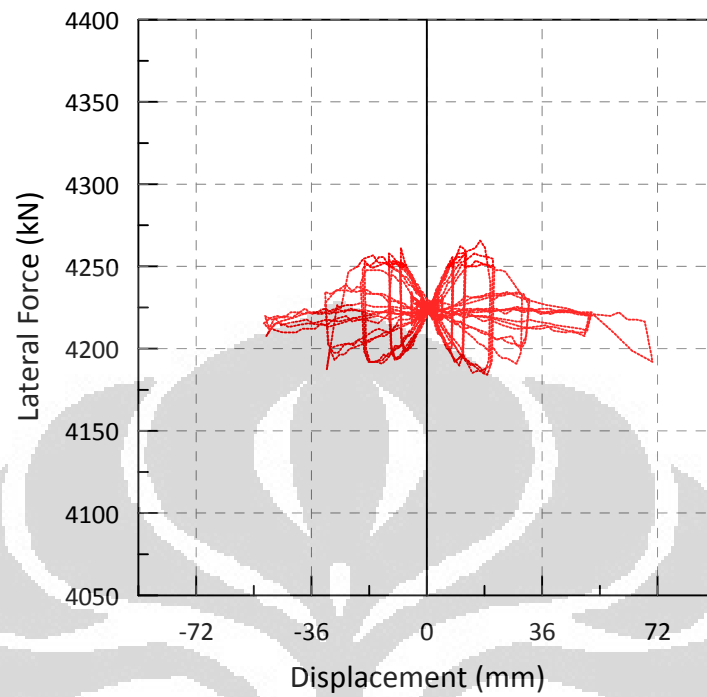

Figure B.6 Applied axial load of Column B4
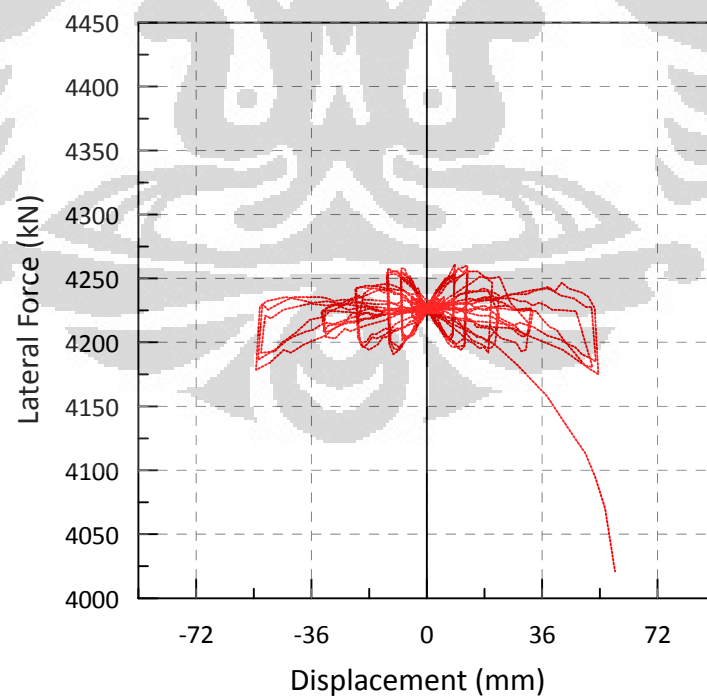
Figure B.7 Applied axial load of Column S1

Figure B.8 Applied axial load of Column S2